Polymeric Filler Reinforced Glass Fiber Epoxy Nanocomposites for Improved Impact Strength

A thesis submitted in the partial fulfillment of the requirements
for the award of degree of

Doctor of Philosophy

by

Daksh Shelly
(Registration No. 901808001)

Under the supervision of

Dr. Tarun Nanda
Professor
Mechanical Engineering Department
Thapar Institute of Engineering & Technology
Patiala

Dr. Rajeev Mehta
Professor and Head
Chemical Engineering Department
Thapar Institute of Engineering & Technology
Patiala

Mechanical Engineering Department
Thapar Institute of Engineering & Technology
Patiala, Punjab, India
March 2023

This Thesis is dedicated to

My mentors, Dr. Tarun Nanda and Dr. Rajeev Mehta, who taught me the principles of life,

My parents, who never stop giving of themselves in countless ways,

My sister, who led me through the valley of darkness with light of hope and support,

My friends and relatives who stood by me when things looked bleak.

TO RAISE NEW QUESTIONS, NEW POSSIBILITIES, TO REGARD OLD PROBLEMS FROM A NEW ANGLE, REQUIRES CREATIVE IMAGINATION AND MARKS REAL ADVANCE IN SCIENCE.

Certificate

This is to certify that the thesis entitled, **"Polymeric Filler Reinforced Glass Fiber Epoxy Nanocomposites for Improved Impact Strength"** submitted by **Daksh Shelly,** Ph.D. student (Registration Number: 901808001) for the partial fulfillment of the requirements for the award of degree of Doctor of Philosophy in Mechanical Engineering Department, Thapar Institute of Engineering and Technology, Patiala, is a record of the candidate's own work carried out by him from July 2018 to September 2022 in this institute under our supervision. The matter presented in this thesis has not been submitted in part or full for the award of any degree in any university or institute.

Date: 15/3/2023

Daksh Shelly
(Daksh Shelly)

Dr. Tarun Nanda
Professor
Mechanical Engineering Department
Thapar Institute of Engineering & Technology
Patiala

Rajeev Mehta

Dr. Rajeev Mehta
Professor and Head
Chemical Engineering Department
Thapar Institute of Engineering & Technology
Patiala

Acknowledgement

First and foremost, I would like to thank the Almighty whose countless blessings have made me who I am today. He enabled me with philosophy, perception, and motivation to present this work, after handling the tough times with empathy, professionalism, and clarity.

During the course of this thesis, several personnel directly or indirectly contributed in making this doctoral dissertation possible and I will always remain deeply indebted to them.

Firstly, from the core of my heart, I would like to express special thanks to my esteemed supervisors, Prof. Tarun Nanda and Prof. Rajeev Mehta for encouraging my research and for allowing me to grow as a research scholar. Their consistent support, dynamic supervision, valuable and innovative suggestions have enlightened my knowledge and skills in the area of fiber reinforced polymer nanocomposites. Both of them have been tremendous mentors now and forever.

Besides my supervisors, I wish to express humble and special thanks to Dr. T. K. Bera and Dr. T.P. Singh for providing me necessary facilities in the department along with their encouragement and constant moral support to accomplish this task. I would also like to acknowledge the valuable suggestions of the members of the Doctoral Committee, Dr. Shruti Sharma, Dr. J.S. Saini, Dr. H.L. Bhowmick, for their insightful comments and questions during my presentations. I sincerely appreciate the whole hearted cooperation and valuable help rendered by teaching and non-teaching staff of the Mechanical Engineering Department (MED), TIET, Patiala.

I am grateful to Dr. Sandeep Sharma, Mr. Munish Kashyap, and Mr. Shubham kaushal who provided me with the experimental set-up to carry out my research work over the past four years. A special thanks to Dr. Haripada Bhunia, CHED, TIET, for also providing me with the equipment for carrying out my research work. Without his benevolent motivation and support, it would not have been possible to conduct this research. Thanks also goes to Dr. Rafat Siddique, Dean of Research and Sponsored Projects for providing the possible research facilities.

It is my pleasure to extend my gratitude to Prof. Rajeev Mehta and his family members for their support throughout my Doctoral research work. I owe a special thanks to Prof. Tarun Nanda and his family members for supporting me whenever I needed. Whenever I needed time and inputs from Prof. Tarun Nanda, his family always welcomed me with a smile. It is only with the blessings and help of Ms. Archana Nanda that I was able to complete the present research.

I thank my seniors, Dr. Bikramjit Sharma, Dr. Karanbir Singh, Dr. Sandeep Sharma, Dr. Jyoti Sharma, and Dr. Shivani Kalotra, along with fellow research scholars, Dr. Saudagar Dongare, Ms. Gloria Ahuja, Ms. Anushka Garg, Ms. Simran Guleria, Mr. Sachin Jaidka, Mr. Rahul Gupta, Mr. Nikhil Sharma, and Mr. Rajat Kumar with whom I have spent these years of research and enjoyed many interactive sessions. I am also thankful to all the laboratory staff members who maintained all the machines, sources, and equipment so efficiently, which helped me in performing the experiments accurately. Special thanks are due to my friends Mr. Lalit Mann Singh and Mr. Amandeep Singh for always supporting me and inspiring me to reach higher accomplishments in my research career.

The financial assistance rendered by Science & Engineering Research Board-Department of Science & Technology (SERB-DST), New Delhi, India for setup of lab equipment, carrying out experiments, mechanical testing, and characterization of materials gratefully acknowledged. The financial support acted as a catalyst and helped me in achieving tremendous results in my research.

Special thanks is also due to my family members. Words cannot express how grateful I am to my parents and sister for all their sacrifice that they had made on my behalf and who have always been my strongest support and my source of motivation during moments of despair and discouragement. My sister and brother-in-law Dr. Richa Shelly and Dr. Tanuj Sharma who had been always there for me and keep me free from worries by efficiently managing all the odds faced by the family. My family members have always acted as an energy booster for me to keep me motivated to provide more inputs to the research.

I want to thank my relatives and friends who have supported me by any means over the past four years in my pursuit of completing my Doctoral Degree.

I extend my special thanks to all who kept me well-balanced and have tried to make this challenging task a pleasant journey.

Place: *Patiala*

Date: 15/3/2023

Daksh Shelly

(Daksh Shelly)

Abstract

Commercially used fiber reinforced polymer composites mostly comprise of glass fibers as the reinforcement and epoxy as the matrix (epoxy based GFRPs). These GFRPs have high specific strength and stiffness and are used in various structural applications. However, safe operation of structures for the required lifetime demands not only good static mechanical properties but also high impact strength. For this reason, the current research in this field of work focuses on improvement in impact strength of epoxy based GFRPs. Epoxy toughening has remained an interesting and challenging topic. Significant efforts have been paid on epoxy-based systems toughened by reinforcement of micrometre-sized liquid rubbers, core-shell rubber particles, thermoplastic particles etc. Addition of rubbery toughening agents provides impressive toughening effect but tends to cause severe deterioration in strength and processing difficulties due to high viscosity. Further, introduction of thermoplastic particles typically gives a moderate toughening effect only. Nanoclay reinforcement to glass fiber reinforced epoxy based composite system shows substantial improvements in static mechanical properties (tensile properties, flexural properties, microhardness etc.) but only marginal improvements in impact strength of the resulting GFRP nanocomposite. So, the impact behaviour of GFRP nanocomposites is still an area of concern. In the present research, it was envisaged that incorporation of thermoplastic fillers as an additional second filler along with nanoclay as the first filler can considerably increase the impact strength and tensile properties of epoxy based GFRPs. Thus, the research work was designed to process epoxy based GFRPs through addition of nanoclay (nano-filler) and thermoplastic fibers (micro-filler) using vacuum assisted hand lay-up technique. Nanoclay was added in a fixed loading of 2 phr in GFRPs. Nanoclay concentration was kept low in order to avoid abrupt increase in viscosity of resulting GFRPs on addition of thermoplastic fibers and nanoclay. Three different thermoplastic fibers viz. (i) ultra high molecular weight polyethylene fiber (loading: 0.125–0.500 phr), para-aramid fibers (0.50–2.00 phr), and Inviya (spandex) fibers (0.50–2.00 phr) were used separately as the micro-filler in GFRPs. A major challenge was to improve the compatibility of thermoplastic fibers with other constituents of epoxy based GFRPs. Surface treatment (compatibilization) of the nano-filler was done with silane agent (silanization) and that of thermoplastic micro-fillers was done using various methods viz. potassium permanganate treatment for UHMWPE fibers, phosphoric acid treatment for para-aramid and Inviya fibers, silanization with 3-aminopropyltriethoxy silane agent, UV-assisted maleic

anhydride grafting (MAH) grafting, and/or a combination of these treatments. For MAH grafting of thermoplastic fibers, the optimum treatment time (for exposure of MAH-acetone solution containing thermoplastic fibers to UV radiations) was determined to be 4.5 h, 02 h, and 4.5 h for UHMWPE fibers, para-aramid fibers, and Inviya fibers respectively.

Processing of multi-scale filler reinforced epoxy GFRPs was done using a series of processing steps including homogenization, probe ultrasonication etc. Characterization techniques including XRD and TEM analysis confirmed the dispersion of nanoclay platelets at a nano-level in developed GFRPs.

Three different types of montmorillonite nanoclays viz. (i) CA, (ii) IE, and (iii) PG were separately reinforced in the reference epoxy based GFRP to investigate the effect on Izod impact strength and tensile properties of resulting GFRPs. PG nanoclay showed the best combination of mechanical properties, and thus, was chosen as the nano-filler for the present research. PG nanoclay was subjected to silanization for further improvement in mechanical properties of GFRPs containing the nanoclay. For silanization, silane agent concentration was varied in the range of 100–400% as a proportion of nanoclay loading (1X, 2X, 3X, and 4X). Silanization was confirmed through FTIR analysis. GFRPs reinforced with 2 phr of 3X silanized nanoclay of 'no-washing' case (3X2PGAW*C) showed maximum improvement of 27% and 16% in Izod impact strength and tensile strength respectively over the reference sample.

Addition of pristine thermoplastic polymeric fibers to GFRP nanocomposite system resulted in deterioration of mechanical properties. Pristine thermoplastic fibers did not interact effectively with other constituents of GFRP system due to lack of polar functional groups owing to chemically inert and mechanically smooth surface. To resolve this issue, thermoplastic fibers were subjected to surface treatment. Surface modification of thermoplastic fibers improved their interfacial adhesion with other constituents of GFRP based nanocomposite system and resulted in significant improvements in impact strength of resulting nanocomposites. Epoxy based GFRPs (containing 2 phr of silanized nanoclay) reinforced with 0.250 phr of treated UHMWPE fibers (potassium permanganate treatment followed by silanization) showed 30% and 17% improvement in impact strength and tensile strength respectively over the reference composite. Epoxy based GFRPs (containing 2 phr of silanized nanoclay) reinforced with 1.00 phr of MAH treated para-aramid fibers showed 34% and 6% improvement in impact strength and tensile strength respectively over the reference composite. Epoxy based GFRPs (containing 2 phr of

silanized nanoclay) reinforced with 1.50 phr of treated Inviya fibers (phosphoric acid treatment followed by silanization) showed 150% and 4% improvement in impact strength and tensile strength respectively over the reference composite.

These newly developed multi-scale filler reinforced epoxy GFRPs displaying significantly improved impact strength along with good tensile properties can be utilized in high impact applications where safety is a critical prerequisite like dashboards, bumpers, and other structural components of automobiles. In addition to this, the newly developed GFRPs can be used in aviation parts (radome, stabilizers etc.), marine industry (decks, hulls etc.), and sports industry (vault poles, archery bows etc.).

List of publications

The following publications in peer reviewed SCI Journals have been published during the Ph.D. tenure.

Publications from present research work

1. **D. Shelly**, T. Nanda, R. Mehta, Reinforcement of compatibilized nanoclay/Inviya fibers to epoxy based glass fiber nanocomposites for high impact strength applications, *Archives of Civil and Mechanical Engineering*. (2023). **(IF: 4.042)** *https://doi.org/10.1007/s43452-023-00610-0*
2. **D. Shelly,** T. Nanda, R. Mehta, Novel epoxy-based glass fiber reinforced composites containing compatibilized para-aramid fibers and silanized nanoclay for improved impact strength, *Polymer Composites*, 43 (2022) 1357–1370. **(IF: 3.531)** *https://doi.org/10.1002/pc.26453*
3. **D. Shelly**, T. Nanda, R. Mehta, Addition of compatibilized nanoclay and UHMWPE fibers to epoxy based GFRPs for improved mechanical properties, *Composites Part A: Applied Science and Manufacturing*, 145 (2021) 106371. **(IF: 9.463)** *https://doi.org/10.1016/j.compositesa.2021.106371*
4. **D. Shelly**, T. Nanda, R. Mehta, Addition of compatibilized nanoclay to GFRCs for improved Izod impact strength and tensile properties, *Proceedings of the Institution of Mechanical Engineers, Part L: Journal of Materials: Design and Applications*, 235 (2021) 2022–2035. **(IF: 2.663)** *https://doi.org/10.1177/14644207211009923*

Other publications

1. T. Nanda, K. Singh, **D. Shelly**, R. Mehta, Advancements in multi-scale filler reinforced epoxy nanocomposites for improved impact strength: a review, *Critical Reviews in Solid State and Materials Sciences*, 46 (2021) 281–329. **(IF: 11.178)** *https://doi.org/10.1080/10408436.2020.1777934*
2. T. Nanda, G. Sharma, R. Mehta, **D. Shelly**, K. Singh, Mechanisms for enhanced impact strength of epoxy based nanocomposites reinforced with silicate platelets. *Materials Research Express*, 6 (2019) 065061. **(IF: 2.025)** *https://doi.org/10.1088/2053-1591/ab1023*
3. M. Raturi, B.J. Singh, **D. Shelly**, K. Singh, T. Nanda, R. Mehta, Tensile behaviour and characterization of epoxy-clay-poly (ethylene terephthalate) nanocomposites, *Materials Research Express*, 6 (2019) 115014. **(IF: 2.025)** *https://doi.org/10.1088/2053-1591/ab43e9*
4. **D. Shelly**, K. Singh, T. Nanda, R. Mehta, Addition of nanomer clays to GFRPs for enhanced impact strength and fracture toughness, *Materials Research Express*, 5 (2018) 105013. **(IF: 2.025)** *https://doi.org/10.1088/2053-1591/aadb0d*

Acronyms & symbols

Acronym	Meaning/Full form
AM	Acrylamide
APTES	3-amimopropyltriethoxysilane
ASTM	American society for testing and materials
C	Carbon
CNTs	Carbon nanotubes
DGEBA	Diglycidyl ether of bisphenol A
EDS	Energy dispersive spectroscopy
EH	Epichlorohydrin
EHPEA	Epichlorohydrin coating followed by poly(propylene glycol) bis(2-aminopropyl ether)
EPDM	Ethylene propylene diene monomer
FE-SEM	Field emission scanning electron microscopy
FTIR	Fourier transform infrared spectroscopy
GFRP	Glass fiber reinforced plastic
GMA	Glycidyl methacrylate
HDPE	High-density polyethylene
IFSS	Interfacial shear strength
ILSS	Interlaminar shear strength
K	Potassium
$KMnO_4$	Potassium permanganate
MAH	Maleic anhydride
MMT	Montmorillonite
Mn	Manganese
MS	γ-methacryloxypropyltrimethoxysilane
MWCNT	Multi-walled carbon nanotubes
N	Nitrogen
Na	Sodium
NaOH	Sodium hydroxide
O	Oxygen
OMMT	Organically modified montmorillonite
P	Phosphorus
PANI	Polyaniline
PCBs	Printed circuit boards
PEI	Polyetherimide
PEN	Polyarylene ether nitrile
PEN-t-Ph	Polyarylene ether nitrile terminated with phthalonitrile
PET	Polyethylene terephthalate fibers
Phr	Per hundred resin
PI	Polyimide
PMMA	Poly(methyl methacrylate)
PP	Polypropylene fibers
R_a	Average surface roughness

SEM	Scanning electron microscopy
Si	Silicon
TEM	Transmission electron microscopy
TETA	Triethylenetetramine
TFBT	Transverse fiber bundle test
UHMWPE	Ultra high molecular weight polyethylene
UTM	Universal testing machine
UV	Ultra violet
VARIM	Vacuum assisted resin infusion moulding
vol.%	Volume percentage
VS	Vinylytriethoxysilane
wt.%	Weight percentage
X	Nanoclay loading
XRD	X-Ray diffraction
ZnNW	Zinc oxide nanowire
θ	Theta
°	Degrees
℃	Degree Celsius

Nomenclature

S. No.	Sample Designation	Detail of nanoclays and processed GFRPs
1.	CA	Cloisite®15A nanoclay
2.	IE	Nanomer® I.28E nanoclay
3.	PG	Nanomer® PGV nanoclay
4.	1XPGAW	1X silane treated Nanomer® PGV with acetone washing(1X means that silane agent amount for surface treatment of nanoclay was 100% as proportion of nanoclay loading)
5.	2XPGAW	2X silane treated Nanomer® PGV with acetone washing
6.	3XPGAW	3X silane treated Nanomer® PGV with acetone washing
7.	4XPGAW	4X silane treated Nanomer® PGV with acetone washing
8.	1XPGAW*	1X silane treated Nanomer® PGV without acetone washing
9.	2XPGAW*	2X silane treated Nanomer® PGV without acetone washing
10.	3XPGAW* (PG* designation used in multi-filler reinforced epoxy based GFRPs)	3X silane treated Nanomer® PGV without acetone washing
11.	4XPGAW*	4X silane treated Nanomer® PGV without acetone washing
12.	RC	GFRP nanocomposite without nanoclay
13.	2CAC	GFRP nanocomposite reinforced with 2 phr of Cloisite®15A
14.	2IEC	GFRP nanocomposite reinforced with 2 phr of Nanomer® I.28E
15.	2PGC	GFRP nanocomposite reinforced with 2 phr of Nanomer® PGV
16.	1X2PGAWC	GFRP nanocomposite reinforced with 2 phr of 1X silanized Nanomer® PGV with acetone washing
17.	2X2PGAWC	GFRP nanocomposite reinforced with 2 phr of 2X silanized Nanomer® PGV with acetone washing
18.	3X2PGAWC	GFRP nanocomposite reinforced with 2 phr of 3X silanized Nanomer® PGV with acetone washing
19.	4X2PGAWC	GFRP nanocomposite reinforced with 2 phr of 4X silanized Nanomer® PGV with acetone washing
20.	1X2PGAW*C	GFRP nanocomposite reinforced with 2 phr of 1X silanized Nanomer® PGV without acetone washing
21.	2X2PGAW*C	GFRP nanocomposite reinforced with 2 phr of 2X silanized Nanomer® PGV without acetone washing
22.	3X2PGAW*C (2PG*C designation used in multi-filler reinforced epoxy based GFRPs)	GFRP nanocomposite reinforced with 2 phr of 3X silanized Nanomer® PGV without acetone washing
23.	4X2PGAW*C	GFRC nanocomposite reinforced with 2 phr of 4X silanized Nanomer® PGV without acetone washing
24.	T1	Potassium permanganate treatment

25.	T2	Silanization with 3-aminopropyltriethoxy silane
26.	T3	Potassium permanganate treatment followed by silanization
27.	T4	UV-assisted MAH grafting
28.	T5	Phosphoric acid treatment
29.	T6	Phosphoric acid treatment followed by silanization
30.	2PG*0.125UC	GFRP nanocomposite reinforced with 2 phr of silanized nanoclay and 0.125 phr of pristine UHMWPE fibers
31.	2PG*0.250UC	GFRP nanocomposite reinforced with 2 phr of silanized nanoclay and 0.250 phr of pristine UHMWPE fibers
32.	2PG*0.375UC	GFRP nanocomposite reinforced with 2 phr of silanized nanoclay and 0.375 phr of pristine UHMWPE fibers
33.	2PG*0.500UC	GFRP nanocomposite reinforced with 2 phr of silanized nanoclay and 0.500 phr of pristine UHMWPE fibers
34.	2PG*0.25UPC	GFRP nanocomposite reinforced with 2 phr of silanized nanoclay and 0.250 phr of UHMWPE fibers treated with potassium permanganate solution
35.	2PG*0.25UAC	GFRP nanocomposite reinforced with 2 phr of silanized nanoclay and 0.250 phr of UHMWPE fibers silanized with 3-aminopropyltriethoxy silane agent
36.	2PG*0.25UPAC	GFRP nanocomposite reinforced with 2 phr of silanized nanoclay and 0.250 phr of UHMWPE fibers treated with potassium permanganate solution followed by silanization with 3-aminopropyltriethoxy silane agent
37.	2PG*0.25UMC	GFRP nanocomposite reinforced with 2 phr of silanized nanoclay and 0.250 phr of UHMWPE fibers after UV-assisted MAH grafting
38.	2PG*0.5PC	GFRP nanocomposite reinforced with 2 phr of silanized nanoclay and 0.50 phr of pristine para-aramid fibers
39.	2PG*1.0PC	GFRP nanocomposite reinforced with 2 phr of silanized nanoclay and 1.00 phr of pristine para-aramid fibers
40.	2PG*1.5PC	GFRP nanocomposite reinforced with 2 phr of silanized nanoclay and 1.50 phr of pristine para-aramid fibers
41.	2PG*2.0PC	GFRP nanocomposite reinforced with 2 phr of silanized nanoclay and 2.00 phr of pristine para-aramid fibers
42.	2PG*1.0PPC	GFRP nanocomposite reinforced with 2 phr of silanized nanoclay and 1.00 phr of para-aramid fibers treated with phosphoric acid
43.	2PG*1.0PAC	GFRP nanocomposite reinforced with 2 phr of silanized nanoclay and 1.00 phr of para-aramid fibers silanized with 3-aminopropyltriethoxy silane agent
44.	2PG*1.0PPAC	GFRP nanocomposite reinforced with 2 phr of silanized nanoclay and 1.00 phr of para-aramid fibers treated with phosphoric acid solution followed by silanization with 3-aminopropyltriethoxy silane agent

45.	2PG*1.0PMC	GFRP nanocomposite reinforced with 2 phr of silanized nanoclay and 1.00 phr of para-aramid fibers after UV-assisted MAH grafting
46.	2PG*0.5IC	GFRP nanocomposite reinforced with 2 phr of silanized nanoclay and 0.50 phr of pristine Inviya fibers
47.	2PG*1.0IC	GFRP nanocomposite reinforced with 2 phr of silanized nanoclay and 1.00 phr of pristine Inviya fibers
48.	2PG*1.5IC	GFRP nanocomposite reinforced with 2 phr of silanized nanoclay and 1.50 phr of pristine Inviya fibers
49.	2PG*2.0IC	GFRP nanocomposite reinforced with 2 phr of silanized nanoclay and 2.00 phr of pristine Inviya fibers
50.	2PG*1.5IPC	GFRP nanocomposite reinforced with 2 phr of silanized nanoclay and 1.50 phr of Inviya fibers treated with phosphoric acid
51.	2PG*1.5IAC	GFRP nanocomposite reinforced with 2 phr of silanized nanoclay and 1.50 phr of Inviya fibers silanized with 3-aminopropyltriethoxy silane agent
52.	2PG*1.5IPAC	GFRP nanocomposite reinforced with 2 phr of silanized nanoclay and 1.50 phr of Inviya fibers treated with phosphoric acid solution followed by silanization with 3-aminopropyltriethoxy silane agent
53.	2PG*1.5IMC	GFRP nanocomposite reinforced with 2 phr of silanized nanoclay and 1.50 phr of Inviya fibers after UV-assisted MAH grafting

Table of contents

List of figures

List of tables

Chapter 1. Introduction

1.1 Overview

This chapter provides an introduction to polymer nanocomposites. It discusses the characteristics of nanoclay reinforced epoxy nanocomposites and presents the different types of nanoclay morphologies that can exist in epoxy nanocomposites. It discusses the properties and limitations of glass fiber reinforced epoxy nanocomposites. The chapter elaborates on the need for compatibilization of various constituents of nanocomposites. It discusses the applications of fiber reinforced polymer composites and finally brings forth the origin of the present research work.

1.2 Polymer nanocomposites

Polymer nanocomposites are defined as polymeric matrices containing nano-fillers, with one of the dimensions being less than or equal to 100 nm [1]. Polymer nanocomposites have received great attention, both in academic community as well as industrial sector, because of their notable improvements in properties over virgin polymers and conventional micro/macro-composites. Conventional composites usually need high filler content (> 10 wt.%) to perform the required functions/applications. Higher filler loading increases the density of composite and also creates processing difficulties. This degrades the overall mechanical performance of composites. Comparatively, nanocomposites show significant improvements in mechanical properties with a lower nano-filler content (< 5 wt.%) [2–4]. It is reported that 3–5 wt.% of nano-filler loading offers the same improvement in properties as is with 20–30 wt.% of micro-filler content [5]. This indicates that nanocomposites offer much greater interfacial area as compared to micro-composites (Figure 1.1) for the same filler content [6].

Nano-fillers are classified into three types based on size. These include (i) one dimensional (nanotubes, nanowires, etc.), (ii) two dimensional (nanoclay, graphene, etc.), (iii) three dimensional (spherical and cubical nanoparticles) [5]. Nano-fillers are utilized in polymer nanocomposites due to their inherent characteristics like high surface-to-volume ratio which improves the matrix-filler interaction and hence provide remarkable improvements in the mechanical properties [3,5,7,8]. Uniformly dispersed nano-fillers boost the mechanical performance whereas agglomerated nanoparticles deteriorate the performance of polymer

nanocomposites. Agglomerates act as crack propagation sites. Thus, the level of nano-filler dispersion in polymer matrices is very imperative [9].

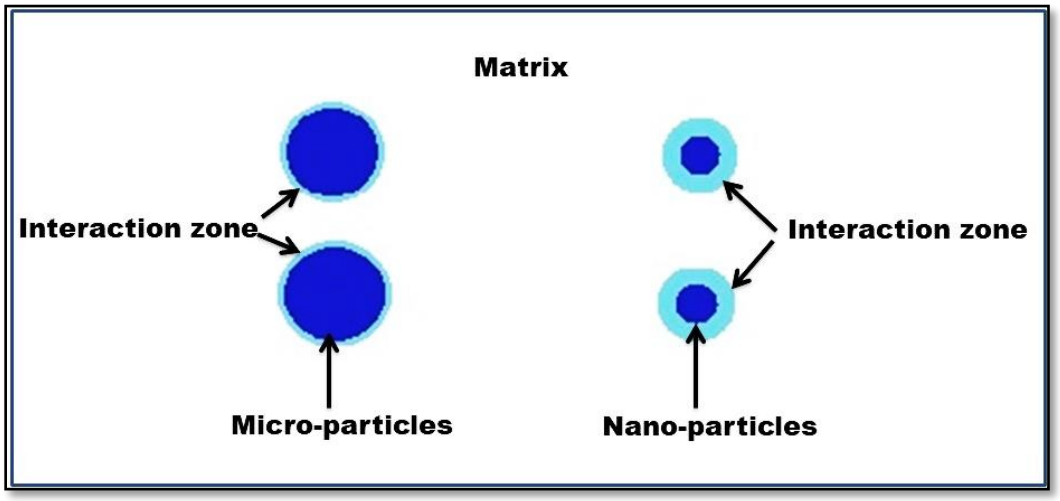

Figure 1.1. Schematic comparison of nano-particle and micro-particle interaction with polymer matrix [6].

Some of the main mechanisms reported in literature which cause improvement in properties of nano-filler reinforced polymer nanocomposites are discussed as follows:

a) **Crack pinning:** The dispersed nano-filler restricts the propagation of cracks and produces a secondary non-linear source. The crack pins at that point. Higher energy is required for further propagation of the crack because energy required to propagate the crack depends on length of crack. This mechanism is known as *'dispersion hardening'* and offers higher obstruction (requires higher energy absorption) owing to lower inter-particle distance among dispersed nano-fillers [10].
b) **Crack deflection:** Uniformly dispersed and stiff nano-fillers cause the cracks to twist or tilt which modifies the crack propagation plane and increases the surface area of cracks. Consequently, more energy is required to cause failure of the material [11].
c) **Debonding and voids:** Debonding is an important phenomenon which induces toughness in composites. The crack tips are not restricted within a void; hence, crack growth is facilitated [12].
d) **Immobilized polymer:** Uniformly dispersed nano-fillers restrict the movement of polymeric chains. Consequently, chain displacement becomes difficult and higher energy is needed to displace the chains [13].

1.3 Nanoclay reinforced polymer nanocomposites

Among the wide variety of nano-fillers viz. nanoclay, carbon nanotubes, graphene, silica nanoparticles, etc., nanoclay has been utilized extensively in polymer composites owing to its unmatchable characteristics like higher aspect ratio, large active surface area, well-studied intercalation chemistry, ease of availability, and low cost [1,2,14–19]. Polymer nanocomposites reinforced with nanoclay provide significantly improved strength and modulus, higher resistance to chemical attack, decreased flammability, and lower gas permeability [1–3,7]. Figure 1.2 shows the general structure of nanoclay (montmorillonite). The structure of nanoclay comprises of octahedral and tetrahedral layers. The octahedral alumina layer is sandwiched between two tetrahedral silica layers. Oxygen atoms of tetrahedral layer are shared with the octahedral layer. The crystal lattice has an overall negative charge due to the isomorphous substitution of aluminium for silicon in the tetrahedral layer and magnesium or iron for aluminium in the octahedral layer. The negatively charged region between the layers attracts cations (e.g. Ca^{2+}, Fe^{2+} and Na^{+}). This results in a positively charged region between the two negatively charged layers. The whole crystal structure is made up of these type of layers. The thickness of nanoclay is around 1 nm. However, the lateral dimensions vary from angstrom to microns or even more. These dimensions of nanoclay result in high aspect ratio and large active surface area (700–800 m^2/g). These layers are available in an inherent parallel stacked structure. The region between two parallel layers is termed as d-spacing or interlayer spacing/gallery [2,3].

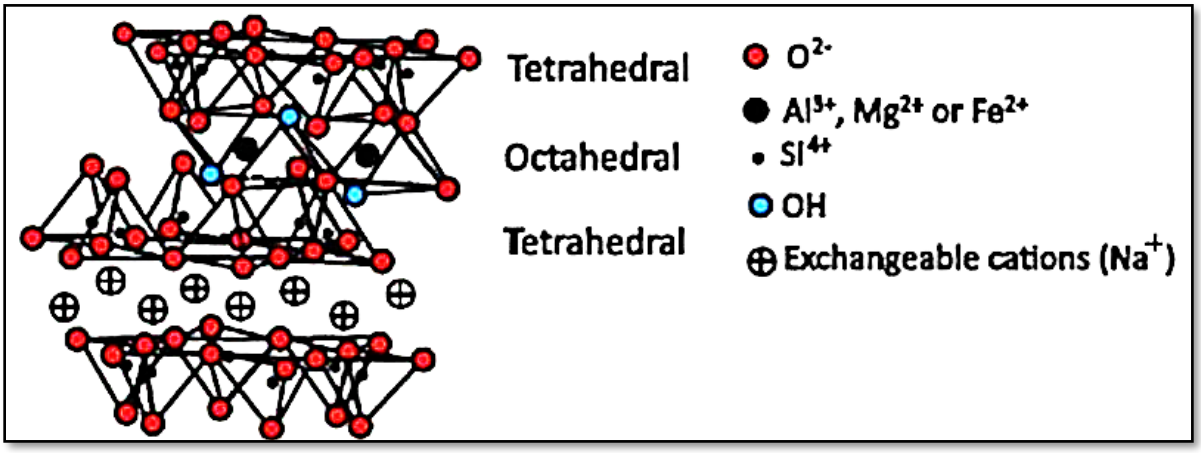

Figure 1.2. Schematic of montmorillonite nanoclay structure [20].

1.4 Various morphologies of nanoclay in polymer nanocomposites

The dispersion of nanoclay in a polymer matrix can result in three different morphologies/structures based on the d-spacing or interlayer spacing/galleries between two nanoclay layers.

a) **Phase separated morphology:** When polymer chains are not able to penetrate between the nanoclay layers, a phase-separated morphology is achieved (Figure 1.3). Polymer nanocomposites with a phase-separated morphology are not able to show significant improvement in properties. Improvement in properties is in the range of conventional composites [2,3].

b) **Intercalated morphology:** When polymer chains are able to penetrate between the nanoclay layers, the d-spacing between them increases. A symmetrically arranged multi-layer structure is seen in which polymer chains and clay layers are alternatively placed. This type of morphology with increased d-spacing as compared to phase-separated morphology is termed as intercalated morphology (Figure 1.3) [2].

c) **Exfoliated morphology:** When polymer chains are able to penetrate between the nanoclay layers and randomly disperse the nanoclay layers in the polymer matrix, an exfoliated morphology is achieved (Figure 1.3). The orientation of nanoclay layers in the polymer matrix is random, and the d-spacing between layers increases extensively. An exfoliated morphology is also known as disordered morphology [2,3,7].

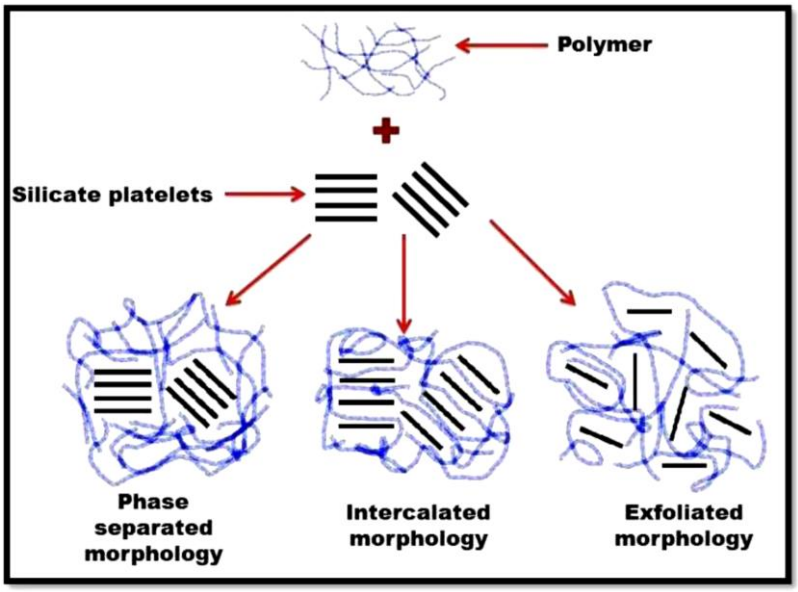

Figure 1.3. Various morphologies of nanoclay in polymer nanocomposites [3].

1.5 Glass fiber reinforced epoxy nanocomposites

For the last half-century, tremendous expansion has been witnessed in the area of fiber reinforced polymer composites owing to their myriad applications in various fields from electronics to aviation [15,21–23]. Fiber reinforced polymer composites comprise of a polymer matrix with high strength fiber(s) as reinforcement. Generally, glass fibers, para-aramid fibers, carbon fibers, polyethylene fibers, ceramic fibers, and natural fibers are used as reinforcement [15,24–30]. Among the various fibers, glass fibers and carbon fibers are most commonly used due to their freedom to be used with either thermoset or thermoplastic matrix [24]. The imperative characteristics of glass fibers include their low cost, high strength and modulus, high chemical resistance, good heat resistance, and excellent insulating properties [31,32]. Epoxy is the most commonly used thermosetting matrix in fiber reinforced polymer nanocomposites because of its characteristics like low density, high chemical stability, excellent bonding ability, and good mechanical properties [14,15,25,33]. Glass fiber reinforced epoxy composites exhibit good static mechanical properties but lack in impact strength. Epoxy resins during curing with a hardener get cross-linked through a polymerization reaction. The resulting cured resins demonstrate superior properties viz. high strength, stiffness, and glass transition temperature. But, this is also accompanied by increased brittleness, resulting in reduced impact strength [1,32,34,35]. Researchers, in the recent past, have tried to obtain a combination of good static mechanical properties along with good impact strength [36–39]. Thermoplastic fibers (polypropylene fibers, polyethylene terephthalate fibers, glass fibers, carbon fibers etc.) or nano-fillers (nanoclay, carbon nanotubes, graphene, silica nanoparticles, etc.) have been used for the purpose by various researchers. Nano-filler (e.g. nanoclay) reinforced epoxy nanocomposites show significantly improved tensile and flexural properties but impact strength improves only marginally [40–43]. On the other hand, thermoplastic fiber reinforced epoxy composites show low mechanical performance due to lack of compatibility of these polymeric fibers with other constituents of epoxy composites. With reinforcement of compatibilized thermoplastic fibers, there is improvement in impact strength but tensile/flexural properties of composites degrade [1,32,34,44]. It is evident from literature that to improve the properties of epoxy based composites with addition of thermoplastic fibers, compatibilization (surface treatment) of thermoplastic fibers is necessary [1,32–34,44,45]. Further, there is still a need to develop epoxy based nanocomposites showing good combination of impact strength-static mechanical properties.

1.6 Compatibilization (surface treatment) of fillers

Compatibilization or surface treatment of reinforcements (nano-filler and/or thermoplastic fibers) results in better interfacial interaction among various constituents of epoxy nanocomposites. This results in development of a robust interface between matrix and reinforcement leading to improved mechanical performance of epoxy nanocomposites [1,32–35,44]. Several surface modification techniques are reported in literature for compatibilization which include chemical treatment (using sodium hydroxide, sulphuric acid etc.), silanization (using different silane agents viz. vinyltriethoxysilane, 3-aminopropyltriethoxysilane etc.), UV-assisted methods (using maleic anhydride grafting, acrylic acid grafting etc.), corona discharge treatment, and plasma modification etc. [1,32–35,44,46–50].

Surface modification techniques either make the fiber surface rough or add functional groups to the fiber surface resulting in better interfacial interaction among various constituents of composite system. Silanization technique and UV-assisted maleic anhydride (MAH) grafting are well known for improving the compatibility between two dissimilar materials (organic and inorganic constituents) [1,34,35].

Table 1.1. Applications of fiber reinforced polymer nanocomposites in various industries.

Industry	Applications	References
Aircraft and Military	Baggage doors, Vertical fins, Vertical and horizontal stabilizers, Rotor blades, Outer flaps, Radome, Tail cone etc.	[15,32,51]
Space Industry	Payload bay door, Remote manipulator arm, Support structures for smaller components (solar arrays, antennas, mirror substrates) etc.	[51]
Automotive Industry	Hood or door panels, Radiator support, Bumper beams, Roof and door frames, Engine valve covers, Timing chain covers, etc.	[15,32,44,51]
Marine Industry	Boat hulls, Decks, Frames, Masts, Bulkheads, Propulsion shafts, etc.	[15,32,35,51,52]
Sporting Goods Industry	Bicycle frames for racing, Tennis rackets, Hockey sticks, Baseball bats, Arrows, Javelins, Athletic shoe soles, heels etc.	[15,32,35,51]
Miscellaneous Industries	Printed circuit boards (PCBs), Floor beams, Transformer housing, Implants, prosthetics etc.	[51,52]

1.7 Applications of fiber reinforced polymer nanocomposites

Fiber reinforced nanocomposites are low-cost/light-weight and are extensively used due to their unique characteristics like excellent strength-to-weight ratio, high tensile and flexural properties

(strength and modulus), good interfacial shear strength, and resistance to degradation from chemicals and environment. These materials are used in aviation, automotive, marine, and military industry and result in reduced overall weight, higher fuel efficiency, and reduced emissions [36,53–60]. The major applications of FRPs are listed in Table 1.1.

1.8 Origin of the present study

Commercially used fiber reinforced polymer composites mostly comprise of glass fibers as reinforcement and epoxy as the matrix (epoxy based GFRPs). These GFRPs have high specific strength and stiffness and are used in various structural applications. However, safe operation of structures for the required lifetime demands not only good static mechanical properties but also high impact strength (e.g. in aerospace applications, during a flight, there is high possibility of impact damage to GFRPs due to runway debris or hail strike [1,32,34,35,51,61–63]. Epoxy, when polymerized, is an amorphous and a highly cross-linked material. The cross-linked structure results in many useful properties such as high modulus and failure strength etc. However, it also leads to an undesirable property whereby the polymer becomes relatively brittle and has poor resistance to crack initiation and growth (i.e. low impact strength). The main disadvantage of polymeric composite materials is represented by the non-visible impact damage, the repairing process being different from the one applied for metal structures. For these reasons, the research in this field focuses on improvement of mechanical properties (especially impact strength) of epoxy based GFRPs to enhance their efficiencies. Epoxy toughening has been an interesting and challenging topic for over four decades. Significant efforts have been paid on epoxies toughened with micrometer-sized liquid rubbers, core-shell rubber particles, thermoplastic particles etc. The addition of rubbery toughening agents has usually resulted in an impressive toughening effect but also tends to cause severe deterioration in strength etc. and also causes processing difficulties due to high viscosity. The introduction of thermoplastic particles typically gives a moderate toughening effect but cannot produce satisfactory results [1,15,32–36,44,64,65]. Consequently, there is still a significant need to develop alternative toughening approaches to significantly increase the fracture resistance of brittle epoxies without compromising on other desirable mechanical properties.

It is reported that reinforcement of nanoclay to fiber reinforced epoxy nanocomposites shows substantial improvements in static mechanical properties (tensile properties, flexural properties, microhardness etc.) along with only marginal improvements in impact strength. So, the impact

behaviour of such nanocomposites is still an area of concern [1,15,16,33,39,66]. To further improve the properties, especially the impact behaviour, one of the ways can be to incorporate second phase fillers (polymer/elastomer filler) into the epoxy resin [1,32,34].

In the light of aforesaid, it was proposed to modify epoxy based GFRP nanocomposites (epoxy/nanoclay/glass fiber nanocomposite systems) through addition of thermoplastic fibers (polymeric fillers) as an additional filler for enhanced impact strength. However, the key to improved properties of multi-constituent reinforced epoxy nanocomposites lies in good compatibility among various constituents of the composite system. For improving the compatibility of polymeric filler with other constituents of the composite system, different compatibilization techniques viz. chemical treatment, silanization, UV-assisted MAH grafting, or combination of these treatments were used in the present research for surface treatment of polymer fillers. Polymer fillers used in the present work include ultra high molecular weight polyethylene (UHMWPE), para-aramid (Kevlar), and Inviya (Spandex) fibers. These polymers vary greatly in their elasticity, ductility, and rigidity. It was envisaged that effective compatibilization of polymeric fillers and their subsequent reinforcement will result in enhanced interfacial interaction/bonding among constituents of the composite system leading to significant improvements in impact strength without any appreciable loss in tensile properties.

Ultra high molecular weight polyethylene (UHMWPE) fibers are high performance fibers because of low density, good mechanical properties in ambient/cryogenic temperature conditions (high toughness, high tensile modulus and strength), good resistance to chemicals and wear, low cost, and light-weight. Inviya fibers are segmented polymers having more than 85% segmented polyurethane. Inviya fibers have higher stretch and elastic recovery due to alternative flexible and rigid structures. These fibers are also known as elastane due to their exceptional ability to stretch (five times their original length). Para-aramid fibers are high-performance fibers having high specific toughness ratio, high strength and modulus, low density, high chemical resistance, and excellent thermal stability.

It was a tremendous processing challenge to compatibilize the various constituents and processes these highly viscous multi-scale reinforced composite systems with minimal defects.

1.9 Outline of the thesis

This research work investigated the effect of reinforcing pristine/compatibilized nano-filler (nanoclay) and pristine/compatibilized micro-filler (thermoplastic fibers) on the mechanical performance of epoxy based GFRPs. Epoxy based GFRPs containing 2 phr nanoclay (fixed concentration; 'phr' means per hundred resin) and thermoplastic fibers (varying concentration) were processed using hand lay-up assisted vacuum assisted resin infusion moulding (VARIM) technique. For improving the compatibility among constituents of composite system, nanoclay and thermoplastic fibers were subjected to compatibilization (surface modification). Silanization method was used for surface modification of nanoclay. For compatibilization of thermoplastic fibers, different surface modification methods viz. chemical treatment, silanization, UV-assisted MAH grafting, and combination of any of these two surface modification methods were used.

There are eight chapters in this thesis. The outline of the chapters is as follows:

- **Chapter 1.** This chapter presents an overview of some basic terms/topics used in the present research work viz. polymer nanocomposites, nanoclay reinforced polymer nanocomposites, morphologies of nanoclay in polymer nanocomposites, glass fiber reinforced epoxy nanocomposites (epoxy based GFRPs) and their applications in different sectors. The importance of compatibilization/surface modification of various fillers and its effect on interfacial interaction of various constituents of multi-scale reinforced nanocomposites is also discussed. The latter part of the chapter presents the need for improving the impact strength of epoxy based GFRPs, and thus, presents origin of the present research work.
- **Chapter 2.** This chapter presents a comprehensive review of literature on processing methods and resulting mechanical properties of (a) nanoclay reinforced polymer composites, (b) UHMWPE fiber reinforced polymer composites, (c) para-aramid fiber reinforced polymer composites, (d) spandex fiber reinforced polymer composites, and (e) multi-scale reinforced polymer composites. The chapter also presents a summary of the reviewed literature and highlights the major gaps in existing literature.
- **Chapter 3.** This chapter presents design of the present research work. Research objectives are formulated in the light of literature gaps. The details of various constituent materials, processing methodology, equipment used for processing/mechanical testing/characterization of epoxy based GFRP nanocomposites are included. The details of procedure used for surface modification of nanoclay and thermoplastic fibers are also presented in this chapter.

- **Chapter 4.** This chapter presents the details of surface modification procedure followed to determine the silane concentration of 3-aminopropyltriethoxy silane agent for silanization of nanoclay. Silane concentration was varied in the range of 1X−4X, where X was the wt.% of nanoclay. In the present research, nanoclay loading was fixed at 2 phr. Impact strength and tensile properties of epoxy based GFRPs (with all constituents except for thermoplastic fibers) containing 2 phr clay treated with various silane concentrations was evaluated. Silane concentration which provided best combination of impact strength and tensile properties for nanocomposites was selected for processing of epoxy based GFRPs. The chapter also describes the effect of acetone washing and no washing after silanization of nanoclay on the properties of composites. FTIR analysis for validation of silanization, XRD/TEM analysis for ascertaining the nanoclay morphology, and SEM analysis for determining the mechanisms causing improvements in mechanical properties are also described in this chapter.
- **Chapter 5.** This chapter presents the effect of reinforcing different concentrations of UHMWPE fibers, both pristine as well as surface treated fibers (0.125–0.500 phr; with an increment of 0.125 phr) on the impact strength/tensile properties of epoxy based GFRPs containing 2 phr of silanized nanoclay. For the pristine UHMWPE fibers, 0.250 phr reinforced GFRPs showed the best mechanical performance. This concentration (0.250 phr) was selected for reinforcing surface modified UHMWPE fibers. Four different compatibilization techniques viz. (i) potassium permanganate treatment, (ii) silanization with 3-aminopropyltriethoxy silane agent, (iii) combination of potassium permanganate treatment and silanization, and (iv) UV-assisted MAH grafting were used. The chapter further presents the results of mechanical testing of epoxy based GFRPs containing 0.250 phr of UHMWPE fibers treated with various compatibilization techniques. Finally, the characterization procedures (FTIR and SEM-EDS analysis) to confirm surface modification of fibers and fracture surface of GFRP nanocomposites (SEM micrographs) fractured under impact testing are also discussed.
- **Chapter 6.** This chapter presents the effect of reinforcing different concentrations of para-aramid fibers, both pristine as well as surface treated fibers (0.50–2.00 phr; with an increment of 0.50 phr) on the impact strength/tensile properties of epoxy based GFRPs containing 2 phr of silanized nanoclay. For pristine para-aramid fibers, 1.00 phr reinforced GFRPs showed the best mechanical performance. This concentration (1.00 phr) was selected for reinforcing surface modified para-aramid fibers. Four different compatibilization techniques viz. (i)

phosphoric acid treatment, (ii) silanization with 3-aminopropyltriethoxy silane agent, (iii) combination of phosphoric acid treatment and silanization, and (iv) UV-assisted MAH grafting were used. The chapter further presents the results of mechanical testing of epoxy based GFRPs containing 1.0 phr of para-aramid fibers treated with various compatibilization techniques. Finally, the characterization procedures (FTIR and SEM-EDS analysis) to confirm surface modification of fibers and fracture surface of GFRP nanocomposites (SEM micrographs) fractured under impact testing are also discussed.

- **Chapter 7.** This chapter presents the effect of reinforcing different concentrations of Inviya fibers, both pristine as well as surface treated fibers (0.50–2.00 phr; with an increment of 0.50 phr) on the impact strength/tensile properties of epoxy based GFRPs containing 2 phr of silanized nanoclay. For pristine Inviya fibers, 1.50 phr reinforced GFRPs showed the best mechanical performance. This concentration (1.50 phr) was selected for reinforcing surface modified Inviya fibers. Four different compatibilization techniques viz. (i) phosphoric acid treatment, (ii) silanization with 3-aminopropyltriethoxy silane agent, (iii) combination of phosphoric acid treatment and silanization, and (iv) UV-assisted MAH grafting were used. The chapter further presents the results of mechanical testing of epoxy based GFRPs containing 1.5 phr of Inviya fibers treated with various compatibilization techniques. Finally, the characterization procedures (FTIR and SEM-EDS analysis) to confirm surface modification of fibers and fracture surface of GFRP nanocomposites (SEM micrographs) fractured under impact testing are also discussed.
- **Chapter 8:** This chapter covers the summary of results and major findings from the present research work. The major conclusions from the research are discussed. Finally, the chapter presents the future scope in this area of research.

As per the outline, the next chapter presents a comprehensive literature review on processing procedures, compatibilization methods and their effect on mechanical properties of polymer composites reinforced with nanoclay and/or thermoplastic fillers.

Chapter 2. Literature review

2.1 Overview

This chapter presents a comprehensive literature review on polymer matrix composites reinforced with one or more of the following constituents viz. nanoclay, glass fibers, UHMWPE fibers, para-aramid fibers, and spandex fibers. The chapter also presents literature on multi-scale constituent reinforced polymer composites. It discusses the influence of processing conditions, compatibilization procedures, and fabrication techniques on the mechanical performance of polymer composites. The literature review is broadly classified into five sections viz. (i) nanoclay reinforced polymer composites, (ii) UHMWPE fiber reinforced polymer composites, (iii) para-aramid fiber reinforced polymer composites, (iv) spandex fiber reinforced polymer composites, and (v) multi-scale filler reinforced polymer composites. The chapter finally summarizes the reviewed literature and discusses the major gaps in the existing literature.

2.2 Nanoclay reinforced polymer composites

Thongchom *et al.* (2022) [67] explored the influence of reinforcing nanoclay, graphene, and basalt fibers on the performance of polypropylene (PP) based nanocomposites. Different loadings of nanoclay (3.00 and 6.00 wt.%), graphene (0.75 and 1.5 wt.%), and basalt fibers (10.00 and 20.00 wt.%) were used. Hot compression moulding technique was used for processing of nanocomposites. Addition of 20.00 wt.% basalt fibers improved the tensile strength, tensile modulus, and impact performance (Charpy test) by 32%, 64%, and 18%, respectively over pristine PP matrix material. Addition of 0.75 wt.% graphene improved the tensile strength and impact performance (Charpy test) by 15% and 20% respectively (over pristine PP). Addition of nanoclay improved the tensile modulus (maximum increase of 59% at 6 wt.%). Maximum tensile strength (17% improvement) was observed at 3 wt.% nanoclay reinforcement. At low loading, the nano-fillers (nanoclay, graphene, and basalt fibers) dispersed uniformly resulting in good adhesion between nano-filler and matrix. However, at higher nano-filler loading, agglomerates formed which deteriorated the properties.

Merzah *et al.* (2022) [68] observed the effect of reinforcing pristine/sulphuric acid treated nanoclay (1–3 wt.%; increment of 1 wt.%.) on the properties of epoxy composites. Addition of 2.0 wt.% of pristine nanoclay improved the tensile strength and modulus by 111% and 41% respectively. Addition of sulphuric acid treated nanoclay further improved the tensile properties

(maximum improvement of 140% in tensile strength at 2 wt.% loading; maximum improvement of 75% in tensile modulus at 3.0 wt.%). The acid treated nanoclay dispersed more uniformly as compared to pristine nanoclay, due to which better mechanical performance was shown by acid treated nanoclay reinforced epoxy nanocomposites.

Chee et al., (2021) [69] explored the influence of reinforcing different types of nanoclay (unmodified and modified nanoclay, and halloysite nanotubes) on the mechanical performance of bamboo and kenaf fiber reinforced epoxy nanocomposites. Fixed nanoclay loading (1.0 wt.%) was used in the work. Hand-layup method was used for processing of nanocomposites. The bamboo and kenaf fiber reinforced epoxy nanocomposites reinforced with modified nanoclay showed best mechanical performance among all fabricated nanocomposites. Tensile strength, flexural strength, and impact strength of is nanocomposite showed improvement of 44%, 67%, and 53% respectively over nanocomposite without nanoclay. Nanoclay owing to higher aspect ratio than halloysite nanotubes had more bonding sites between epoxy-nanoclay and fibers. Also modified nanoclay uniformly dispersed (due to organic modification) in epoxy resin and resulted in stronger interfacial bonding between epoxy-nanoclay and fibers.

Sivaperumal and Jancirani (2021) [70] explored the influence of reinforcing nanoclay (0.5–2.5 wt.; with an increment of 0.5 wt.%.) on the mechanical performance of Ramie fiber (40.0 wt.%) reinforced epoxy nanocomposites. Addition of nanoclay improved mechanical properties till 1.5 wt.%, beyond this decreasing trend was observed owing to formation of agglomerates. Ramie fiber reinforced epoxy nanocomposite reinforced with 1.5 wt.% nanoclay showed 48%, 34%, and 84% improvement in tensile strength, flexural strength, and impact strength respectively, as compared to Ramie fiber reinforced epoxy composite (without nanoclay). The improvement was witnessed due to micro fibril mechanism of Ramie fiber. Also, absence of fiber pullout confirmed good interfacial bonding among constituents of the nanocomposite systems.

Nayak *et al.* (2020) [71] evaluated the influence of reinforcing nano-silica particles (1.0 wt.%) and nanoclay platelets (2.0 wt.%) on the flexural properties and glass transition temperature of epoxy based GFRPs. Manual hand lay-up technique was used for processing of GFRPs. Flexural strength improved by 11% over the reference sample (epoxy based GFRP without any nano-reinforcement) owing to improved bonding between constituents on the addition of nano-reinforcements. Flexural modulus didn't change with nano-silica and nanoclay reinforcement. Glass transition temperature decreased from 101℃ to 91℃.

Shettar *et al.* (2020) [72] examined the influence of reinforcing nanoclay on tensile/flexural properties of epoxy based GFRPs. Glass fiber concentration was varied from 40–60 wt.% (increment of 10 wt.%). Nanoclay concentration was varied as 2.0 wt.% and 4.0 wt.%. Manual compressing was used for processing of GFRPs. Reinforcement of 60 wt.% of glass fibers to pristine epoxy showed improvement of 15% and 10% in tensile strength and modulus respectively with respect to reference sample (containing 40 wt.% glass fibers and no clay). Epoxy composite reinforced with 60 wt.% glass fibers and 4 wt.% nanoclay showed the highest improvement of 28% and 29% in tensile strength and modulus respectively over the reference sample. Similar trends were also observed in flexural properties. Flexural strength and modulus improved by 15% and 43%, respectively over the reference sample.

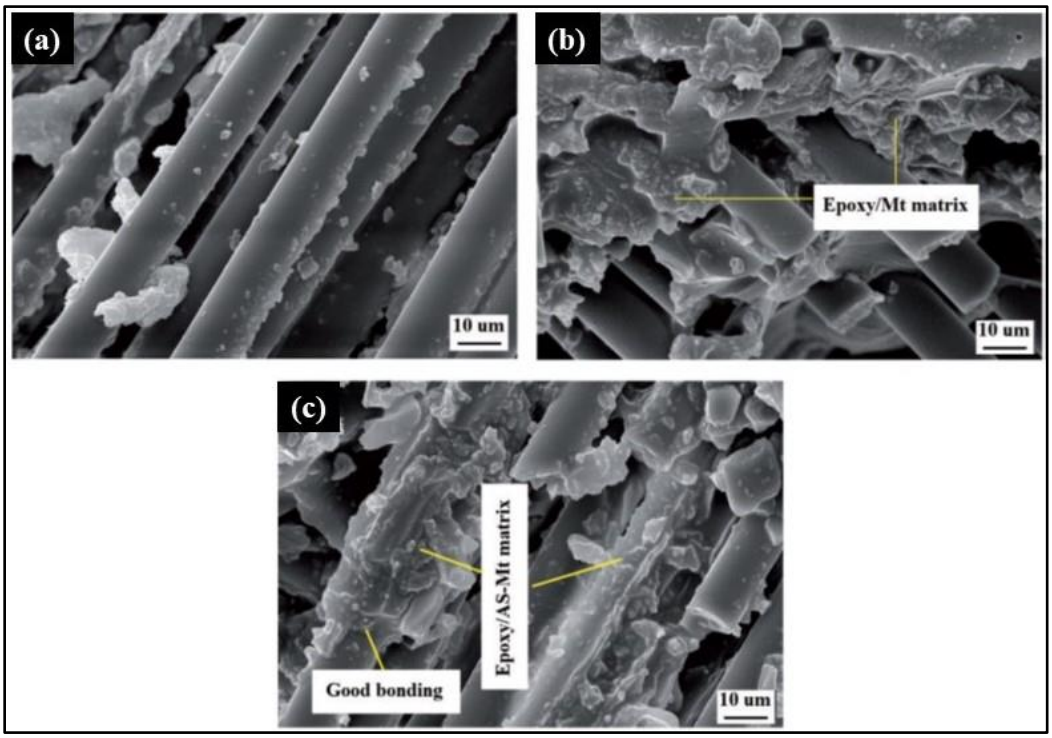

Figure 2.1. SEM micrographs of fractured surface after tensile testing (a) GFRP having no nanoclay, (b) GFRP having 2 phr pristine nanoclay, and (c) GFRP having 2 phr silanized nanoclay [73].

Feiz and Khosravi (2019) [73] examined the influence of silanized nanoclay (1–7 wt.%; increment of 2 wt.%) on the performance of epoxy based GFRPs. Hand lay-up technique followed by cold pressing was used. All properties improved till 5 wt.% silanized nanoclay loading. Maximum improvement in tensile, flexural, and compressive strengths was 18%, 38%, and 53% respectively (compared to GFRP epoxy composite without nanoclay). GFRP having no nanoclay showed a smooth surface (Figure 2.1a). The roughness of GFRP surface increased with addition

of nanoclay, however, silanized nanoclay showed the roughest surface (Figure 2.1b). Silanized nanoclay acted as an interlocking agent between epoxy and glass fibers, thereby improving the interfacial bonding between them.

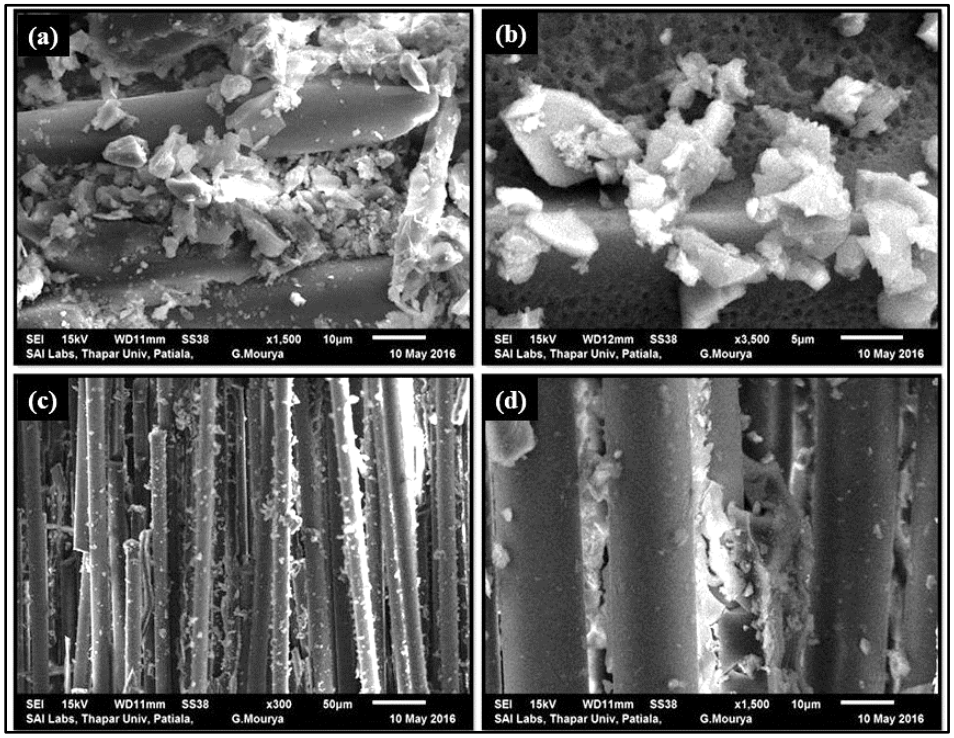

Figure 2.2. SEM micrographs of surface after fracture toughness of GFRP having 2 phr nanoclay loading (a–b) Nanomer PGV, and (c–d) Nanomer I.28E [15].

Shelly *et al.* (2018) [15] examined the influence of reinforcing nanoclay (Nanomer PGV and Nanomer I.28E used separately; 0–4 phr with increment of 0.5 phr) on performance of glass fiber VARIM technique (vacuum assisted resin infusion moulding) was used for fabricating nanocomposites. GFRPs reinforced with Nanomer PGV showed a slight improvement in tensile properties, whereas GFRPs reinforced with Nanomer I.28E didn't show any significant improvement in tensile properties. The impact strength of GFRPs reinforced with Nanomer PGV, and Nanomer I.28E improved by 22 % and 15 %, respectively, as compared to GFRP (having no nanoclay). The fracture toughness of GFRPs reinforced with Nanomer PGV and Nanomer I.28E was improved by 73 % and 57 %, respectively, as compared to GFRP (having no nanoclay). The random dispersion of nanoclay made the path of crack more torturous and thus inhibited crack propagation (Figure 2.2 b−c). It was revealed that epoxy-nanoclay strongly adhered to glass fibers (Figure 2.2a and 2.2d). Consequently, GFRPs reinforced with nanoclay showed better mechanical performance.

Withers *et al.* (2015) [66] examined the influence of reinforcing nanoclay (2.0 and 4.0 wt.%.) on the tensile properties of epoxy based GFRPs. Tensile strength and modulus were maximum for GFRP containing 2 wt.% nanoclay. GFRPs without nanoclay showed a more brittle-like matrix behavior that was more susceptible to failure (Figure 2.3a). The fractured surface of epoxy based GFRP composite containing 2 wt.% nanoclay showed toughened and more ductile epoxy matrix (Figure 2.3b), which supported the improved tensile properties.

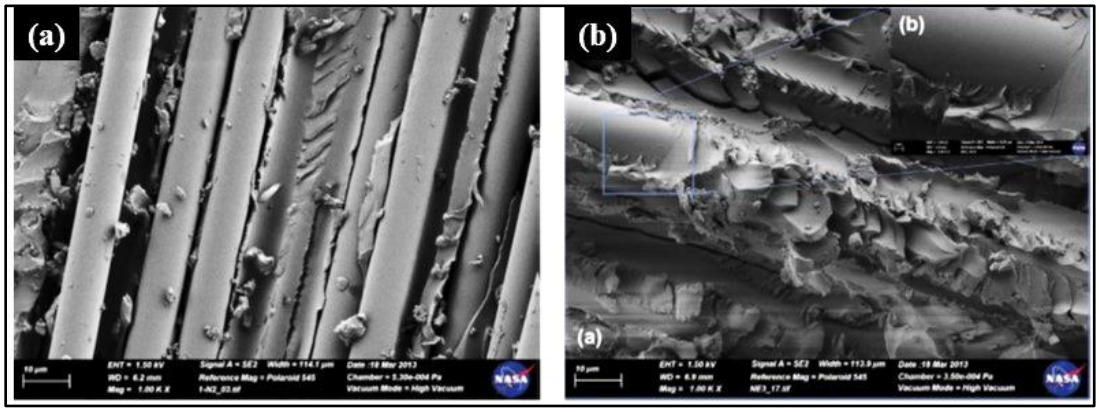

Figure 2.3. SEM micrographs of fractured surface after tensile testing (a) GFRP having no clay, and (b) GFRP having 2 phr nanoclay [66].

Rafiq *et al.* (2018) [39] observed the influence of reinforcing nanoclay (1.5 wt.% and 3.0 wt.%) on the flexural strength and fracture toughness of epoxy based GFRP nanocomposites. Epoxy based GFRPs reinforced with 1.5 wt.% nanoclay showed the best mechanical performance (15% and 77% improvement in flexural and fracture strength respectively, over GFRP without nanoclay). Mechanical performance improved owing to good dispersion of nanoclay in epoxy resin. Crack arrest and crack deflection mechanisms also helped in boosting the performance.

Kumar *et al.* (2010) [74] examined the influence of reinforcing nanoclay on the tensile and flexural properties of epoxy based GFRPs. Nanoclay loading was varied as 2, 3, 5, and 12 wt.%. Tensile properties and flexural properties showed maximum improvement at 5 wt.% loading with enhancement of 133%, 58%, 56.8%, and 103.6 % in tensile strength, tensile modulus, flexural strength, and flexural modulus respectively over the neat epoxy sample. Uniform dispersion of clay helped in improving the bonding between epoxy and glass fibers. At 12 wt.% nanoclay loading properties deteriorated due to poor dispersion of nanoclay and air entrapment in the fabricated GFRPs.

Table 2.1. Summary of literature on nanoclay reinforced epoxy nanocomposites.

S.No.	Composition	Effect on mechanical properties and underlying mechanisms/reasons for change in properties	References
1.	**Matrix**: Epoxy **Reinforcement**: Nanoclay	Authors explored the effect of nanoclay addition on properties of epoxy composites. Tensile strength, tensile modulus, flexural strength, flexural modulus, impact strength, and fracture toughness improved till an optimum loading. Improvement in modulus was observed due to high stiffening effect of nanoclay. Strength improved due to uniform dispersion of clay which deflected/restricted the crack advancement, thus resulting in improved performance. Beyond the optimum nanoclay loading, properties deteriorated due to formation of agglomerates, increased viscosity, and void formation. Voids and clay agglomerates acted as stress concentration sites. Thus, pre-mature failure of epoxy nanocomposites occurred.	Isik *et al.* 2003 [40]; Zunjarrao *et al.* 2006 [75]; Qi *et al.* 2006 [76]; Wang *et al.* 2006 [77]; Kim *et al.* 2008 [78]; Lim *et al.* 2011 [42]; Alamri *et al.* 2012 [79]; Bakar *et al.* 2012 [80]; Shokrieh *et al.* 2012 [81]; Kusmono *et al.* 2013 [41]; Rafiq *et al.* 2014 [39]; Alsagayar *et al.* 2015 [82]; Nguyen *et al.* 2021 [83]
2.	**Matrix**: Epoxy **Reinforcements**: Nanoclay, Carbon fibers/ Glass fibers	Authors investigated the influence of nanoclay addition on the performance of epoxy/carbon fiber nanocomposites. Nanoclay reinforcement to carbon fiber reinforced epoxy nanocomposites improved the tensile and flexural properties, impact strength, fracture toughness, and interlaminar shear strength. at a low nanoclay loading (generally less than 5 wt.%). Improvement in properties was witnessed due to mechanisms like micro-cracks and voids, crack tip bifurcation, crack pinning, and crack deflection. Curing at higher temperatures also enhanced the properties owing to complete cross linking of polymer nanocomposites. Damping characteristics and loss modulus also improved. At higher nanoclay loadings, aggregates were formed. These flaws/unwanted agglomerates initiated cracks and resulted in failure of materials at lower stress/strain. Some authors reported use of silanized nanoclay which further enhanced the properties due to formation of chemical bond between epoxy/clay/fibers. Breakage of fibers was the dominating mechanism observed in such cases. Fiber pull-out from epoxy matrix was not generally observed after reinforcement of nanoclay.	Timmerman *et al.* 2002 [84]; Haque *et al.* 2003 [37]; Kornmann *et al.* 2005 [38]; Siddiqui *et al.* 2007 [85]; Xu *et al.* 2008 [86]; Karippal *et al.* 2011 [87]; Khan *et al.* 2011 [88]; Phonthammachai *et al.* 2011 [89]; Kanny *et al.* 2014 [90]; Islam *et al.* 2015 [91]; Sharma *et al.* 2016 [92]; Jeyakumar *et al.* 2017 [93]; Annappa *et al.* 2021 [94]; Tay *et al.* 2021 [95]

Bozkurt *et al.* (2007) [36] investigated the effect of reinforcing montmorillonite clay (MMT) and organically modified montmorillonite clay (OMMT) on the performance of epoxy based GFRPs. Clay loadings were 1, 3, 6, and 10 wt.%. Tensile modulus remained almost constant by addition of MMT and OMMT till 6 wt.% of clay over neat epoxy. Tensile strength was slightly higher for MMT/epoxy composite as compared to OMMT/epoxy composites (for all clay loadings). Maximum improvement in flexural strength (16%) and modulus (13%) was obtained at 6 wt.% clay (OMMT) content. The presence of clay layers at fiber-matrix interface helped in boosting

the interfacial bonding between epoxy and glass fiber till an optimum loading. However, at 10 wt.% nanoclay reinforced GFRPs showed deterioration in properties due to agglomeration of clay particles. These agglomerates acted as stress concentration sites, resulting in pre-mature failure.
A summary of additional literature available on nanoclay reinforced epoxy nanocomposites is presented in Table 2.1.

2.3 UHMWPE fiber reinforced polymer composites

Steinke and Sodano (2022) [96] examined the effect of aramid nanofiber grafting on the interfacial shear strength (IFSS) of UHMWPE fibers. Dip coating process was used for grafting aramid nanofibers on the surface of UHMWPE fibers. Different time periods used for dip coating were 1, 3, 5, and 7 min. Average surface roughness (R_a) of UHMWPE fibers increased with an increase in coating time period. R_a increased from 11 nm (for pristine fibers) to 36 nm for surface modified UHMWPE fibers (dipped in aramid nanofiber coating for 7 min). Maximum improvement of 173% (over pristine fibers) was observed in IFSS of UHMWPE fibers treated for 3 min in aramid nanofiber coating. Aramid nanofiber coating made the UHMWPE fiber surface rougher and formed polar functional groups like amide, hydroxyl, carboxyl, and ketone, thus, strengthening the bonding between fibers and epoxy. Hence, higher IFSS was showed by modified UHMWPE fibers. Treatment for longer periods (> 3 min) resulted in non-uniform and porous coating. Larger time periods also caused formation of aramid agglomerates.

Steinke and Sodano (2022) [97] observed the influence of zinc oxide nanowire (ZnNW) grafting on the IFSS of UHMWPE fibers. UHMWPE fiber surface was modified with oxygen plasma treatment followed by ZnNW grafting. Dip coating was used for grafting ZnNW on UHMWPE fiber surface. Time periods used for oxygen plasma treatment were 15 s, 30 s, 60 s, and 90 s. IFSS of pristine UHMWPE fiber was 3.13 MPa. UHMWPE fibers treated with oxygen plasma treatment (for 30 s) followed by ZnNW grafting showed maximum improvement of 135% in IFSS (7.35 MPa) over pristine fibers. With 90 s time period, IFSS had improved to a value of 4.75 MPa. The possible mechanisms for improved IFSS were (i) uniform grafting of ZnNW on the surface of UHMWPE fibers, (ii) increased surface area of UHMWPE fibers after grafting, (iii) improved mechanical interlocking after surface modification.

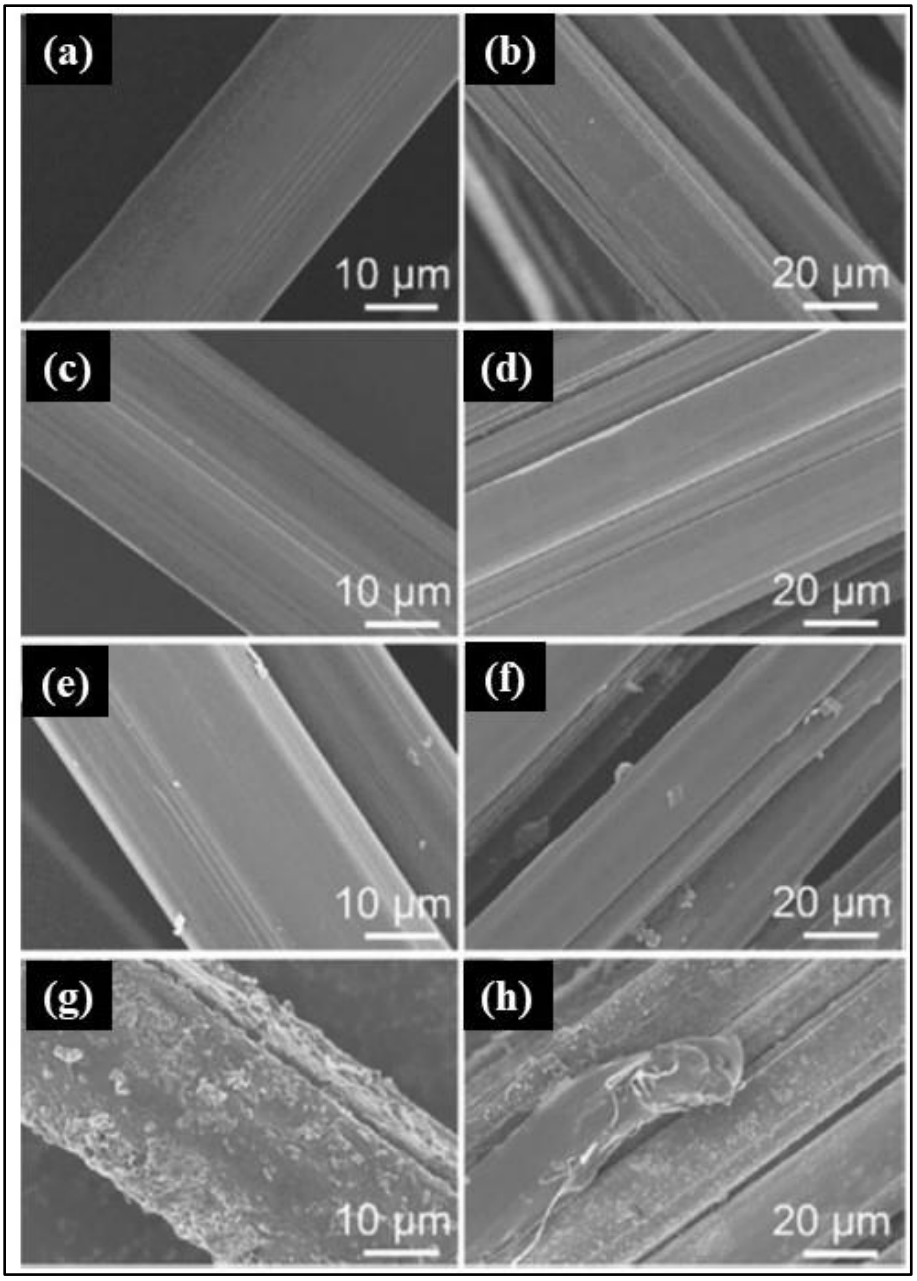

Figure 2.4. SEM micrographs of pristine/compatibilized UHMWPE fibers (a–b) pristine, (c–d) plasma treated, (e–f) PANI grafted, and (g–h) plasma treatment followed by PANI grafting [98].

Zhang *et al.* (2022) [98] investigated the influence of different surface treatments on the H pull-out force of UHMWPE fibers. UHMWPE fibers were subjected to three different surface modification techniques viz. (a) plasma treatment, (b) polyaniline (PANI) grafting, and (c) plasma treatment followed by PANI grafting. H pull-out force of UHMWPE fibers improved after each surface modification technique. Maximum H pull-out force was observed in case of the third technique (i.e. plasma treatment followed by PANI grafting) with 68% improvement in H pull-out

force compared to pristine fibers. The surface of UHMWPE fibers became rough after surface modification (Figure 2.4). Plasma treatment followed by PANI grafted UHMWPE fibers showed the roughest surface (Figure 2.4g–h). Plasma treatment increased the functional groups on fibers' surface whereas PANI grafting on plasma treated surface made it rougher, hence interfacial bond strength increased owing to mechanical interlocking.

Li *et al.* (2019) [99] examined the influence of reinforcing compatibilized UHMWPE fibers on the performance of epoxy composites. Compatibilization of UHMWPE fibers was done using chromic acid solution. UHMWPE fibers were used in a fixed loading of 0.3 wt.%. Impact strength improved both with addition of pristine UHMWPE fibers (88.7 to 90.8 kJ/m^2) and compatibilized UHMWPE fibers (88.7 to 92.6 kJ/m^2) as compared to pristine epoxy. Addition of pristine UHMWPE fibers deteriorated the tensile strength of composites. Addition of compatibilized fibers improved the tensile strength by 7.5%. Surface treatment made the surface of fibers rougher and increased the oxygen contacting group.

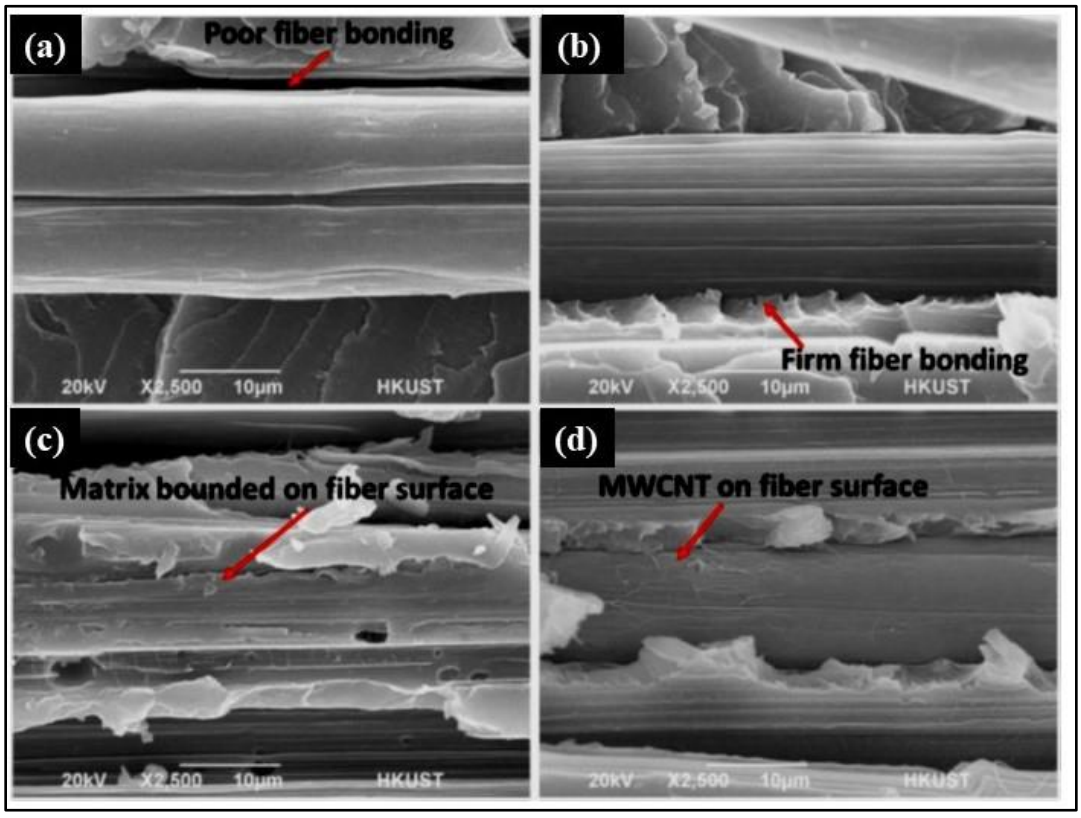

Figure 2.5. SEM micrographs of ELIUM nanocomposites showing (a) pristine UHMWPE fibers reinforced ELIUM composites, (b) dopamine modified UHMWPE fibers reinforced ELIUM composites, (c) 0.03 wt.% MWCNTs and dopamine modified UHMWPE fibers reinforced ELIUM nanocomposites, and (d) 0.10 wt.% MWCNTs and dopamine modified UHMWPE fibers reinforced ELIUM nanocomposites [100].

Shanmugam *et al.* (2019) [100] investigated the influence of reinforcing dopamine modified multi-walled carbon nanotubes (MWCNT) on the mechanical properties of UHMWPE fibers/ELIUM composites. MWCNTs loading was 0.01, 0.03, 0.05, and 0.10 wt.%. Dip coating was used for dopamine treatment of MWCNTs. UHMWPE fibers/ELIUM composites reinforced with 0.03 wt.% of dopamine modified MWCNTs showed 42.5% improvement in TFBT (transverse fiber bundle test) bonding strength over pristine UHMWPE fibers reinforced ELIUM composites. The fracture surface of test specimen after TFBT bonding strength test showed that poor bonding between pristine fiber and ELIUM matrix (Figure 2.5a). Interfacial bonding between matrix and compatibilized UHMWPE fibers improved after surface modification (Figure 2.5). Nanocomposite reinforced with 0.03 wt.% MWCNTs and dopamine modified UHMWPE fibers showed the best interfacial bonding (Figure 2.5c). MWCNTs impeded crack propagation in the interface owing to bridging effect. Surface modification of UHMWPE fibers with dopamine modified MWCNTs made the surface rougher and resulted in mechanical interlocking between epoxy and UHMWPE fibers.

He *et al.* (2018) [101] observed the influence of reinforcing plasma treated UHMWPE fibers on the performance of high-density polyethylene (HDPE) composites. UHMWPE fibers were mixed with HDPE resin using a twin screw extruder. Surface of UHMWPE fibers was modified with oxygen plasma treatment for 5 min at three different powers: (i) 200 W, (ii) 300 W, and (iii) 400 W. Different concentrations of UHMWPE fibers used for fabricating composites were 5, 10, 15, and 20 wt.%. Tensile modulus continuously increased with increase in UHMWPE fiber content till 20 wt.%. Composites reinforced with 20 wt.% of treated UHMWPE fibers (300 W, 5 min) exhibited 175% increase in tensile modulus (compared to pristine HDPE). Impact strength increased with an increase in UHMWPE fiber loading till 15 wt.% (136% increase; 300 W, 5 min); beyond this, impact strength decreased. Plasma treatment increased the surface roughness and added functional groups on the surface of UHMWPE fibers; hence, oxygen concentration increased which improved the chemical bonding between UHMWPE fibers and HDPE.

Meng *et al.* (2018) [102] explored the influence of reinforcing surface modified UHMWPE fibers (treated with chromic acid solution) on the performance of UHMWPE fiber reinforced polyurethane composites. Flexural strength improved by 9% with addition of pristine UHMWPE fibers (0.3 wt.%) to the polyurethane matrix. Further, improvement (18% as compared to pristine polyurethane) occurred with addition of chromic acid treated UHMWPE fibers. Similarly, addition

of pristine UHMWPE fibers (0.3 wt.%) improved the impact strength of composites to 26.1 kJ/m^2 from 1.9 kJ/m^2 for pristine polyurethane. Addition of surface treated fibers further improved the impact strength to 33.1 kJ/m^2. Chemical cross-linking between treated UHMWPE fibers and polyurethane matrix improved the interfacial adhesion between the two.

Mohammadalipour and Masoomi (2018) [103] studied the effect of reinforcing nanoclay and compatibilized UHMWPE fibers on the performance of epoxy nanocomposites. Nanoclay concentration was varied as 1, 3, and 5 wt.% and fibers were used in fixed concentration of 2.5 wt.%. Performance improved with addition of nanoclay till 1 wt.%. Tensile strength, tensile modulus, and toughness of nanocomposite containing 1.0 wt.% nanoclay and 2.5 wt.% treated UHMWPE fibers improved by 48%, 27%, and 30% respectively (over pristine epoxy).

Li *et al.* (2018) [104] observed the influence of reinforcing potassium permanganate treated UHMWPE fibers (fixed loading of 0.3 wt.%) on the performance of epoxy composites. Impact strength and interlaminar shear strength (ILSS) of treated UHMWPE/epoxy composites showed improvement of 11% and 28% respectively over the neat epoxy. Properties improved due to formation of rougher surface of UHMWPE fibers after treatment resulting in better interfacial adhesion between fibers and matrix. Surface roughness of fibers was examined using atomic force microscopy and SEM microscopy.

Tang *et al.* (2017) [105] examined the effect of adding NaOH treated UHMWPE fibers (5–30 wt.%; increment of 5 wt.%.) and silica particles (20 wt.%) on the performance of poly(methyl methacrylate) (PMMA) composites. Tensile strength/flexural strength improved with increase in pristine UHMWPE fiber content till 20 wt.%; beyond this, the properties deteriorated. Further, composites reinforced with 20 wt.% treated UHMWPE fibers and 20 wt.% silica particles exhibited 87.5% and 97% increase in tensile strength and flexural strength respectively over pristine PMMA. Surface modification enhanced the average surface roughness of UHMWPE from 200 nm (pristine fibers) to 879 nm (surface treated for 15 min). XPS analysis confirmed that oxygen-containing groups increased on the treated UHMWPE fiber surface. This had the most decisive impact to strengthen the bond between UHMWPE fibers and epoxy.

Li *et al.* (2017) [106] explored the effect of reinforcing surface treated UHMWPE fibers (0.1–0.5 wt.%; increment of 0.1 wt.%.) on the performance of epoxy composites. Addition of both, treated as well as untreated fibers to the pristine epoxy resulted in reduced tensile strength due to random dispersion of fibers. This caused stress concentration leading to premature failure of composites.

ILSS increased with increase in UHMWPE fiber loading till 0.3 wt.%. ILSS of 0.3 wt.% surface treated UHMWPE fibers/epoxy composites was 129.40 MPa, an improvement of 7% and 27% as compared to pristine epoxy and pristine UHMWPE fiber reinforced epoxy composites respectively. Pristine UHMWPE fiber reinforced epoxy composites showed crack propagation through the epoxy matrix and also de-bonding of fibers at the interface. SEM micrographs revealed that treated UHMWPE fiber/epoxy composites exhibited a closely packed fiber-matrix interfacial bonding.

Tang *et al.* (2017) [107] investigated the effect of reinforcing alkali treated UHMWPE fibers on the ILSS of polyimide (PI) composites. For alkali treatment, 20 wt.% of NaOH solution was used (treatment time: 5, 10, and 15 min). Tensile strength, tensile modulus, and ILSS of PI composites reinforced with treated UHMWPE fibers for 5 min improved by 14%, 17%, and 6% respectively (compared to pristine UHMWPE fiber reinforced PI composites). Increase in treatment time (10 min and 15 min) deteriorated the tensile properties and ILSS due to formation of conglomerate and non-uniform dispersion of fibers, reducing the integrity of composite.

Jin *et al.* (2016) [108] examined the influence of compatibilized UHMWPE woven fabric on the performance of epoxy composites. Plasma treatment and pyrrole treatment were utilized for surface treatment. Vacuum assisted resin transfer moulding was used for processing of composites. Combination of plasma treatment followed by pyrrole grafting showed the best mechanical performance which had increased the average roughness of fibers from 0.095 μm to 0.371 μm. IFSS, compressive strength, and bending strength of epoxy composites reinforced with modified UHMWPE fibers (combination treatment) improved by 848%, 54%, and 44% respectively (compared to composite reinforced with pristine UHMWPE fibers). The results showed that hydrogen-bonding interaction between plasma treated UHMWPE and pyrrole improved the fiber-matrix-fiber load transfer process. Thus, mechanical performance of composite enhanced.

Li *et al.* (2016) [109] observed the influence of reinforcing surface modified (chromic acid treated) UHMWPE fibers on the tensile strength, modulus, elongation at break of UHMWPE fibers. Dip coating was used for surface modification. Modified UHMWPE fibers showed degradation in tensile strength and elongation at the break by 6.87 % and 8.29 % respectively as compared to pristine fibers. However, tensile modulus enhanced by 21.66%. Chromic acid effectively modified the surface of UHMWPE fibers. The surface of fibers became rough with and long grooves (Figure 2.6). Treated UHMWPE fibers caused chain scission of macromolecules resulting in lower

molecular weight and strength. Consequently, the flexibility decreased. The existence of oxygen on the surface started cross-linking. Thus, chain movement was constrained and resulted in decreased elongation at break after surface modification.

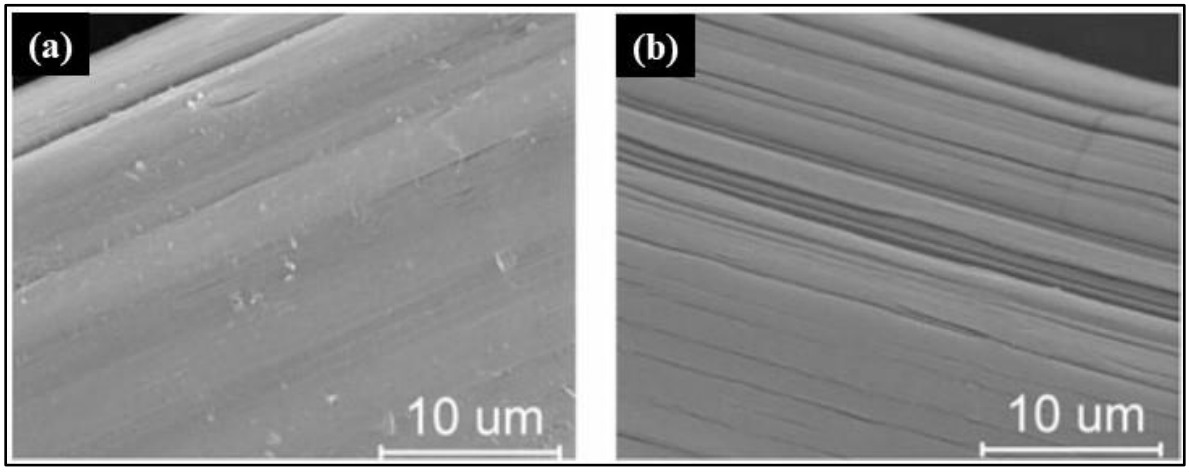

Figure 2.6. SEM micrographs of UHMWPE fibers (a) pristine, and (b) chromic acid treated [109].

Ahmadi *et al.* (2015) [110] investigated the effect of addition of carbon nano-fibers (0.5, 1.0, 1.5, and 3 wt.%) on the performance of epoxy/UHMWPE composites. UHMWPE fibers were used in a fixed loading of 2.2 wt.%. UHMWPE fiber surface was modified using glycidyl methacrylate (GMA). Nanocomposite reinforced with 1.0 wt.% carbon nano-fibers and 2.2 wt.% GMA treated UHMWPE fibers showed 119% and 98% improvement in tensile and flexural strength respectively (over pristine epoxy). Addition of carbon nano-fibers and surface modified UHMWPE fibers strengthened the bonding among constituents and provided more resistance to crack initiation and propagation.

Firouzi *et al.* (2014) [111] examined the influence of nylon coating on the toughness and tensile strength of UHMWPE fibers evaluated at three different temperatures (25 ℃, 50 ℃, and 70 ℃). Nylon coating improved the tensile strength of UHMWPE fibers, however, with increase in coating temperature, the tensile strength decreased. Highest tensile strength was 17% higher than that of pristine UHMWPE fibers observed for nylon coated UHMWPE fibers coated at 25℃. Toughness increased after nylon coating and with increase in coating temperature, toughness further improved. Highest toughness was 169% higher than that of pristine UHMWPE fibers observed for nylon coated UHMWPE fibers at 70 ℃. Flexibility and ductile nature of nylon were attributed for improved toughness.

Broujerdi *et al.* (2013) [112] investigated the effect of reinforcing surface modified UHMWPE fibers on the performance of epoxy/UHMWPE composites. Glycidyl methacrylate (GMA) treatment was used for surface modification. GMA was grafted on UHMWPE fibers in three different weight percentage for processing of composites (11 wt.% GMA grafted UHMWPE fibers, 25 wt.% GMA grafted UHMWPE fibers, and 40 wt.% GMA grafted UHMWPE fibers). Epoxy composite reinforced with 11 wt.% GMA grafted UHMWPE fibers showed the highest improvement in toughness (19% higher than pristine fibers reinforced composite) and tensile strength (47% higher than pristine fiber reinforced composite). SEM/FTIR analysis confirmed that GMA grafting on the surface of UHMWPE fibers added functional groups which resulted in strong chemical bonds between epoxy and surface modified UHMWPE fibers.

Li and Chen (2012) [113] examined the influence of reinforcing maleic anhydride (MAH) grafted high density polyethylene (HDPE) granules on the tensile strength/impact strength of clay reinforced polyetherimide (PEI) composites. Nanoclay was used in the range of 1–9 wt.%, with an increment of 2 wt.%. Tensile strength improved by 33% with addition of 9 wt.% nanoclay. Addition of MAH-HDPE showed further improvement (75%) in clay/PEI composites. Impact strength increased with addition of nanoclay to the PEI matrix (from 45 to 50 kJ/m^2). Addition of MAH-HDPE further increased the impact strength (to 65 kJ/m^2).

Wang *et al.* (2006) [114] investigated the influence of reinforcing UV-assisted acrylamide (AM) grafted UHMWPE fibers on the performance of epoxy based and vinyl ester based composites. Surface modified UHMWPE fiber reinforced epoxy resin showed higher improvement in single fiber pull-out strength (49% higher than pristine fiber reinforced epoxy composite) as compared to modified UHMWPE fiber reinforced vinyl ester. Improvement in interlaminar shear strength (ILSS) was almost same for both type of composites. ILSS of modified UHMWPE fiber reinforced epoxy and vinyl ester composites improved by 114% and 116% respectively as compared to pristine UHMWPE fiber reinforced epoxy and vinyl ester composites respectively.

A summary of additional literature available on UHMWPE fiber reinforced epoxy nanocomposites is presented in Table 2.2.

Table 2.2. Summary of literature on UHMWPE fiber reinforced epoxy nanocomposites.

S.No.	Composition	Effect on mechanical properties and underlying mechanisms/reasons for change in properties	References
1.	**Matrix**: Epoxy **Reinforcement**: UHMWPE fibers/particles	Authors investigated the influence of reinforcing UHMWPE fillers on properties of epoxy composites. Reinforcement of pristine UHMWPE fibers to epoxy resulted in decreased mechanical performance owing to exceptionally smooth and chemically inert surface of UHMWPE fibers which resulted in a weak bond between UHMWPE and epoxy. Addition of compatibilized UHMWWPE fillers showed superior performance (tensile and flexural properties, impact strength, pull-out strength, tribological properties, and interlaminar shear strength). Main factors affecting the properties included wettability, curing schedule, and interfacial bonding between matrix-reinforcement. Surface modification increased the oxygen groups on surface of UHMWPE increasing its wettability and intensity of polar groups on fiber surface.	Gutowski *et al.* 1993 [115]; Ogawa *et al.* 2000 [116]; Arshad *et al.* 2020 [117]; Belgacemi *et al.* 2020 [118]; Han *et al.* 2020 [119]; Wang *et al.* 2020 [120]; Yan *et al.* 2020 [121]; Chhetri *et al.* 2021 [122]; Pundhir *et al.* 2021 [123]; Tian *et al.* 2021 [124]; Wu *et al.* 2021 [125]; Guo *et al.* 2022 [126]; Wu *et al.* 2022 [127]
2.	**Matrix**: Epoxy **Reinforcements**: UHMWPE fibers/particles and nano-filler (graphene oxide, silicon carbide, aluminium oxide etc.)	Authors examined the combined effect of reinforcing compatibilized UHMWPE fillers and a separate nano-filler on the properties of epoxy composites. Reinforcement of these fillers in the pristine state deteriorated the properties of resulting composites. To improve the overall performance, both UHMWPE fibers and the nano-filler were subjected to surface modification. For UHMWPE, silanization, MAH grafting, plasma treatment, chromic acid treatment, potassium permanganate treatment, or combination of these treatments is reported. For nano-fillers, generally silanization technique is used. Reinforcement of compatibilized UHMWPE fibers and nano-fillers improved the tensile and flexural properties, impact strength, and interlaminar shear strength of resulting epoxy nanocomposites. Compatibilization of fillers formed hydrogen bonding between constituents of nanocomposite system resulting in formation of a polymer network. The dispersed nano-fillers bear the load applied on the matrix along with the fibers. The other mechanisms reported are matrix-cracking, fiber necking and breaking, shear yield deformation etc. Glass transition temperature and storage modulus also improved with addition of compatibilized fillers due to restriction in polymer chain movement.	Ahmadi *et al.* 2016 [128]; Belgacemi *et al.* 2020 [129]; Liu *et al.* 2020 [130]; Shanmugam *et al.* 2020 [131]; Shanmugam *et al.* 2020 [132]; Belgacemi *et al.* 2021 [133]; Belgacemi *et al.* 2021 [134]; Chhetri *et al.* 2021 [122]; Mehelli *et al.* 2022 [135]; Zhang *et al.* 2022 [136]

2.4 Para-aramid fiber reinforced polymer composites

Alsaadi (2022) [137] examined the effect of adding silicon carbide (5–20 wt.%; increment of 5 wt.%.) having particle size of 35 μm on the fracture toughness and flexural properties of carbon/aramid epoxy composites. Carbon fiber/silicon carbide epoxy composites showed better performance than aramid fiber/silicon carbide epoxy composites. Epoxy composites reinforced with carbon fiber mat (weight percent varied between 55−60 wt.%) and 5 wt.% silicon carbide

showed the highest improvement in properties. Fracture toughness improved from 1515 to 2034 J/m^2. Flexural strength and modulus increased from 645 MPa and 45.3 GPa to 680 MPa and 48.4 GPa, respectively. Addition of silicon carbide particles improved the bonding between carbon/aramid fibers and epoxy matrix.

Zuo *et al.* (2022) [138] examined the influence of reinforcing polyarylene ether nitrile terminated with phthalonitrile (PEN-t-Ph) of different molecular weights on the performance of aramid fiber reinforced/PEN-t-Ph composites. Hand lay-up assisted hot pressing was used for fabricating composites. Dip coating was used for surface modification of aramid fibers with PEN-t-Ph. Sample coding used was PEN a, PEN b, PEN c, and PEN d with decreasing molecular weights. PEN-t-Ph modified aramid fiber reinforced/PEN c composites showed the best performance. Impact strength, flexural strength, and IFSS improved by 43%, 47%, and 95% respectively as compared to the lowest values among all the four samples. The lower molecular weight of PEN-t-Ph resin increased the collision probability of modified aramid fibers and PEN-t-Ph resin. Thus, a more stable cross-linked structure was formed. The lower molecular weight of PEN-t-Ph resin had more fluidity and easily penetrated between the fibers during the processing of laminates. If the molecular weight of PEN-t-Ph resin was low, it decreased the entanglement of molecular chains. Consequently, the interfacial compatibilization was reduced between constituents.

Li *et al.* (2021) [139] examined the influence of reinforcing compatibilized para-aramid fibers on the mechanical properties of epoxy composites. Vacuum assisted resin infusion moulding (VARIM) was used for processing of epoxy composites. Two different surface modification techniques were used for para-aramid fibers, (a) epichlorohydrin coating (EH) and (b) epichlorohydrin coating followed by poly(propylene glycol) bis(2-aminopropyl ether) (EHPEA). Surface modification with EH resulted in formation of epoxy group on the para-aramid surface. Further, poly(propylene glycol) bis(2-aminopropyl ether) treatment increased the reactive functional groups (oxygen and nitrogen content) on the surface of para-aramid fibers, and thus, increased the polarity between para-aramid fibers and epoxy. Consequently, compatibilized para-aramid fibers reinforced epoxy composites exhibited better mechanical performance. Epoxy composites reinforced with epichlorohydrin coating followed by poly (propylene glycol) bis (2-aminopropyl ether) coating para-aramid fibers showed 29% and 24% improvement in IFSS and flexural strength respectively over pristine para-aramid fiber reinforced epoxy composites.

Khan *et al.* (2021) [140] evaluated the effect of adding micro-silica particles and glass microspheres separately on the performance of para-aramid fiber reinforced polyvinyl butyral composites. Concentration of particles was varied from 1–4 wt.% with increment of 1 wt.%. Flexural strength increased with both the particles till the maximum loading of 4.0 wt.% (86% and 143% improvement with glass microspheres and micro silica particles respectively). Flexural modulus increased till 3 wt.% (144% and 137% improvement with glass microspheres and micro silica particles respectively). Maximum improvement in Charpy impact strength was observed in polyvinyl butyral composites reinforced with para-aramid fiber and 3 wt.% glass microspheres (from 30.6 to 53.86 kJ/m^2). Fiber breakage and delamination mechanisms during fracture resulted in improved mechanical performance.

Lin *et al.* (2020) [141] studied the influence of reinforcing compatibilized para-aramid fibers on the performance of rubber composites. Para-aramid fibers were pre-treated with calcium chloride and sodium hydroxide solutions. Two different methods were used for surface modification of para-aramid fibers, (a) silanization, and (b) in-situ silica modification. Rubber composites reinforced with surface modified para-aramid fibers (pre-treatment followed by silanization) showed the highest tensile strength and DIN abrasion. Tensile strength and DIN abrasion improved by 32% and 16% respectively over rubber composite reinforced with pristine para-aramid fibers. The presence of reactive functional groups on the surface of treated para-aramid fibers enhanced the interfacial bonding among constituents of composite system.

Lu *et al.* (2018) [46] evaluated the influence of reinforcing surface modified para-aramid fibers on the performance of epoxy sheets. Para-aramid fibers were treated with phosphoric acid solution of various concentrations viz. 10, 20, 30, and 40 wt.% at 40 ℃ for 2h followed by vacuum drying at 105 ℃ for 4h. Tensile strength of compatibilized para-aramid fiber (20% concentration) reinforced epoxy sheet improved from 2.41 to 3.41 kN/m^2 (increment of 42%). Tensile strength enhanced due to improved interfacial bonding between para-aramid fibers and epoxy after functionalization of para-aramid fibers. This was owing to formation of carboxyl and amino groups (confirmed by FTIR analysis). The functionalization of para-aramid fibers made the surface rough which resulted in mechanical interlock effect (Figure 2.7).

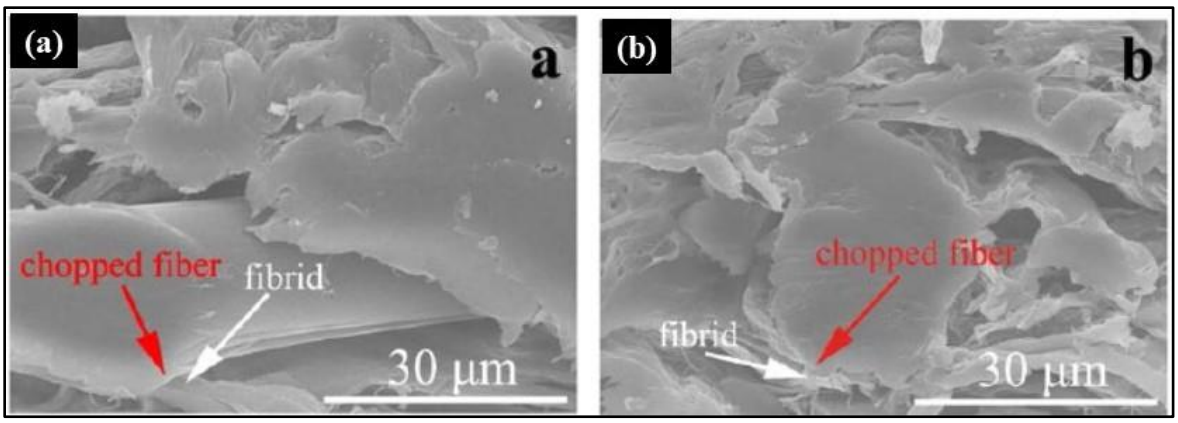

Figure 2.7. SEM micrographs of para-aramid/epoxy sheet (a) having pristine para-aramid fibers, and (b) having phosphoric acid treated para-aramid fibers [46].

Yang *et al.* (2018) [142] evaluated the effect of reinforcing aramid nanofibers on the properties of para-aramid paper. Hand sheets forming technique was used for fabricating paper. Addition of 6.0 wt.% aramid nanofibers enhanced the ultimate tensile strength and dielectric strength by 145% and 44% respectively as compared to pristine para-aramid paper. Properties improved owing to improved interfacial bonding of aramid nanofibers acting as the bridging binders, fillers, inlaying nails, and self-assembly fragmented films. Aramid nanofiber reinforced paper was a light-weight material exhibiting good heat resistance, insulating properties, tensile strength.

Fan *et al.* (2018) [143] investigated the influence of reinforcing low temperature plasma treated para-aramid fibers on the interfacial shear strength (IFSS) of epoxy composites. Orthogonal array experimental design was used for identification of optimum conditions for treatment. Sixteen different combinations were used for surface modification of aramid fibers. The decreasing order of different parameters affecting the IFSS of modified para-aramid fiber reinforced epoxy composites included treatment power (67.5 W), treatment time (11 min), and treatment pressure (2500 Pa). IFSS of epoxy composites reinforced with para-aramid fibers treated under optimum conditions increased by 36% as compared to pristine para-aramid fiber reinforced epoxy composites. For the treated fibers reinforced in composites, interfacial interaction improved due to Vander Waals' forces, interfacial friction, and chemical bonding.

Akhil *et al.* (2016) [144] observed the effect of adding para-aramid fibers (30.0, 35.0, and 40.0 wt.%) using VARIM technique on the performance of epoxy composites. Epoxy composite reinforced with 35 wt.% para-aramid fibers showed the best tensile strength (6% higher than

pristine epoxy) and hardness (18% improvement) and that reinforced with 30 wt.% para-aramid fibers showed the best impact strength (29% improvement).

Deng *et al.* (2016) [145] investigated the influence of surface treatment of para-aramid fibers by sulphuric acid under microwave irradiation on the breaking strength of fibers. Aramid fibers were dipped in sulfuric acid solution of various concentrations viz. 5, 10, 20, 30, 40, and 50 g/L for a fixed time period of 4 min. Breaking strength of fibers deteriorated after sulphuric acid treatment. The loss of strength was marginal till 20.0 g/L concentration (only 7% drop in strength), but beyond this level, the strength decreased significantly. Decrease in breaking strength was associated with the etching effect of sulfuric acid.

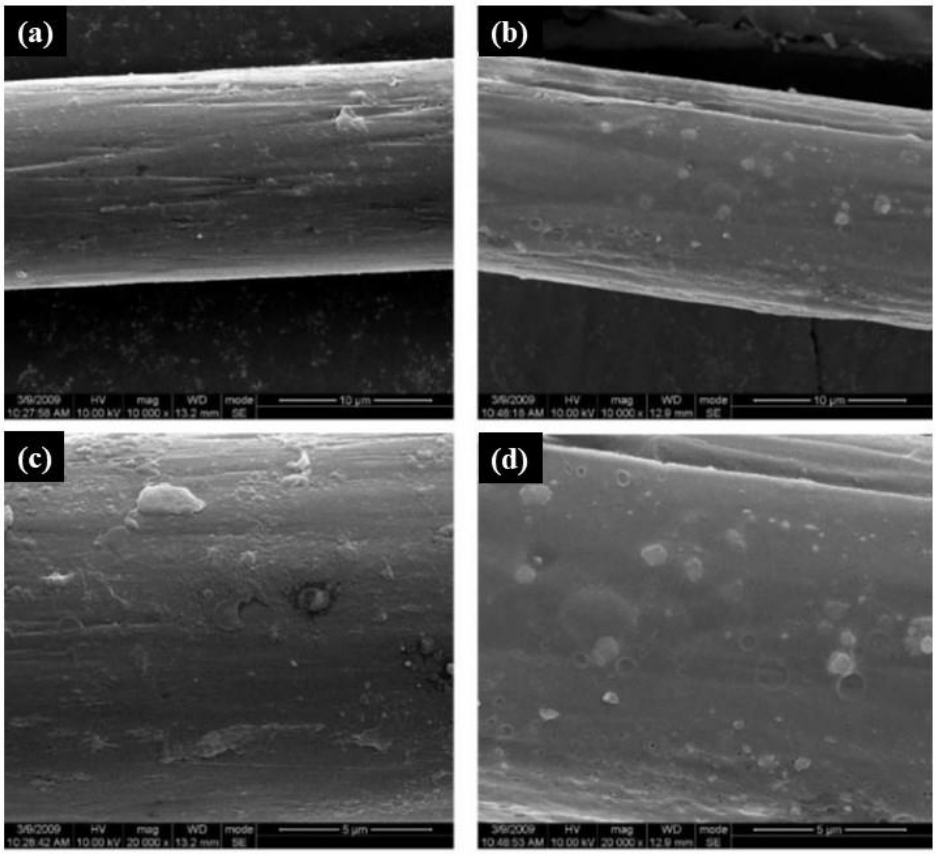

Figure 2.8. SEM micrographs of para-aramid fibers (a and c) pristine, and (b and d) direct fluorinated [146].

Peng *et al.* (2012) [146] evaluated the influence of reinforcing compatibilized para-aramid fibers on the ILSS and tensile strength of epoxy composites. Direct fluorination technique was used for surface treatment of fibers. Para-aramid fibers were used in fixed quantity of 65 wt.%. ILSS and tensile strength of epoxy composite reinforced with fluorinated para-aramid fibers improved from 42.2 to 56.2 MPa (33% higher) and 2089 to 2340 MPa (12% higher) respectively as compared to

epoxy composite reinforced with pristine para-aramid fibers. Difference in the surface of pristine and fluorinated para-aramid fibers was easily observable (Figure 2.8). Fluorination did not damage the fiber surface, though formation of gibbous particles was observed (Figure 2.8b). In contrast to other treatments, at higher magnification, fluorinated para-aramid fibers showed a smoother surface (Figure 2.8d) as compared to pristine fibers (Figure 2.8c) owing to formation of a thin layer around para-aramid fibers after fluorination. Fluorination was able to activate the surface of para-aramid fibers owing to which a better interface developed between epoxy and para-aramid fibers.

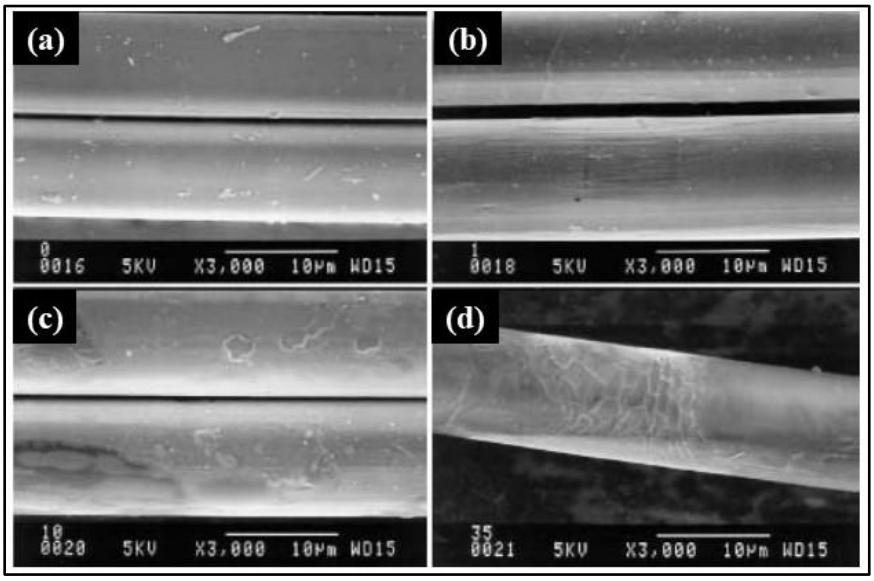

Figure 2.9. SEM micrographs of para-aramid fibers (a) pristine, (b) treated with 1 wt.% phosphoric acid, (c) treated with 10 wt.% phosphoric acid, and (d) treated with 35 wt.% phosphoric acid [147].

Park *et al.* (2002) [147] examined the influence of reinforcing surface modified para-aramid fibers using hot press with vacuum bagging on the performance of epoxy composites. Different concentrations of phosphoric acid were used for surface modification (1, 10, and 35 wt.%). Maximum improvement in interlaminar shear strength (82%) and fracture toughness (71%) was observed for nanocomposite reinforced with 10 wt.% phosphoric acid treated para-aramid fibers. SEM micrographs of surface of pristine and 1 wt.% phosphoric acid treated para-aramid fibers did not show any significant changes (Figure 2.9a–b). However, 10 wt.% phosphoric acid treated para-aramid fibers effectively made the surface of fiber rough (Figure 2.9c) which resulted in improved interfacial bonding. The surface of 35 wt.% phosphoric acid treated para-aramid fibers was more rough (Figure 2.9d) but at the same time it deteriorated the properties of fibers owing to excess concentration of phosphoric acid. Thus, mechanical properties exhibited by 35 wt.% phosphoric

acid treated para-aramid fibers reinforced epoxy composites deteriorated. Impact strength of phosphoric acid treated para-aramid fiber reinforced epoxy composites was less than that of pristine para-aramid fiber reinforced composites owing to increased impact stiffness resulting in more brittle behavior of composites.

A summary of additional literature available on para-aramid fiber reinforced epoxy nanocomposites is presented in Table 2.3.

Table 2.3. Summary of literature on para-aramid fiber reinforced epoxy nanocomposites.

S.No.	Composition	Effect on mechanical properties and underlying mechanisms/reasons for change in properties	References
1.	**Matrix**: Epoxy **Reinforcement**: Para-aramid fibers	Addition of pristine para-aramid fibers to epoxy resin resulted in deteriorated mechanical properties due to high crystallinity, surface smoothness, surface inertness, and less polar groups availability resulting in weak interface between para-aramid fibers and epoxy resin. The fibers detached from epoxy matrix owing to weak interfacial bonding between them. Reinforcement of surface modified para-aramid fibers showed improvement in interfacial shear strength, tensile and flexural properties, impact strength, and pull-out strength. Surface modified fibers added more polar groups and grooves on the fiber surface. Polar groups increased oxygen contacting groups and resulted in higher fiber surface energy causing increased wettability.	Shu-hui *et al.* 2006 [148]; Zhang *et al.* 2008 [149]; Zhang *et al.* 2008 [150]; Gu *et al.* 2012 [151]; Gao *et al.* 2013 [152]; Zhao *et al.* 2013 [153]; Cheng *et al.* 2016 [154]; Deng *et al.* 2017 [50]; Cheng *et al.* 2018 [155]; Moraes *et al.* 2020 [156]; Li *et al.* 2021 [139]; Zhang *et al.* 2021 [157]
2.	**Matrix**: Epoxy **Reinforcements**: Para-aramid fibers and nano-fillers (graphene oxide, silicon carbide, carbon nanotubes etc.)	Addition of nano-fillers (graphene oxide, silicon carbide, carbon nanotubes etc.) marginally improved the mechanical performance of para-aramid fiber reinforced epoxy nanocomposites. For further enhancement in properties, para-aramid fibers and/or nano-fillers were subjected to surface modification for improving the interfacial interaction with other constituents of the nanocomposite system. Para-aramid fibers were compatibilized with different surface modification treatments including poly-p-paraphenylene terephthalamide treatment, dopamine treatment, fluorination, plasma treatment etc. Composites containing both the compatibilized reinforcements showed highest mechanical properties. Compatibilization of fillers enhanced active functional groups on fibers and also their surface roughness. This resulted in strong chemical bonding and robust mechanical interlocking between para-aramid fibers and epoxy matrix. Generally, three types of failures are witnessed: (i) resin failure, (ii) fiber failure, and (iii) adhesion failure of interface layers. Compatibilized para-aramid fibers changed the fracture from clean shear (with pristine fibers) to shear and peal. Presence of nano-filler boosted further the bond strength between fibers and epoxy resin.	Bilisik *et al.* 2018 [158]; Cheng *et al.* 2018 [155]; Bilisik *et al.* 2019 [159]; Gong *et al.* 2019 [160]; Suresh *et al.* 2020 [161]; Obradović *et al.* 2021 [162]; Zhang *et al.* 2021 [157]; Zhang *et al.* 2021 [163]

2.5 Spandex fiber reinforced polymer composites

Lei *et al.* (2021) [164] investigated the influence of grafting of carbon nanotubes/silver nanoparticles on the sensitivity of spandex fiber strain sensor. The surface of spandex fibers was modified with a solution prepared by mixing carbon nanotubes (5 mg/ml), sodium dodecyl benzene sulfonate (8 mg/ml), Ag nanoparticles (50 mg/ml), polystyrene sulfonic acid, and polymer polyvinyl alcohol respectively. The said solution was prepared using a magnetic stirrer and an ultrasonicator. The dipping and drying process was repeated about 20 times. When the strain sensor was stretched in the range of 0–20%, the strain sensitivity reached up to 58.5, which was 5 times higher than the strain sensor made of only carbon nanotubes. The sensor could detect mechanical strains as small as 0.053% with a very short response time of 42 ms. Carbon nanotubes/silver nanoparticles were uniformly distributed on the surface of spandex fibers as shown in Figure 2.10. The coating was strongly bonded to spandex fibers and didn't detach. Thus, these sensors could easily be sewn into gloves, clothes etc.

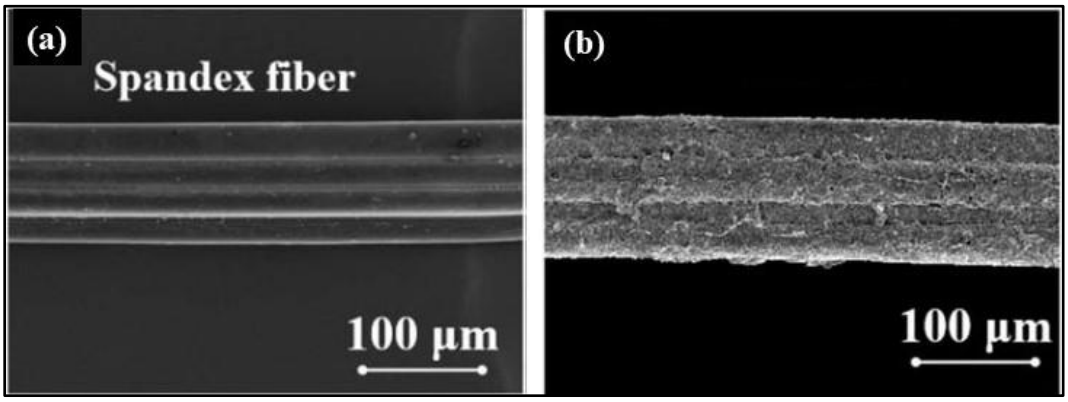

Figure 2.10. SEM micrographs of spandex fibers (a) pristine, and (b) carbon nanotubes/silver nanoparticles grafted [164].

Ali *et al.* (2021) [165] examined the effect of grafting carbon nanotubes (CNTs) on the electrical conductivity of Nylon 6/Spandex fibers. Dip coating was used for surface modification of Nylon 6/Spandex fibers. The fibers were pre-treated with sodium hydroxide before grafting the CNTs. This pre-treatment etched the surface of Nylon 6/Spandex fibers which helped in more effective grafting of CNTs owing to mechanical interlocking. CNTs were dispersed in distilled water and pH of solution was maintained around 6.5 pH with the help of acetic acid. Nylon 6/Spandex fibers were dispersed in this solution for 30 min at room temperature followed by drying at 50 ℃. This process was repeated for 5, 10, 15, and 20 times. It was revealed that electrical resistivity decreased

(from 260 Ω.m for 5 dipping cycles to 50 Ω.m for 20 dipping cycles) with increase in number of dipping cycles due to grafting of the conductive CNTs on the surface of Nylon 6/Spandex yarn. Durability of modified Nylon 6/Spandex fibers was checked by severe washing with water. Minor changes were observed in resistivity before and after severe washing, which was negligible. This suggested that CNTs strongly adhered to the fibers and did not detach even with severe washing.

Chen *et al.* (2020) [166] examined the effect of carbon nanotubes (CNT)/ultra-thin polyurethane coating on the strain sensing performance of spandex fibers. CNT loading was varied from 1–5 wt.% with increment of 1 wt.%. 1-pyrenecarboxylic acid treatment was used for surface modification of CNTs. CNTs/polyurethane suspension was prepared with the help of an ultrasonicator (40 kHz; 2 h at room temperature). A spin coater was used for grafting on the surface of spandex fibers. Two different types of coatings were used for grafting on spandex fibers: (a) CNTs/polyurethane coating, and (b) modified CNTs/polyurethane coating. It was observed that electrical conductivity increased with increase in CNT loading till the maximum value of 5 wt.%. Modified CNTs/polyurethane coated spandex fibers showed more electrical conductivity as compared to CNTs/polyurethane coated spandex fibers. Modified spandex fibers exhibited large workable strain, high sensitivity, excellent repeatability, and stability. Sensors fabricated with modified spandex fibers demonstrated high sensitivity over a wide working range. Modified CNTs/polyurethane coated spandex fibers exhibited gauge factor of 6.7 and 14191.5 at strains of 0–20% and 170–200% respectively. The relative resistance of samples with spandex fibers came out to be approximately constant with time for bending motion ($\Delta R/R$~55%).

Vo *et al.* (2020) [167] examined the influence of addition of graphene and silver nanowires on the properties of spandex composites for preparing highly stretchable strain sensors. N,N-dimethylformamide and graphene suspension (1.2 mg/mL) was prepared. Spandex fibers were dispersed in suspension (400 rpm, 12h, 80 ℃). Now, silver suspension (0.5 wt.% in isopropyl alcohol) was put in this suspension (400 rpm, 12h, 80 ℃). This final suspension was poured in a mould, dried at 60 ℃, and composite film having thickness of 50 μm was prepared. The fabricated strain sensor could experience large strains till 120% and low hysteresis with a high gauge factor (150.3) at a strain of 120%. The prepared sensors found applications in observing human motions (body movements, heart rate etc.).

Kong *et al.* (2018) [168] examined the influence of combined addition (5–20 wt.%; increment of 5 wt.%.) of reduced graphene oxide and acid treated carbon nanotubes on the super-stretchability

and electrical conductivity of spandex composite membranes. Graphene oxide was synthesized using modified Hummers method. CNTs were treated in a solution containing equal amounts of nitric acid and sulphuric acid. Acid treated CNTs (0.75 mg/mL, 120 ml) and graphene oxide (0.5 mg/mL, 60 ml) in aqueous solution were ultrasonicated individually for 1h each. Now both solutions were mixed and pH of solution was maintained at 10 by addition of potassium hydroxide. After this, hydrazine (300 mg) was added. The prepared solution was mixed for 3.5 h at 95 ℃. The suspension was washed until a constant pH was obtained. The obtained black precipitate was mixed ultrasonically for 30 min and solution-casting method was used for fabricating composites. Maximum stretchability (elongation at break: 387%) and electrical conductivity (49.5 Scm^{-1}) were achieved at 20 wt.%. The modified CNTs attached on the surface of graphene oxide. It signified that modified CNTs could act as a steric interruption to inhibit the aggregation of graphene oxide (Figure 2.11). A 3D network was formed by the overlap of CNTs and graphene oxide. This could facilitate fabrication of electrically conductive composite.

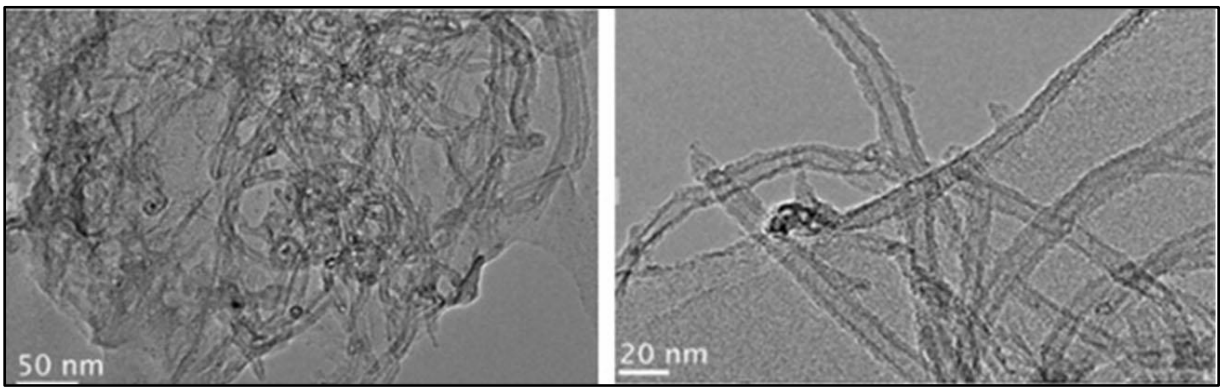

Figure 2.11. TEM micrographs of CNT/graphene oxide precipitate [168].

Chen *et al.* (2018) [169] investigated the influence of CNT/polyurethane coating on the properties of spandex fibers used for strain sensing applications. CNT loading varied from 1–5 wt.% with increment of 1 wt.%. CNTs were put in dimethylformamid and sonicated for 2h at room temperature. Polyurethane granules were dispersed in CNT suspension with the help of a magnetic stirrer for 1h. The suspension (containing thermoplastic polyurethane) was sonicated for 2h and dried at 80 ℃ for 24h. This prepared suspension was coated on spandex fibers with the help of a spray coater. The process was repeated for 1, 2, 3, 4, and 5 times. Electrical conductivity increased with increase in CNT loading. Maximum electric conductivity was observed for spandex fibers

coated with 5 wt.% CNT/polyurethane coating. Conductivity also increased with increase in number of coats due to more grafting of CNTs on the surface of spandex fibers (Figure 2.12).

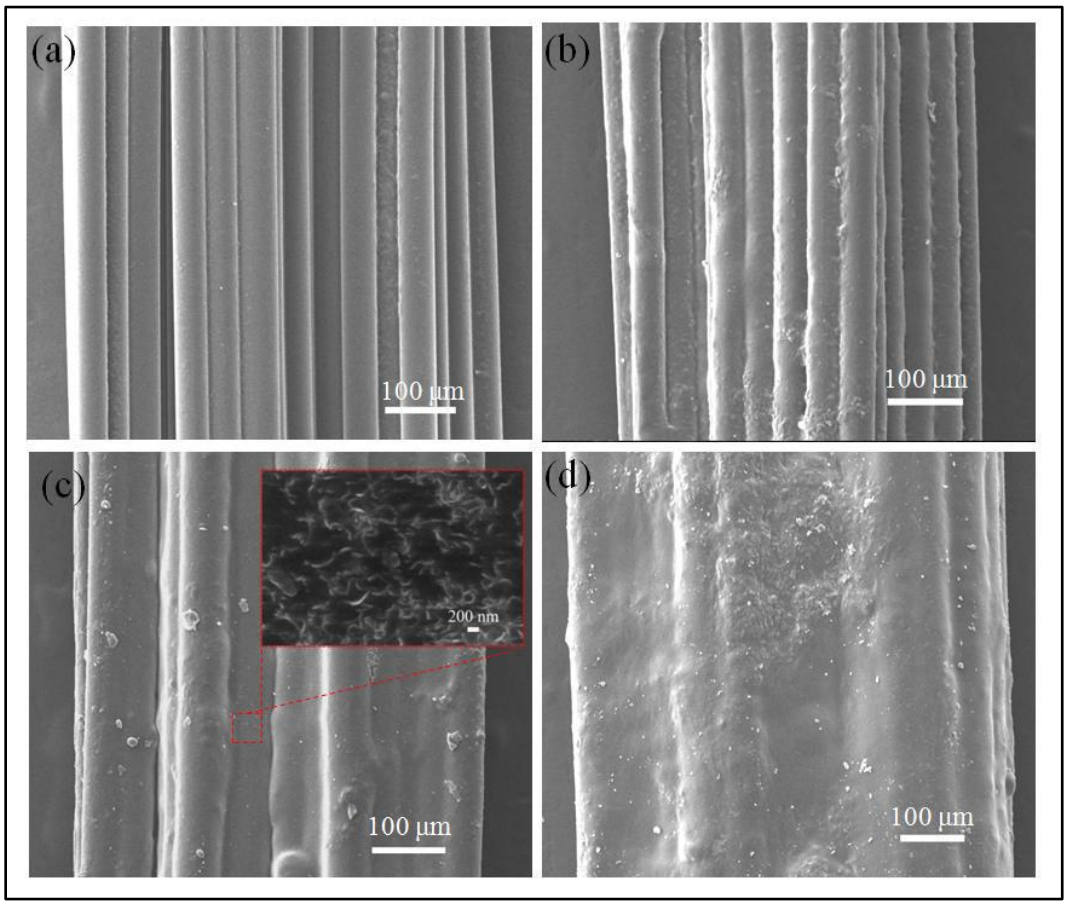

Figure 2.12. SEM micrographs of spandex fibers (a) pristine, (b) after 1 coating, (c) after 3 coatings, and (d) after 5 coatings [169].

Sun *et al.* (2012) [170] examined the effect of reinforcing spandex fibers (20, 40, and 60 vol.%) on the tensile properties of epoxy composite. The different loading of spandex fiber used was 20%, 40%, and 60 vol.%. 20 vol.% spandex fiber reinforced epoxy composites showed 50%, 28%, and 16% improvement in tensile stress, Young's modulus, and fracture strain respectively (over virgin epoxy). Increase in spandex loading beyond 20 vol.% resulted in deterioration of tensile properties due to low modulus and intensity of spandex fibers. At lower spandex loading, fibers acted as crack stoppers.

Sun *et al.* (2012) [171] examined the influence of reinforcing acid treated CNTs on spandex fiber reinforced epoxy composites. Loading of carbon nanotubes varied as 0.6, 1.0. 1.5, 2.5, and 4.5 wt.%. Elastic modulus of CNT (4.5 wt.%) reinforced spandex fiber/epoxy composite was

maximum (improved by 300% as compared to spandex fiber/epoxy composite without CNTs). Maximum tensile strength was shown by CNT (0.6 wt.%) reinforced spandex fiber/epoxy composite (improved by 67%). The increased loading of CNT in epoxy resin increased the viscosity of the epoxy/CNT/spandex fiber suspension owing to which removal of entrapped air from suspension became difficult and some air bubbles remained entrapped in the nanocomposite. These entrapped air bubbles acted as stress concentrators and pre-mature failure of material occurred.

A summary of additional literature available on spandex fiber reinforced nanocomposites is presented in Table 2.4.

Table 2.4. Summary of literature on spandex fiber reinforced nanocomposites.

S.No.	Composition	Effect on mechanical/electrical properties and underlying mechanisms/reasons for change in properties	References
1.	Spandex fiber related or spandex fiber reinforced composites	Most of the literature available on spandex fibers or spandex fiber reinforced composites discusses electric conductivity, sensitivity strain range etc. These materials find applications in the field of sensors for monitoring human motions. Different nano-fillers (carbon nanotubes, silver nano-particles, graphene, and graphene oxide etc.) are grafted on the surface of the spandex fibers to make them conductive for sensor related applications. Spandex fiber based sensors offer high sensitivity, workable strain range, excellent repeatability, long-term stability, low weight, and flexibility. Some authors have grafted polyaniline on spandex fibers to be used as humidity sensor. Currently, efforts have been made by various researchers for making wearable sensors from spandex based sensors.	Sun *et al.* 2015 [172]; Foroughi *et al.* 2016 [173]; Yang *et al.* 2017 [174]; Guo *et al.* 2018 [175]; Montazerian *et al.* 2019 [176]; Bi *et al.* 2021 [177]; Myant *et al.* 2022 [178]

2.6 Multi filler-reinforced polymer composites

Gokuldass and Ramesh (2019) [179] investigated the effect of modifying the epoxy resin with micro-rubber and nano-silica on the mechanical properties of woven fabric glass/Kevlar based hybrid composites. Eight layers of weaved fiber were used for fabricating the nanocomposite sheets. Three stacking sequences [GG-KK-KK-GG], [GG-KK-GG-KK], and [GG-GG-KK-KK] were used. Nine sets of hybrid E-glass/Kevlar weaved fibers were made with virgin epoxy, epoxy blended micro-rubber (9 wt.%) and nano-silica (11 wt.%), and epoxy with micro rubber (9 wt.%) to form hybrid composites. Addition of nano-silica in epoxy composites provided maximum tensile strength of 275 MPa (improved by 40%) as compared to pristine epoxy. Epoxy/micro-rubber composites exhibited higher fracture toughness compared to virgin epoxy and epoxy/micro-rubber/nano-silica composites. The stacking sequence of GG/GG/KK/KK provided superior

mechanical properties than other stacking sequences. The pristine epoxy did not adhere effectively to the glass/Kevlar fiber which caused pre-mature failure. Addition of nano-silica particles resulted in formation of more bonding sites between epoxy resin and glass/Kevlar fibers resulting in higher mechanical properties.

Gokuldass and Ramesh (2019) [180] examined the outcome of modifying epoxy resin with micro-rubber and nano-silica on the mechanical properties of intra-ply and mono-fiber woven glass/Kevlar fabric based hybrid composites. Epoxy resin was modified with 9 wt.% of micro-rubber and 11 wt.% of nano-silica. Epoxy resin modified with rubber and nano-silica and reinforced with intra-ply woven mat showed maximum improvement in fracture toughness (from 9.5 to 48.5 MPa). Tensile strength and modulus improved by 71% and 73% respectively over the pristine epoxy. Epoxy nanocomposite reinforced with intra-ply woven fiber mat showed higher mechanical performance than epoxy nanocomposite reinforced with mono fiber woven mat. This improvement was due to intra-ply fibers which offered more barrier layers.

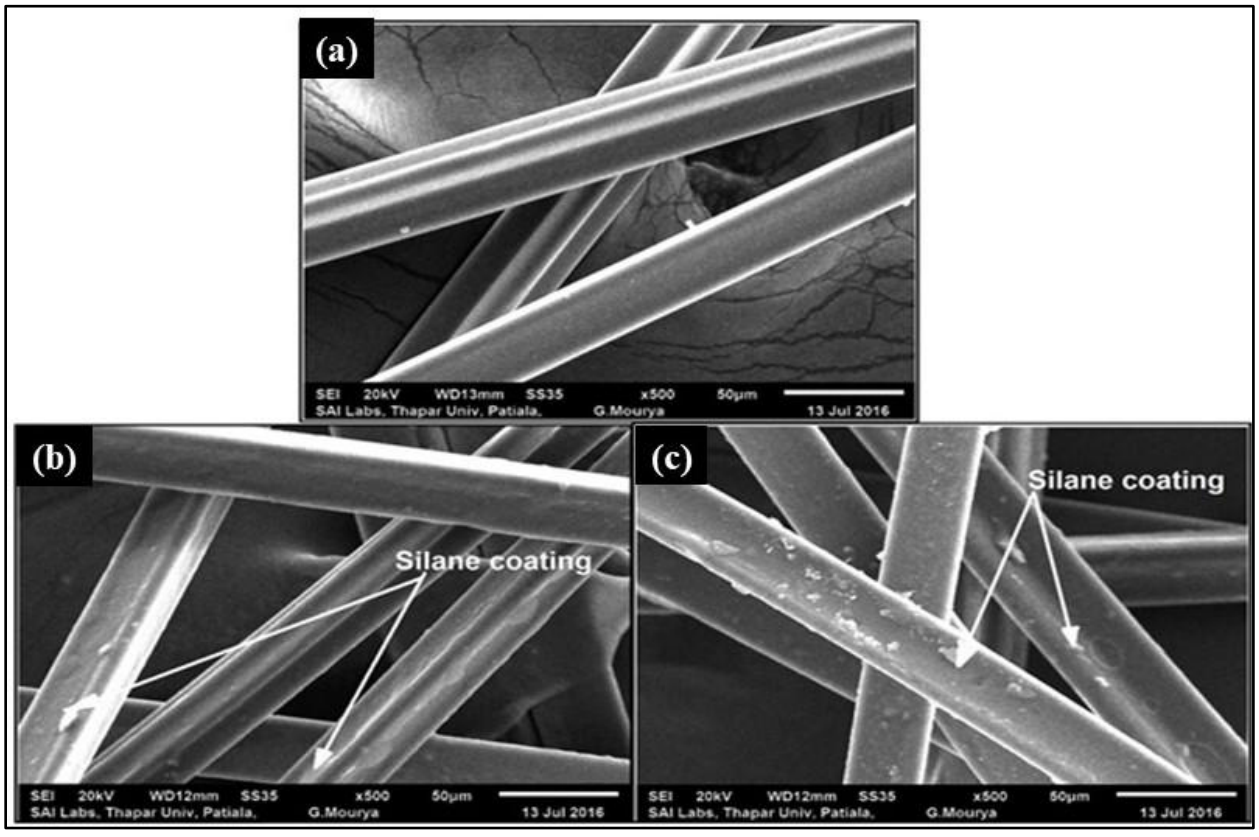

Figure 2.13. SEM micrographs of PET fibers at X500 (a) pristine PET fibers, (b) MS treated PET fibers, and (c) VS treated PET fibers [34].

Singh *et al.* (2017) [34] investigated the effect of adding compatibilized polyethylene terephthalate (PET) fibers as micro-reinforcement on the impact strength of epoxy based GFRPs containing 1 phr nanoclay as the nano-reinforcement. Two separate methods, (i) silane treatment, and (ii) UV-assisted maleic anhydride (MAH) grafting were used for compatibilization of PET fibers. Silane agents used were γ-methacryloxypropyltrimethoxysilane (MS) and vinylytriethoxysilane (VS). Epoxy based GFRPs were prepared using vacuum-assisted hand lay-up technique. Grafting of silane agents on PET fibers was confirmed by SEM-EDS. SEM micrographs showed that the surface of pristine fibers was smooth (Figure 2.13). However, the surface of silane treated PET fibers was relatively rough. EDS analysis confirmed the presence of silicon on the surface of silane treated PET fibers. Addition of 1 phr nanoclay to epoxy based GFRPs improved impact strength by only 4% over the GFPR with no nanoclay. Addition of pristine PET fibers (1, 2, and 3 phr) to epoxy based GFRP having 1 phr nanoclay deteriorated the impact strength owing to lack of compatibility among the constituents of composite system. Addition of 2 phr MS treated PET fibers, VS treated PET fibers, and MAH grafted PET fibers to epoxy based GFRP (containing 1 phr nanoclay) improved the impact strength by 12%, 19%, and 8% respectively over GFRP with no nanoclay. Improvement in impact strength was obtained due to increased interfacial interaction among various constituents after compatibilization.

Singh *et al.* (2017) [32] investigated the effect of reinforcing compatibilized polypropylene (PP) fibers as micro-reinforcement on the impact strength of epoxy based GFRPs containing 1 phr nanoclay as the nano-reinforcement. Two different methods (i) silane treatment, and (ii) UV-assisted maleic anhydride (MAH) grafting were used for compatibilization of PET fibers. Silane agents used were γ-methacryloxypropyltrimethoxysilane (MS) and vinylytriethoxysilane (VS). Epoxy based GFRPs were prepared using vacuum-assisted hand lay-up technique. Addition of 1 phr nanoclay to epoxy based GFRPs improved the impact strength by 4% over GFPR with no nanoclay. Addition of pristine PP fibers (1, 2, and 3 phr) to epoxy based GFRPs (containing 1 phr nanoclay) deteriorated the impact properties due to lack of compatibility of constituents. FTIR and SEM-EDS analysis confirmed the successful compatibilization of PP fibers after different surface treatments. XRD and TEM analysis confirmed the partially exfoliated clay morphology in the processed GFRPs. Addition of 2 phr MS treated PP fibers and MAH grafted PP fibers to epoxy based GFRP (containing 1 phr nanoclay) improved impact strength by 44% and 13% respectively over GFRP without nanoclay. GFRP composite (having no nanoclay/PP fibers) showed a very

smooth and brittle surface (Figure 2.14a) which resulted in less resistance during failure under impact loading. GFRP reinforced with 1 phr nanoclay showed a rough surface appearance due to presence of epoxy/clay mixture on the surface of glass fibers (Figure 2.14b). GFRPs reinforced with compatibilized PP fibers (silane treated/MAH grafted) showed improvement in interfacial interaction among the constituents of the composite system (Figure 2.14e–f). As a result better mechanical properties were shown by GFRPs reinforced with compatibilized PP fibers.

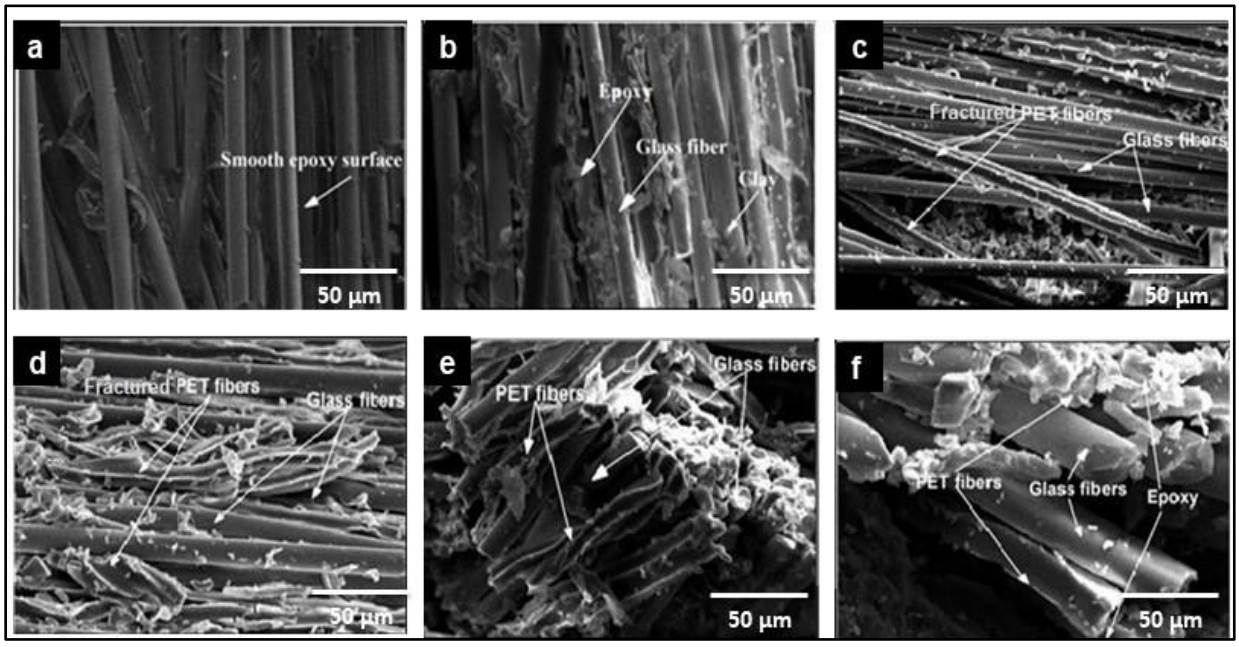

Figure 2.14. SEM micrographs of epoxy based GFRPs after impact testing (a) GFRP without clay/PP, (b) GFRP containing only nanoclay, (c) GFRP having 2 phr pristine PP fiber, (d) GFRP having 2 phr MS treated PP fibers, (e) GFRP having 2 phr VS treated PP fibers, and (f) GFRP having 2 phr MAH grafted PP fibers [32].

Singh *et al.* (2017) [35] investigated the effect of adding compatibilized ethylene propylene diene monomer (EPDM) rubber as micro-reinforcement on the impact strength of epoxy based GFRPs containing 1 wt.% nanoclay as nano-reinforcement. Two different methods (i) silane treatment using bis-(3-triethoxysilyl-propyl)-tetrasulfane, and (ii) maleic anhydride (MAH) grafting were used for surface modification of EPDM particles. Composites were prepared using vacuum-assisted hand lay-up technique. EPDM particles concentration used was 2.5, 5.0, 7.5, and 10.0 wt.%. Addition of 1 phr nanoclay to epoxy based GFRPs improved the impact strength by 13% over GFPR (having no nanoclay). XRD and TEM analysis confirmed partially exfoliated clay morphology in processed GFRPs. Addition of EPDM particles till 5.0 wt.% resulted in improved impact strength. Beyond this concentration, impact strength deteriorated due to lesser compatibility among constituents. Addition of 5 wt.% of silane treated EPDM particles and MAH

grafted EPDM particles to epoxy based GFRP (containing 1 phr nanoclay) improved the impact strength by 68% and 26% respectively over reference GFRP (having no nanoclay).

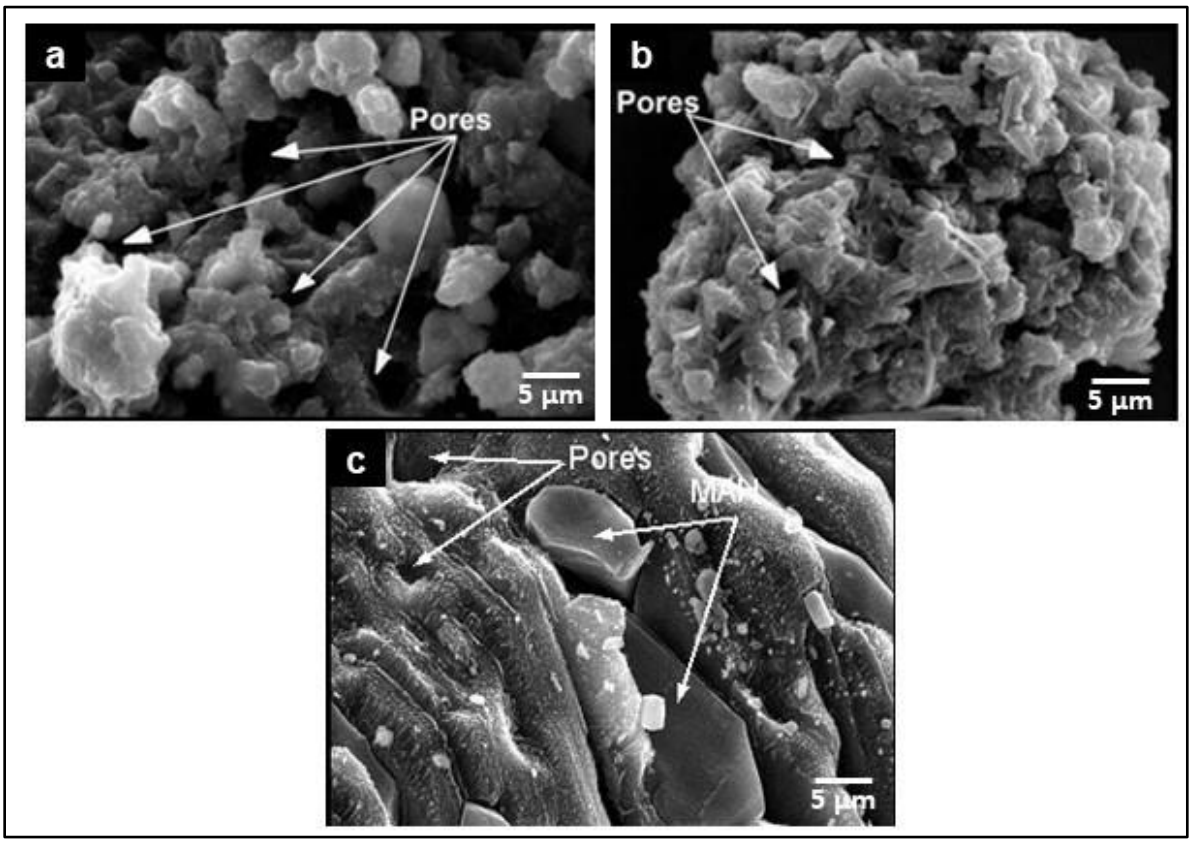

Figure 2.15. SEM micrographs of EPDM particles (a) pristine, (b) silanized EPDM particles, and (c) MAH grafted EPDM particles [35].

FTIR and SEM-EDS analysis confirmed successful compatibilization of EPDM particles after different surface treatments. SEM micrographs of EPDM particles are shown in Figure 2.15. It was clear that pristine EPDM particles showed a large number of large sized pores (Figure 2.15a); however, the number and size of pores decreased in compatibilized EPDM particles (Figure 2.15b). The relatively dense and compact morphology was attributed to presence of compatibilized agents.

A summary of literature available on multi-scale filler-reinforced polymer nanocomposites is presented in Table 2.5.

Table 2.5. Summary of literature on multi-scale filler reinforced polymer nanocomposites.

S.No.	Composition	Effect on mechanical properties and underlying mechanisms/reasons for change in properties	References
1.	**Matrix**: Epoxy **Reinforcements**: Nano-reinforcement (silica); Micro-reinforcement (rubber particles), Woven fiber mat (Glass and Kevlar fibers)	Epoxy resin was modified with micro-rubber and nano-silica particles. It revealed that addition of nano-silica showed highest improvement in tensile strength owing to uniform dispersion of silica particles. The uniformly dispersed silica particles resulted in more number of bonding sites. Thus, higher tensile strength was exhibited. However, maximum fracture toughness was witnessed in nanocomposites reinforced with nano-silica and micro-rubber. It was also observed that nanocomposite reinforced with intra-ply fiber mat showed higher mechanical performance as compared to nanocomposite reinforced with inter-ply fiber mat.	Gokuldass *et al.* 2019 [179]; Gokuldass *et al.* 2019 [180]
2.	**Matrix**: Epoxy **Reinforcements**: Nano-reinforcement (clay); Micro-reinforcement (thermoplastic fibers), Woven fiber mat (Glass fiber)	Epoxy nanocomposites containing more than two reinforcement at different scales are known as multi-scale filler reinforced epoxy nanocomposites. The addition of nano- and micro- fillers in the pristine state generally deteriorated the mechanical properties (impact strength, tensile and flexural properties) of the nanocomposite system due to lack of compatibility among constituents. To improve the mechanical performance of multi-scale filler reinforced epoxy nanocomposites, compatibilization of fillers is vital. Various surface modification techniques viz. chemical treatment, silanization, UV-assisted MAH grafting are used. Addition of compatibilized micro-fillers (soft/ductile fibers) improve the impact strength along with slight drop in tensile and flexural properties. Compatibilization resulted in additional functional groups on the surface of micro-fillers and enhanced interfacial bonding with epoxy resin. Reinforcement of surface modified mico-fillers thus enhanced the impact strength.	Nanda *et al.* 2020 [1]; Singh *et al.* 2017 [32]; Singh *et al.* 2018 [34]; Singh *et al.* 2017 [35]

2.7 Summary of the reviewed literature

- Effect of nanoclay addition (pristine as well as silanized) on the tensile properties, flexural properties, impact strength, and fracture toughness of epoxy based GFRP nanocomposites has been reported. Tensile modulus, flexural modulus, and flexural strength are reported to increase significantly with increase in nanoclay content till an optimum value (improvements have been more with silanized clay). Tensile strength, impact strength, and fracture toughness are reported to show only minor improvements with addition of nanoclay to GFRP composites. [15,36,39,66–68,71–74].
- Several authors have investigated the effect of polymer fiber addition (ultra-high molecular weight polyethylene (UHMWPE), para-aramid, and spandex) on the tensile strength, interlaminar shear strength (ILSS), impact strength, and fracture toughness of epoxy based composites. It is reported that reinforcement of pristine fibers generally degrades all the

mechanical properties. Surface modification (compatibilization) of fibers is necessary before reinforcement for improving interfacial adhesion between fibers and matrix. [46,96,97,99,101–103,107,139,143,146,181].

- Few authors have investigated the effect of reinforcing nano-fillers, both pristine and surface modified (nanoclay, nano-silica, silicon carbide particles, carbon nanotubes etc.) on the fiber (para-aramid, UHMWPE, and glass fibers) reinforced polymer composites. With addition of compatibilized nano-fillers, polymer composites were reported to exhibit improved tensile properties, flexural properties, and interlaminar shear strength [100,137,140,179,180].
- Several authors have investigated the effect of nano-filler grafting (silver particles, graphene, carbon nanotubes, etc.) on spandex fibers to improve the electrical conductivity and strain sensing performance of spandex fiber based strain sensors. The grafting procedures improved the conductivity, stretchability, and sensitivity of spandex fiber based strain sensors [164–169].
- A few authors have investigated the effect of polymer fiber addition (PET and PP fibers) and elastomer particles addition (EPDM particles) on the impact strength and tensile/flexural properties of epoxy based GFRPs (containing nanoclay). It was reported that addition of pristine thermoplastic fibers and elastomeric particles deteriorated the mechanical properties. Compatibilized fibers/particles (silane treated and UV-assisted MAH grafted fibers) enhanced the impact strength of epoxy based GFRPs with some loss in tensile properties [32,34,35].

2.8 Gaps in the existing literature

- Very few authors have investigated the effect of nanoclay addition on the impact strength of glass fiber reinforced epoxy nanocomposites (epoxy/nanoclay/GFRP nanocomposites). The effect of reinforcing silanized nanoclay on the impact strength of epoxy based GFRPs has not been investigated to date.
- A few authors have investigated the combined effect of thermoplastic fiber reinforcement and nanoclay addition on the tensile and flexural properties of polymer composites. However, the effect on impact strength has not been investigated.
- Singh *et al.* [32,34,35] investigated the effect of reinforcing thermoplastic/elastomeric fibers/particles (PP fibers, PET fibers, and EPDM particles) on the impact strength of epoxy-nanoclay based GFRPs. These studies successfully established the concept of adding polymer fibers to nanoclay reinforced epoxy based GFRPs for significantly improving the impact

strength. There is a large spectrum of thermoplastic fibers having diverse chemical structures from the very flexible (Inviya, popularly known as spandex) to the very rigid (Para-aramid, popularly known as Kevlar). Thus, there is a potential to achieve much greater impact strength with this approach. The effect of reinforcing different types of polymer fibers viz. ultra-high molecular weight polyethylene (UHMWPE), para-aramid, Inviya, etc. on the impact strength of epoxy based GFRPs has not been investigated.

The next chapter discusses the design of the current research work. The chapter presents a detailed discussion on the origin of current research, objectives and key issues, and the materials and methods used in the present work.

Chapter 3. Design of the study

3.1 Overview

This chapter utilizes the gaps in existing literature to establish the research objectives and key issues of the present study. This chapter also presents the details of materials and methodology used in the present research. The chapter also presents the details of equipment used for mechanical testing and characterization of fabricated GFRPs.

3.2 Objective and key issues

The overall objective of the present research is "*to improve the impact strength of epoxy based GFRP composites with addition of nanoclay and polymer filler through selection of suitable composition and processing conditions.*"

The key issues addressed are as follows:

- Fabrication of epoxy/clay/GFRP nanocomposite laminates reinforced with varying concentration of untreated and compatibilized polymer filler.
- Evaluation of mechanical properties (impact strength, tensile strength, and tensile modulus) and characterization of the processed nanocomposites for structure-property-processing relationship.

3.3 Methodology

The following methodology was followed to achieve the research objectives:

- Compositional details including range of weight concentration of various constituents of epoxy based GFRP nanocomposites was obtained through a detailed literature survey. Table 3.1 presents the detail of constituents.
- Silanization of nanoclay was done with varying concentration of silane agent (1X–4X; X is the nanoclay loading). For each case, the silanized nanoclay was reinforced in epoxy based GFRP and mechanical properties were evaluated. Nanoclay (both pristine and silanized) were dispersed in epoxy using homogenizer (at 20,000 rpm for 10 min) and probe ultrasonicator (at 80% amplitude for 10 min; pulse on 40 s; pulse off 20 s). Optimum concentration of silane

agent for silanization of nanoclay was selected from the case which showed maximum improvement in mechanical performance of silanized nanoclay reinforced GFRP.

- Compatibilization (surface modification) of various polymer fibers (UHMWPE, para-aramid, and Inviya fibers) by different methods including (i) chemical treatment, (ii) silanization, (iii) UV-assisted MAH grafting, and (iv) combination of chemical treatment followed by silanization.

Table 3.1. Details of various constituents used in the fabrication of multi-reinforced epoxy based GFRPs.

S.No.	Constituent	Specification	Quantity	Compatibilization method
1.	Nanoclay	Nanomer PGV	In a fixed amount (2 phr)	Silanization with 3-aminopropyltriethoxysilane (APTES)
2.	Glass fiber mat	E-glass fiber mat	2 plies for tensile samples and 12 plies for impact samples	Pristine state (no surface treatment)
3.	Thermoplastic polymer fibers			
a)	Ultra-high molecular weight polyethylene (UHMWPE)	Thermoplastic polymer fibers	0.125–0.500 phr; with an increment of 0.125 phr	(i) Potassium permanganate treatment, (ii) silanization with 3-aminopropyltriethoxy silane agent, (iii) Potassium permanganate treatment followed by silanization, and (d) UV-assisted MAH grafting
b)	Polyparaphenylene terephthalamide (para-aramid)		0.50–2.00 phr; with an increment of 0.50 phr	(i) Phosphoric acid treatment, (ii) silanization with 3-aminopropyltriethoxy silane agent , (iii) Phosphoric acid treatment followed by silanization, and (d) UV-assisted MAH grafting
c)	Polyether-polyurea copolymer (Inviya)		0.50–2.00 phr; with an increment of 0.50 phr	(i) Phosphoric acid treatment, (ii) silanization with 3-aminopropyltriethoxy silane agent, (iii) Phosphoric acid treatment followed by silanization, and (d) UV-assisted MAH grafting
4.	Resin and hardener system	Araldite CY 230 and Aradur HY951	Balance quantity. Resin-hardener ratio to be kept as 10:1 by wt.% (as recommended by the supplier)	Pristine state (no surface treatment)

- Polymer fibers (pristine or compatibilized, as per the case) were dispersed into epoxy-silanized nanoclay suspension by using homogenizer (at 10,000 rpm for 10 min), probe ultrasonicator (at 80% amplitude for 10 min), followed by homogenizer (at 15,000 rpm for 5 min).
- Curing agent was added to the epoxy-silanized nanoclay-polymer fiber suspension using mechanical stirrer (at 500 rpm for 10 min).
- The prepared suspension was used to lay up glass fiber mat to the desired thickness for processing GFRP nanocomposite laminates with the help of VARIM (Vacuum Assisted Resin Infusion Moulding) process.
- Mechanical properties (impact strength and tensile strength) of multi-scale filler reinforced epoxy based GFRP nanocomposites were evaluated to determine the most suitable composition of constituents (nanoclay and polymer fiber content) of nanocomposite system.
- The fracture surface of epoxy based GFRP which exhibited maximum improvement in impact strength was subjected to SEM analysis to determine the mechanisms causing improvements.
- GFRPs were characterized (XRD, TEM, FTIR, and SEM etc.) with respect to their mechanical properties and also to ascertain the dispersion and type of morphology of nanoclay in GFRPs.

3.4 Materials

Epoxy is one of the most important thermosetting resins employed as a matrix material for polymer based composites. Epoxy resin offers several benefits like easy processing, absence of by-products, good adhesion, good chemical resistance, and high failure strength [14,15,33]. Epoxy based fiber reinforced composites are extensively used in numerous industries starting from aviation to electronic industries [1,32,34,35]. Fiber reinforced composites are used in myriad applications viz. aerospace parts (rotor blades, radome), automobile components (bumper, roof, and door frames), marine spare parts (ship decks, hulls), sporting goods (arrows, archery bows, vault poles), racing car chassis and bodies, and several civil applications [1,32–34]. Different thermoplastic and natural fibers are used for reinforcing epoxy composites, most commonly used fibers are glass fibers, carbon fibers, and para-aramid fibers [182,183]. Glass fiber reinforced epoxy composites (GFRP) are attracting huge attention because of their outstanding characteristics like high specific strength and stiffness [184,185]. The use of nano-fillers in fiber reinforced composites has also attracted great interest. A small amount of nano-fillers (less than 5 wt.%) leads to significant improvements

in mechanical, barrier, and thermal properties of FRPs because of their unique exfoliation/intercalation characteristics, high aspect ratio, and large active surface area [2,7,41,42,186,187]. Epoxy based GFRP nanocomposites exhibit good static mechanical properties (tensile, flexural, and interfacial shear strength) but lack in impact strength. Consequently, epoxy based GFRPs find limited use in high impact applications [1,32,34,35].

In the present study, different thermoplastic fibers viz. UHMWPE, para-aramid, and Inviya fibers (micro-filler) were utilized with E-glass fiber mat (bi-directional) and nanoclay (nano-filler) to improve the impact strength of epoxy based GFRPs.

UHMWPE fibers (chemical structure is given in Figure A6, Appendix-I) have attracted tremendous attention because of their high tensile strength, high tensile modulus, light weight, low cost, and excellent resistance to chemical and physical degradation. UHMWPE fibers have record values of tensile strength and Young's modulus amongst polymer fibers. In terms of specific strength, these fibers have properties superior to all known fibers [98,99,106,188–191].

Para-aramid fibers (chemical structure is given in Figure A7, Appendix-I) are high-performance fibers that attract commercial and academic interest because their highly crystalline structure offers high specific toughness ratio and strength. They are widely used as an excellent reinforcement material for advanced polymer composites in aircrafts, aerospace, and missile applications [46,50,140,142,146].

Inviya fibers (chemical structure is given in Figure A8, Appendix-I) are one of the most important thermoplastic-elastomeric fibers commercially produced worldwide. Inviya fibers are made of long chain synthetic polymers comprising mainly of segmented polyurethanes. Polymer chains in segmented polyurethanes consist of two chemically distinct structural units (hard and soft segments). These structural units have glass transition temperatures above and below the room temperature respectively. Inviya fibers offer advantages of high strength, light-weight, exceptional elasticity, and recovery rate. These fibers are used for swimwear, cycling jerseys and shorts, dance belts for male ballet dancers, and other net ball body suits etc. [165,168,170,172,192].

The present work used epoxy (Araldite CY230) and curing agent (Aradur HY951) supplied by Huntsman Advanced Materials, India. Araldite CY230 is diglycidyl ether of bisphenol A (DGEBA) epoxy. Epoxy used was off-white in colour, tasteless, odourless, and non-toxic with low shrinkage. Curing agent, Aradur HY951 (triethylenetetramine [TETA]) was yellow in colour. Specific gravity of epoxy and hardener at 25 ℃ were 1.1 g/cm^3 and 0.98 g/cm^3 respectively.

Epoxy-curing agent weight ratio was kept as 10:1. 'Nanomer PGV' nanoclay was supplied by Sigma-Aldrich, India. WR 360 E-glass woven roving mats (bi-directional; 0°/90°) of 360 g/m^2 areal density were supplied by Owens Corning, India. Further, UHMWPE and para-aramid fibers were procured from Minifibers, USA. Inviya (Spandex) fibers were supplied by Indorama Pvt. Ltd., Singapore. All other chemicals (acetone, ethanol, silane agents, acetic acid, MAH granules, phosphoric acid, and potassium permanganate) were supplied by Tokyo Chemicals Industry, Japan.

3.5 Silanization of nanoclay

Silane agent used for silanization of nanoclay was 3-amimopropyltriethoxysilane (chemical structure is given in Figure A5, Appendix-I). The concentration of silane agent to be used for silane treatment of nanoclay was optimized in the present research. Silane agent concentration was selected as a proportion of weight of nanoclay (X). Silane agent concentration chosen for the study was 1X, 2X, 3X, and 4X as per earlier reported literature [16,193,194]. Beyond 4X concentration, viscosity of the system increased drastically making processing extremely difficult. Thus, silane agent concentration was restricted to 4X.

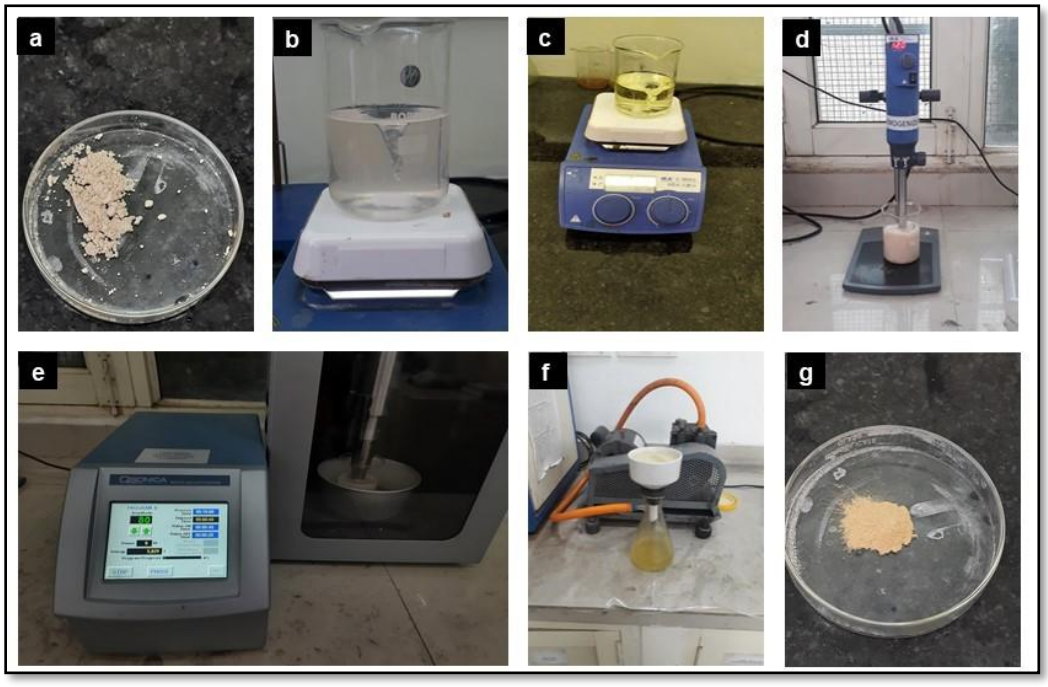

Figure 3.1. Real time images of processing during silanization of nanoclay showing (a) pristine nanoclay, (b) mixing of silane agent in acetone, (c) solution after hydrolysis, (d) homogenization of nanoclay in hydrolyzed solution, (e) ultrasonication of nanoclay in hydrolyzed solution, and (f) silanized nanoclay.

Pristine nanoclay was dried at 110 ℃ for 18 h before the silanization process. APTES silane agent was added to acetone during magnetic stirring (IKA, C-MAG HS4, India) at 750 rpm. Acetic acid was added to this solution to adjust pH value in the range of 4.5–5.5 pH. This hydrolysis step was done for 30 min. The solution was homogenized (IKA, T 25 digital Ultra-Turrax, India) at 12000 rpm for 3 min after adding nanoclay to it. This was followed by ultrasonication using probe sonicator (Qsonica, Q700, USA) at 80% amplitude for 10 min for proper dispersion of nanoclay. Now two separate cases were used viz. (i) with acetone washing, and (ii) without acetone washing to complete the silanization process. In the first case ('with acetone washing'), the silanized nanoclay was washed with acetone after sonication and was then extracted using vacuum filtration process. The purpose of washing the nanoclay with acetone was to rinse out any unreacted/excess silane agent. In the second case ('without acetone washing'), the silanized nanoclay was not washed with acetone after sonication and the silanized nanoclay was directly extracted using vacuum filtration process. The silanized nanoclays (under the two separate cases) were dried in a vacuum oven (60 ℃; 48 h). The dried nanoclay particles were crushed into fine particles using pestle and mortar. The real time images of silanization procedure followed for nanoclay are shown in Figure 3.1.

3.6 Compatibilization of polymer fibers

In the present research, three different thermoplastic fibers were used separately as a micro-reinforcement. These included (i) UHMWPE fibers, (ii) para-aramid fibers, and (iii) Inviya fibers. The fibers were subjected to four different surface treatment methods (compatibilization procedures). Surface modification (compatibilization) of UHMWPE fibers was done using (i) potassium permanganate treatment (T1), (ii) silanization with 3-aminopropyltriethoxy silane (T2), (iii) potassium permanganate treatment followed by silanization (T3), and (d) UV-assisted MAH grafting (T4). Surface modification (compatibilization) of para-aramid fibers and Inviya fibers was done using (i) phosphoric acid treatment (T5), (ii) silanization with 3-aminopropyltriethoxy silane (T2), (iii) phosphoric acid treatment followed by silanization (T6), and (d) UV-assisted MAH grafting (T4).

3.6.1 Potassium permanganate treatment

5 g of $KMnO_4$ was added to 50 g of nitric acid to prepare $KMnO_4$-HNO_3 solution. Thermoplastic fibers to be treated were dipped in this solution for 1 min at 35 ℃. Distilled water was used to wash out excess solution to obtain a constant pH value (around 5 pH). The treated fibers were dried for 12 h at 35℃ using a vacuum oven (at 1 bar). The colour of fibers changed from white to dark brown. Potassium permanganate is an oxidizing agent and on treatment with fibers, it itself gets reduced and oxidizes the fibers. The colour change confirmed the oxidation of fibers. The real time images of potassium permanganate treatment are shown in Figure 3.2.

3.6.2 Phosphoric acid treatment

Phosphoric acid solution (20 wt.%) was prepared by mixing phosphoric acid (60 ml) in distilled water (300 ml). Thermoplastic fibers to be treated were dipped in the prepared solution followed by magnetic stirring at 40 ℃ for 2 h. Treated fibers were rinsed in distilled water to obtain a constant pH value by removing excess acid. These were then dried (110 ℃, 6h). The real time images of phosphoric acid treatment are shown in Figure 3.3.

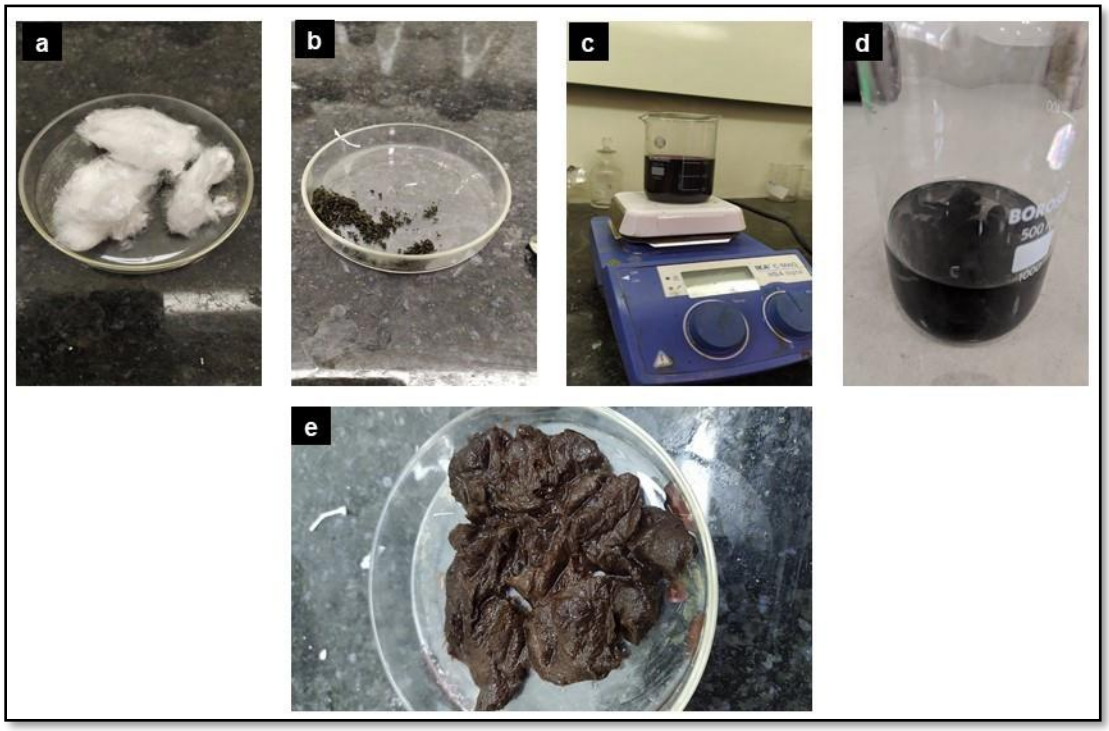

Figure 3.2. Real time images of potassium permanganate treatment of UHMWPE fibers (a) pristine UHMWPE fibers, (b) potassium permanganate granules, (c) mixing of potassium permanganate in nitric acid with the help of magnetic stirring, (d) UHMWPE fibers dipped in potassium permanganate solution, and (e) potassium permanganate treated UHMWPE fibers.

3.6.3 Silane treatment

For silane treatment of fibers, ethanol solution (95 vol. %) and distilled water (5 vol.%) were taken in a beaker. Silane agent (2 vol.% of solution) was added to ethanol solution using magnetic stirring. This was followed by adjusting the pH of solution in the range of 4.5–5.5 by adding acetic acid. Magnetic stirring was continued for another 30 min to facilitate completion of hydrolysis process. Required amount of fibers were dipped in this prepared solution for 10 min. Treated fibers were washed with ethanol solution twice to remove excess silane agent. The fibers were taken out from the solution and were cured in a vacuum oven at 110℃ for 10 min (at 1 bar). The real time images of silanization of fibers is shown in Figure 3.4.

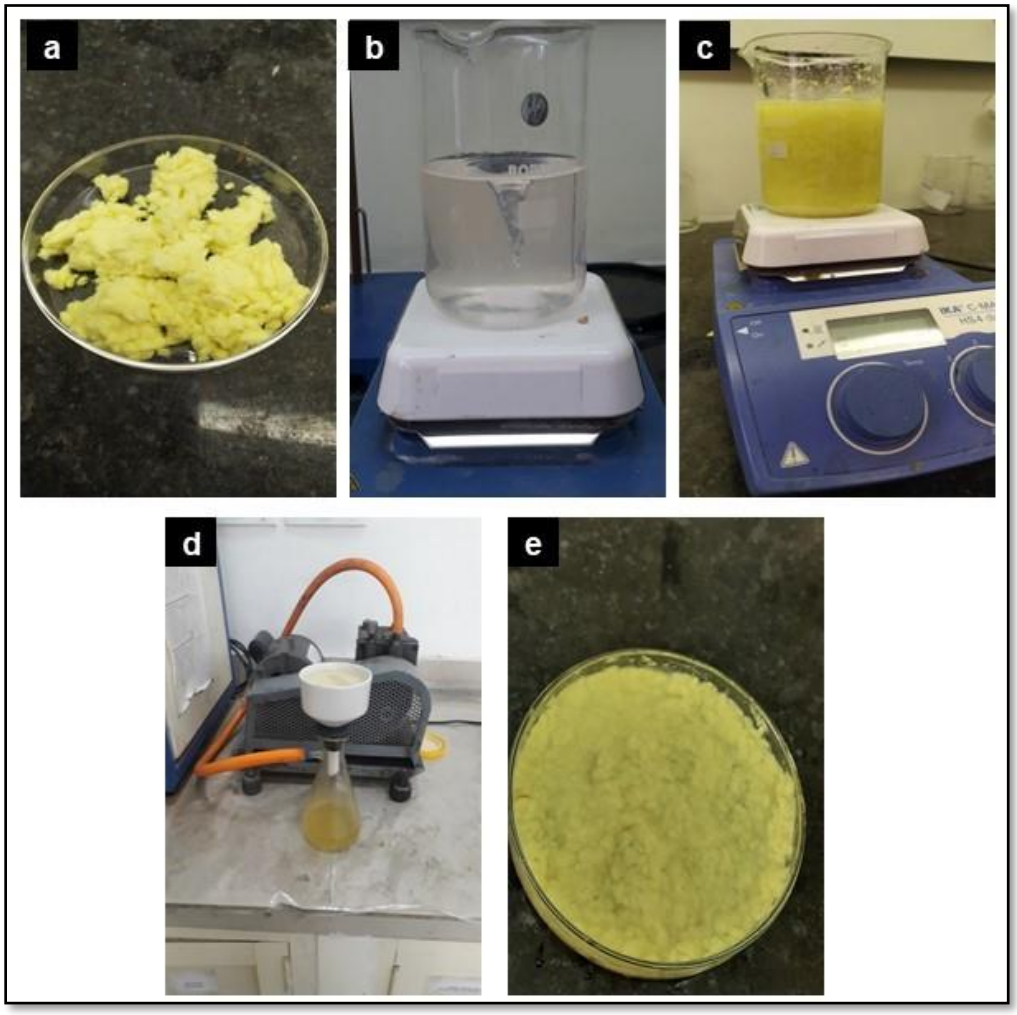

Figure 3.3. Real time images of phosphoric acid treatment of para-aramid fibers showing (a) pristine para-aramid fibers, (b) preparation of phosphoric acid solution with the help of magnetic stirring, (c) para-aramid fibers being magnetically stirred in phosphoric acid solution, (d) vacuum filtration of para-aramid fibers after treatment, and (e) phosphoric acid treated para-aramid fibers.

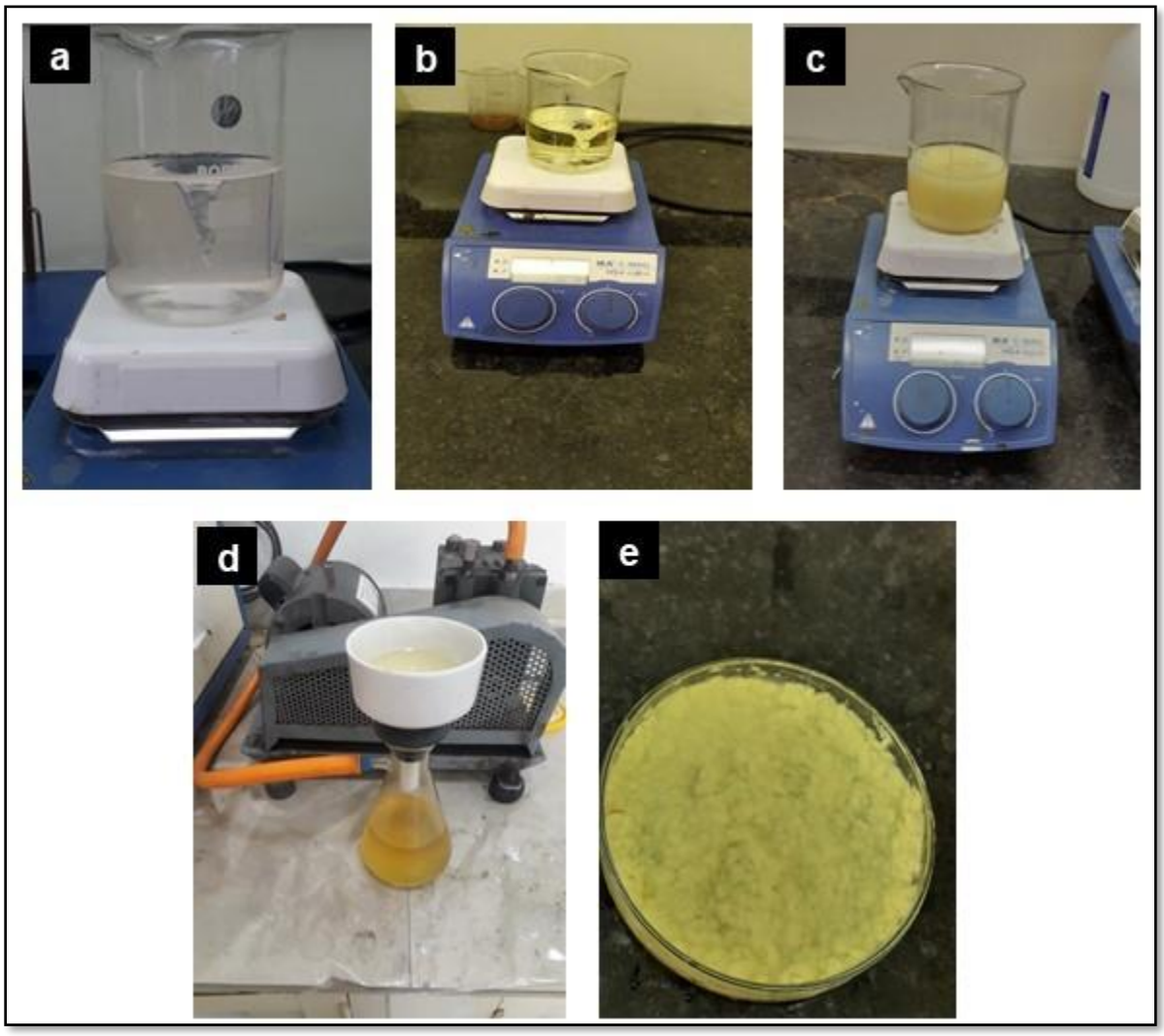

Figure 3.4. Real time images of silane treatment of para-aramid fibers (a) mixing of acetone and silane agent with help of magnetic stirrer, (b) hydrolyzed solution, (c) para-aramid fibers being mixed with silane agent solution with the help of magnetic stirrer, (d) vacuum filtration of para-aramid fibers after silanization, (e) silanized para-aramid fibers.

3.6.4 UV-assisted MAH grafting

MAH granules equal to the weight of fibers to be treated were dissolved in acetone. A fixed quantity of fibers was dipped in acetone-MAH solution and exposed to UV rays for different time periods (0.5–7 h) to determine the optimum time for MAH grafting. After exposure to UV radiations, treated fibers were washed with acetone to wash out unreacted MAH solution. The treated fibers were dried in an oven. Finally, the weight of dried fibers was noted. The real time

images of UV-assisted MAH grafting are shown in Figure 3.5. The weight gain details of different thermoplastic fibers after MAH grafting are given in Table 3.2–3.4.

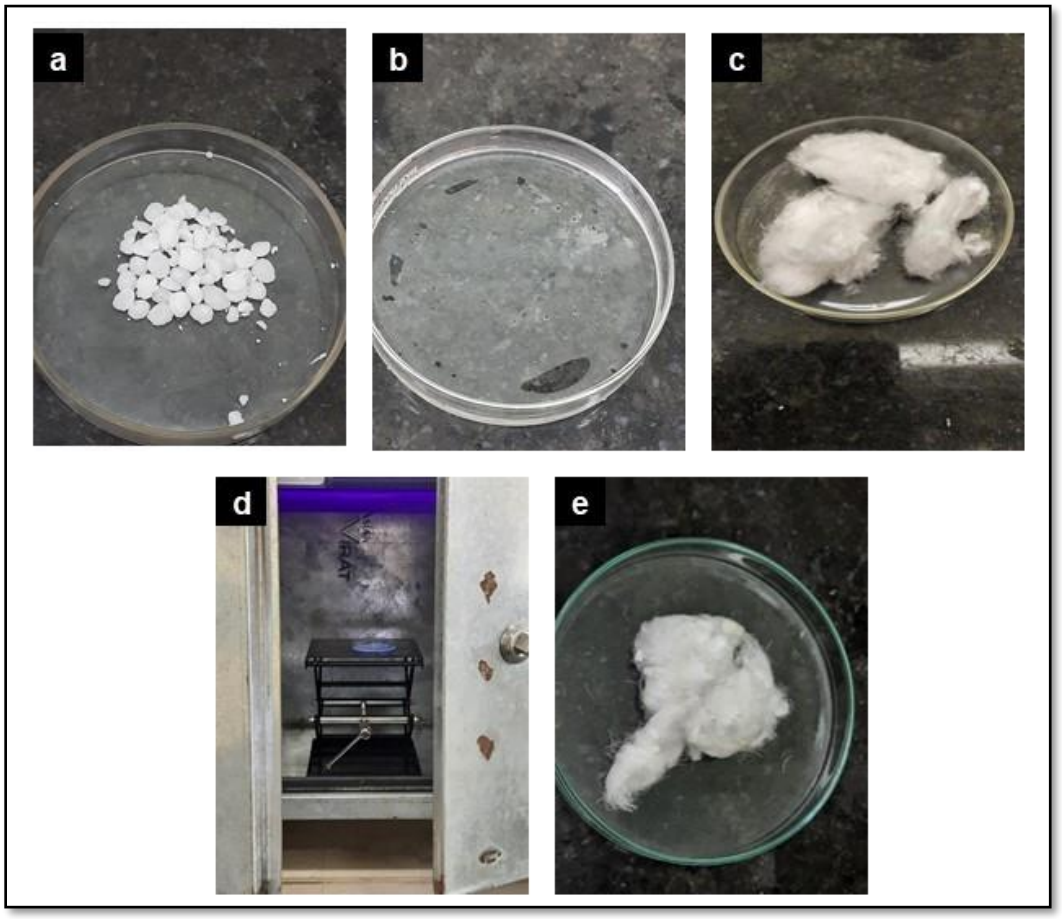

Figure 3.5. Real time images of UV-assisted MAH grafting of UHMWPE fibers showing (a) MAH granules, (b) MAH granules dispersed in acetone, (c) pristine UHMWPE fibers, (d) UHMWPE fibers dipped in MAH/acetone solution exposed to UV radiations, and (e) MAH grafted UHMWPE fibers.

Table 3.2. Details of weight gain of UHMWPE fibers after MAH grafting.

S. No.	Initial weight (g)	Time period (h)	Final weight (g)	Percentage weight gain (%)
1	2.000	1.0	2.110	5.50
2	2.000	2.0	2.170	8.50
3	2.000	3.0	2.340	17.00
4	2.000	4.0	2.400	20.00
5	**2.000**	**4.5**	**2.790**	**39.50**
6	2.000	5.0	2.620	31.00
7	2.000	5.5	2.440	22.00
8	2.000	6.0	2.225	11.25
9	2.000	7.0	2.170	8.50

Table 3.3. Details of weight gain of para-aramid fibers after MAH grafting.

S. No.	Initial weight (g)	Time period (h)	Final weight (g)	Percentage weight gain (%)
1	3.000	0.5	3.940	31.33
2	3.000	1.0	4.091	36.37
3	3.000	1.5	4.210	40.33
4	**3.000**	**2.0**	**4.855**	**61.83**
5	3.000	2.5	4.245	41.50
6	3.000	3.0	3.751	25.03
7	3.000	3.5	3.210	7.00
8	3.000	4.0	3.160	5.33
9	3.000	4.5	3.008	0.27

Table 3.4. Details of weight gain of Inviya fibers after MAH grafting.

S. No.	Initial weight (g)	Time period (h)	Final weight (g)	Percentage weight gain (wt.%)
1.	1.000	1	1.005	0.5
2.	1.000	2	1.202	20.2
3.	1.000	3	1.230	23
4.	1.000	4	1.271	27.1
5.	**1.000**	**4.5**	**1.341**	**34.1**
6.	1.000	5	1.304	30.4
7.	1.000	5.5	1.131	13.1
8.	1.000	6	1.100	10
9.	1.000	7	1.100	10

3.7 Fabrication of multi-filler reinforced epoxy based GFRPs

3.7.1 Processing of epoxy-nanoclay suspension

For processing of epoxy-nanoclay suspension, nanoclay (2 phr; fixed quantity) was dried in vacuum oven at 110 ℃ for 15 min. Epoxy resin and nanoclay (pristine or silanized, as per the case) were hand mixed with a stirrer. The suspension was homogenized at 20000 rpm for 10 min. Ultrasonication was done at 80% amplitude for 10 min (pulse on 40 s; pulse off 20 s). The real time images of processing of epoxy-nanoclay suspension are shown in Figure 3.6.

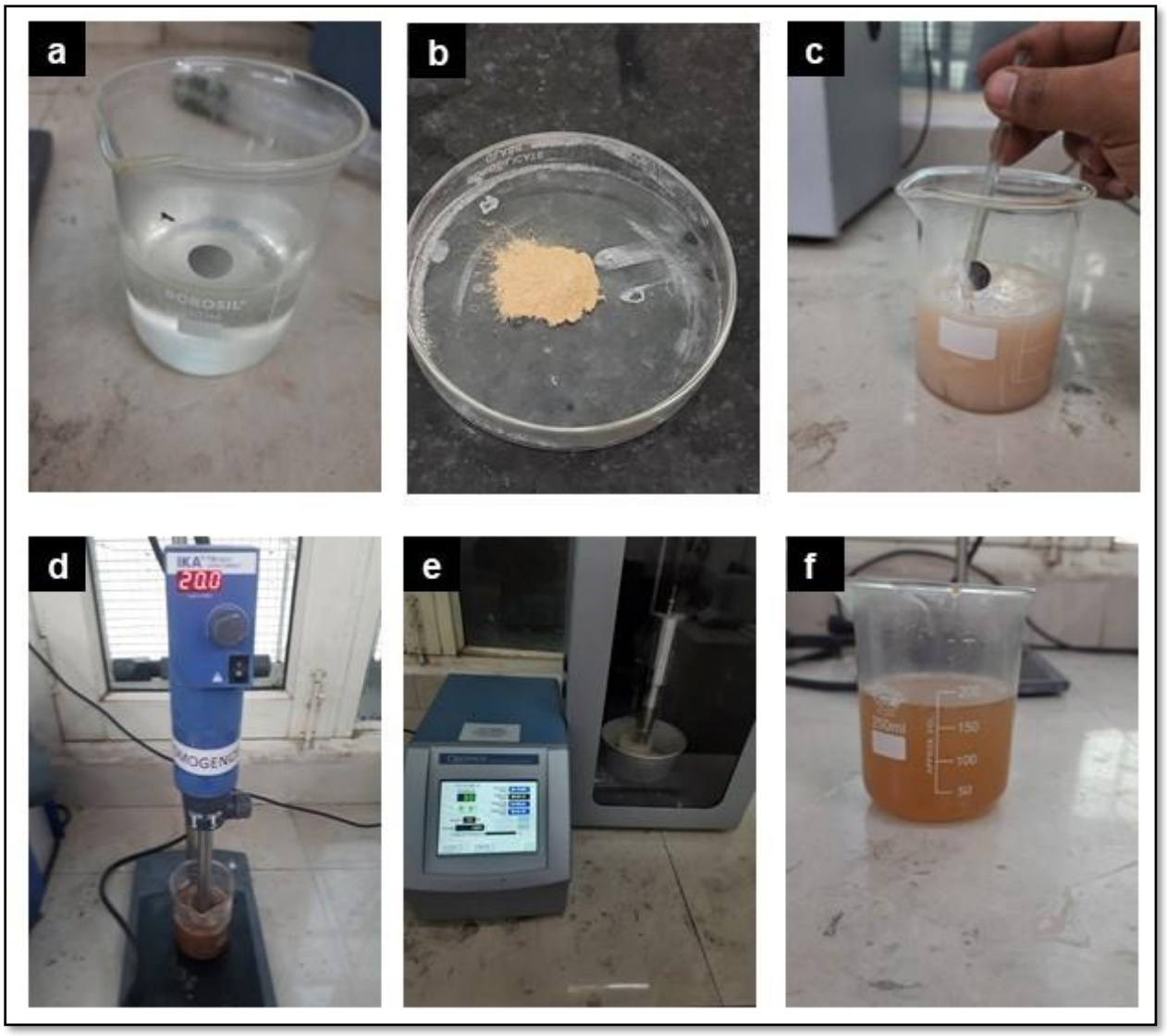

Figure 3.6. Real time images of dispersion of nanoclay in epoxy matrix showing (a) pristine epoxy, (b) silanized nanoclay, (c) hand mixing of nanoclay in epoxy, (d) homogenization of nanoclay in epoxy, (e) ultrasonication of nanoclay in epoxy, and (f) epoxy-nanoclay suspension.

3.7.2 Processing of epoxy-nanoclay-polymer fibers suspension

Thermoplastic fibers (pristine or modified, as per the case) were added to the epoxy-nanoclay suspension during homogenization (10,000 rpm; 5 min) followed by high speed homogenization (15,000 rpm; 5 min). Ultrasonication was done for 10 min. Again, the suspension was homogenized (10,000 rpm; 5 min). After cooling, as the temperature of suspension reached 35℃, curing agent was added and mechanical stirring was done for proper mixing. The suspension was

degassed with the help of a vacuum desiccator for 30 min for removal of trapped air. The real time images of processing of epoxy-nanoclay-thermoplastic fiber suspension are shown in Figure 3.7.

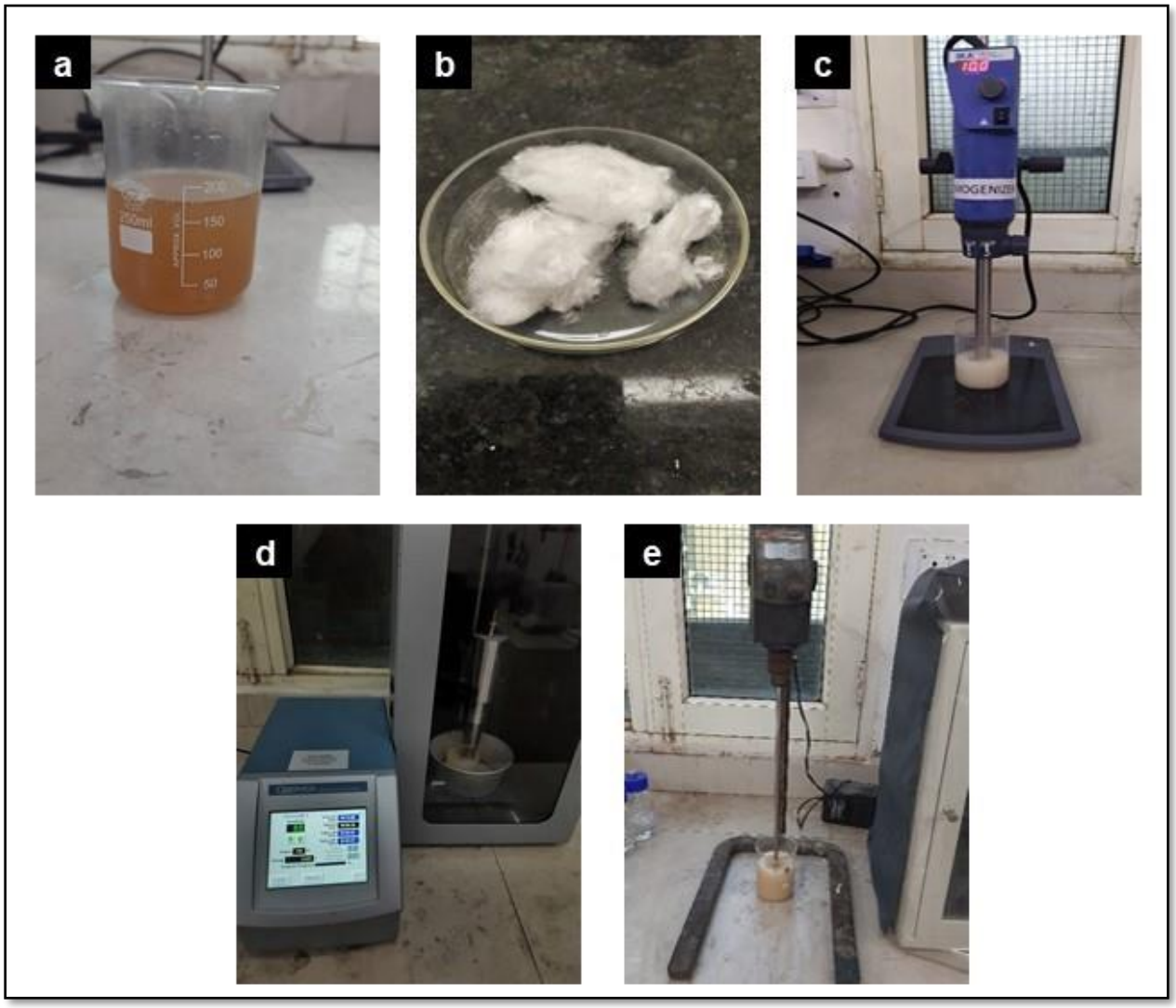

Figure 3.7. Real time images of dispersion of thermoplastic fibers in epoxy-nanoclay suspension showing (a) epoxy-nanoclay suspension, (b) pristine/compatibilized UHMWPE fibers, (c) homogenization of UHMWPE fibers in epoxy-clay suspension, (d) ultrasonication of UHMWPE fibers in epoxy-clay suspension, and (e) epoxy-nanoclay-UHMWPE-hardener suspension.

3.7.3 Processing of multi-filler reinforced epoxy based GFRPs through VARIM technique

VARIM set-up was used for processing of GFRPs. Glass fiber mats were cut in the required sizes (for impact samples, 30×10 mm; for tensile samples, 30×30 mm) and were placed on the VARIM table. These glass fiber mats were laid up using the epoxy-based suspension. The process was repeated to obtain the desired thickness (required number of plies) for testing as per the ASTM

standards. 2 plies of glass fiber mat were used for preparing tensile samples and 12 plies were used for impact samples. After the required number of plies were laid-up, the samples were covered with a separator cloth, followed by a perforated sheet, and finally a wire mesh. For removal of entrapped air, connections were made between this lay-up and vacuum ports of VARIM table with the help of a breather cloth and a vacuum bagging sheet. Curing and post-curing time schedule was (35 ℃ for 6 h) and (60 ℃ for 6 h) respectively. The real time images of fabrication of multi-scale filler reinforced epoxy based GFRPs through VARIM process are shown in Figure 3.8.

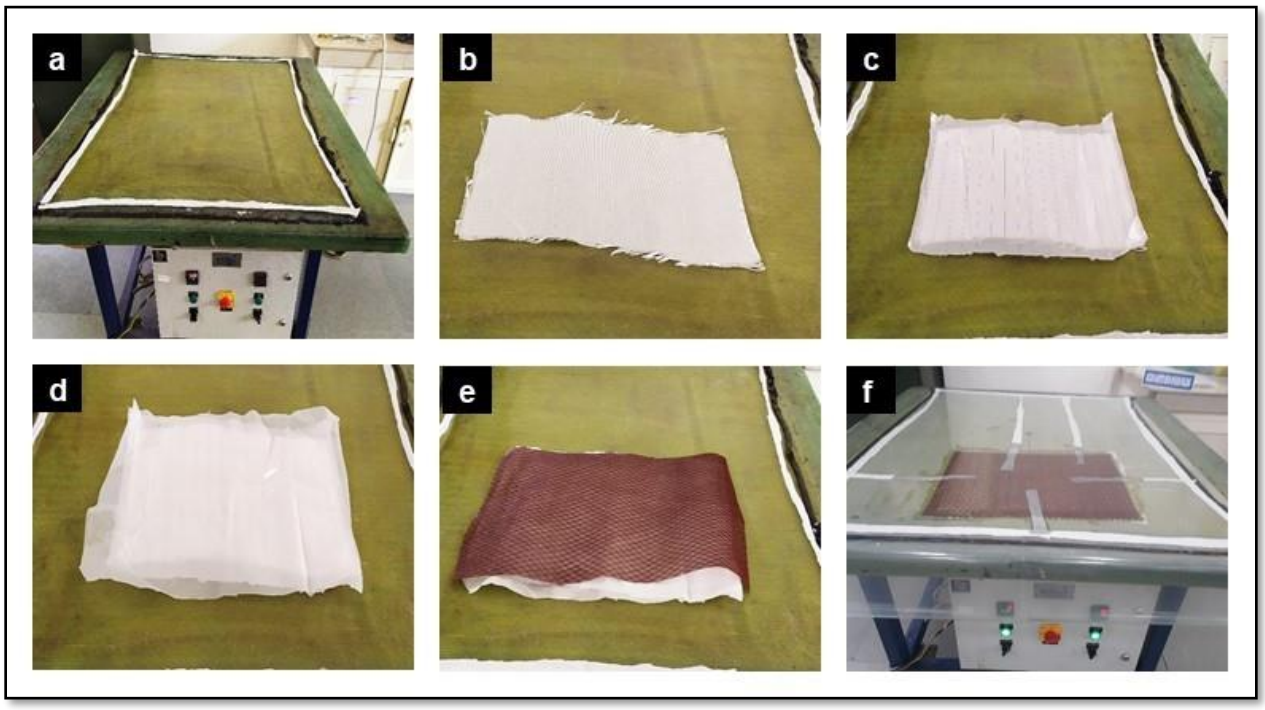

Figure 3.8. Real time images of processing of multi-scale filler reinforced epoxy based GFRP nanocomposites showing (a) breather cloth being applied on VARIM set-up, (b) glass fiber mat cut in required size kept on the VARIM table, (c) glass fiber mats laid-up with suspension covered with separating cloth, (d) separating cloth covered with perforated sheet, (e) perforated sheet covered with wire mesh, and (f) VARIM set-up prepared for air tight connections with the help of vacuum bagging sheet and sealant tape.

Details of sample designations used for different nanoclays and various GFRPs processed in the present research are presented in Table 3.5.

Table 3.5. Sample designations of nanoclays and epoxy based GFRP nanocomposites

S. No.	Sample Designation	Detail of nanoclays and processed GFRPs
1.	CA	Cloisite®15A nanoclay
2.	IE	Nanomer® I.28E nanoclay
3.	PG	Nanomer® PGV nanoclay
4.	1XPGAW	1X silane treated Nanomer® PGV with acetone washing(1X means that silane agent amount for surface treatment of nanoclay was 100% as proportion of nanoclay loading)
5.	2XPGAW	2X silane treated Nanomer® PGV with acetone washing
6.	3XPGAW	3X silane treated Nanomer® PGV with acetone washing
7.	4XPGAW	4X silane treated Nanomer® PGV with acetone washing
8.	1XPGAW*	1X silane treated Nanomer® PGV without acetone washing
9.	2XPGAW*	2X silane treated Nanomer® PGV without acetone washing
10.	3XPGAW* (PG* designation used in multi-filler reinforced epoxy based GFRPs)	3X silane treated Nanomer® PGV without acetone washing
11.	4XPGAW*	4X silane treated Nanomer® PGV without acetone washing
12.	RC	GFRP nanocomposite without nanoclay
13.	2CAC	GFRP nanocomposite reinforced with 2 phr of Cloisite®15A
14.	2IEC	GFRP nanocomposite reinforced with 2 phr of Nanomer® I.28E
15.	2PGC	GFRP nanocomposite reinforced with 2 phr of Nanomer® PGV
16.	1X2PGAWC	GFRP nanocomposite reinforced with 2 phr of 1X silanized Nanomer® PGV with acetone washing
17.	2X2PGAWC	GFRP nanocomposite reinforced with 2 phr of 2X silanized Nanomer® PGV with acetone washing
18.	3X2PGAWC	GFRP nanocomposite reinforced with 2 phr of 3X silanized Nanomer® PGV with acetone washing
19.	4X2PGAWC	GFRP nanocomposite reinforced with 2 phr of 4X silanized Nanomer® PGV with acetone washing
20.	1X2PGAW*C	GFRP nanocomposite reinforced with 2 phr of 1X silanized Nanomer® PGV without acetone washing
21.	2X2PGAW*C	GFRP nanocomposite reinforced with 2 phr of 2X silanized Nanomer® PGV without acetone washing
22.	3X2PGAW*C (2PG*C designation used in multi-filler reinforced epoxy based GFRPs)	GFRP nanocomposite reinforced with 2 phr of 3X silanized Nanomer® PGV without acetone washing
23.	4X2PGAW*C	GFRC nanocomposite reinforced with 2 phr of 4X silanized Nanomer® PGV without acetone washing
24.	T1	Potassium permanganate treatment
25.	T2	Silanization with 3-aminopropyltriethoxy silane
26.	T3	Potassium permanganate treatment followed by silanization

27.	T4	UV-assisted MAH grafting
28.	T5	Phosphoric acid treatment
29.	T6	Phosphoric acid treatment followed by silanization
30.	2PG*0.125UC	GFRP nanocomposite reinforced with 2 phr of silanized nanoclay and 0.125 phr of pristine UHMWPE fibers
31.	2PG*0.250UC	GFRP nanocomposite reinforced with 2 phr of silanized nanoclay and 0.250 phr of pristine UHMWPE fibers
32.	2PG*0.375UC	GFRP nanocomposite reinforced with 2 phr of silanized nanoclay and 0.375 phr of pristine UHMWPE fibers
33.	2PG*0.500UC	GFRP nanocomposite reinforced with 2 phr of silanized nanoclay and 0.500 phr of pristine UHMWPE fibers
34.	2PG*0.25UPC	GFRP nanocomposite reinforced with 2 phr of silanized nanoclay and 0.250 phr of UHMWPE fibers treated with potassium permanganate solution
35.	2PG*0.25UAC	GFRP nanocomposite reinforced with 2 phr of silanized nanoclay and 0.250 phr of UHMWPE fibers silanized with 3-aminopropyltriethoxy silane agent
36.	2PG*0.25UPAC	GFRP nanocomposite reinforced with 2 phr of silanized nanoclay and 0.250 phr of UHMWPE fibers treated with potassium permanganate solution followed by silanization with 3-aminopropyltriethoxy silane agent
37.	2PG*0.25UMC	GFRP nanocomposite reinforced with 2 phr of silanized nanoclay and 0.250 phr of UHMWPE fibers after UV-assisted MAH grafting
38.	2PG*0.5PC	GFRP nanocomposite reinforced with 2 phr of silanized nanoclay and 0.50 phr of pristine para-aramid fibers
39.	2PG*1.0PC	GFRP nanocomposite reinforced with 2 phr of silanized nanoclay and 1.00 phr of pristine para-aramid fibers
40.	2PG*1.5PC	GFRP nanocomposite reinforced with 2 phr of silanized nanoclay and 1.50 phr of pristine para-aramid fibers
41.	2PG*2.0PC	GFRP nanocomposite reinforced with 2 phr of silanized nanoclay and 2.00 phr of pristine para-aramid fibers
42.	2PG*1.0PPC	GFRP nanocomposite reinforced with 2 phr of silanized nanoclay and 1.00 phr of para-aramid fibers treated with phosphoric acid
43.	2PG*1.0PAC	GFRP nanocomposite reinforced with 2 phr of silanized nanoclay and 1.00 phr of para-aramid fibers silanized with 3-aminopropyltriethoxy silane agent
44.	2PG*1.0PPAC	GFRP nanocomposite reinforced with 2 phr of silanized nanoclay and 1.00 phr of para-aramid fibers treated with phosphoric acid solution followed by silanization with 3-aminopropyltriethoxy silane agent
45.	2PG*1.0PMC	GFRP nanocomposite reinforced with 2 phr of silanized nanoclay and 1.00 phr of para-aramid fibers after UV-assisted MAH grafting
46.	2PG*0.5IC	GFRP nanocomposite reinforced with 2 phr of silanized nanoclay and 0.50 phr of pristine Inviya fibers
47.	2PG*1.0IC	GFRP nanocomposite reinforced with 2 phr of silanized nanoclay and 1.00 phr of pristine Inviya fibers
48.	2PG*1.5IC	GFRP nanocomposite reinforced with 2 phr of silanized nanoclay and 1.50 phr of pristine Inviya fibers
49.	2PG*2.0IC	GFRP nanocomposite reinforced with 2 phr of silanized nanoclay and 2.00 phr of pristine Inviya fibers
50.	2PG*1.5IPC	GFRP nanocomposite reinforced with 2 phr of silanized nanoclay and 1.50 phr of Inviya fibers treated with phosphoric acid
51.	2PG*1.5IAC	GFRP nanocomposite reinforced with 2 phr of silanized nanoclay and 1.50 phr of Inviya fibers silanized with 3-aminopropyltriethoxy silane agent

52.	2PG*1.5IPAC	GFRP nanocomposite reinforced with 2 phr of silanized nanoclay and 1.50 phr of Inviya fibers treated with phosphoric acid solution followed by silanization with 3-aminopropyltriethoxy silane agent
53.	2PG*1.5IMC	GFRP nanocomposite reinforced with 2 phr of silanized nanoclay and 1.50 phr of Inviya fibers after UV-assisted MAH grafting

3.8 Testing and characterization

X-ray diffraction (X'Pert3 Powder diffractometer, PANalytical, Almelo, Netherlands) was used to determine the d-spacing (d_{001} peak) of nanoclay when it was in the pristine state (both unmodified and silanized state). Further, X-ray diffraction was also used for determining the nanoclay morphology (along with d-spacing details) when nanoclay was dispersed in the processed GFRP nanocomposites. The range of 2θ angle was selected in the range of 2−10°. The fabricated samples were crushed into a fine powder using a high speed mixer. The powder was used for XRD analysis. For TEM analysis (Hitachi, H-7500, Japan), the crushed fine powder was dispersed in ethanol with the help of a sonication bath (30 min). This suspension was used for preparing sample for TEM analysis on copper grid. The quality of dispersion of nanoclay in the processed GFRP system (whether uniformly distributed or not) and also its type of morphology obtained were ascertained by TEM analysis.

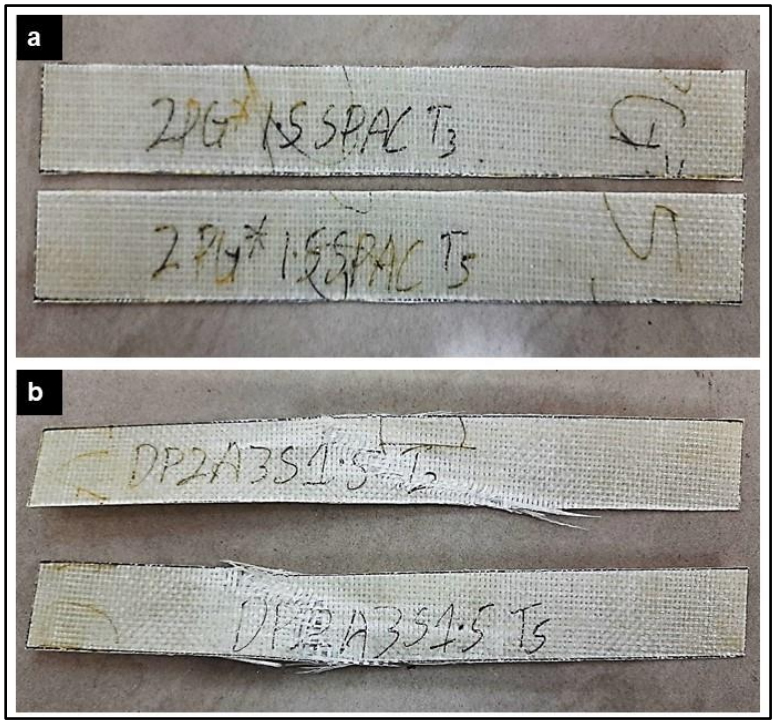

Figure 3.9. Actual images of tensile samples used in the present research (a) before, and (b) after tensile testing.

For FTIR samples, the samples (fibers/clay) mixed in potassium bromide and pellets were made, which was used as sample for FTIR analysis. Surface treatments of nanoclay and thermoplastic fibers were confirmed by FTIR analysis (Perkin-Elmer FTIR spectrometer RX-IFTIR, Massachusetts, US) conducted in the scanning range of 4000–400 cm^{-1}. Further, SEM (JSM-6510LV, JEOL, Tokyo, Japan)/FESEM-EDS (Carl Zeiss Sigma 500, ZEISS, Jena, Germany) micrographs were also used for confirming the surface treatment of thermoplastic fibers. Tensile specimens (as per ASTM D-3039 standard) and impact specimens (as per ASTM D 256–02 standard) were prepared using a diamond cutter. For illustration, the actual images of tensile and impact samples (before and after testing) for one of the compositions used in the present research are shown in Figure 3.9 and Figure 3.10 respectively. Universal testing machine (Zwick/Roell, Germany) having a load cell of 10 kN was used for tensile testing and Izod impact tester (ATS FAAR, Italy) having a least count of 0.01 J/m^2 was used for impact testing (Figure 3.11). Four samples were tested for each composition and property, and the mean value was reported. All the tests (tensile and impact tests) were evaluated at room temperature. For maintaining uniform environmental conditions in the laboratory, air conditioners were used. Temperature and humidity level of room was maintained at 25 ℃ and 40% respectively. Before performing the tests, the samples were kept at 25 ℃ for 48 h as per the requirements of ASTM standards.

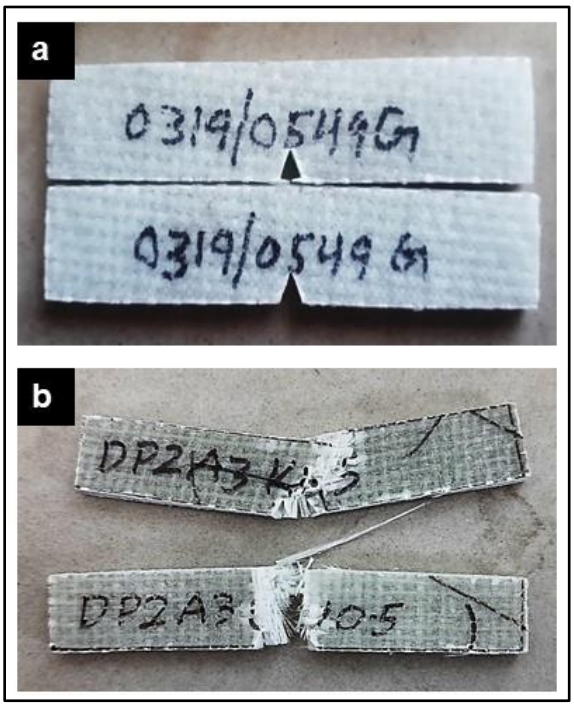

Figure 3.10. Actual images of impact samples used in the present research (a) before, and (b) after impact testing.

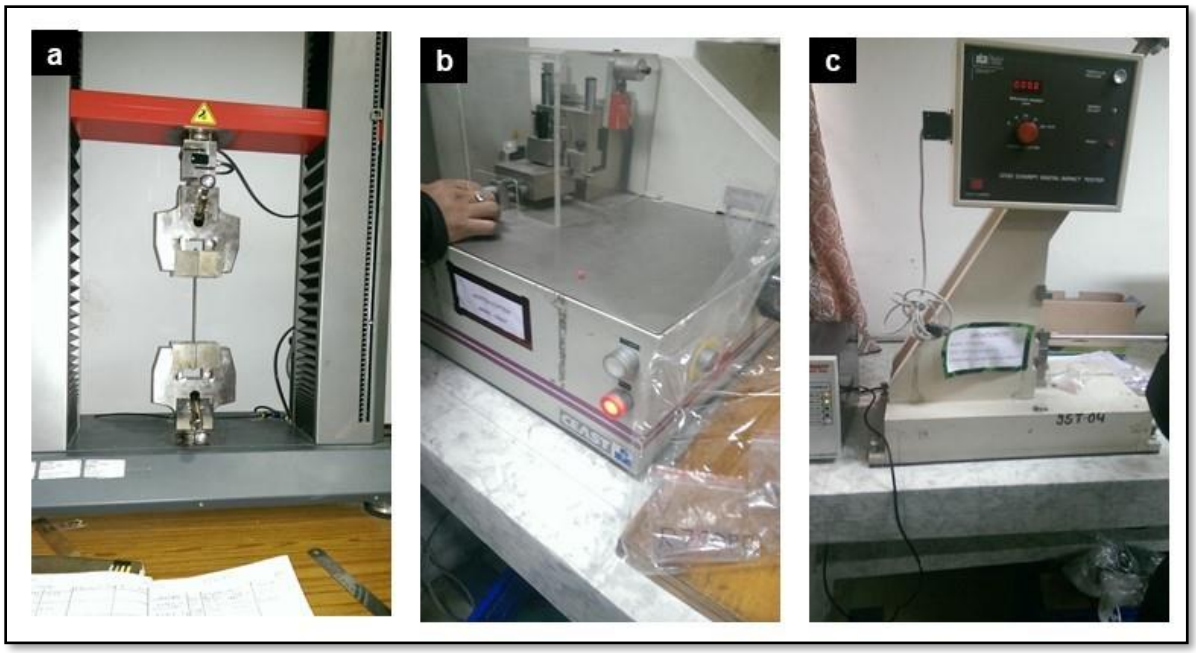

Figure 3.11. Real time images of the testing equipment showing (a) universal testing machine (UTM), (b) notch cutter for Izod impact test specimens, and (c) impact tester.

For better understanding of the mechanisms responsible for improved impact strength, SEM (JSM-6510LV, JEOL Limited, Tokyo, Japan) and FESEM (Carl Zeiss Sigma 500, ZEISS, Jena, Germany) analysis of fracture surface of impact test specimen of GFRP showing the highest impact strength was done.

The next chapter presents the results and discussion on the effect of reinforcing silanized nanoclay (different concentrations of silane agent used for silanization of nanoclay) on the impact strength and tensile properties of epoxy based GFRP nanocomposites.

Chapter 4. Effect of reinforcing nanoclay on the mechanical properties of GFRPs

4.1 Overview

This chapter presents the results and discussion on the impact strength and tensile properties obtained for the processed epoxy based GFRPs reinforced with silanized nanoclay. Different concentrations of silane agent were used for the silanization of nanoclay. During the silanization of nanoclay, there were two options viz. (a) rinse the silanized clay with acetone (acetone washing), and (b) do not rinse the silanized nanoclay with acetone (no-washing). The effect of acetone washing and no-washing after silane treatment on the mechanical properties of epoxy based GFRPs containing the reinforced silanized nanoclay is also discussed. The results of various characterization techniques (XRD, TEM, FTIR and SEM) used for validation of silanization of nanoclay, determination of morphology of nanoclay in the matrix material, and effectiveness of interfacial bonding between the constituents of nanocomposite system are also presented.

4.2 Mechanical properties of pristine/silanized nanoclay reinforced GFRPs

GFRP composite without nanoclay (RC; reference composite) showed an impact strength of 153 kJ/m^2. Different pristine nanoclays (CA, IE, and PG; defined in Table 3.5, Chapter 3) were reinforced separately into the reference composition to investigate the influence on impact strength of resulting composite system. Nanoclay loading was fixed at 2 phr in GFRPs. This was in line with an earlier research study of our research group [15]. Addition of each type of pristine nanoclay improved the impact strength of reference GFRP system (Figure 4.1 and Table 4.1). Maximum improvement in Izod impact strength (23.5% over the reference sample) was observed for the GFRP reinforced with pristine PG nanoclay (i.e. 2PGC nanocomposite sample). Addition of the other two types of pristine nanoclays (CA and IE respectively) resulted in only minor improvements in impact strength (6.5% and 4.0% respectively) of GFRP system. For this reason, only PG nanoclay was considered for further investigations (related to silanization of nanoclay under different conditions and its subsequent reinforcement in GFRPs for studying improvement in mechanical properties).

Figure 4.2 and Table 4.1 present the tensile strength and tensile modulus of processed GFRPs. Tensile stress versus percentage elongation behaviour is presented in Figure A1, Appendix I. Addition of 2 phr PG nanoclay to RC showed 14% and 4% improvement in tensile modulus and

tensile strength respectively. However, addition of IE and CA nanoclays resulted in deterioration of tensile strength and also the tensile modulus.

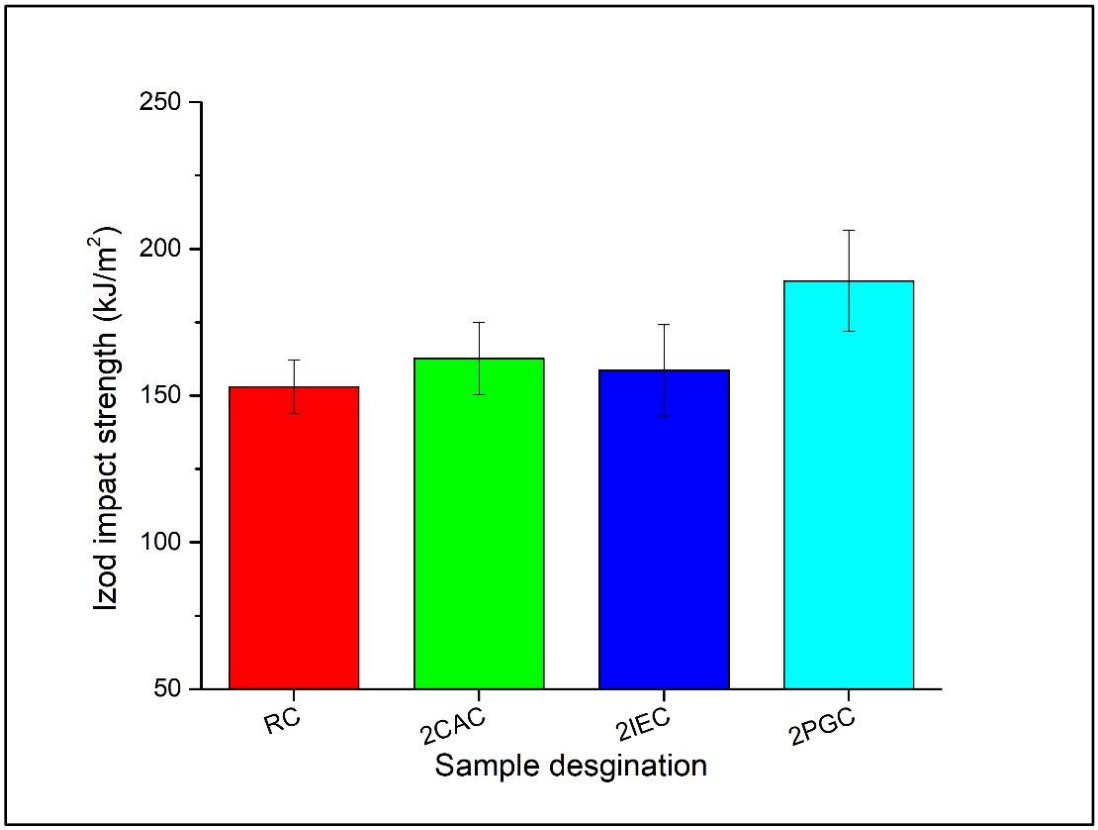

Figure 4.1. Impact strength of reference composite and various GFRPs reinforced with 2 phr of different pristine nanoclays.

Table 4.1. Mechanical properties of GFRPs reinforced with 2 phr of various pristine nanoclays and those reinforced with surface treated PG nanoclay under different silanization conditions.

S. No.	Sample Designation[#]	Impact Strength (kJ/m^2)	Tensile Strength (MPa)	Tensile Modulus (GPa)
1.	**RC**	**153±9**	**338±7**	**7.48±0.10**
2.	2PGC	189±17	351±4	8.51±0.04
3.	2CAC	163±12	326±6	7.31±0.06
4.	2IEC	159±15	331±3	7.33±0.04
5.	1X2PGAWC	169±11	320±9	7.31±0.08
6.	2X2PGAWC	209±3	344±7	7.71±0.03
7.	3X2PGAWC	187±13	319±3	7.59±0.11
8.	4X2PGAWC	180±10	335±6	7.55±0.06
9.	1X2PGAW*C	174±12	379±6	8.08±0.03
10.	2X2PGAW*C	189±3	348±7	7.98±0.10
11.	**3X2PGAW*C**	**194±2**	**392±9**	**7.91±0.02**
12.	4X2PGAW*C	187±2	356±7	7.88±0.01

#: Details of various designations is given in nomenclature

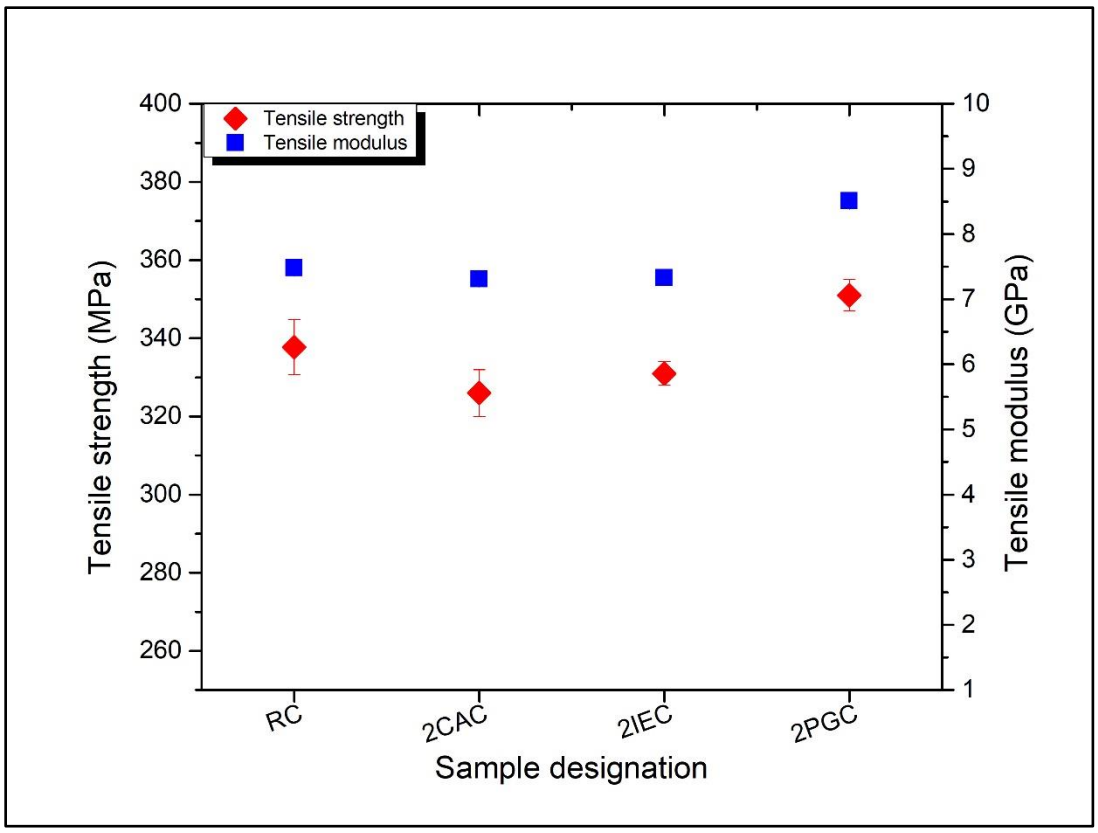

Figure 4.2. Tensile properties of reference composite and various GFRPs reinforced with 2 phr of different pristine nanoclays showing tensile strength and tensile modulus values.

The impact strength values obtained for reference composite and various GFRPs reinforced with silanized nanoclay are presented in Figure 4.3 and Table 4.1. PG nanoclay was silanized with four different concentrations of silane agent (1X–4X, where X signifies that silane agent amount used for surface treatment as a proportion of nanoclay loading). For all these concentrations, two cases of processing were used (a) 'with acetone washing', and (b) 'without acetone washing' (explained in Section 3.5, Chapter 3). All GFRPs reinforced with silanized nanoclay ('with acetone washing') showed improved impact strength over the RC composite. Highest impact strength (37% higher than RC) was shown by 2X2PGAWC nanocomposite (Figure 4.3). Similarly, all GFRPs reinforced with silanized nanoclay ('without acetone washing') also showed improved impact strength over the RC composite, though the improvements were slightly lesser with regard to their 'with acetone washing' counterparts for a given silane concentration-GFRP composition. Highest Izod impact strength for this category was shown by 3X2PGAW*C nanocomposite (27% higher than RC; Figure 4.3). For both the cases, impact strength of nanocomposites reinforced with silanized

nanoclay improved with increase in silane concentration till an optimum concentration (2X for the case of 'with acetone washing' and 3X for the case of 'without acetone washing').

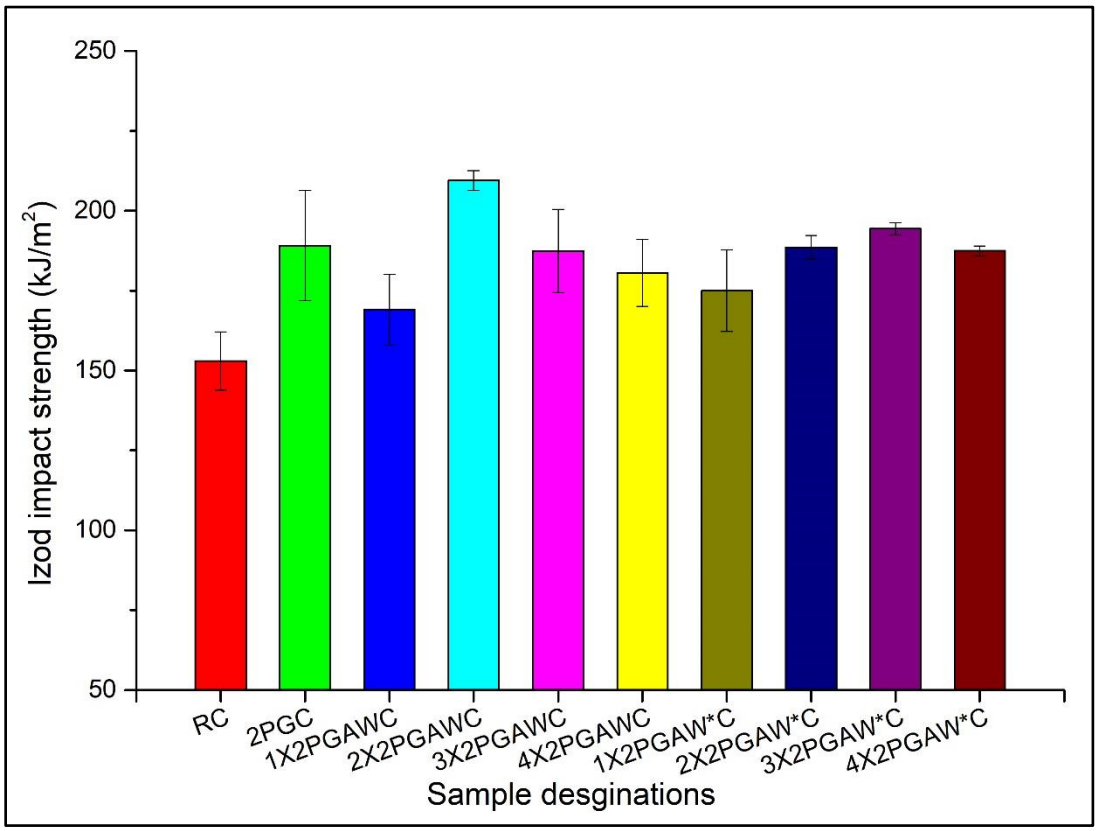

Figure 4.3. Impact strength of reference composite and various GFRPs reinforced with 2 phr of surface treated PG nanoclay under different silanization conditions.

Tensile properties of GFRPs did not improve with reinforcement of silanized nanoclay for the case of 'washing with acetone' (Table 4.1 and Figure 4.4). However, GFRPs reinforced with silanized nanoclay for the case of 'without acetone washing' showed improvements in tensile properties. Maximum improvement in tensile strength and tensile modulus (16% and 6% higher respectively than RC) was observed for 3X2PGAW*C nanocomposite (GFRP reinforced with 2 phr of 3X silanized PG clay 'without acetone washing').

Further, 3X2PGAW*C nanocomposite also showed 27% improvement in impact strength over RC (as discussed earlier). Though, increase in impact strength was lesser than 'with acetone washing' counterpart (27% and 37% respectively), but considering improvement in both the properties (tensile properties as well as impact strength), the performance of GFRPs reinforced with silanized clay of 'without acetone washing' case was better.

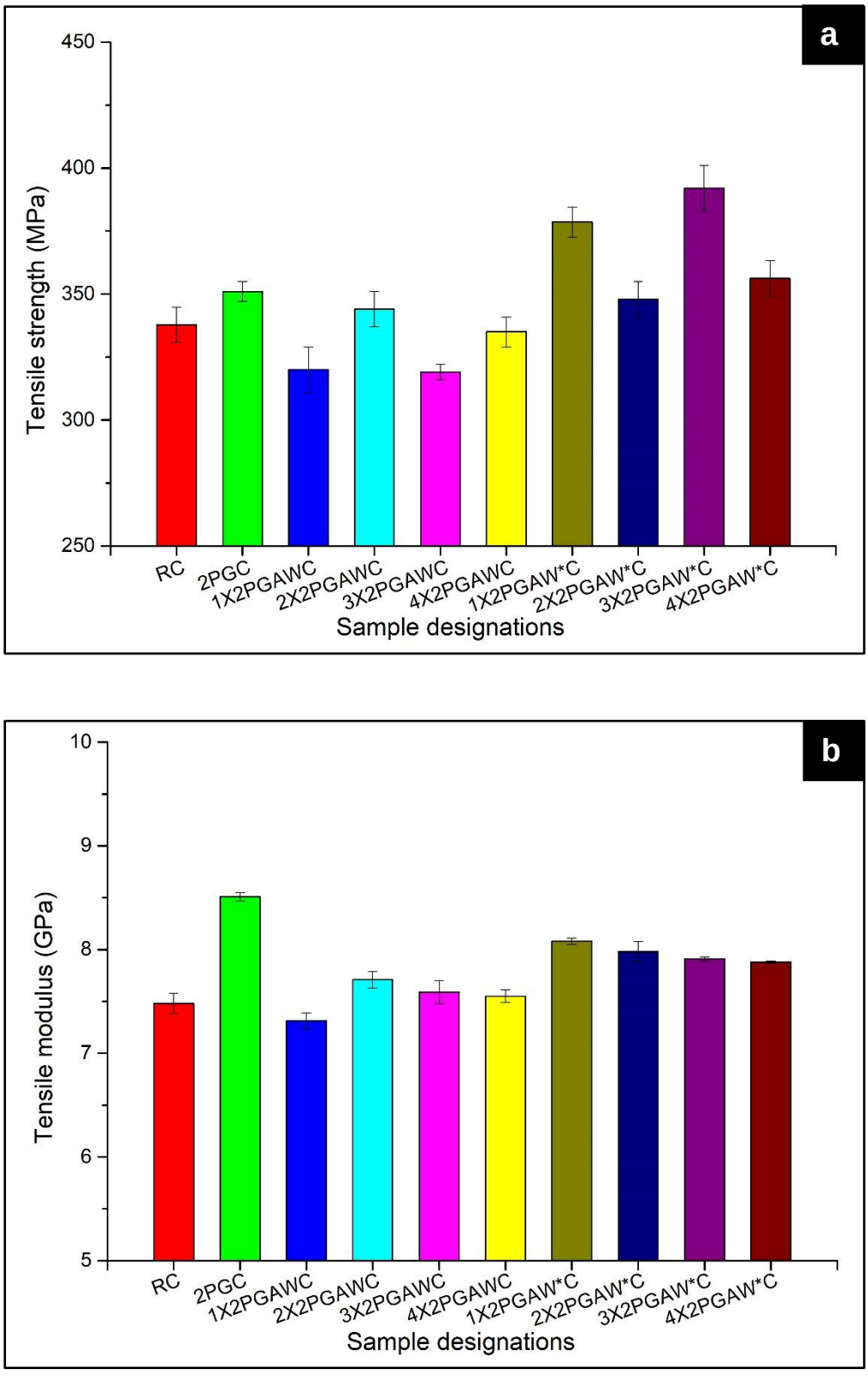

Figure 4.4. Tensile properties of reference composite and various GFRPs reinforced with 2 phr of surface treated PG nanoclay under different silanization conditions showing (a) tensile strength, and (b) tensile modulus values for composites.

Maximum improvement in all the properties was not achieved in a single composition because different mechanisms come into play for different strength behaviour.

Maximum improvement in tensile modulus was obtained for 2PGC composition. Addition of pristine nanoclay which is very rigid to the epoxy-hardener G FRP system improved the stiffness and hence the tensile modulus of 2PGC composite. Further, addition of silanized nanoclay to the epoxy-hardener GFRP system decreased the tensile modulus (as compared to 2PGC composition) because of the plasticizing effect of silane agent. Maximum improvement in tensile strength was obtained for 3X2PGAW*C composite. For this composition, since acetone washing was not done after silanization, the small nano-sized stacks of a few silicate layers were retained which resulted in better interfacial bonding among constituents of GFRPs. However, highest impact strength was observed for 2X2PGAWC composition due to the use of optimum silane concentration. The 3X2PGAW*C composition (without acetone washing) didn't show the highest impact strength due to excess of silane molecules which may act as plasticizers and deteriorated the impact strength.

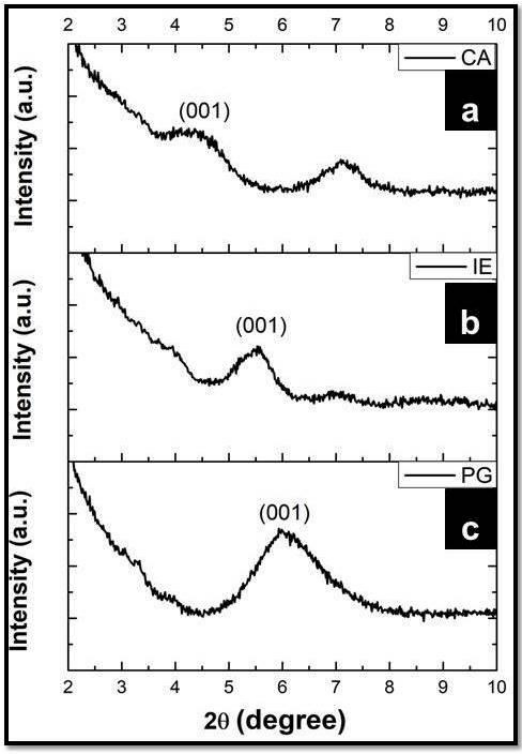

Figure 4.5. XRD micrographs of different pristine nanoclays to determine the location of d_{001} peak for (a) Cloisite®15A (CA), (b) Nanomer® I.28E (IE), and (c) Nanomer® PGV (PG) nanoclay.

For the silanized nanoclay, the layer of amino silane agent around the nanoclay surface reduces the platelet interaction and results in breaking of natural stacking sequence of platelets. This promotes uniform dispersion of clay at nano-level [20,92,195] which was validated through XRD and TEM analysis in the present research. Uniform clay dispersion results in more number of bonding sites between the epoxy-silanized nanoclay-glass fibers. Clay platelets dispersed at a nano-level also act as obstacles to crack propagation and result in crack deflection, crack pinning, and crack impeding [14,15].

4.3 XRD and TEM analysis

4.3.1 XRD diffractograms of different nanoclays for d-spacing values

Figure 4.5 presents the XRD diffractograms for various pristine nanoclays investigated in the present research.

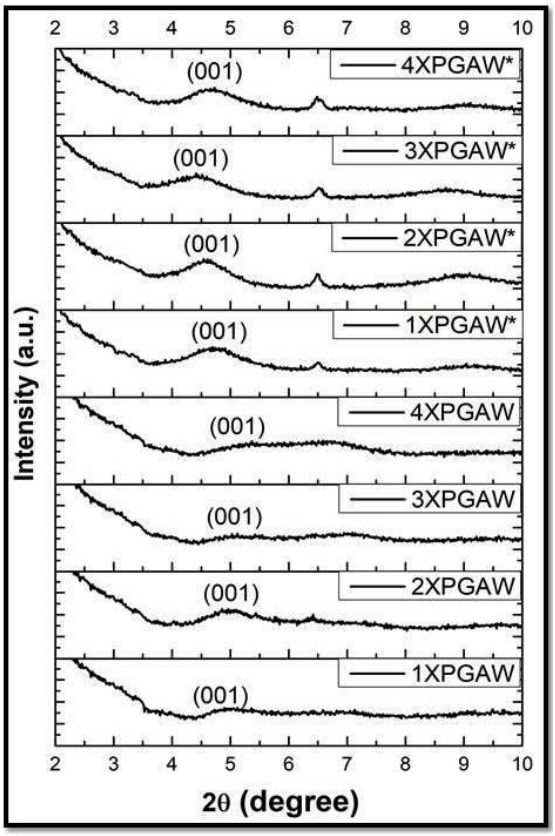

Figure 4.6. XRD diffractograms of silanized 'PG' nanoclay under different conditions.

The '2θ' values for the 'd_{001}' peak for 'CA', 'IE', and 'PG' nanoclays were determined as 4.57°, 5.55°, and 5.97° respectively corresponding to d-spacing value of 19.32 Å, 15.83 Å, and

14.80 Å, respectively. The d-spacing values for organically modified clays (i.e. 'CA' and 'IE' nanoclays) were higher than their unmodified hydrophilic counterpart ('PG' nanoclay). Similar observations had been also reported by Shelly *et al.* (2018) [15]. As stated earlier, 'PG' nanoclay was selected for silane treatment and also for further study in the present research because its reinforcement in the pristine state in GFRP resulted in better mechanical properties of GFRPs as compared to the other two counterparts ('IE' and 'CA' nanoclays).

4.3.2 XRD diffractograms of silanized PG nanoclay for d-spacing values

For silanization of PG nanoclay, silane agent concentration was selected as a proportion of weight of nanoclay (X) to be reinforced in the GFRP system. Silane agent concentrations considered to determine the optimum concentration for silane treatment were 1X, 2X, 3X, and 4X. Grafting of amino silane molecules (silane treatment) on the silicate platelets (nanoclay) shifted the d_{001} peak towards lower '2θ' angles (Figure 4.6). Silane treated nanoclay (for all cases) showed substantially higher d-spacing values than the pristine nanoclay (Table 4.2).

Hydroxyl groups present on the internal surfaces and edges of clay platelets react with amino silane and shift the d_{001} peak towards lower 2θ angles (thereby increasing the d-spacing). Si─O─Si covalently bonded 'bridge' between clay and silane agent pulls the outer clay layers [196–198]. Increase in interlayer galleries gives more chance to silane molecules to penetrate into the galleries resulting in more d-spacing [195].

Table 4.2. Values of d-spacing for different nanoclays.

	Sample Designation	2θ angle (degrees)	d_{001} spacing (Å)
1.	**Pristine nanoclays**		
	a) CA	4.570	19.319
	b) IE	5.577	15.834
	c) PG	5.968	14.797
2.	**'PG' nanoclay treated with different concentrations of silane agent**		
	a) 1XPGAW	5.293	16.683
	b) 2XPGAW	4.973	17.755
	c) 3XPGAW	4.878	18.100
	d) 4XPGAW	4.949	17.840
	e) 1XPGAW*	4.914	17.969
	f) 2XPGAW*	4.618	19.121
	g) 3XPGAW*	**4.464**	**19.780**
	h) 4XPGAW*	4.511	19.573

The highest d-spacing value (with maximum shifting of d_{001} peak towards the left) was observed for nanoclay treated with 3X silane agent, for both type of cases viz. 'with acetone washing' and 'without acetone washing'. The 2θ shift was from 5.968° to 4.878° and from 5.968° to 4.464° for the two cases respectively. Increase in d-spacing value was till an optimum concentration of silane agent (here 3X). These observations were attributed to availability of silane molecules in abundance which could intercalate between the clay layers forming a silane three-dimensional network. Beyond a limit, new silane molecules could not further intercalate between the clay layers owing to which no further increase in d-spacing was observed [195]. Further, for any given silane concentration, the silane treated clays of the case, 'without acetone washing', showed more d-spacing than nanoclays washed with acetone after silane treatment ('with acetone washing' case). This suggested that nano-sized clay platelets were being 'washed out' of the material on washing with acetone. As a result, comparatively large sized clay particles were being retained after washing which provided lesser d-spacing [25].

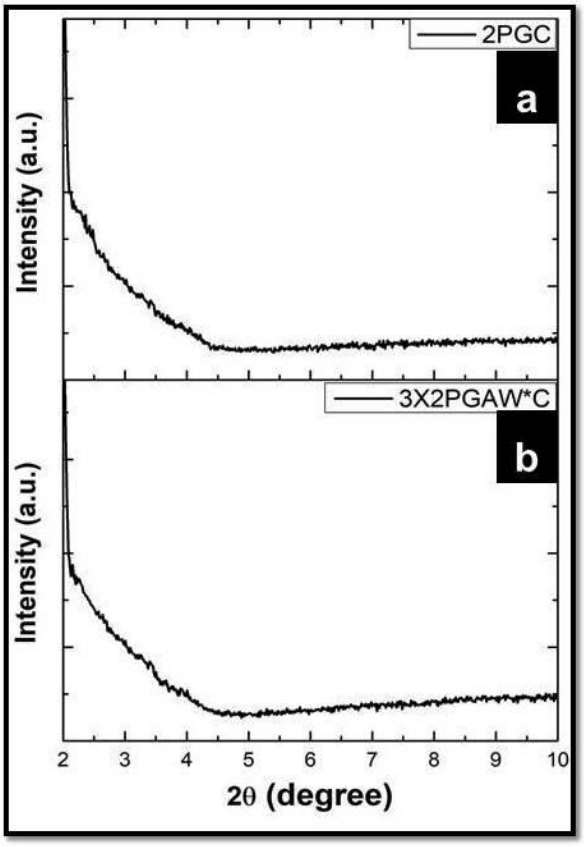

Figure 4.7. XRD diffractograms of (a) 2PGC nanocomposite and (b) 3X2PGAW*C nanocomposite for observing the type of nanoclay morphology obtained in GFRPs.

4.3.3 XRD and TEM analysis of GFRPs for clay morphology

GFRPs reinforced with pristine PG nanoclay as well as those containing silanized PG nanoclay did not show any d_{001} peak in XRD diffractograms indicating partially/fully exfoliated clay morphology in the processed GFRPs. Figure 4.7 shows diffractograms for two of the processed GFRPs (a) 2PGC nanocomposite (i.e. GFRP containing 2 phr of pristine PG nanoclay), and (b) 3X2PGAW*C nanocomposite (i.e. GFRP showing the best combination of impact strength and tensile properties containing 2 phr of 3X silanized PG nanoclay of 'without acetone washing' case).

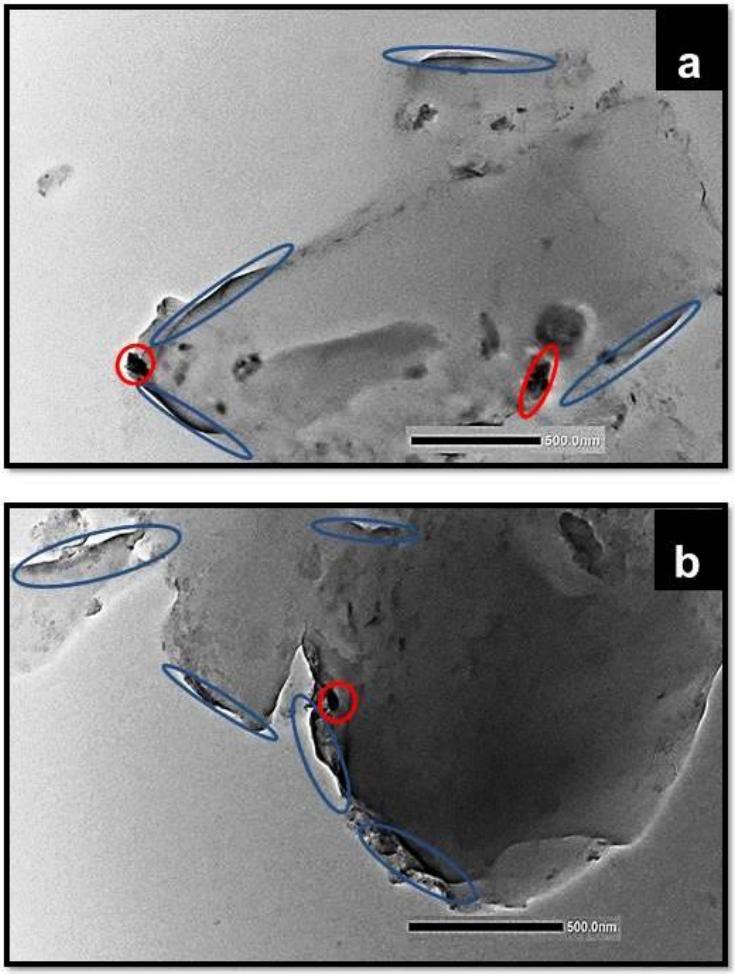

Figure 4.8. TEM micrographs of (a) 2PGC, and (b) 3X2PGAW*C nanocomposites for observing the type of nanoclay morphology obtained in GFRPs.

For validation of XRD results, TEM analysis of two of the processed GFRPs was performed (Figure 4.8). TEM micrographs revealed a mixed type of nanoclay morphology comprising of (a) mainly exfoliated silicate platelets dispersed randomly (blue highlighted areas), and (ii)

intercalated structures at a few places (red highlighted areas). This showed that the epoxy resin monomers were able to penetrate into the interlayer galleries of silicate platelets. Consequently, either exfoliated platelets were randomly dispersed (complete exfoliation) or the interlayer galleries between the platelets increased (intercalation); thus, the nanoclay morphology achieved in the GFRPs processed in the present research has been mentioned as partially exfoliated. This exfoliated morphology confirmed that the processing conditions used in the present research for dispersion of nanoclay were effective, and thus, similar processing methodology was used for processing of all the GFRPs in the present work.

4.4 FTIR analysis to confirm silanization of nanoclay

FTIR analysis was used to confirm the silanization of clay platelets. FTIR spectrographs of pristine nanoclay and various silanized nanoclays are presented in Figure 4.9.

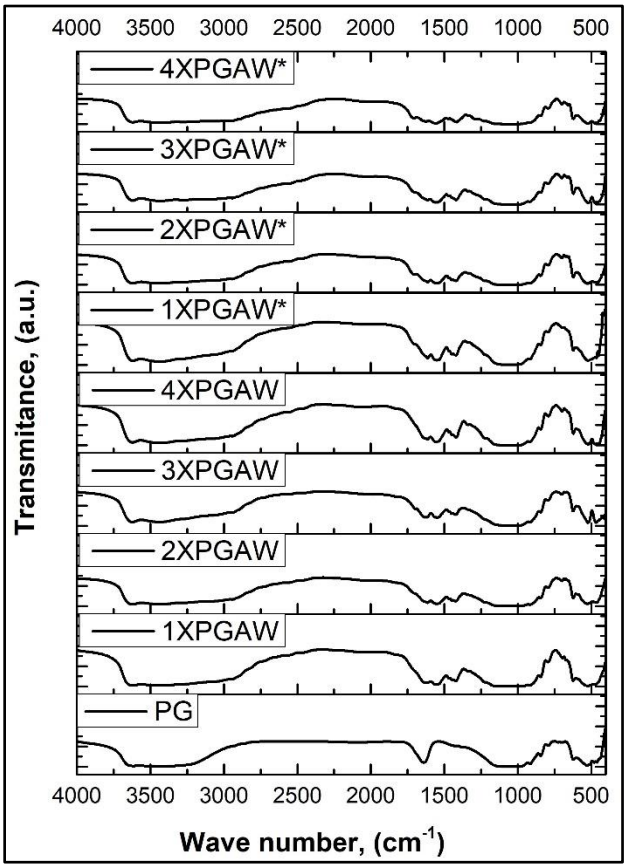

Figure 4.9. FTIR spectra of pristine nanoclay and silanized nanoclays under various conditions.

Montmorillonite nanoclay has been used in the present research. Its structure comprises of repeated units of two tetrahedral sheets and one octahedral sheet. Hydroxyl groups (OH groups) which are

formed from trapped water molecules or free silanol groups of the silane agents are generally available at the broken edges of platelets. Hydroxyl groups have good reactive ability, especially with the multi-functional silane agents [196,199]. OH groups are capable of getting condensed with hydrolysed–SiOH groups, or with water existing in silane molecules, or with $–SiOCH_2CH_3$ molecules present in other organic solvents [20,200–202].

The peak observed around 3620 cm^{-1} (for both, pristine as well as silanized nanoclays) corresponds to Al–OH or Mg–OH groups present in the nanoclay. This peak may also be linked to methanol group, silanol, or water [20,203]. Further, the broad peak observed around 3433 cm^{-1} (for both, pristine as well as silanized nanoclays) corresponds to the OH or N–H groups. OH group may have come from trapped water molecules from the surface of silicate platelets or from the free silanol groups of silane agents attached chemically/physically on the surface of nanoclay [195]. The peak shift from 1638 cm^{-1} to 1615 cm^{-1} after silane treatment corresponded to hydroxyl bending in absorbed water. The intensity of this peak reduced after silanization of nanoclay, which may be ascribed to covalent bonding of hydroxyl groups with silane agent. The new peak observed around 1550 cm^{-1} in silanized clays signified the bending vibration of –NH2 group [204]. The peaks observed in the range of 1500–700 cm^{-1} correspond to Si–O stretching [203]. Si–O–Si stretching vibration peak was detected around 1055 cm^{-1} in pristine clay. This peak around 1055 cm^{-1} broadened after silane treatment due to formation of extra Si–O–Si bonds. This broadening of the peak around 1055 cm^{-1} confirmed successful grafting of trifunctional amino silane into the interlayer galleries of silicate platelets [20]. Some peaks were observed around 844 cm^{-1}, 790 cm^{-1}, and 700 cm^{-1} (for both, pristine as well as silanized clays) which corresponded to the Al–Al–OH and Al–Mg–OH bending vibrations [205].

4.5 SEM analysis of fracture surface of impact test specimens of nanoclay reinforced GFRPs

SEM micrographs of the facture surface of Izod impact test samples of base composite and different GFRPs reinforced with pristine nanoclays are presented in Figure 4.10. Fracture surface of the reference composite (RC) presented a fine and smooth glass fiber surface (Figure 4.10a). It was observed that matrix material was not adhering to the glass fiber surface indicating lack of interaction between glass fibers and epoxy matrix. This resulted in lower Izod impact strength of the reference sample. Figure 4.10b–d presents the fracture surface of impact specimens of 2PGC, 2CAC, and 2IEC nanocomposites. The micrographs showed relatively rougher surface of glass

fibers as compared to that in the reference composite (RC). GFRP reinforced with PG nanoclay showed the roughest surface (Figure 4.10b) amongst pristine nanoclay reinforced GFRPs. This validated its highest impact strength among the GFRPs reinforced with different pristine nanoclays.

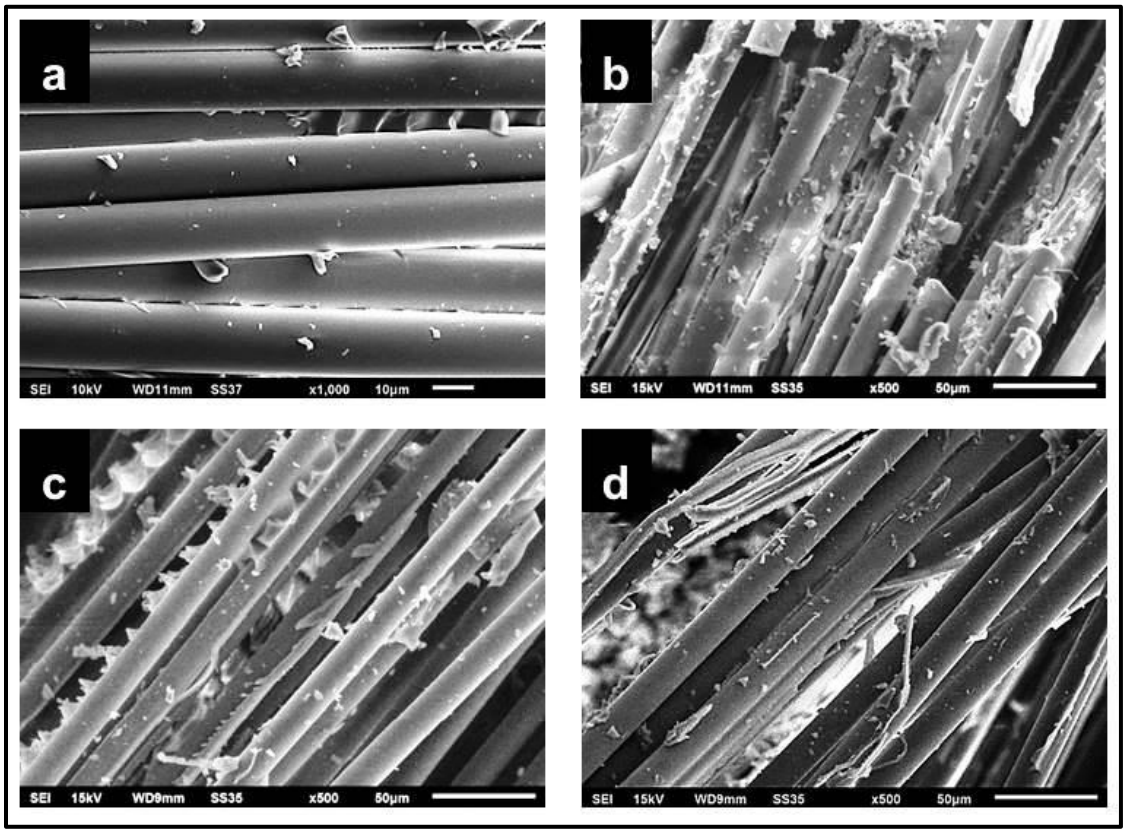

Figure 4.10. SEM micrographs of fracture surface of impact test specimens of (a) RC, (b) 2PGC, (c) 2CAC, and (d) 2IEC composites.

SEM micrographs of nanocomposites reinforced with 2X silane treated nanoclay for 'with acetone washing' case (2X concentration showed best combination of mechanical properties for 'with acetone washing' case) and 3X silane treated nanoclay for 'without acetone washing' (3X concentration showed best combination of mechanical properties for 'without acetone washing' case) are shown in Figure 4.11. Comparing the results of Figure 4.11a and Figure 4.11c with Figure 4.10b, it is clear that glass fiber surface is rougher in GFRPs reinforced with silanized clay (Figure 4.11a/Figure 4.11c) compared to the GFRP with pristine clay (Figure 4.10b). This indicated that addition of silanized nanoclay enhanced the interfacial interaction among various constituents of GFRPs. Figure 4.11a and Figure4.11c reveal that epoxy-silanized clay mixture was more uniformly distributed on the glass fiber surface due to affinity of silanized nanoclay layers with

glass fibers. This also suggested that there was a strong bonding among constituents of GFRPs reinforced with silanized nanoclay which improved the impact strength. Further, Figure 4.11b and Figure 4.11d revealed that there was no fiber pull-out, signifying significant interfacial bonding. For these reasons, GFRPs reinforced with silanized nanoclay showed superior impact strength.

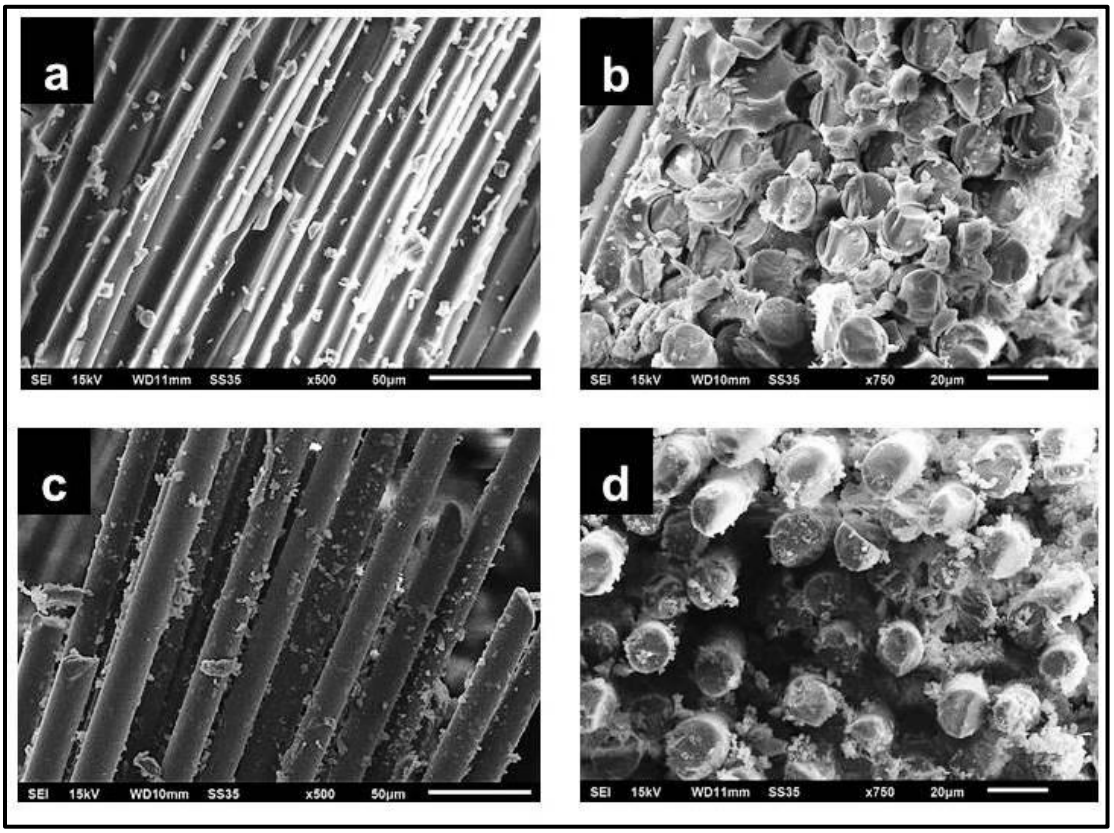

Figure 4.11. SEM micrographs of fracture surface of impact test specimens of GFRPs reinforced with 2 phr of silanized nanoclay for (a) 2X2PGAWC at X500, (b) 2X2PGAWC at X750, (c) 3X2PGAW*C at X500, and (d) 3X2PGAW*C at X750.

Reinforcement of 2 phr of 3X silane treated nanoclay ('without acetone washing') to the reference composite exhibited 27%, 16%, and 6% improvement in impact strength, tensile strength and tensile modulus respectively for the resulting GFRP nanocomposite.

The next chapter presents the results and discussion on the effect of reinforcing silanized nanoclay along with ultra high molecular weight polyethylene fibers (UHMWPE) on the impact strength and tensile properties of epoxy based GFRP nanocomposites.

Chapter 5. Effect of reinforcing UHMWPE fibers and silanized nanoclay on the mechanical properties of GFRPs

5.1 Overview

This chapter presents the results and discussion on the mechanical properties of epoxy based GFRPs reinforced with silanized nanoclay and ultra high molecular weight polyethylene (UHMWPE) fibers. Silanized nanoclay was added in a fixed amount and UHMWPE fibers were added in varying amounts for processing of various GFRPs. UHMWPE fibers were used both in the pristine as well as in the surface treated (compatibilized) state. Four compatibilization methods were used including (i) potassium permanganate treatment, (ii) silanization with 3-aminopropyltriethoxy silane agent, (iii) potassium permanganate treatment followed by silanization, and (iv) UV-assisted MAH grafting. The chapter also discusses the results of various characterization techniques (SEM, EDS, and FTIR) used for validation of compatibilization of UHMWPE fibers and for observing the interaction among various constituents of nanocomposite system.

5.2 Mechanical properties of nanoclay-UHMWPE fiber reinforced GFRPs

Figures 5.1–5.2 and Table 5.1 present the results of impact strength, tensile strength, and tensile modulus values obtained for GFRPs reinforced with 2 phr of silanized nanoclay and different concentrations of UHMWPE fibers (pristine as well as compatibilized). The tensile stress versus percentage elongation behaviour is given in Figure A2, Appendix I.

Impact strength and tensile properties improved after addition of 2 phr of PG nanoclay to the reference composite (RC). Epoxy based GFRP reinforced with 2 phr of pristine nanoclay (i.e. 2PGC) showed an improvement in mechanical properties (23.5%, 4%, and 14% improvement in impact strength, tensile strength, and tensile modulus respectively over reference composite, RC). Further, when epoxy based GFRP was reinforced with 2 phr of silanized nanoclay (i.e. 2PG*C) there was further improvement in impact strength and tensile strength (27% and 16% improvement respectively over RC). The improvement in mechanical properties was attributed to better bonding of silanized clay with epoxy. Silanized clay-epoxy bonding improved because of increased d-spacing of nanoclay after silanization (as discussed in Chapter 4). Further, the partially exfoliated morphology of nanoclay obtained in 2PG*C composite resulted in more number of interfacial bonding sites for epoxy-silanized clay-glass fiber system.

Table 5.1. Mechanical properties of GFRPs reinforced with 2 phr of silanized nanoclay and different concentrations of UHMWPE fibers (pristine as well as compatibilized).

S. No.	Sample Designation[#]	Impact Strength (kJ/m^2)	Tensile Strength (MPa)	Tensile Modulus (GPa)
1.	**RC**	**153±9**	**338±7**	**7.48±0.10**
2.	2PGC	189±17	351±4	8.51±0.04
3.	2PG*C	194±2	392±9	7.91±0.03
4.	2PG*0.125UC	144±14	368±4	7.58±0.04
5.	2PG*0.250UC	158±10	259±3	6.74±0.03
6.	2PG*0.375UC	147±3	315±2	7.34±0.05
7.	2PG*0.500UC	136±9	318±4	7.38±0.08
8.	2PG*0.25UPC	189±9	405±9	8.29±0.03
9.	2PG*0.25UAC	161±3	398±6	8.58±0.02
10.	**2PG*0.25UPAC**	**199±10**	**396±7**	**8.22±0.05**
11.	2PG*0.25UMC	191±1	364±7	8.46±0.06

#: Details of various designations is given in nomenclature

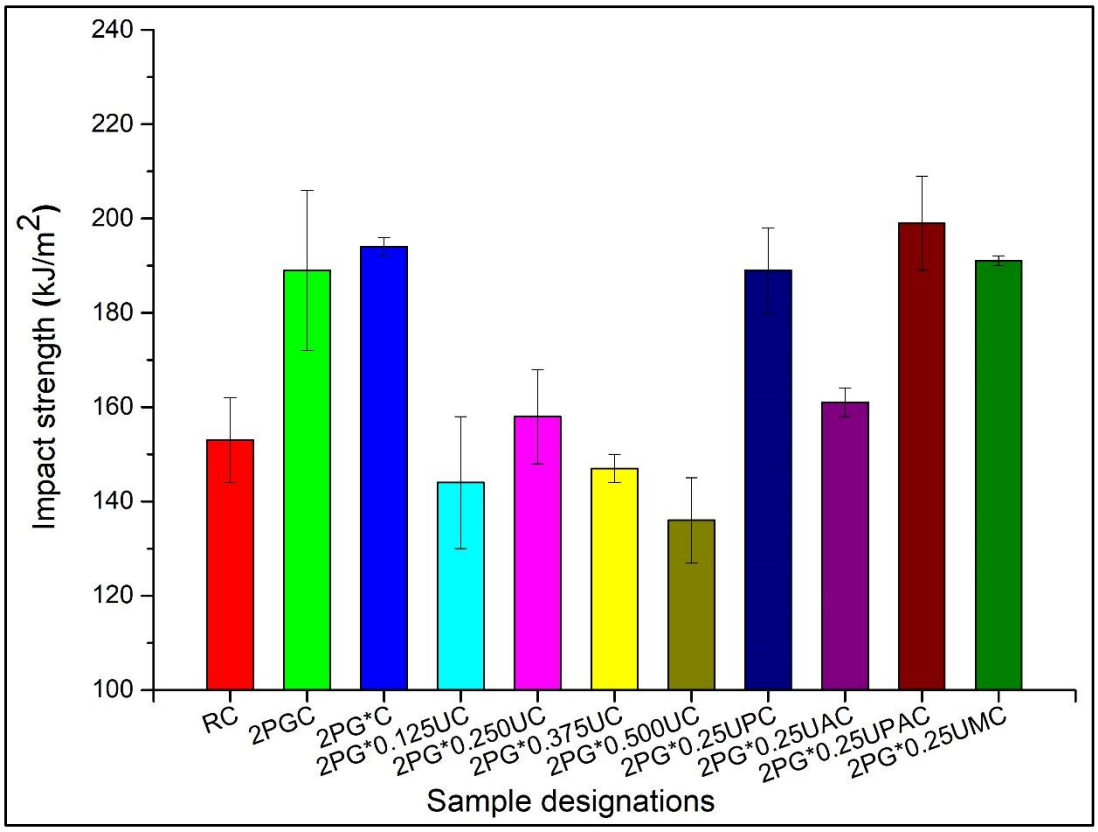

Figure 5.1. Impact strength of reference composite and various GFRPs reinforced with 2 phr of silanized PG nanoclay and different concentrations of UHMWPE fibers (pristine as well as compatibilized).

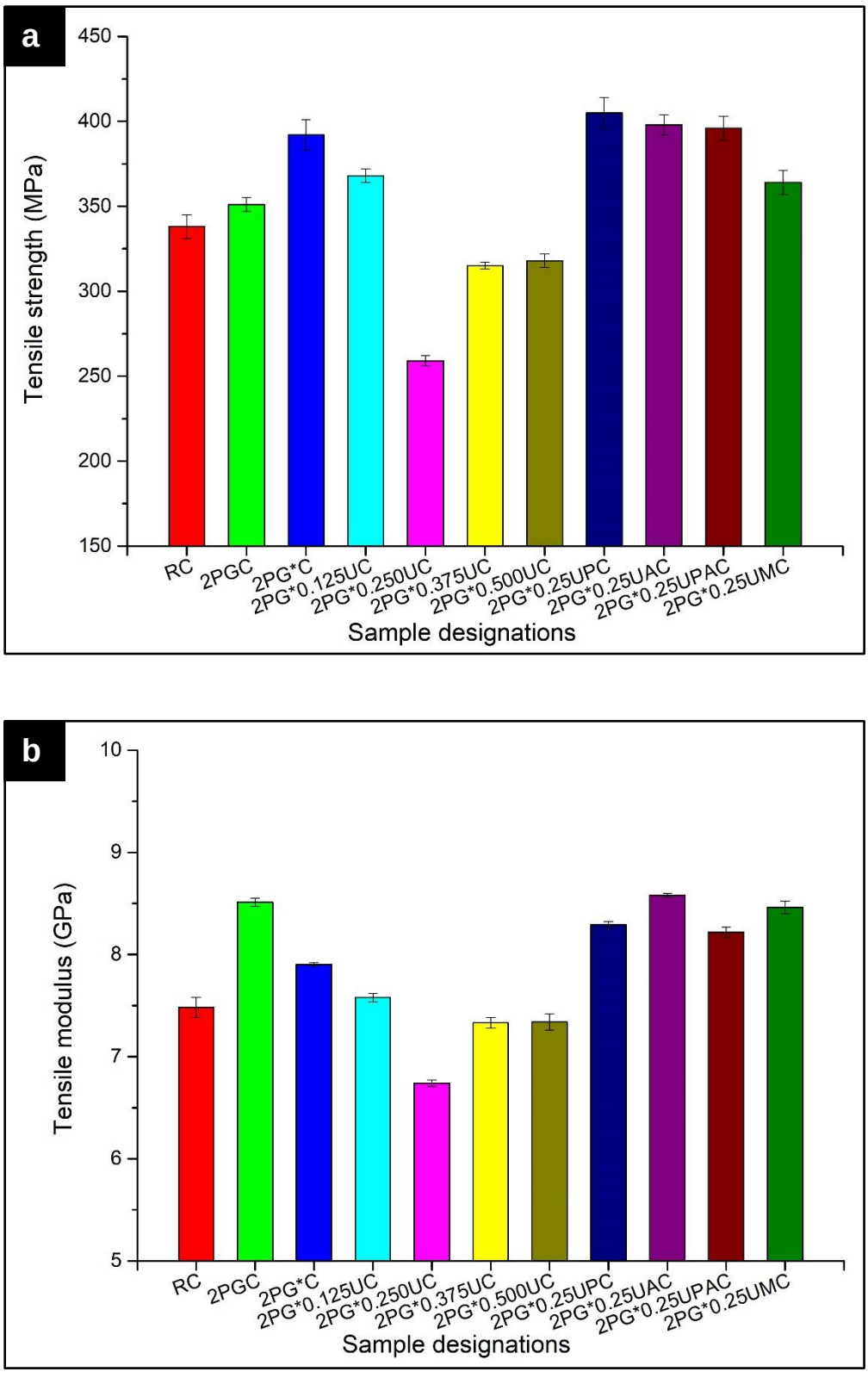

Figure 5.2. Tensile properties of reference composite and various GFRPs reinforced with 2 phr of silanized PG nanoclay and different concentrations of UHMWPE fibers (pristine as well as compatibilized) showing (a) tensile strength, and (b) tensile modulus values for composites.

Reinforcement of pristine UHMWPE fibers (in any concentration; 0.125−0.50 phr) to 2PG*C composite deteriorated the mechanical properties of resulting GFRP nanocomposites (2PG*0.125UC, 2PG*0.250UC, 2PG*0.375UC, and 2PG*0.500UC). Pristine UHMWPE fibers are chemically inert having a linear long chain with high degree of orientation and crystallinity [99,206,207]. This renders the pristine UHMWPE fibers unsuitable for interaction with epoxy causing poor interfacial bonding between the two, and hence, lower mechanical performance of resulting composites. To resolve this issue, UHMWPE fibers were subjected to surface treatment (compatibilization) using four different techniques viz. (i) potassium permanganate treatment (T1), (ii) silanization with 3-aminopropyltriethoxy silane agent (T2), (iii) potassium permanganate treatment followed by silanization (T3), and (iv) UV-assisted MAH grafting (T4). Among the pristine UHMWPE fiber reinforced epoxy-nanoclay based GFRPs, the best results (mechanical properties) were obtained with 0.250 phr UHMWPE fiber concentration. For this reason, 0.250 phr fiber loading was selected for processing of epoxy-nanoclay based GFRPs reinforced with compatibilized UHMWPE fibers (0.250 phr) and silanized nanoclay (2 phr). Reinforcement of these compatibilized UHMWPE fibers treated with T1, T2, T3, and T4 treatments resulted in increase in impact strength and tensile strength of resulting GFRPs by 24% & 20%, 5% & 18%, 30% & 17%, and 25% & 8% respectively over the reference composite (RC). It was noted that 2PG*0.250UPAC composite (GFRP having 2 phr of silanized nanoclay and 0.250 phr of T3 surface treated UHMWPE fibers) showed the best combination of properties. Compared to its counterpart containing pristine UHMWPE fibers, the 2PG*0.250UPAC composite showed improvement of 53%, 22%, and 26% in tensile strength, tensile modulus, and impact strength respectively.

For validation of results, current results compared with the available literature. Several studies are available in literature which investigate the effect of reinforcing either nano-particles, or thermoplastic fibers, or both on the properties of resulting composites. Different nano-reinforcements used include nanoclay, alumina, titanium dioxide, and carbon nanotubes. Addition of nano-particles showed improvements mainly in tensile properties, flexural properties, and inter-laminar shear strength with only minor improvement in impact strength [1,14–16,33,194,208–211]. Different thermoplastic fibers used as reinforcement in epoxy resin include polypropylene (PP), polyethylene terephthalate (PET), para-aramid, and polyethylene fibers. Addition of pristine (untreated) fibers showed either deterioration or only minor improvement in mechanical properties

due to lack of compatibility of thermoplastic fibers with other constituents of composites. To improve compatibility, surface modification (compatibilization) of fibers is reported in literature. Reinforcement of compatibilized fibers showed significant improvement in mechanical performance of composites [99,104,106,188,207,212–214]. In the context of present research, three studies are available in literature. Singh's group [32,34,35] fabricated epoxy based GFRPs with addition of pristine nanoclay and different micro-fillers viz. (i) PP, (ii) PET, (iii) EPDM (ethylene propylene diene monomer) to investigate their effect on mechanical properties of resulting GFRPs. The results showed significant improvements in impact strength with degradation in tensile and flexural properties. However, in the present work, both impact strength as well as tensile properties showed significant improvements.

UHMWPE fibers were treated in four different ways. GFRPs containing 2 phr of silanized nanoclay and 0.250 phr of T3 surface treated UHMWPE fibers showed the best combination of properties. The advantages of potassium permanganate treatment followed by silanization of UHMWPE fibers (i.e. T3 treatment) are discussed here. After a given treatment, the surface of treated fibers had a coating of the treating solution over it. The presence of coating on the surface of fibers impeded the fiber-fiber contact and reduced agglomeration of fibers during processing of GFRPs. This led to uniform distribution of fibers in the GFRPs. Further, the layer of coating solution on the fiber surface was irregular. This irregular surface boosted the bonding among constituents of nanocomposite by mechanical interlocking [97,98,215]. The irregular surfaces for surface treated fibers were observed in the present research also and were shown in Figure 5.3. Silane agents were used to improve the bonding between treated thermoplastic fibers and other constituents of GFRP system. Silane agents have two functional groups, one group attaches to an organic constituent and the other group attaches to an inorganic constituent. General chemical formula of silane agent is $R_3Si–X$ (where R is organofuntional group, Si is silicon, and X is hydrolyzable group) [32,35]. Silane agent forms a bridge of covalent bonds between the fiber(s) and the matrix. The X group reacts with epoxy matrix. The Si–OR bonds hydrolyze quickly in aqueous solution to make silanol Si–OH groups and react with hydroxyl group of fiber [32]. The silane agent used in the present research contained X group of 3-aminopropyl and the R group was ethoxy. During drying after silanization, reverse condensation takes place and silanol and –OH groups form polysiloxane on the surface, here UHMWPE fibers [195]. The X group present on the surface of fibers reacts with the epoxy and a stable covalent bond is formed between them. On

completion of all the reactions, the strong primary bonds act as a bridge between fibers and epoxy matrix. Consequently, multi-scale filler reinforced GFRPs reinforced with 2 phr of silanized nanoclay and 0.250 phr of compatibilized UHMWPE fibers (potassium permanganate treatment followed by silanization) exhibited best mechanical performance among GFRPs reinforced with compatibilized UHMWPE fibers.

5.3 SEM and EDS analysis for confirming surface treatment of UHMWPE fibers

Figure 5.3−5.4 present the SEM-EDS analysis of UHMWPE fibers used in the present research. SEM micrograph of the pristine UHMWPE fibers showed that their surface was very smooth (Figure 5.3a). EDS analysis of pristine fibers showed presence of carbon (C) and oxygen (O) only. After T1 treatment (potassium permanganate), the surface of fibers became rougher compared to pristine UHMWPE fiber surface (Figure 5.3b). Increased roughness of fibers indicated that $KMnO_4$ treatment successfully modified the surface UHWMPE fibers. EDS analysis also validated the presence of potassium (K) and manganese (Mn) along with C and O (Figure 5.4b). After T2 treatment, no major difference was observed between surface of pristine fibers and that of treated fibers (compare Figure 5.3a and Figure 5.3c). Only minor changes in surface roughness were observed for silane treated fibers. EDS analysis confirmed the silane treatment with presence of silicon (Si) along with C and O. After T3 treatment, the surface of UHMWPE fibers obtained was the roughest among all the cases of UHMWPE fibers (Figure 5.3d). T3 treatment was a combination of T1 and T2 treatments, applied in sequence. EDS results showed presence of K, Mn, Si along with C and O (Figure 5.4d). Finally, grafting of maleic anhydride (MAH) on the surface of fibers was observed (Figure 5.4e). EDS analysis was not able to validate the MAH grafting. To confirm the presence of MAH grafting on the surface of UHMWPE fibers, FTIR analysis was done (discussed in Section 5.4).

All the four compatibilization methods used for surface treatment of UHMWPE fibers enhanced the properties of nanocomposites reinforced with these compatibilized fibers. The best combination of mechanical properties was provided by GFRP reinforced with 0.25 phr of T3 treated UHMWPE fibers (2PG*0.25UPAC composites). During the T3 treatment, the surface of UHMWPE fibers became rough when initially subjected to potassium permanganate treatment. $KMnO_4$ treatment increased the irregularities on the surface, thus increasing the surface area of fibers. During the subsequent silane treatment, the irregularities present on the fiber surface helped

in easy silane agent grafting. This coating (potassium permanganate followed by silanization) on the surface of UHMWPE fibers helped in uniform dispersion of fibers by reducing the fiber-fiber interaction.

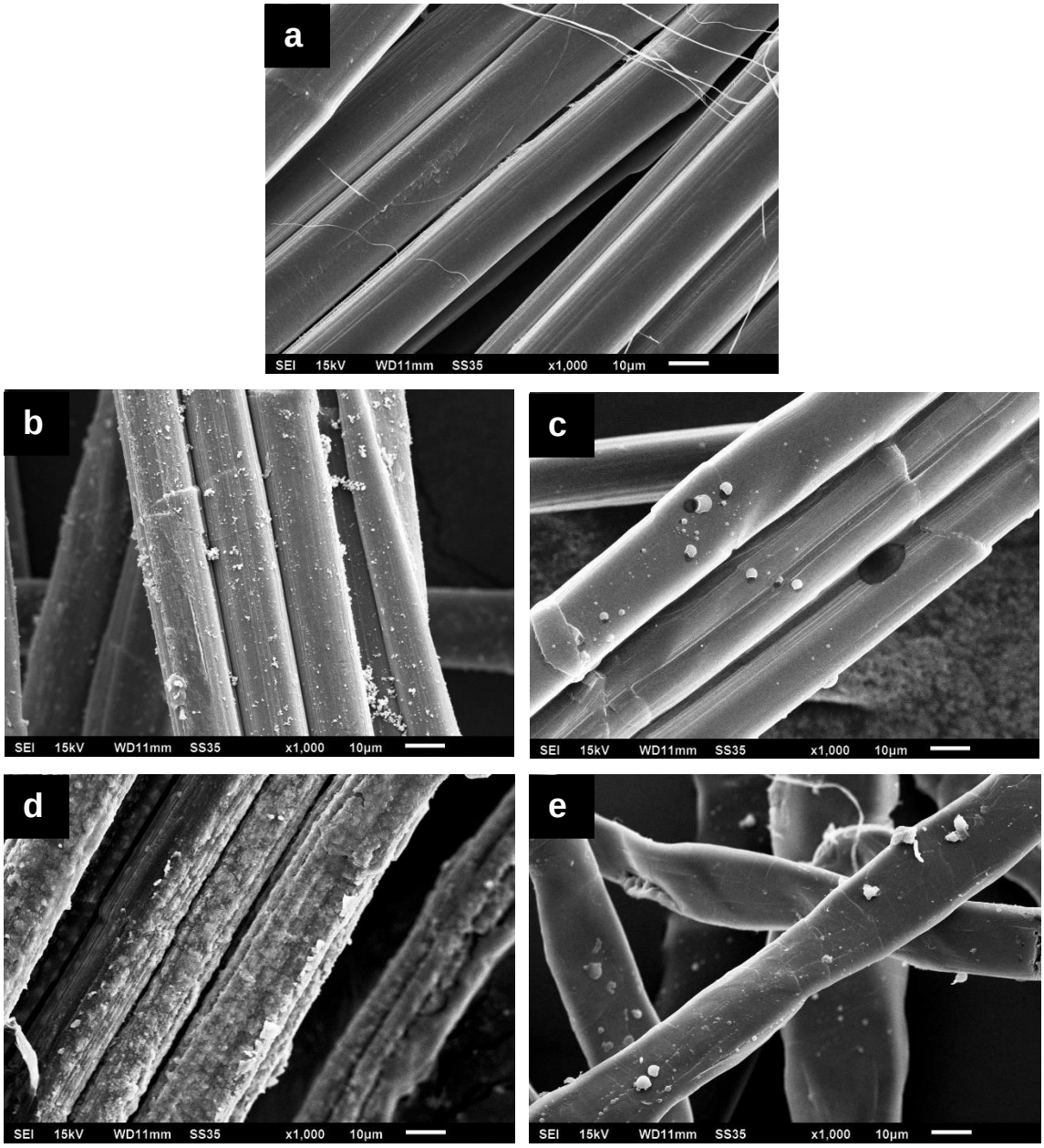

Figure 5.3. SEM micrographs of UHMWPE fibers showing their surface (a) in the pristine state, (b) after T1 treatment, (c) after T2 treatment, (d) after T3 treatment, and (e) after T4 treatment.

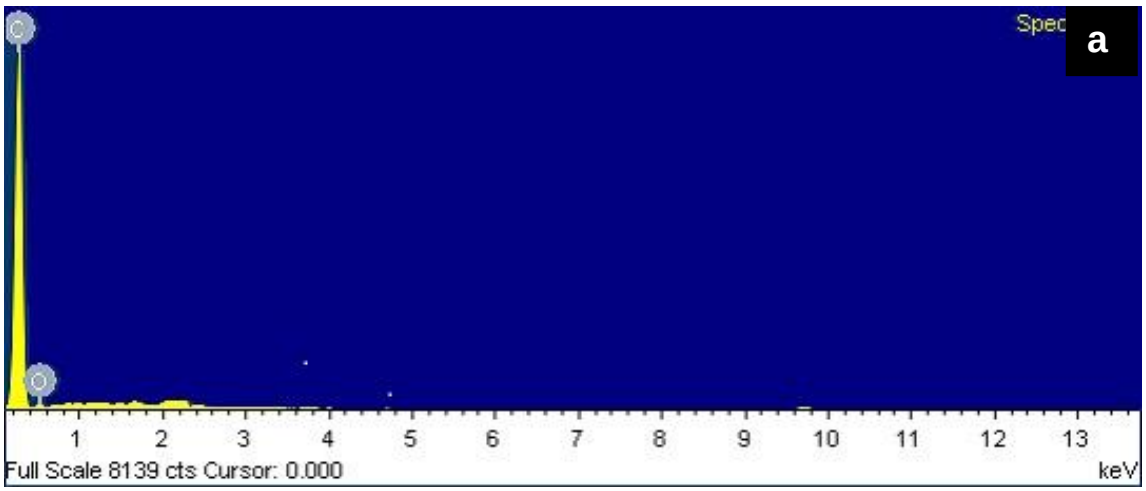
a
O
O
1 2 3 4 5 6 7 8 9 10 11 12 13
Full Scale 8139 cts Cursor: 0.000
keV

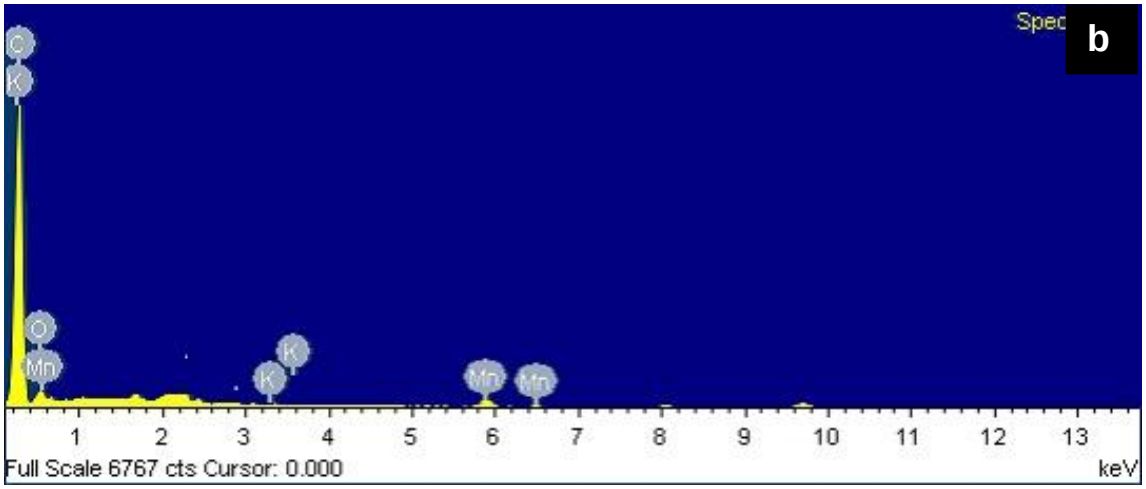
b
O
K
O
Mn
K
K
Mn
Mn
1 2 3 4 5 6 7 8 9 10 11 12 13
Full Scale 6767 cts Cursor: 0.000
keV

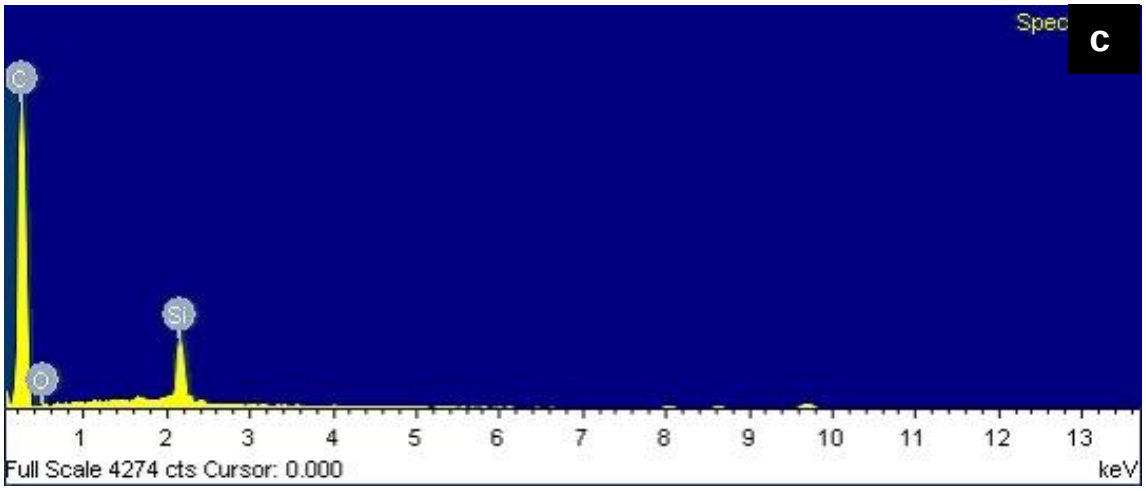
c
O
Si
O
1 2 3 4 5 6 7 8 9 10 11 12 13
Full Scale 4274 cts Cursor: 0.000
keV

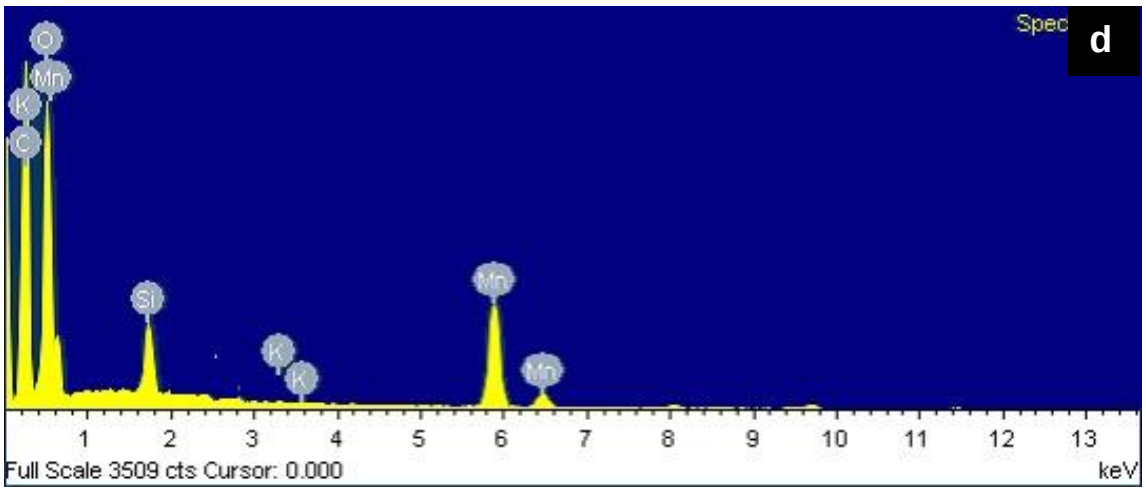

Figure 5.4. EDS spectrographs of UHMWPE fibers showing the presence of various constituents (a) in the pristine state, (b) after T1 treatment, (c) after T2 treatment, and (d) after T3 treatment.

5.4 FTIR analysis to confirm surface treatment of UHMWPE fibers

FTIR spectra of UHMWPE fibers is shown in Figure 5.5. Bands of C–H asymmetric/symmetric stretch vibrations, C–H asymmetric changing angle vibrations, –C–O asymmetric stretch vibrations, and C–H swing in-plane vibrations were observed in the UHMWPE fibers (for both, pristine as well as compatibilized) at around 2912 cm^{-1}, 2846 cm^{-1}, 1468 cm^{-1}, 1100 cm^{-1}, and 716 cm^{-1} respectively [102,206]. The band at 3361 cm^{-1} for potassium permanganate treated UHMWPE fibers (i.e. T1 treated fibers) corresponded to the hydroxyl group [206]. The band around 1030 cm^{-1} and 821 cm^{-1} in potassium permanganate treated UHMWPE fibers (i.e. T1 treated fibers) corresponded to C–O stretching and out of plane C–H bending respectively [99,102,206]. A new band in silanized UHMWPE fibers (i.e. T2 treated fibers) was observed at 1021 cm^{-1} which corresponded to Si–O–Si [16,20,195]. UHMWPE fibers treated with combination of potassium permanganate and silanization (i.e. T3 treated fibers) showed all peaks that were observed for UHMWPE fibers when treated with individual treatments (i.e. T1 and T2 treatments). This confirmed the combination of treatments. After MAH grafting of UHMWPE fibers (i.e. T4 treated fibers), the bands observed at 2605 cm^{-1} and 1706 cm^{-1} corresponded to the C–H vibrations and C=O stretching of anhydride present in MAH respectively [216,217]. The band at 1555 cm^{-1} corresponded to the –COOH group [34]. The –C–O– stretching band was observed at 1258 cm^{-1} [218]. New bands were observed after MAH grafting due to the formation of new polar groups from MAH on the PE fiber surface, thus confirming the MAH grafting. Thus, FTIR study validated the results obtained through SEM and EDS.

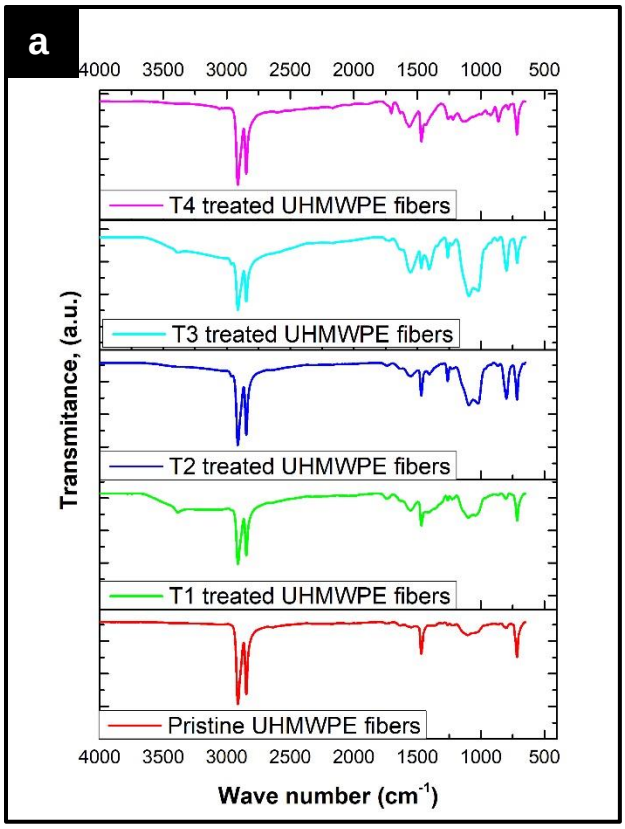

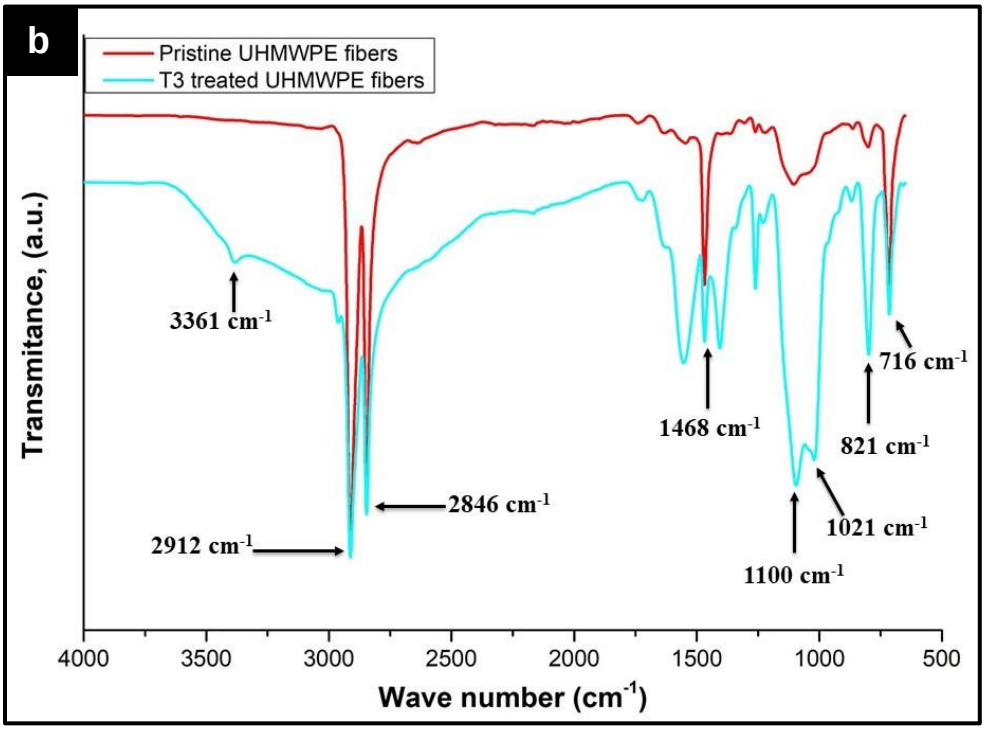

Figure 5.5. FTIR spectra of (a) all the cases of UHMWPE fibers, (b) pristine versus T3 treated UHMWPE fibers.

5.5 SEM analysis of fracture surface of impact test specimens of GFRPs containing silanized nanoclay and UHMWPE fibers

Figure 5.6 shows the SEM micrographs of impact test specimens of (i) RC, (ii) 2PGC, and (iii) 2PG*C. SEM image of RC composite showed smooth surface of glass fibers with no traces of epoxy attached to them (Figure 5.6a). This indicated that the bond/interface between glass fibers and epoxy matrix was weak. Consequently, glass fibers were easily de-bonded from the matrix without much resistance under impact loading. However, the fracture surface of 2PGC (Figure 5.6b) and 2PG*C (Figure 5.6c) nanocomposites were observed to be very rough as compared to RC composite due to the incorporation of nanoclay. This indicated strong bonding between glass fiber-epoxy-nanoclay. Further, comparing Figure 5.6b and Figure 5.6c, fracture surface of 2PG*C nanocomposite was even more uneven/rough in comparison to 2PGC nanocomposite. These observations corroborated well with the results of mechanical properties (2PG*C nanocomposite showed higher impact strength and tensile properties than 2PGC nanocomposite).

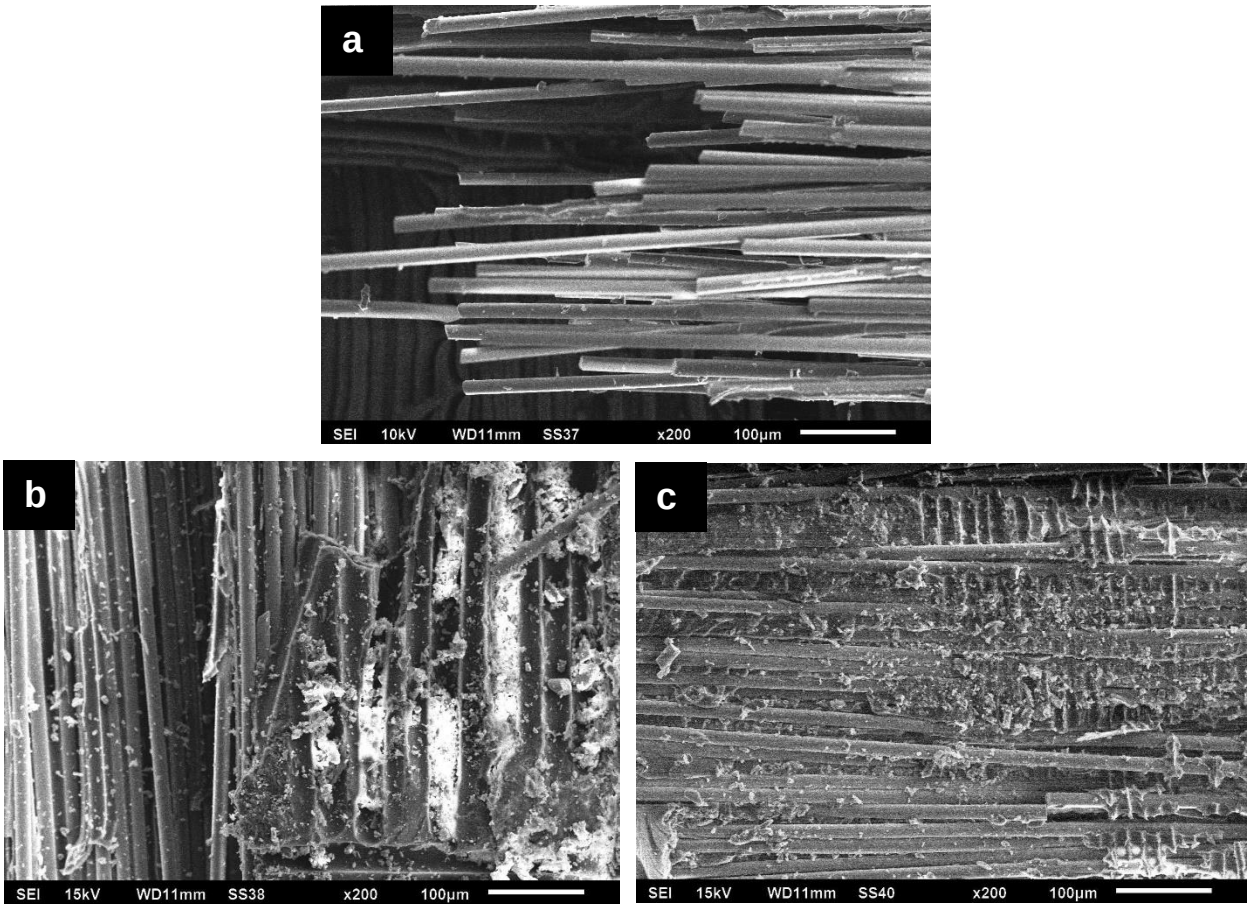

Figure 5.6. SEM micrographs of fracture surface of impact test specimens of (a) RC, (b) 2PGC, and (c) 2PG*C composites.

SEM micrographs of fracture surface of impact test specimens of 2PG*0.25UC, 2PG*0.25UPC, 2PG*0.25UAC, 2PG*0.25UPAC, and 2PG*0.25UMC nanocomposites are presented in Figure 5.7.

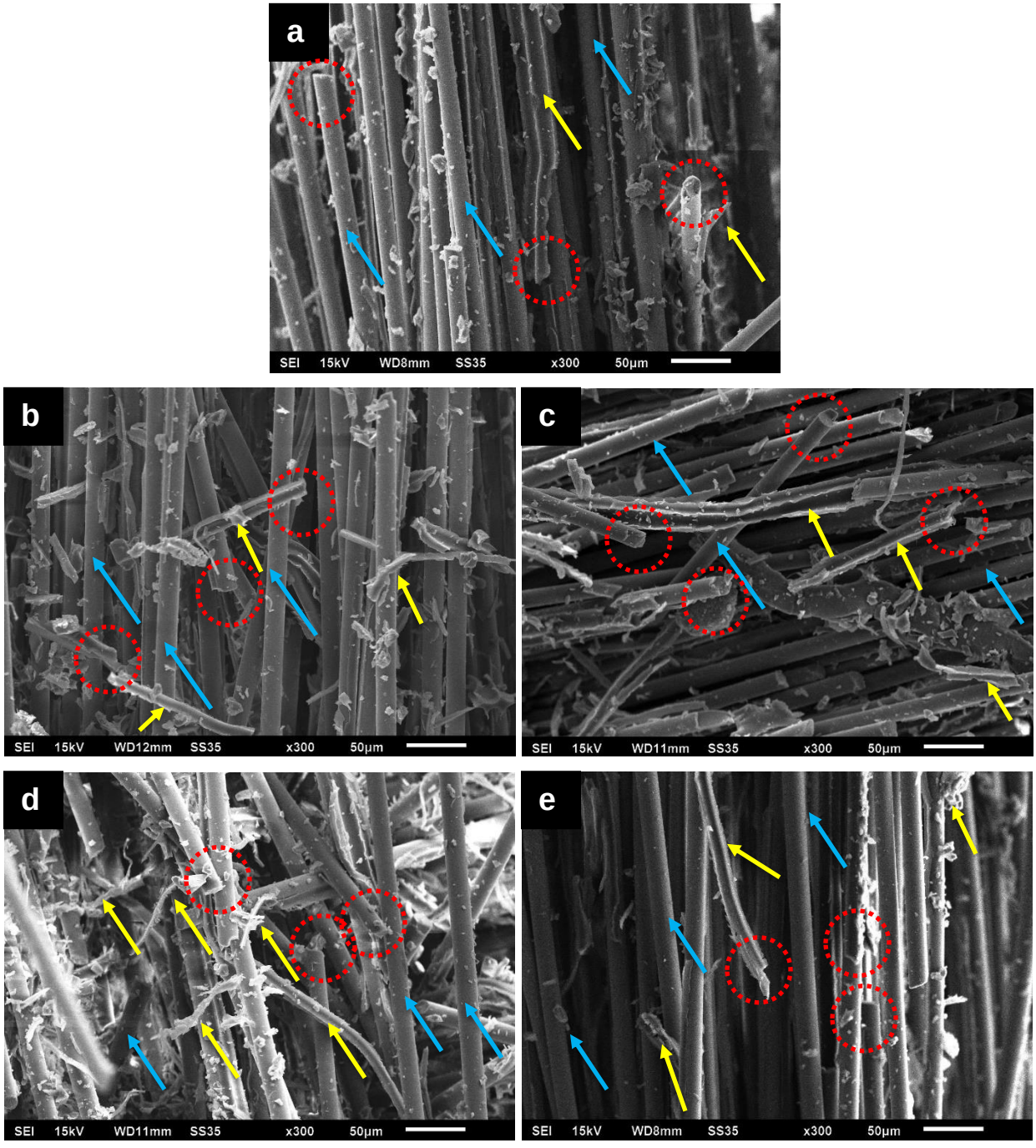

Figure 5.7. SEM micrographs of fracture surface of impact test specimens of GFRPs reinforced with 2 phr of silanized nanoclay and 0.25 phr of UHMWPE fibers for (a) 2PG*0.25UC, (b) 2PG*0.25UPC, (c) 2PG*0.25UAC, (d) 2PG*0.25UPAC, and (e) 2PG*0.25UMC nanocomposites.

UHMWPE fibers and glass fibers are shown with the help of yellow and blue colored arrows respectively in Figure 5.7. The fractured fibers are highlighted with circles in red color. The surface of 2PG*0.25UC nanocomposite showed epoxy-silanized clay mixture attached to glass fibers at a few sites (Figure 5.7a). The UHMWPE fibers (in pristine state) were observed at a few places, but these untreated/pristine UHMWPE fibers were neither attached to the epoxy-silanized clay mixture nor to the glass fibers. This indicated lack of interaction among various constituents of the nanocomposite system. The addition of pristine UHMWPE fibers resulted in brittle fracture due to their characteristics like chemically inert surface, linear long chains with high degree of orientation and crystallinity. This caused poor interface between UHMWPE fibers and other constituents. Thus, lower mechanical performance of nanocomposites reinforced with pristine/untreated UHMWPE fibers was observed.

Comparing the SEM micrographs of fracture surface of 2PG*0.25UPC, 2PG*0.25UAC, 2PG*0.25UPAC, and 2PG*0.25UMC with 2PG*0.25UPC nanocomposite (comparing Figure 5.7b–e with Figure 5.7a), it was observed that fracture surface of GFRPs reinforced with treated UHMWPE were rougher as compared to 2PG*0.250UC. Epoxy-silanized clay mixture was uniformly distributed and was seen attached to the glass fibers. Further, the compatibilized UHMWPE fibers were uniformly distributed and were well bonded to the epoxy-silanized clay mixture because of the surface treatments (both of clay and UHMWPE fibers). Addition of compatibilized UHMWPE fibers enhanced the interfacial bonding among various constituents of GFRPs due to generation of a large number of covalent bonds among the constituents of composite system [219,220]. Further, fracturing of fibers and absence of fiber pull-out indicated effective stress transfer from matrix to reinforcements (nanoclay and glass/UHMWPE fibers) through a strong interface.

Comparing the SEM micrographs of fracture surface of impact test specimens of various GFRPs reinforced with compatibilized UHMWPE fibers (Figure 5.7b–e), it was observed that epoxy-silanized clay mixture and compatibilized UHMWPE fibers were more uniformly distributed in 2PG*0.25UPAC composition (Figure 5.7d) as compared to other composites. This was concluded as the fracture surface of GFRPs reinforced with T3 treated UHMWPE fibers (Figure 5.7d) was the roughest among all GFRPs reinforced with compatibilized UHMWPE fibers (subjected to T1 or T2, or T3 treatment). The uniform distribution of UHMWPE fibers in 2PG*0.25UPAC made

crack propagation very difficult resulting in absorption of more energy and hence higher impact strength.

Epoxy based GFRP reinforced with 2 phr of silanized nanoclay and 0.250 phr of UHMWPE fibers treated with potassium permanganate solution followed by silanization (T3 treatment) exhibited 30% and 17% improvement in impact strength and tensile strength respectively over the reference sample.

The next chapter presents the results and discussion on the effect of reinforcing silanized nanoclay along with para-aramid fibers on the impact strength and tensile properties of epoxy based GFRP nanocomposites.

Chapter 6. Effect of reinforcing para-aramid fibers and silanized nanoclay on the mechanical properties of GFRPs

6.1 Overview

This chapter presents the results and discussion on the mechanical properties of epoxy based GFRPs reinforced with silanized nanoclay and para-aramid fibers. Silanized nanoclay was added in a fixed amount and para-aramid fibers were added in varying amounts for processing of various GFRPs. Para-aramid fibers were used both in the pristine as well as in the surface treated (compatibilized) state. Four compatibilization methods were used including (i) phosphoric acid treatment, (ii) silanization with 3-aminopropyltriethoxy silane agent, (iii) phosphoric acid treatment followed by silanization, and (iv) UV-assisted MAH grafting. The chapter also discusses the results of various characterization techniques (SEM, EDS, and FTIR) used for confirming compatibilization of para-aramid fibers and for observing the interaction among various constituents of nanocomposite system.

6.2 Mechanical properties of nanoclay-para-aramid fiber reinforced GFRPs

Figures 6.1–6.2 and Table 6.1 present the results of impact strength, tensile strength, and tensile modulus values obtained for GFRPs reinforced with 2 phr of silanized nanoclay and different concentrations of para-aramid fibers (pristine as well as compatibilized). The tensile stress versus percentage elongation behaviour is given in as Figure A3, Appendix I.

Impact strength and tensile properties improved after addition of 2 phr of PG nanoclay to the reference composite (RC). Epoxy based GFRP reinforced with 2 phr of pristine (untreated) nanoclay (i.e. 2PGC) showed an improvement in mechanical properties (23.5%, 4%, and 14% improvement in impact strength, tensile strength, and tensile modulus respectively over reference composite, RC). Further, when epoxy based GFRP was reinforced with 2 phr of silanized nanoclay (i.e. 2PG*C) there was further improvement in impact strength and tensile strength (27% and 16% improvement respectively over RC). The increase in impact strength and tensile strength may be attributed to (a) higher d-spacing of silanized nanoclay, (b) very fine-scale dispersion of silicate platelets in the epoxy resulting in increased bonding sites between glass fibers and epoxy-clay mixture, and (c) improved compatibility of silanized clay with epoxy matrix-glass fibers silanization (as discussed in Chapter 4).

Table 6.1. Mechanical properties of GFRPs reinforced with 2 phr of silanized nanoclay and different concentrations of para-aramid fibers (pristine as well as compatibilized).

S. No.	Sample Designation[#]	Impact Strength (kJ/m^2)	Tensile Strength (MPa)	Tensile Modulus (GPa)
1.	**RC**	**153±9**	**338±7**	**7.48±.10**
2.	2PGC	189±17	351±4	8.51±.04
3.	2PG*C	194±2	392±9	7.91±.02
4.	2PG*0.5PC	146±8	369±10	7.38±.05
5.	2PG*1.0PC	150±10	372±4	7.33±.08
6.	2PG*1.5PC	148±6	304±8	7.29±.09
7.	2PG*2.0PC	145±11	369±7	7.40±.04
8.	2PG*1.0PPC	186±6	401±4	8.46±.06
9.	2PG*1.0PAC	195±2	375±9	8.52±.02
10.	2PG*1.0PPAC	187±14	357±4	8.12±.04
11.	**2PG*1.0PMC**	**205±6**	**357±5**	**7.50±.04**

#: Details of various designations is given in nomenclature

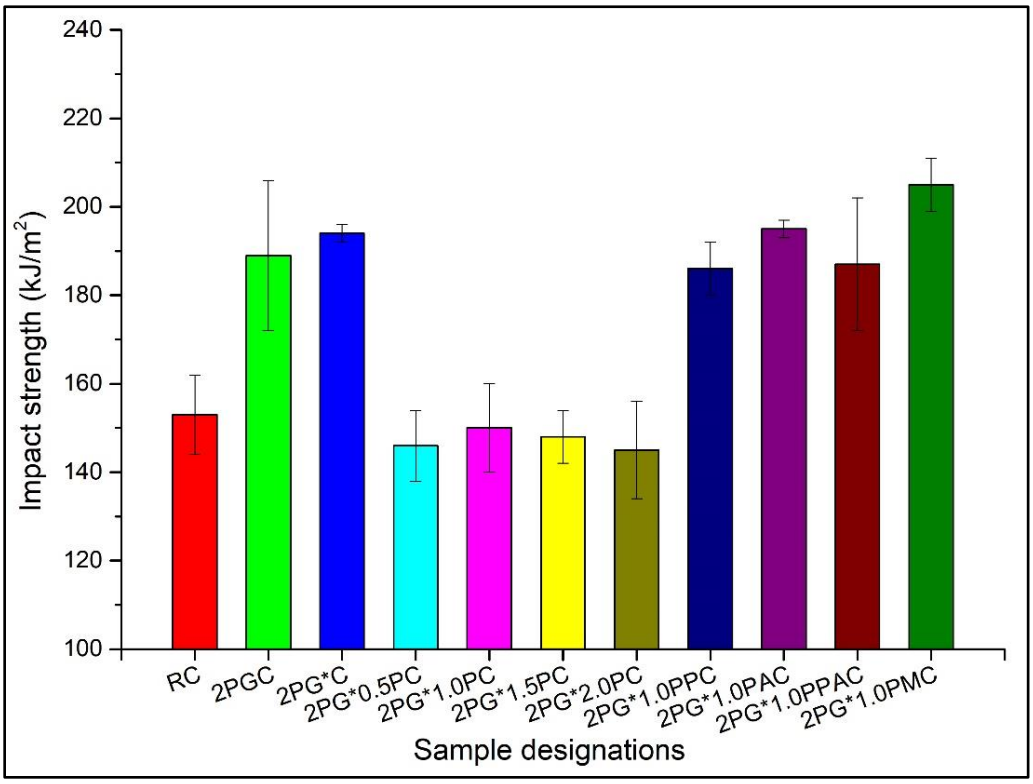

Figure 6.1. Impact strength of reference composite and various GFRPs reinforced with 2 phr of silanized nanoclay and different concentrations of para-aramid fibers (pristine as well as compatibilized).

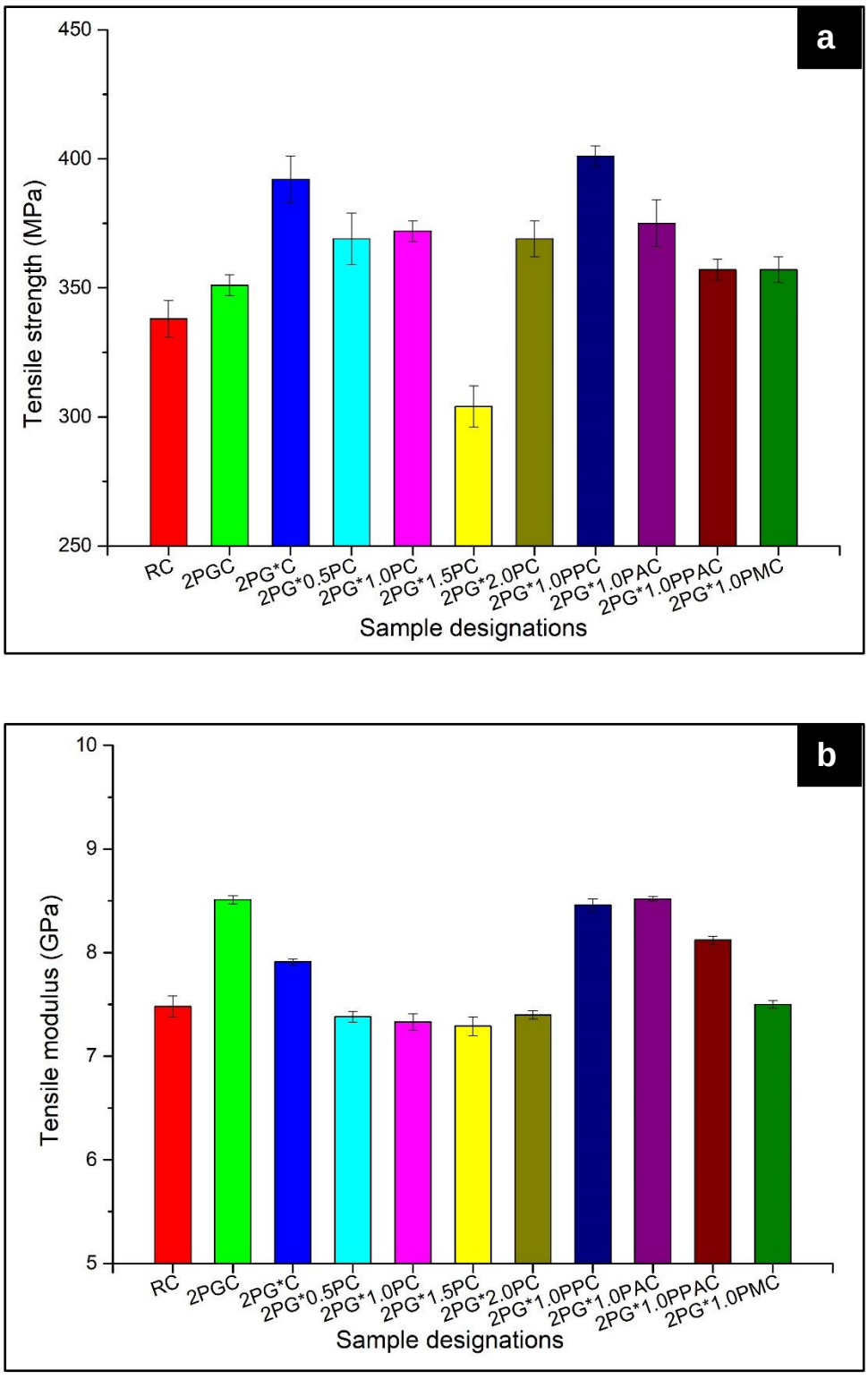

Figure 6.2. Tensile properties of reference composite and various GFRPs reinforced with 2 phr of silanized PG nanoclay and different concentrations of para-aramid fibers (pristine as well as compatibilized) showing (a) tensile strength, and (b) tensile modulus values for composites.

Reinforcement of pristine para-aramid fibers (in any concentration; 0.50−2.00 phr) to 2PG*C composite deteriorated the mechanical properties of resulting GFRP nanocomposites (2PG*0.5PC, 2PG*1.0PC, 2PG*1.5PC, and 2PG*2.0PC). Pristine para-aramid fibers lack in polar functional groups, possess high crystallinity, and have a chemically inert surface [221–223]. For these reasons, the pristine para-aramid fibers were incompatible for interaction with the hydrophobic epoxy resin. To resolve this issue, para-aramid fibers were subjected to surface treatment (compatibilization) using four different techniques viz. (i) phosphoric acid treatment (T5), (ii) silanization with 3-aminopropyltriethoxy silane (T2); same as was used for UHMWPE fibers, (iii) phosphoric acid treatment followed by silanization (T6), and (iv) UV-assisted MAH grafting (T4); same as was used for UHMWPE fibers. Among the pristine para-aramid fiber reinforced epoxy-nanoclay based GFRPs, the best results (mechanical properties) were obtained with 1.00 phr para-aramid fiber concentration. For this reason, 1.00 phr fiber loading was selected for processing of epoxy-nanoclay based GFRPs reinforced with compatibilized para-aramid fibers (1.00 phr) and silanized nanoclay (2 phr). Reinforcement of these compatibilized para-aramid fibers treated with T5, T2, T6, and T4 treatments resulted in increase in impact strength and tensile strength of resulting GFRPs by 22% & 19%, 27% & 11%, 22% & 6%, and 34% & 6% respectively over the reference composite (RC). It was noted that 2PG*1.0PMC composite (GFRP having 2 phr of silanized nanoclay and 1.0 phr of T4 surface treated para-aramid fibers) showed the best combination of properties. Compared to its counterpart containing pristine para-aramid fibers, the 2PG*1.0PC composite showed improvement of 37% in impact strength.

It is well reported in literature that there are different thermoplastic fibers which are used as reinforcement in epoxy resin. These include polypropylene (PP), polyethylene terephthalate (PET), para-aramid, and polyethylene fibers [1,32–34,101,118,157,159,161,207,212,224]. Addition of these fibers in the pristine (untreated) state generally shows deterioration (or only minor improvement) in mechanical properties of the resulting GFRPs containing such fibers [33,44,50]. In the pristine state, there is a lack of compatibility of thermoplastic fibers with other constituents of composites. To improve compatibility, surface modification (compatibilization) of fibers is reported in literature [1,32,34,35,44,99,142,151,215]. Reinforcement of compatibilized fibers has been reported to show significant improvements in mechanical performance of composites [147,153,223,225]. For validation of results, current results compared with the available literature. In the context of present research, three studies are available in literature.

Singh's group [32,34,35] fabricated epoxy based GFRPs with addition of pristine nanoclay and different micro-fillers added separately viz. (i) PP, (ii) PET, (iii) EPDM (ethylene propylene diene monomer) to investigate their effect on the mechanical properties of resulting GFRPs. Singh's group [32,34,35] achieved significant improvements in impact strength, but there was deterioration in tensile properties. However, in the present work, both impact strength and tensile properties showed significant improvements. Maximum improvement in impact strength (34% higher than RC) along with improved tensile strength (6% higher than RC) was achieved with 2PG*1.0PMC composite which contained MAH grafted para-aramid fibers (T4 treated fibers).

With regards to MAH grafting, when MAH is exposed to UV rays, it develops eximers, as illustrated in Equation 1.

$$2MAH^{UV} \rightarrow MAH^{+}\,MAH^{-} \qquad \text{---------- (1)}$$

MAH eximers developed according to Equation 1 are abstracted by hydrogen atoms from para-aramid fibers which promote cross-linking reaction. This leads to grafting of MAH on para-aramid fibers successfully [34]. Successful MAH grafting of para-aramid fibers strengthens the bonding among dissimilar constituents of GFRPs. Thus, higher impact strength was witnessed for GFRPs reinforced with MAH grafted para-aramid fibers (2PG*1.0PMC).

6.3 SEM and EDS analysis for confirming surface treatment of para-aramid fibers

Figure 6.3−6.4 present the SEM micrographs and EDS analysis respectively of the para-aramid fibers used in the present work. Pristine para-aramid fibers showed a very smooth and fine surface (Figure 6.3a). EDS analysis of pristine para-aramid fibers (Figure 6.4a) showed presence of carbon (C), sodium (Na), nitrogen (N), and oxygen (O). Next, the T5 treatment (using phosphoric acid) provided to para-aramid fibers made the surface of fibers rougher as compared to pristine state (Figure 6.3b). EDS results reported presence of C, Na, N, O, and also phosphorus (P) after T5 treatment. The presence of phosphorous in the spectrographs confirmed the presence of phosphoric acid coating (Figure 6.4b). Further, T2 treatment (using APTES silane agent) made the surface of fibers even rougher (Figure 6.3c). EDS results reported presence of C, Na, N, O, and also silicon (Si) after T2 treatment and thus, confirmed grafting of silane agent on the fibers (Figure 6.4c). Next, with T6 treatment (combination of phosphoric acid treatment followed by silanization), only minor changes were observed on the surface of para-aramid fibers (Figure 6.3d). Various elements observed in the EDS spectra included C, Na, N, O, and also P & Si (Figure 6.4d). Finally, T4

treatment (UV-assisted MAH grafting) also made the surface of fibers rougher as compared to the pristine state. Grafting of MAH on the surface of PA fibers was clearly observed (Figure 6.3e). To further confirm the MAH grafting, FTIR analysis of para-aramid fibers was done (same as discussed in Section 6.4). All treatments (T5, T2, T6, and T4) given to para-aramid fibers improved the performance of GFRPs reinforced with these surface-modified para-aramid fibers. Maximum impact strength was obtained in 2PG*1.0PMC nanocomposite system (34% higher than RC).

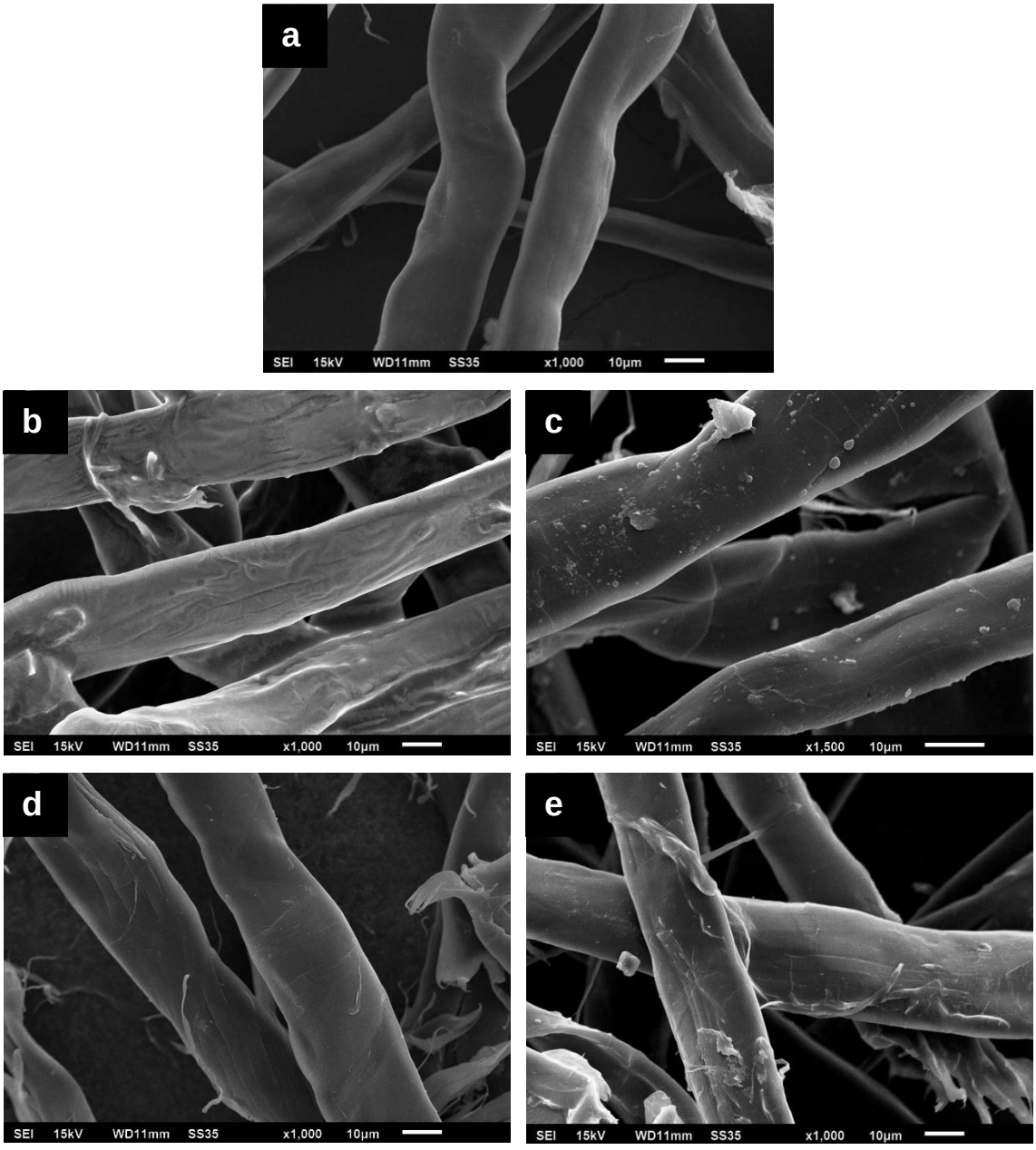

Figure 6.3. SEM micrographs of para-aramid fibers showing their surface (a) in the pristine state, (b) after T5 treatment, (c) after T2 treatment, (d) after T6 treatment, and (e) after T4 treatment.

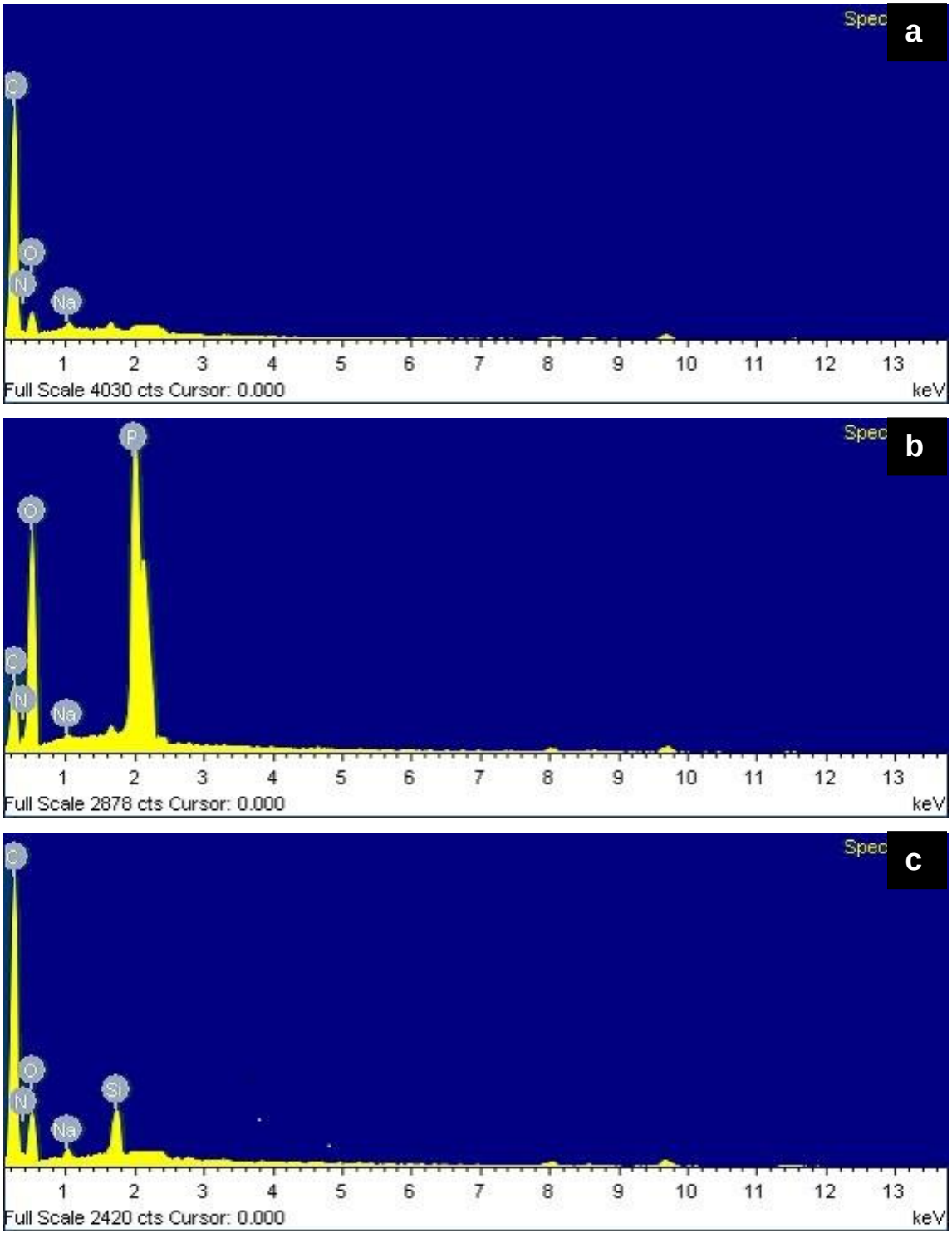
a
C
O
N
Na
1 2 3 4 5 6 7 8 9 10 11 12 13
Full Scale 4030 cts Cursor: 0.000
keV
b
P
O
C
N
Na
1 2 3 4 5 6 7 8 9 10 11 12 13
Full Scale 2878 cts Cursor: 0.000
keV
c
C
O
N
Si
Na
1 2 3 4 5 6 7 8 9 10 11 12 13
Full Scale 2420 cts Cursor: 0.000
keV

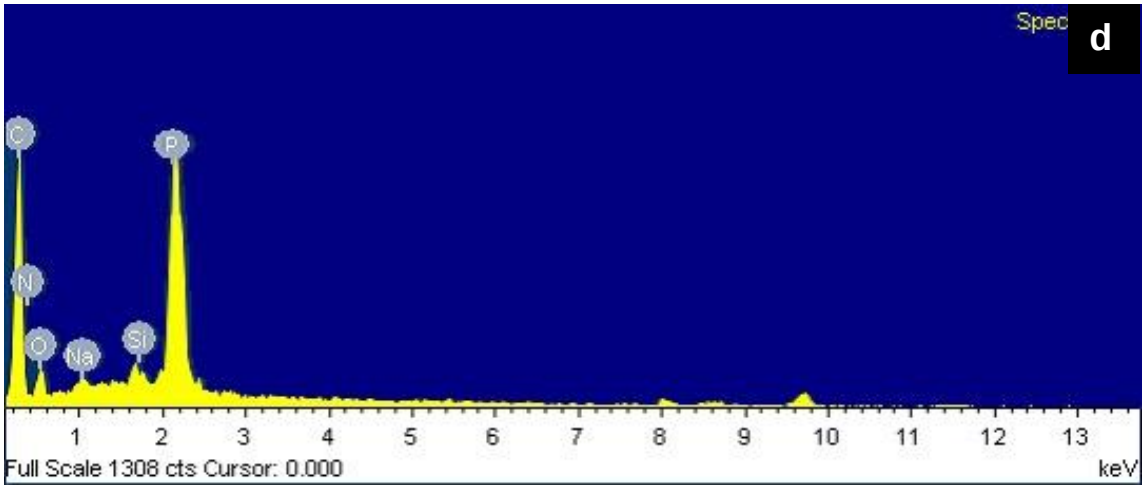

Figure 6.4. EDS spectrographs of para-aramid fibers showing the presence of various constituents (a) in the pristine state, (b) after T5 treatment, (c) after T2 treatment, and (d) after T6 treatment.

6.4 FTIR analysis to confirm surface treatment of para-aramid fibers

FTIR diffractograms of pristine and compatibilized para-aramid fibers are shown in Figure 6.5. The peak around 3310 cm^{-1} observed in pristine and compatibilized para-aramid fibers corresponded to the N–H stretching and stretching vibration of O–H group [226,227]. The three major peaks around 1635 cm^{-1}, 1538 cm^{-1}, and 1305 cm^{-1} present in pristine and compatibilized para-aramid fibers corresponded to Amide I (C=O stretching), Amide II (C–N stretching and in-plane N–H), and Amide III (C–N, C–C, and N–H vibrations) respectively [226,227]. The intensities of all three peaks increased after compatibilization of para-aramid fibers owing to oxidation and etching of fibers [228]. Another possible reason for higher intensities of these peaks after phosphoric acid treatment (T5 treatment) was the presence of increased acidic group on the surface of para-aramid fibers [147]. The intensity of peak at 3310 cm^{-1} increased and broadened after phosphoric acid treatment of para-aramid fibers due to presence of increased O–H group, hence confirmed the surface modification. The peaks observed at around 2750 cm^{-1} and 2355 cm^{-1} corresponded to the weak O–H group and C=O stretching respectively. The higher intensity peak at around 1220 cm^{-1} in silanized para-aramid fibers corresponded to C–N and indicated the successful hydrolysis of $Si{-}OCH_2CH_3$ [229]. The peak observed around 1195 cm^{-1} was due to Si–CH_2–R stretching vibration [230]. The intensities of 1635 cm^{-1}, 1538 cm^{-1}, and 1305 cm^{-1} peaks increased (as discussed above), and confirmed the successful grafting of 3-aminopropyltriethoxy silane (T2 treatment) on the surface of para-aramid fibers. As compared to pristine para-aramid fibers, the MAH grafted para-aramid fibers had some additional peaks at 2925 cm^{-1}, 2595 cm^{-1},

and 1706 cm^{-1}. The peaks at 2925 cm^{-1} and 2595 cm^{-1} corresponded to the C–H vibrations. The peak at 1706 cm^{-1} corresponded to the C=O stretching of anhydride present in MAH [34]. This confirmed the MAH grafting (T4 treatment) of para-aramid fibers. Thus, FTIR study validated the results obtained through SEM and EDS.

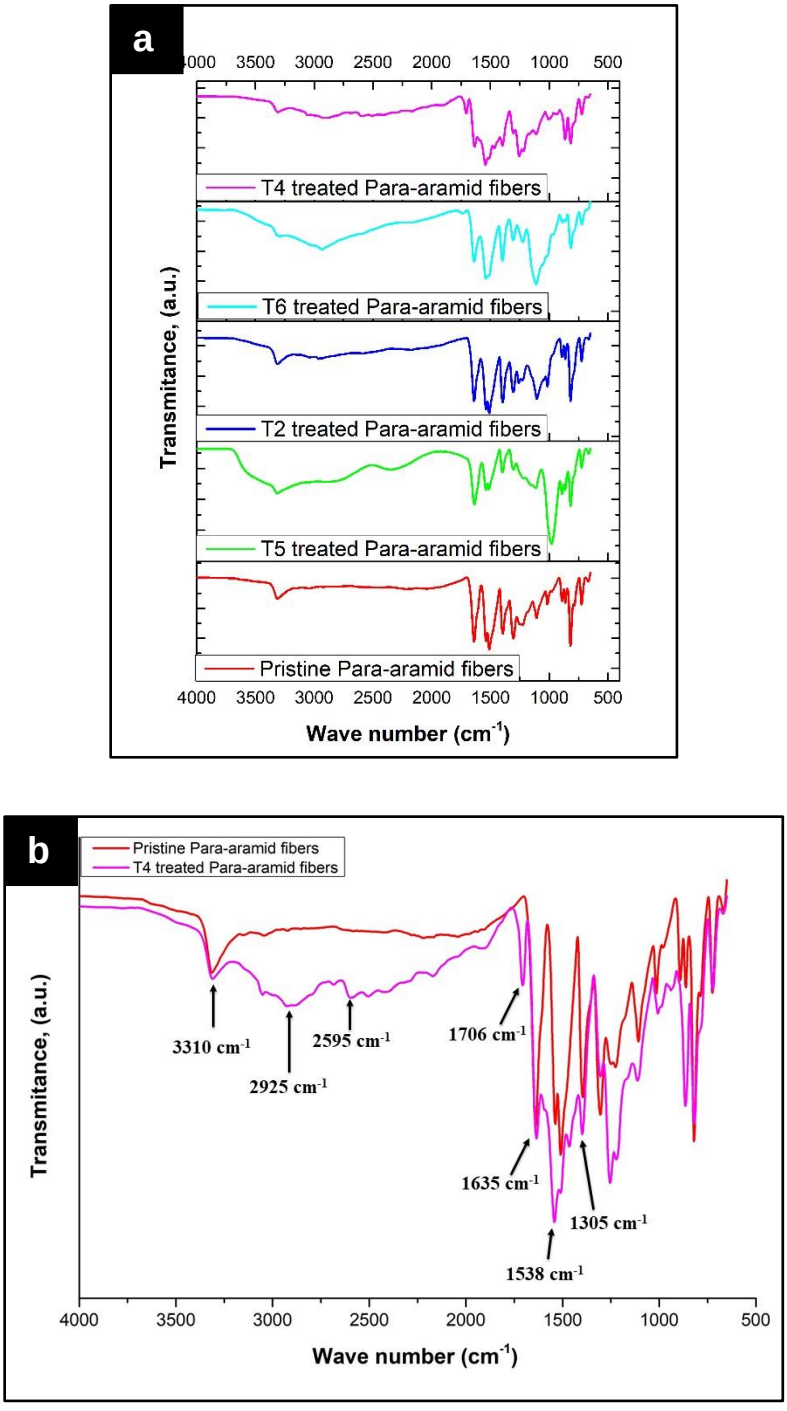

Figure 6.5. FTIR spectra of (a) all the cases of para-aramid fibers, (b) pristine versus T4 treated para-aramid fibers.

6.5 SEM analysis of fracture surface of impact test specimens of GFRPs containing silanized nanoclay and para-aramid fibers

Figure 6.6 presents the SEM micrographs of fracture impact test specimens of (i) reference composite (RC), (ii) 2PGC, and (iii) 2PG*C compositions. Figure 6.6a shows less interaction between glass fibers and epoxy resulting in easy debonding of glass fibers from the matrix material under applied load, and hence, lower mechanical properties. SEM image of 2PGC nanocomposite shows uniformly distributed silicate platelets (Figure 6.6b) which provided resistance to applied load. SEM micrograph of 2PG*C nanocomposite (Figure 6.6c) showed more effective interaction between glass fibers-epoxy because of the presence of silanized nanoclay. The epoxy-silanized clay mixture was more uniformly distributed on the glass fiber surface due to affinity of silanized nanoclay layers for glass fibers. Glass fiber and clay, both are inorganic materials functionalized at the surface with organic molecules which results in polarity match between their respective surfaces [15,25,38].

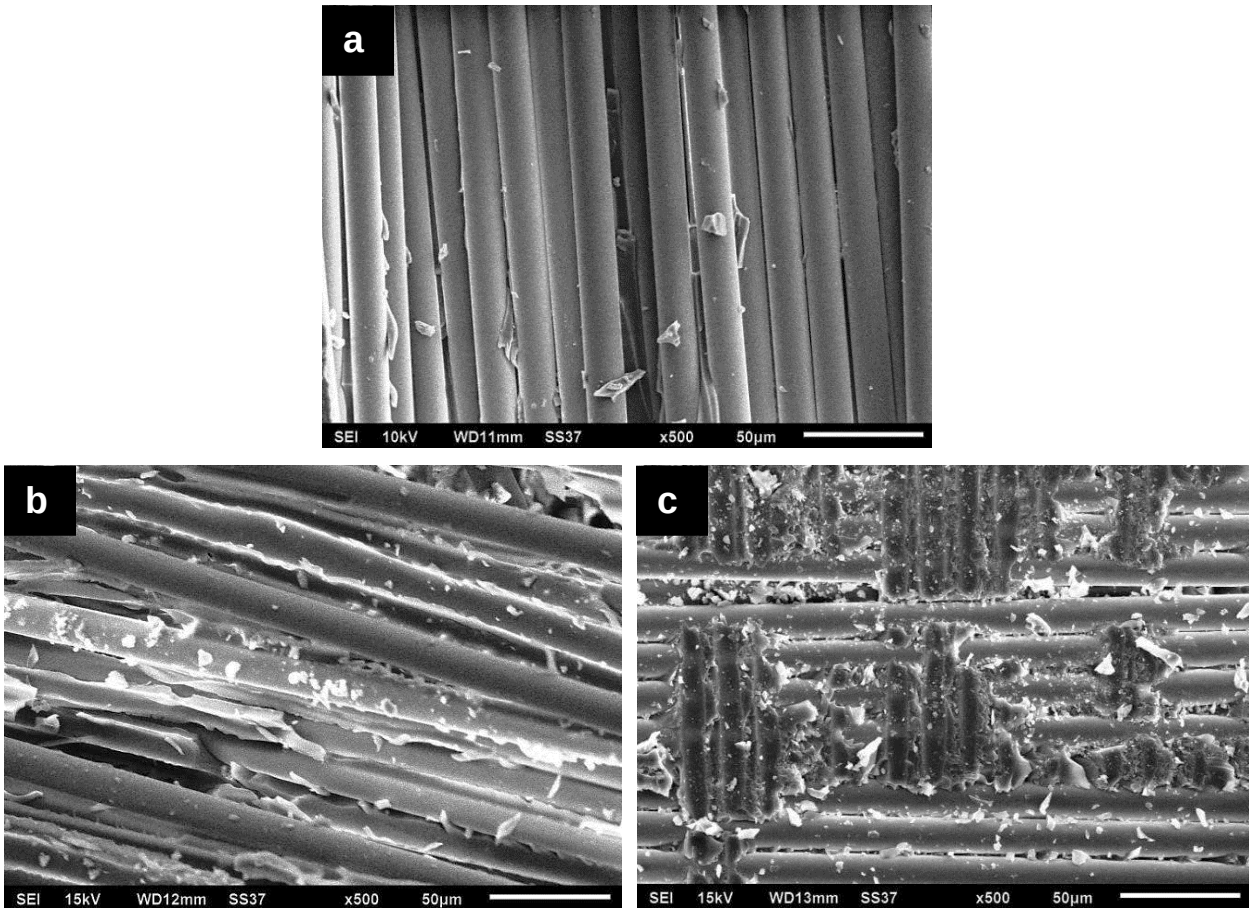

Figure 6.6. SEM micrographs of fracture surface of impact test specimens of (a) RC, (b) 2PGC, and (c) 2PG*C composites.

Figure 6.7 presents the SEM micrographs of fracture surfaces of 2PG*1.0PC, 2PG*1.0PPC, 2PG*1.0PAC, 2PG*1.0PPAC, and 2PG*1.0PMC nanocomposites after Izod impact testing. Green and blue color arrows are indicating para-aramid fibers and glass fibers respectively. Red color circles are indicating fibers which got fractured under loading.

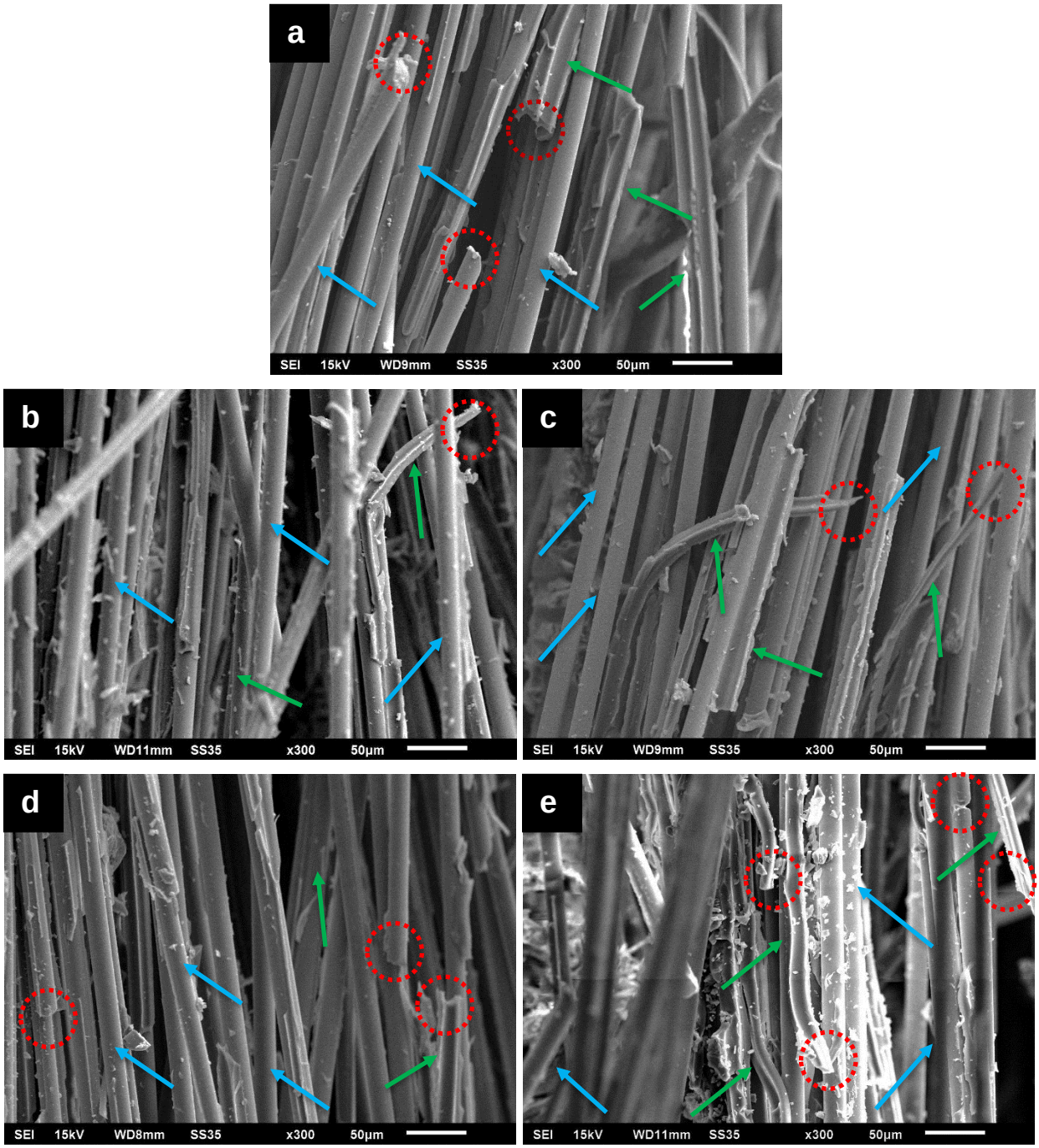

Figure 6.7. SEM micrographs of fracture surface of impact test specimens of GFRPs reinforced with 2 phr of silanized nanoclay and 1.0 phr para-aramid fibers for (a) 2PG*1.0PC, (b) 2PG*1.0PPC, (c) 2PG*1.0PAC, (d) 2PG*1.0PPAC, and (e) 2PG*1.0PMC nanocomposites.

For nanocomposite containing pristine para-aramid fibers (i.e., 2PG*1.0PC), SEM micrographs revealed (i) fine and smooth surface of glass fibers and para-aramid fibers, and (ii) very little epoxy-clay blend bonded to glass fibers and para-aramid fibers (Figure 6.7a). These observations confirmed lack of interfacial bonding of pristine para-aramid fibers with other constituents of GFRPs and so low value of impact strength/tensile properties for the resulting composites. Further, for nanocomposites containing compatibilized para-aramid fibers, SEM micrographs revealed (i) relatively rougher surface of glass fibers and para-aramid fibers (GFRP reinforced with MAH grafted para-aramid fibers was the roughest, Figure 6.7e), and (iii) relatively more amount of epoxy-clay mixture attached to the glass fibers and para-aramid fibers (Figure 6.7b–e). Also, fractured fibers were observed (Figure 6.7b–e). Finally, fiber pull-out was absent which indicated strong bonding among constituents of GFRPs.

Thus, the addition of silanized nanoclay and compatibilized para-aramid fibers resulted in superior mechanical properties of GFRPs. Four different methods were utilized for the compatibilization of para-aramid fibers. Each method provided a coating on the para-aramid fiber surface to prevent fiber-fiber interaction and promoted effective dispersion of fibers in the epoxy-clay-glass fiber system. This led to improved interaction of these micro-fillers with other constituents of GFRPs. Reinforcement of MAH grafted para-aramid fibers provided the best results.

Epoxy based GFRP reinforced with 2 phr of silanized nanoclay and 1.0 phr of para-aramid fibers treated with UV-assisted MAH grafting (T4 treatment) exhibited 34% and 6% improvement in impact strength and tensile strength respectively over the reference sample.

The next chapter presents the results and discussion on the effect of reinforcing silanized nanoclay along with Inviya fibers on the impact strength and tensile properties of epoxy based GFRP nanocomposites.

Chapter 7. Effect of reinforcing Inviya fibers and silanized nanoclay on the mechanical properties of GFRPs

7.1 Overview

This chapter presents the results and discussion on the mechanical properties of epoxy based GFRPs reinforced with silanized nanoclay and Inviya (Spandex) fibers. Silanized nanoclay was added in a fixed amount and Inviya fibers were added in varying amounts for processing of various GFRPs. Inviya fibers were used both in the pristine as well as in the surface treated (compatibilized) state. Four compatibilization methods were used including (i) phosphoric acid treatment, (ii) silanization with 3-aminopropyltriethoxy silane agent, (iii) phosphoric acid treatment followed by silanization, and (iv) UV-assisted MAH grafting. The chapter also discusses the results of various characterization techniques (SEM, EDS, and FTIR) used for confirming compatibilization of Inviya fibers and for observing the interaction among various constituents of nanocomposite system.

7.2 Mechanical properties of nanoclay-Inviya fiber reinforced GFRPs

Figures 7.1–7.2 and Table 7.1 present the results of impact strength, tensile strength, and tensile modulus values obtained for GFRPs reinforced with 2 phr of silanized nanoclay and different concentrations of Inviya fibers (pristine as well as compatibilized). The tensile stress versus percentage elongation behaviour is available as Figure A4, Appendix I.

Impact strength and tensile properties improved after addition of 2 phr of PG nanoclay to the reference composite (RC). Epoxy based GFRP reinforced with 2 phr of pristine nanoclay (i.e. 2PGC) showed an improvement in mechanical properties (23.5%, 4%, and 14% improvement in impact strength, tensile strength, and tensile modulus respectively over the reference composite, RC). Further, when epoxy based GFRP was reinforced with 2 phr of silanized nanoclay (i.e. 2PG*C) there was further improvement in impact strength and tensile strength (27% and 16% improvement respectively over RC). The improvement in mechanical properties was attributed to better bonding of silanized clay with epoxy. Silanized clay-epoxy bonding improved because of increased d-spacing of nanoclay after silanization (as discussed in Chapter 4). Further, the partially exfoliated morphology of nanoclay obtained in 2PG*C composite resulted in more number of interfacial bonding sites for epoxy-silanized clay-glass fiber system.

Table 7.1. Mechanical properties of GFRPs reinforced with 2 phr of silanized nanoclay and different concentrations of Inviya fibers (pristine as well as compatibilized).

S. No.	Sample Designation[#]	Impact Strength (kJ/m^2)	Tensile Strength (MPa)	Tensile Modulus (GPa)
1.	**RC**	**153±9**	**338±7**	**7.48±0.10**
2.	2PGC	189±17	351±4	8.51±0.04
3.	2PG*C	194±2	392±9	7.91±0.02
4.	2PG*0.5IC	153±7	338±5	7.12±0.06
5.	2PG*1.0IC	173±9	345±7	7.52±0.06
6.	2PG*1.5IC	185±10	337±10	7.34±0.07
7.	2PG*2.0IC	155±9	338±10	7.20±0.01
8.	2PG*1.5IPC	144±8	309±6	7.19±0.03
9.	2PG*1.5IAC	188±14	338±3	7.20±0.01
10.	**2PG*1.5IPAC**	**382±10**	**350±6**	**7.22±0.03**
11.	2PG*1.5IMC	355±14	354±10	7.44±0.04

#: Details of various designations is given in nomenclature

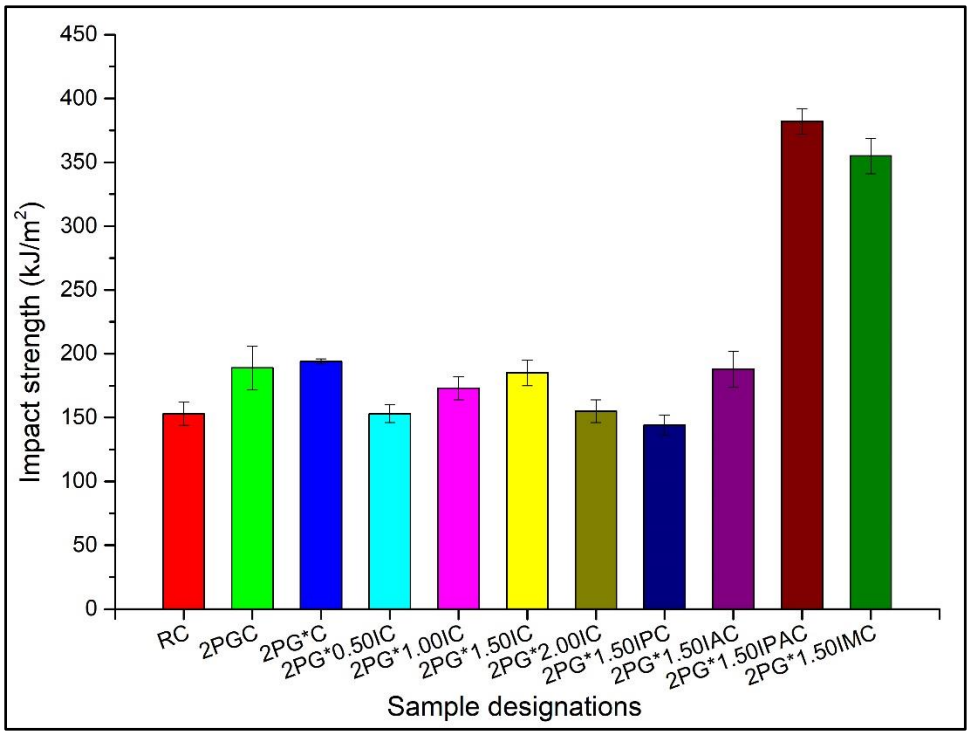

Figure 7.1. Impact strength of reference composite and various GFRPs reinforced with 2 phr of silanized PG nanoclay and different concentrations of Inviya fibers (pristine as well as compatibilized).

Reinforcement of pristine Inviya fibers (in any concentration; 0.50−2.00 phr) to 2PG*C composite deteriorated the mechanical properties of resulting GFRP nanocomposites (2PG*0.50IC, 2PG*1.00IC, 2PG*1.50IC, and 2PG*2.00IC). This drop in properties was owing to lack of compatibility of pristine Inviya fibers with other constituents of epoxy based GFRP system.

Literature reports that for multi-scale filler reinforced composite systems, surface modification of reinforcements/fillers is needed for (i) their uniform distribution in the matrix material, and also (ii) improving their interfacial adhesion with other constituents of the composite system [1,34,35].

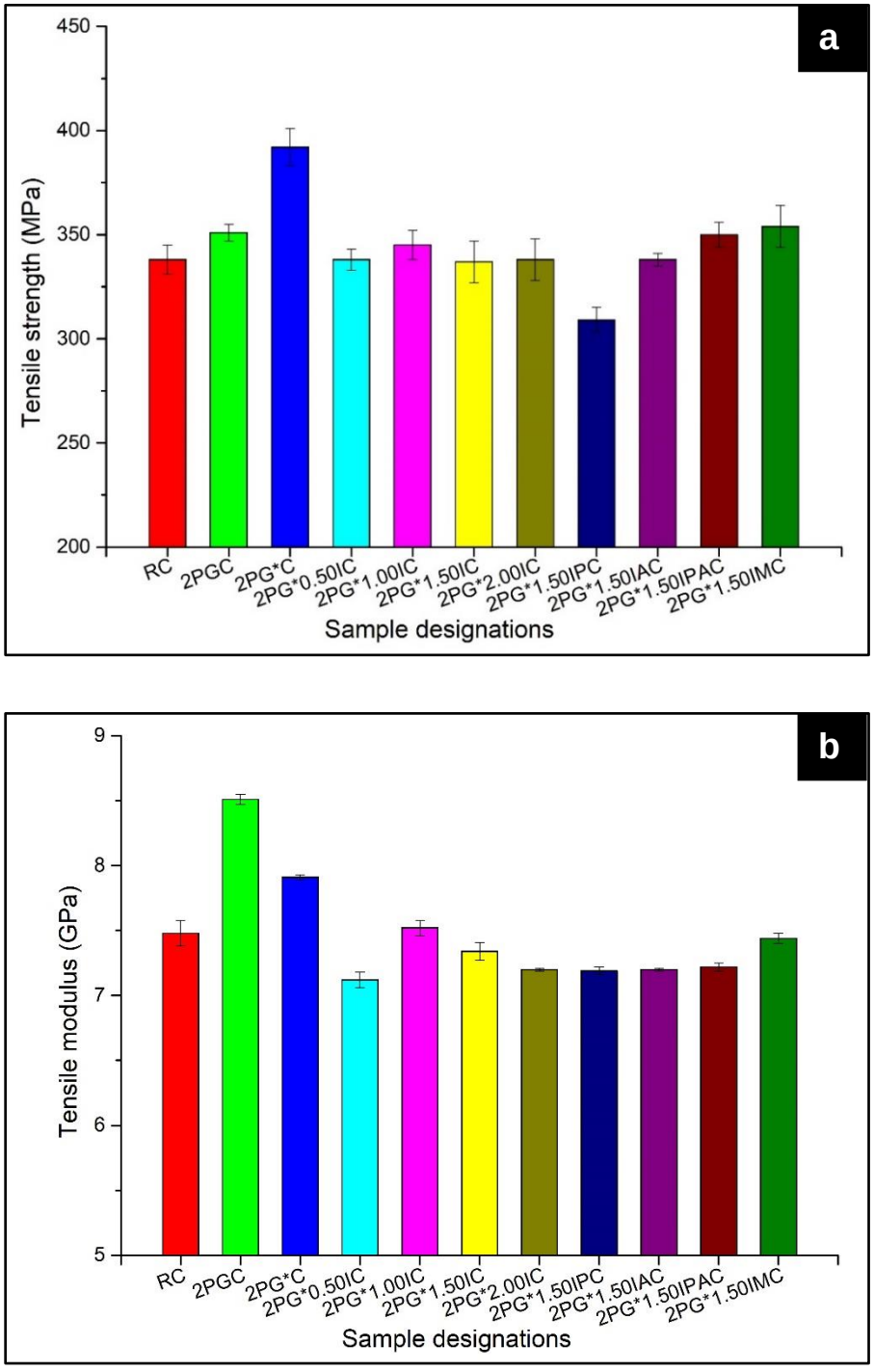

Figure 7.2. Tensile properties of reference composite and various GFRPs reinforced with 2 phr of silanized PG nanoclay and different concentrations of Inviya fibers (pristine as well as compatibilized) showing (a) tensile strength, and (b) tensile modulus values for composites.

To resolve this issue, Inviya fibers were subjected to surface treatment (compatibilization) using four different techniques viz. (i) phosphoric acid treatment (T5); same as was used for para-aramid fibers, (ii) silanization with 3-aminopropyltriethoxy silane (T2); same as was used for UHMWPE fibers, (iii) phosphoric acid treatment followed by silanization (T6); same as was used for para-aramid fibers, and (iv) UV-assisted MAH grafting (T4); same as was used for UHMWPE fibers. Among the pristine Inviya fiber reinforced epoxy-nanoclay based GFRPs, the best results (mechanical properties) were obtained with 1.50 phr Inviya fiber concentration. For this reason, 1.50 phr fiber loading was selected for processing of epoxy-nanoclay based GFRPs reinforced with compatibilized Inviya fibers (1.50 phr) and silanized nanoclay (2 phr). Reinforcement of these compatibilized Inviya fibers treated with T2, T6, and T4 treatments resulted in increase in impact strength and tensile strength of resulting GFRPs by 23% & 0%, 150% & 4%, and 132% & 5% respectively over the reference composite (RC). Reinforcement of T5 treated Inviya fibers to 2PG*C composite didn't show any significant change in impact strength and tensile properties. It was noted that 2PG*1.50IPAC composite (GFRP having 2 phr of silanized nanoclay and 1.50 phr of T6 surface treated Inviya fibers) showed the best combination of properties. Compared to its counterpart containing pristine Inviya fibers (2PG*1.50IC), the 2PG*1.50IPAC composite showed improvement of 106% in impact strength.

For validation of results, current results compared with the available literature. Singh *et al.* [32,34,35] in different studies investigated the influence of addition of PET, PP, and EPDM fibers/particles on the impact strength behaviour of epoxy based nanoclay reinforced GFRPs. It was concluded that addition of unmodified (pristine) PET, PP, EPDM fillers degraded all the mechanical properties of resulting GFRPs, similar to as is observed in the present work. However, addition of surface treated PET, PP, and EPDM fillers showed 19%, 44%, 68% improvement in impact strength along with some loss in tensile properties as compared to the reference GFRP [32,34,35]. However, in the present work, very significant improvements in impact strength (150% with T6 and 132% with T4 treatment) were observed along with minor improvements in tensile strength for GFRPs reinforced with surface treated Inviya fibers.

For Inviya fiber reinforced GFRPs, the best impact strength was obtained with addition of T6 treated Inviya fibers (150% improvement over RC). The reasons for improvement in properties are discussed as follows. Nanoclay and Inviya fibers, in their pristine state are hydrophilic in nature. On being added in the pristine state to the GFRP system, these constituents are not

compatible with the hydrophobic epoxy. Different surface modification techniques are reported to make these constituents hydrophobic for better compatibility with epoxy resin [1,16,32,194,231]. In the present research, silanization technique was used for clay platelets and four separate surface modification techniques were used for Inviya fibers. Surface treatment of fibers prevents fiber-fiber interaction and impedes fiber aggregation, resulting in uniform dispersion of Inviya fibers in the GFRPs. Surface treatment also changes the smooth surface of fibers into an uneven and irregular surface. Thus, mechanical interlocking on these rough surfaces improves the interfacial adhesion among constituents of GFRPs. In T6 treatment, phosphoric acid treatment was followed by silanization. After phosphoric acid treatment, the surface of Inviya fibers became rough which resulted in more surface area for silanization. The silane agent easily grafted over the rough surface of Inviya fibers. Silane agent comprises of two different functional groups, one of which is coupled to an organic and the other to an inorganic constituent. $R_3Si–X$ is the basic chemical formula for silane agent. The silane agent develops a covalent bond bridge among constituents of GFRPs. The epoxy matrix interacts with the X group. In aqueous medium, the Si–OR bonds hydrolyzes swiftly to form silanol Si–OH groups which interact with the hydroxyl group available in fiber surface. The X group of silane agent utilized in this research was 3-aminopropyl, while the R group was ethoxy. Reverse condensation occurs during the drying process performed after silanization; further, the reaction between silanol and –OH groups form poly-siloxane on the surface. When the X group present on fiber surface interacts with epoxy, a stable covalent bond is developed. On accomplishment of all the reactions, the strong primary bonds serve as a link between the thermoplastic fibers and the epoxy matrix [35].

Significant improvement in impact strength of GFRPs (132% improvement over RC) was also achieved by addition of T4 (MAH grafting) treated Inviya fibers. With regards to MAH grafting, it is reported that when MAH is exposed to UV rays, it develops eximers, as illustrated by Equation 1.

$$2MAH^{UV} \rightarrow MAH^{+}\,MAH^{-} \qquad \text{---------- (1)}$$

These MAH eximers are abstracted by hydrogen atoms from Inviya fibers which promotes cross-linking reaction. This leads to grafting of MAH on Inviya fibers successfully [34]. The successful MAH grafting strengthens the interfacial bonding among dissimilar constituents of GFRPs. Consequently, the stress applied on GFRPs is uniformly and effectively transferred to the

reinforcement(s) through the strong interface developed. Thus, higher impact strength was witnessed for GFRPs reinforced with MAH grafted Inviya fibers (2PG*1.5IMC).

7.3 SEM and EDS analysis for confirming surface treatment of Inviya fibers

FE-SEM micrographs and EDS spectra of pristine and compatibilized Inviya fibers (after various surface treatments) are shown in Figure 7.3 and Figure 7.4 respectively.

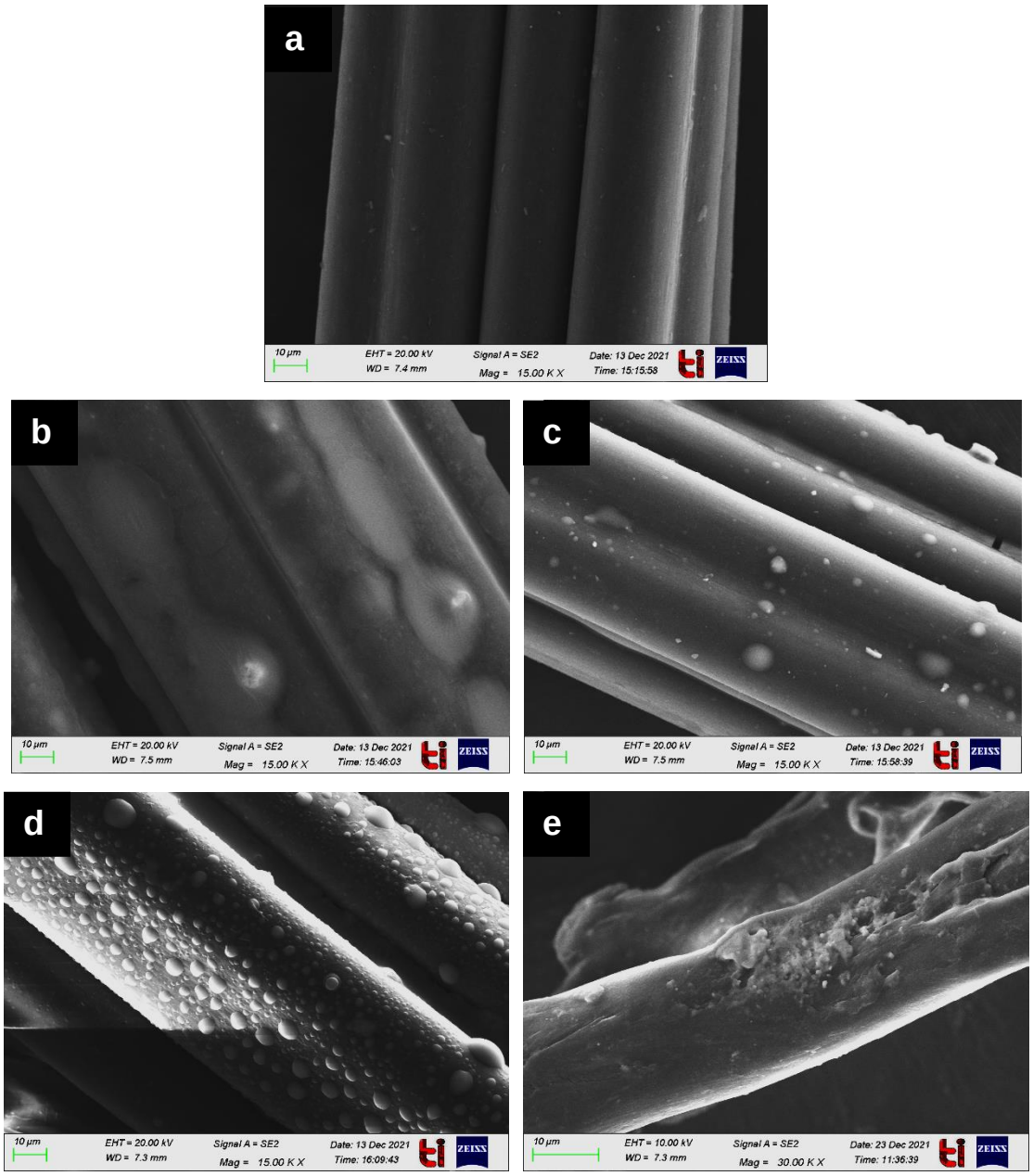

Figure 7.3. FE-SEM micrographs of Inviya fibers showing their surface (a) in the pristine state, (b) after T5 treatment, (c) after T2 treatment, (d) after T6 treatment, and (e) after T4 treatment.

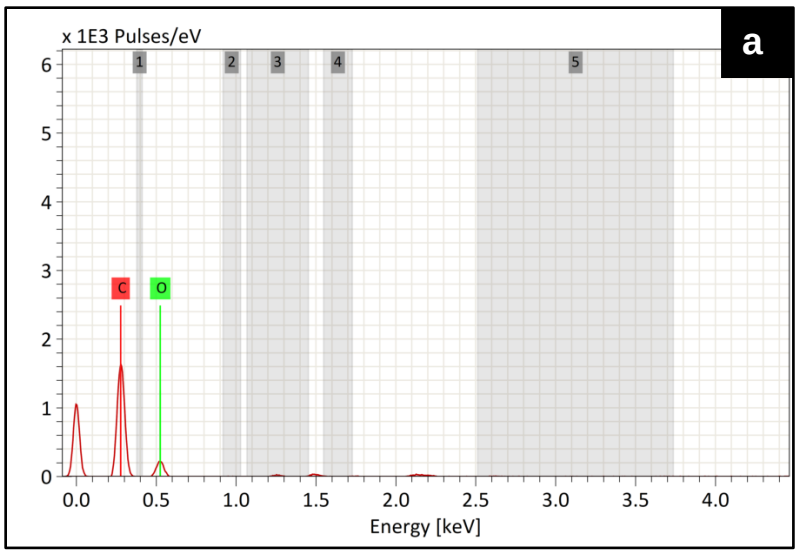
a
x 1E3 Pulses/eV
1
2
3
4
5
C
O
Energy [keV]

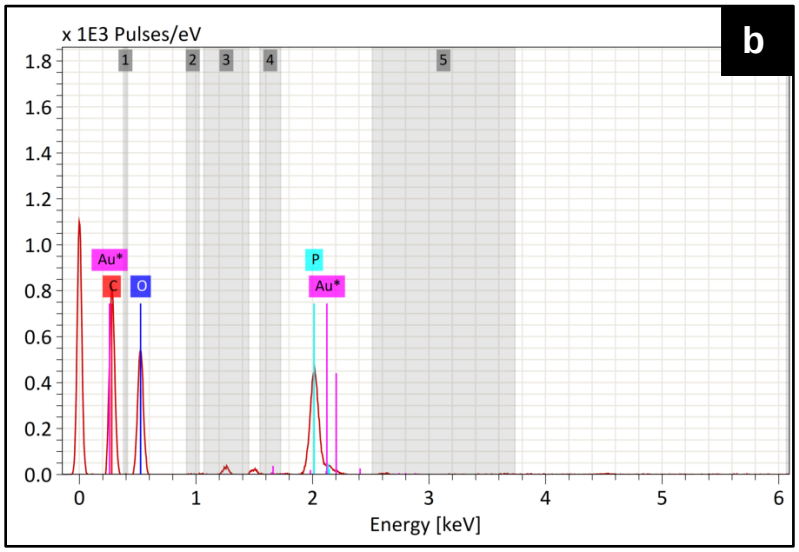
b
x 1E3 Pulses/eV
1
2
3
4
5
Au*
C
O
P
Au*
Energy [keV]

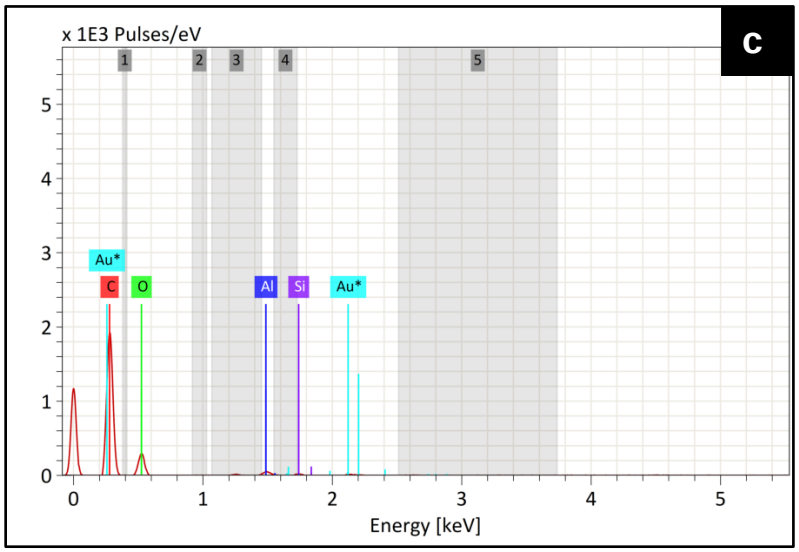
c
x 1E3 Pulses/eV
1
2
3
4
5
Au*
C
O
Al
Si
Au*
Energy [keV]

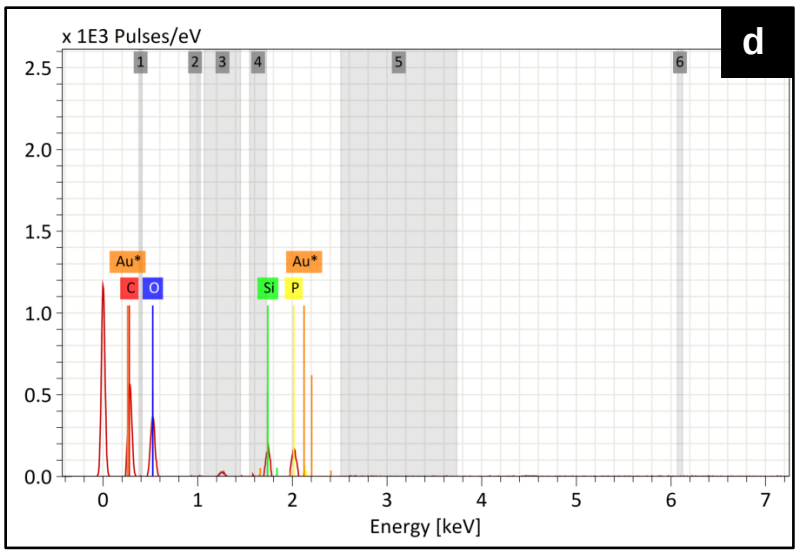

Figure 7.4. EDS spectrographs of Inviya fibers showing the presence of various constituents (a) in the pristine state, (b) after T5 treatment, (c) after T2 treatment, and (d) after T6 treatment.

The surface of pristine Inviya fibers was very smooth and glossy (Figure 7.3a). Carbon (C) and Oxygen (O) were the main elements detected in pristine Inviya fibers through EDS (Figure 7.4a). Phosphoric acid treatment (T5) significantly altered the surface of Inviya fibers. The surface of fibers became more rough/uneven after treatment (Figure 7.3b). Phosphoric acid treatment added one more element, (phosphorus, P), along with C and O (Figure 7.4b). The 'O' content also increased from 17.94% to 41.52%. With regards to silane treatment (T2), silane coating was clearly witnessed on the surface of Inviya fibers after the treatment (Figure 7.3c). The presence of silicon (Si) along with C and O in EDS spectra confirmed the silanization of Inviya fibers (Figure 7.4c). For T6 treatment (combination of phosphoric acid treatment and silanization), the surface of treated Inviya fibers became very bumpy and rough (Figure 7.3d) as compared to Figures 7.3a–c. Phosphoric acid treatment made the surface of Inviya fibers very rough and irregular. This resulted in very effective and uniform silane coating on the fibers (Figure 7.3d) as compared to the case of only silane treatment i.e. T2 treatment (Figure 7.3c). The various elements observed in EDS spectra included C, O, P, and Si (Figure 7.4d). The presence of these elements confirmed the success of the combined treatment (T6 treatment). Figure 7.3e shows the FE-SEM micrograph of Inviya fibers after MAH grafting (T4 treatment). Inviya fiber surface became uneven after this treatment and uniform maleic anhydride coating was observed (Figure 7.3e). EDS analysis could not validate the presence of MAH on T4 treated fibers. To confirm the presence of MAH coating, FTIR analysis was done which is discussed in the next section.

Elemental Au was observed in EDS spectra due to the gold sputtering of samples to make them conductive as required for SEM samples. Further, elemental Al was observed owing to the use of aluminium stabs for EDS analysis.

7.4 FTIR analysis to confirm surface treatment of Inviya fibers

To validate the results of FE-SEM and EDS analysis pertaining to surface treatment of Inviya fibers, FTIR analysis was done. FTIR diffractograms are given in Figure 7.5. The peak around 3320 cm^{-1} corresponded to the stretching of amine group (–NH) in urethane [232,233]. The peak around 1638 cm^{-1} corresponded to presence of carbonyl group which indicated presence of urethane moieties [233]. The peaks around 2938 cm^{-1}, 2854 cm^{-1}, and 2797 cm^{-1} were observed owing to symmetric/asymmetric stretching of C–H bands [232–234]. The peak around 1730 cm^{-1} corresponded to C=O stretching [233–235]. The peak around 1530 cm^{-1} was observed due to C–N stretching or NH bending [232,236]. The weak peak around 1100 cm^{-1} was due to ether (C–O–C) stretching [232,236]. These aforementioned peaks were observed both in pristine as well as all cases of treated fibers. These peaks signified that the fibers under investigation were Inviya fibers (spandex fibers).

For T5 treated Inviya fibers, the peak at 3320 cm^{-1} broadened and its intensity increased after phosphoric acid treatment (as compared to that in case of pristine Inviya fibers) because of the increased O–H group [237]. The increased intensity around 1638 cm^{-1} was due to amide I group [234,237]. The relatively increased intensity of peak at 990 cm^{-1} corresponded to aliphatic phosphates (P–O–C stretching) [235]. These observations confirmed the surface treatment of Inviya fibers with phosphoric acid (T5 treatment).

For T2 treated Inviya fibers, the peak around 3320 cm^{-1} belonged to the amine group or O–H group broadening, and its intensity increased after silanization with 3-aminopropyltriethoxy silane agent [25]. This confirmed the silanization of Inviya fibers (T2 treatment).

For T6 treated Inviya fibers, the peak around 3320 cm^{-1} belonged to the amine group or O–H group broadening; its intensity also increased [25]. The high intensity peak at 990 cm^{-1} corresponded to aliphatic phosphates (P–O–C stretching) and confirmed the combined treatment of phosphoric acid and silanization (T6 treatment) [235].

For T4 treated Inviya fibers, the peak at 3320 cm^{-1} broadened after MAH grafting belonged to the amine group or O–H group. The C=O stretching of anhydride available in MAH boosted the

strength of the peak at 1730 cm^{-1} [237]. The intensities of peaks at 1638 cm^{-1} and l530 cm^{-1} also changed, may be due to formation of carboxy group as a result of reaction between the anhydro group and moisture and due to the existence of COOH group respectively [34]. Thus, FTIR study validated the results obtained through SEM and EDS.

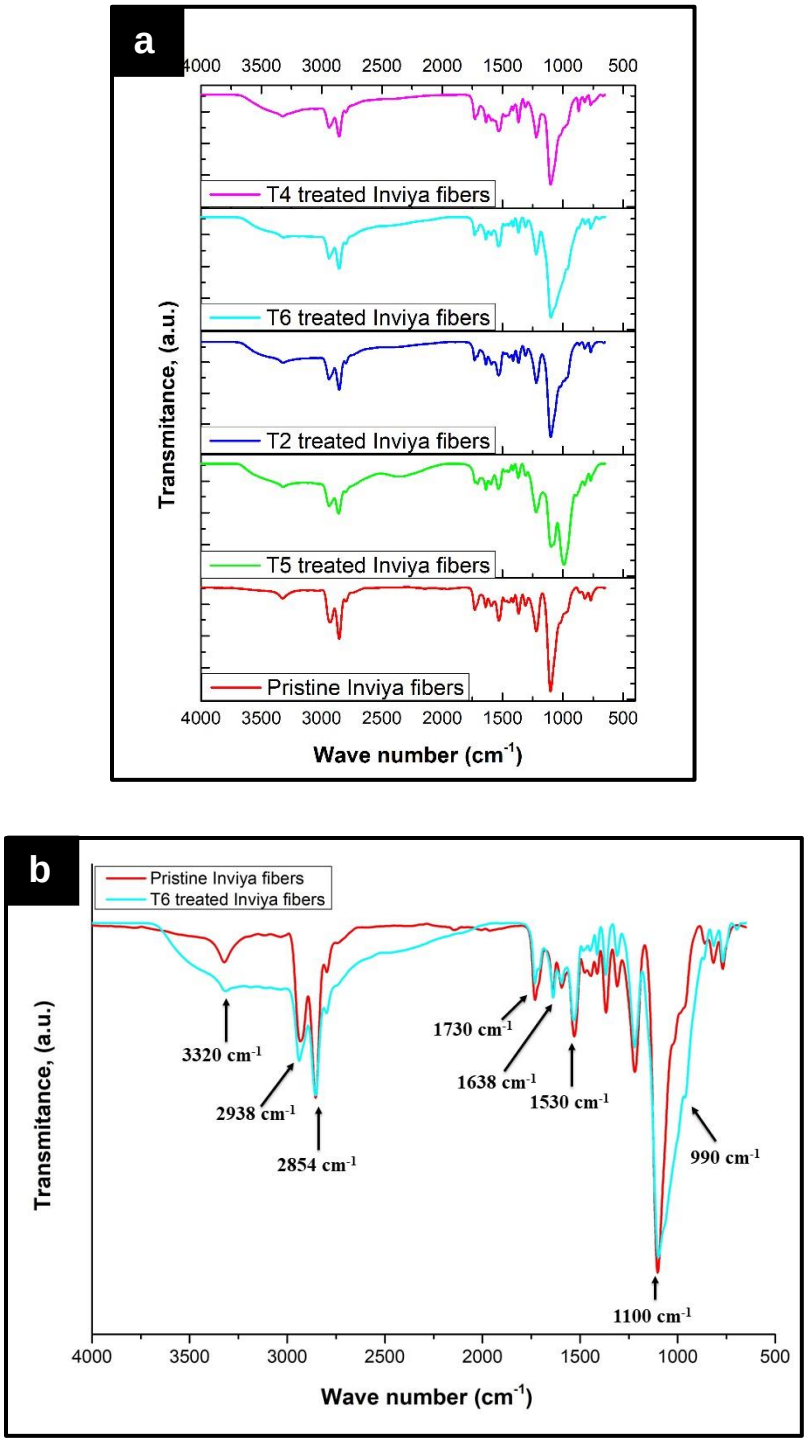

Figure 7.5. FTIR spectra of (a) all the cases of Inviya fibers, (b) pristine versus T6 treated Inviya fibers.

7.5 SEM analysis of fracture surface of impact test specimens of GFRPs containing silanized nanoclay and Inviya fibers

Figure 7.6 shows the micrographs of fracture surface of impact test samples of the reference GFRP sample (RC) and GFRPs containing pristine and silanized nanoclay respectively (2PGC and 2PG*C respectively).

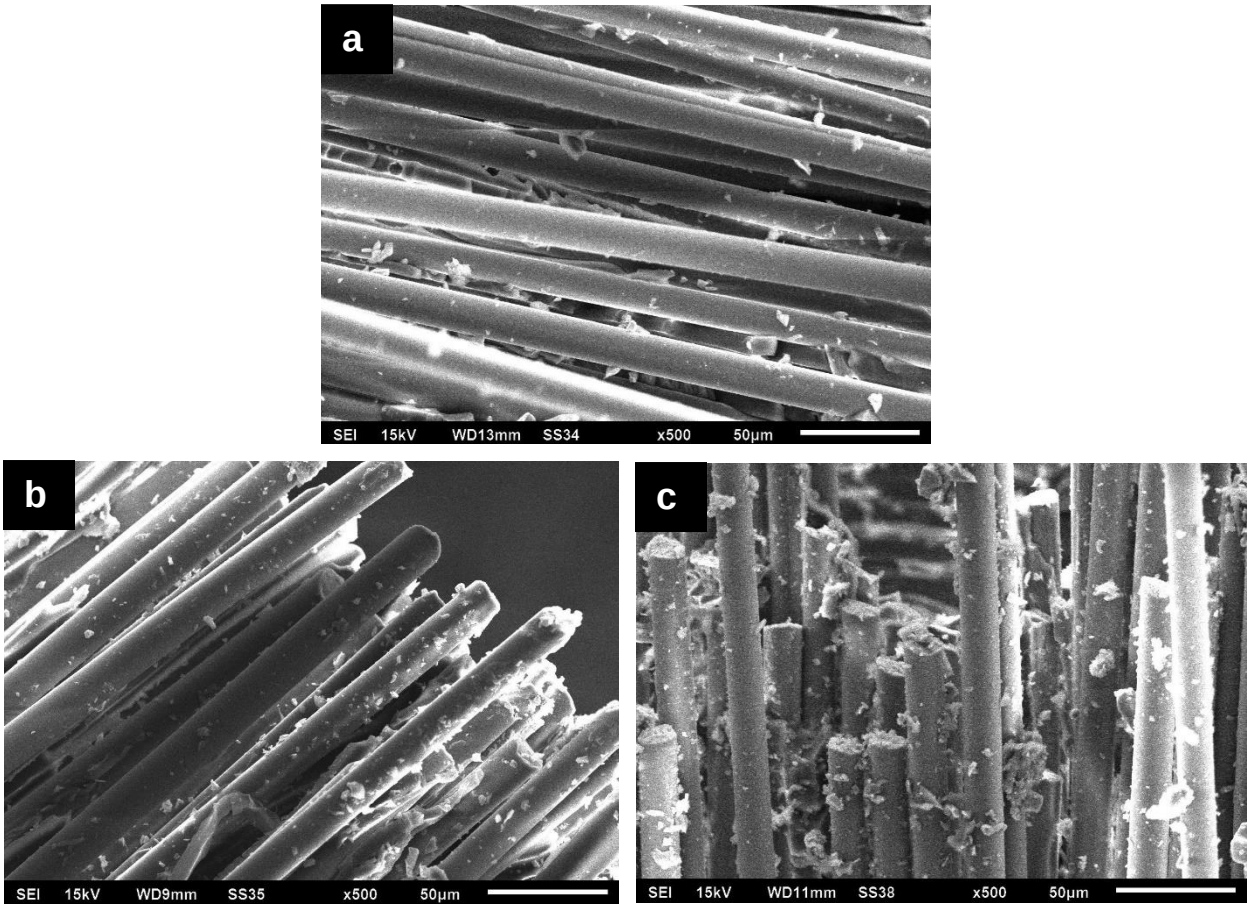

Figure 7.6. SEM micrographs of fracture surface of impact test specimens of (a) RC, (b) 2PGC, and (c) 2PG*C composites.

For the reference sample (RC), the glass fiber surface appeared very smooth. Further, very few traces of epoxy were witnessed on the surface of glass fibers owing to weak interfacial bonding between glass fibers and epoxy resin (Figure 7.6a). For the 2PGC nanocomposite (Figure 7.6b), the surface of glass fibers appeared relatively rough as compared to RC; more traces of epoxy-clay platelets mixture was observed on the glass fiber surface. The pristine clay platelets, on addition to RC, attached to the surface of glass fibers (both being inorganic in nature), making the glass fiber surface rougher, and thus, improving the interfacial bonding between glass fibers and epoxy due to mechanical interlocking effect. For the 2PG*C nanocomposite (reinforced with silanized

clay reinforced), the surface of glass fibers appeared roughest (Figure 7.6c). Silanized platelets showed better dispersion in the nanocomposite GFRP system (due to increased d-spacing). This led to more bonding sites between glass fibers and silanized platelets-epoxy mixture. Hence, higher impact strength was observed for 2PG*C nanocomposite as compared to RC and 2PGC compositions.

Figure 7.7 presents the SEM micrographs of GFRPs reinforced with silanized clay platelets and Inviya fibers (pristine/compatibilized) showing fracture surfaces after impact testing. Inviya fibers and glass fibers are shown with the help of orange and blue colored arrows respectively in Figure 7.7. Inviya/glass fibers which fractured under impact loading are highlighted with circles in red color. As discussed earlier in Section 7.2, addition of pristine thermoplastic fibers deteriorated the impact strength of resulting GFRPs owing to a lack of compatibility among various constituents of GFRPs. Figure 7.7a–b witnessed only a few bonding sites between 'epoxy-silanized clay-Inviya fibers' mixture and glass fibers. It was observed that Inviya fibers did not adhere to the glass fibers. Consequently, lower impact strength was observed for 2PG*1.5IC composition. Higher impact strength of GFRPs was achieved with reinforcement of T6 and T4 treated Inviya fibers. Addition of T6 (combination of phosphoric acid and silanization treatment) and T4 (UV-assisted MAH treated) treated Inviya fibers improved the impact strength by 150% and 132% respectively over RC sample. It was clear from Figure 7.7d–e that T6 and T4 treated Inviya fibers showed better compatibility with other constituents of GFRPs. More bonding sites were observed between 'epoxy-silanized clay-compatibilized Inviya fibers' mixture and glass fibers. Figures 7.7d−e showed that 'epoxy-silanized clay-compatibilized Inviya fibers' mixture was more uniformly present on the surface of glass fibers. Also, surface treatment of Inviya fibers impeded the Inviya fiber-Inviya fiber interaction resulted in more uniform dispersion of Inviya fibers. The uniform distribution of compatibilized nanoclay platelets-Inviya fibers restricted crack propagation under loading by acting as crack impeders/deflectors before failure of the material.

Consequently, newly developed GFRPs absorbed more energy before fracture. Thus, higher mechanical properties (especially impact strength) were witnessed.

Epoxy based GFRP reinforced with 2 phr of silanized nanoclay and 1.5 phr of Inviya fibers treated with phosphoric acid solution followed by silanization (T6 treatment) exhibited 150% and 3.5% improvement in impact strength and tensile strength respectively over the reference sample.

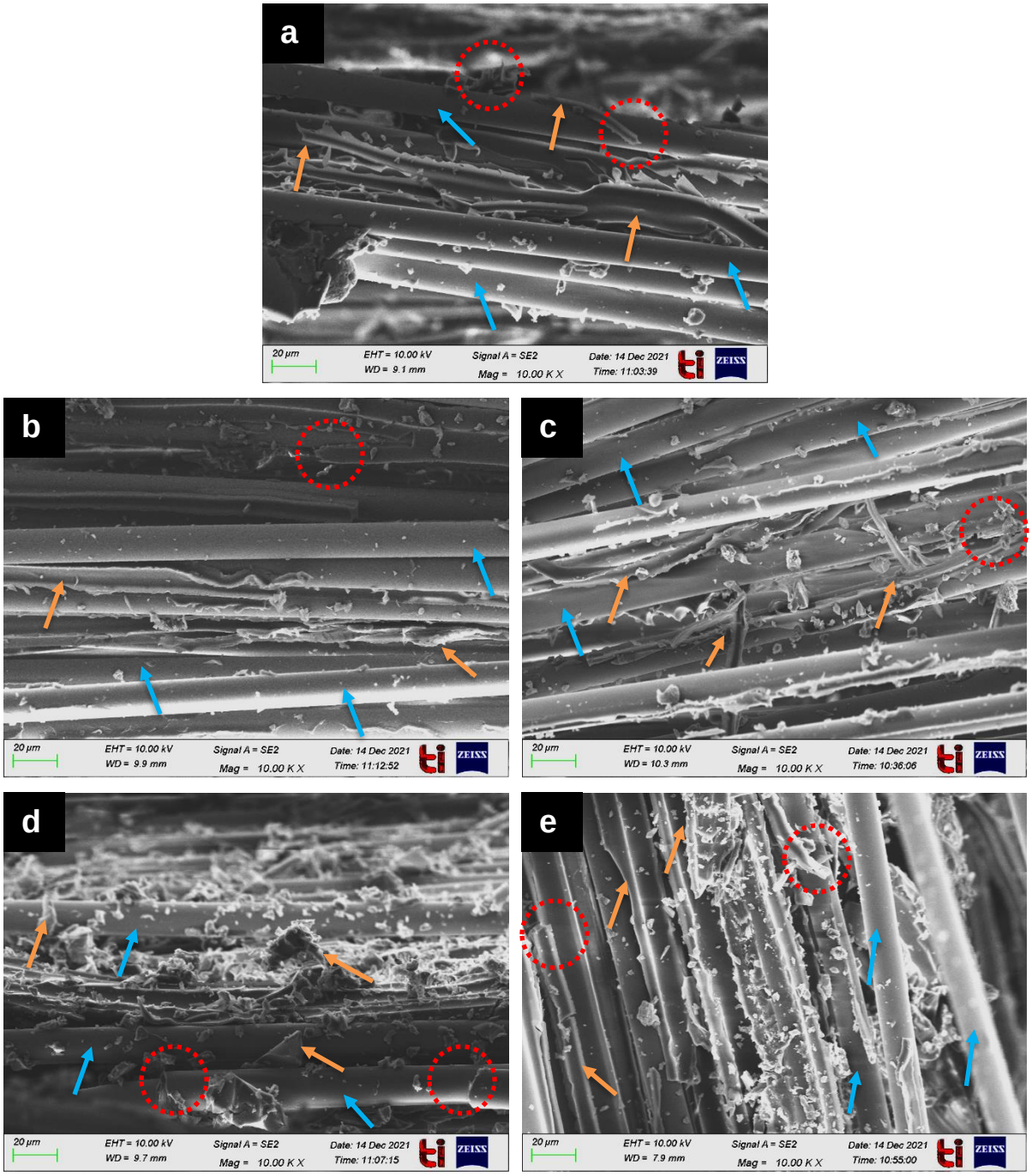

Figure 7.7. FE-SEM micrographs of fracture surface of impact test specimens of GFRPs reinforced with 2 phr of silanized nanoclay and 1.5 phr of Inviya fibers for (a) 2PG*1.5IC, (b) 2PG*1.5IPC, (c) 2PG*1.5IAC, (d) 2PG*1.5IPAC, and (e) 2PG*1.0IMC nanocomposites.

The next chapter presents the main conclusions drawn from the present research and the possible scope for future work.

Chapter 8. Conclusions and future recommendations

8.1 Overview

In the present work, multi-scale filler reinforced epoxy based GFRP nanocomposites were successfully proceesed using vacuum assisted hand lay-up procedure. Silanized nanoclay and compatibilized thermoplastic fibers (including UHMWPE, para-aramid, and Inviya fibers) were added as nano-filler and micro-filler, respectively to glass fiber reinforced epoxy nanocomposites. The resulting GFRP nanocomposites exhibited significant improvements in impact strength without any drop in tensile properties.

The main findings of the present research are discussed in the following sections.

8.2 Processing of multi-scale filler reinforced glass fiber epoxy nanocomposites

Processing these multi-scale filler reinforced epoxy GFRPs was challenging due to the high viscosity of the system. Despite the challenges, multi-scale filler reinforced GFRP nanocomposites with significantly high and reproducibile mechanical performance (especially impact strength) were successfully processed. The main conclusions with regards to the processing adopted in the present research are as follows:

- Nano-filler (nanoclay) and micro-filler (thermoplastic fibers) were effectively dispersed in the epoxy resin with the help of homogenizer and a probe sonicator. For dispersion of nanoclay in the epoxy matrix, homogenization (speed: 20,000 rpm; time: 10 min) was followed by probe sonication (amplitude: 80%; pulse-on time: 40s; pulse-off time: 20s; total sonication time: 10 min). Further, for dispersion of thermoplastic fibers, homogenization (speed: 10,000 rpm; time: 5 min) was followed by high speed homogenization (speed: 15,000 rpm; time: 5 min), and was finally subjected to sonication (amplitude: 80%; pulse-on time: 40s; pulse-off time: 20s; total sonication time: 10 min). Again, the suspension (epoxy/nanoclay/thermoplastic fibers) was homogenized (speed: 10,000 rpm; time: 5 min). Finally, the curing agent (hardener) was mixed in the suspension of epoxy/nanoclay/thermoplastic fibers by using a mechanical stirrer (speed: 500 rpm; total stirring time: 10 min).
- XRD diffractograms obtained for the processed GFRPs containing pristine/silanized nanoclay didn't show the 'd_{001}' peak. This indicated that exfoliated morphology (partially/fully) for the nanoclay was achieved in GFRPs. The results of XRD were confirmed by TEM micrographs, which showed partially exfoliated nanoclay morphology in the processed GFRPs. The results

of XRD and TEM analysis signified that the processing procedure resulted in dispersion of the clay platelets effectively at a nano-level in processed GFRPs.

- For the processed multi-scale filler reinforced epoxy nanocomposites, the key to improved performance was dependent on the success in achieving good interfacial interactions among constituents of GFRP system. To achieve effective interfacial bonding among constituents, silanization technique was used for nanoclay and four different techniques for thermoplastic fibers including (a) chemical treatment using phosphoric acid/potassium permanganate (b) silanization, (c) combination of chemical treatment & silanization, and (d) UV-assisted maleic anhydride were evaluated in the present research.
- For MAH grafting of thermoplastic fibers, the optimum time required for exposure to UV radiations had to be determined for each type of fiber. The optimum exposure time for UHMWPE fibers, para-aramid fibers, and Inviya fibers was determined as 4.5 h, 2.0 h, and 4.5 h respectively. These optimum exposure time durations resulted in weight gain of 39.50%, 61.83%, and 34.1% for UHMWPE fibers, para-aramid fibers, and Inviya fibers respectively.

8.3 Mechanical properties of multi-scale filler reinforced glass fiber epoxy nanocomposites

Multi-scale filler reinforced epoxy based GFRPs with significantly improved impact strength were developed in the present research. The major outcomes with regards to mechanical properties obtained and the associated characterization measures to corroborate the improvements achieved in properties for processed GFRPs are as follows:

- Three different pristine nanoclays were reinforced separately to epoxy based GFRP composite (reference composition) to select the best nanoclay for further processing of epoxy based GFRP nanocomposites. Improvement in mechanical properties was achieved with all the three types of nanoclays. Addition of Nanomer PGV nanoclay provided the maximum improvement in mechanical properties of the resulting GFRP nanocomposite. Impact strength, tensile strength, and tensile modulus improved by 23.5%, 4%, and 14% respectively over the reference sample. For this reason, Nanomer PGV nanoclay was used for further investigations.
- Silane treatment of Nanomer PGV nanoclay and its subsequent reinforcement in epoxy based GFRP composite (reference composition) was effective in further improving the mechanical properties of resulting GFRP (i.e. properties of this resulting GFRP were superior over its counterpart containing pristine nanoclay). The optimum weight concentration of silane agent

for silanization of nanoclay was three times the given weight concentration of nanoclay (i.e. 3X). Reinforcement of 2phr of 3X silane treated nanoclay (without acetone washing) to the reference composite exhibited 27%, 16%, and 6% improvement in impact strength, tensile strength and tensile modulus respectively for the resulting GFRP nanocomposite.

- Reinforcement of thermoplastic fibers in the pristine state to epoxy-silanized nanoclay GFRP system degraded all the mechanical properties of resulting GFRPs. Pristine thermoplastic fibers did not show effective interfacial interaction with epoxy resin due to lack of polar functional groups and also due to chemically inert nature/mechanically smooth surface of pristine fibers. SEM micrographs confirmed poor interfacial bonding of pristine thermoplastic fibers with other constituents of GFRPs. To overcome this issue, different compatibilization techniques were used for surface treatment of thermoplastic fibers.
- Compatibilization procedures used for surface modification of thermoplastic fibers were confirmed through SEM-EDS and FTIR analysis. SEM-EDS analysis confirmed the chemical and morphological changes on the surface of treated thermoplastic fibers. FTIR analysis further validated the results of SEM-EDS. Compatibilization of thermoplastic fibers improved the interfacial bonding among various constituents of GFRP nanocomposite system. As a result, for a given composition, the impact strength and tensile properties of epoxy based GFRPs reinforced with compatibilized thermoplastic fibers were significantly higher than their counterparts reinforced with pristine thermoplastic fibers.
- Ultra high molecular weight polyethylene (UHMWPE) fiber concentration in GFRPs was varied in the range of 0.125–0.500 phr. For pristine UHMWPE reinforced GFRPs, the sample containing 2 phr of silanized nanoclay and 0.250 phr of pristine UHMWPE fibers showed the best results. So, 0.250 phr of UHMWPE fiber loading was selected to process GFRPs containing compatibilized UHMWPE fibers and silanized nanoclay. Epoxy based GFRP reinforced with 2 phr of silanized nanoclay and 0.250 phr of UHMWPE fibers treated with potassium permanganate solution followed by silanization (T3 treatment) exhibited 30% and 17% improvement in impact strength and tensile strength respectively over the reference sample.
- Para-aramid fiber concentration in GFRPs was varied in the range of 0.5–2.0 phr. For pristine para-aramid fiber reinforced GFRPs, the sample containing 2 phr of silanized nanoclay and 1.0 phr of para-aramid fibers showed the best results. So, 1.0 phr of para-aramid fiber loading was

selected to process GFRPs containing compatibilized para-aramid fibers and silanized nanoclay. Epoxy based GFRP reinforced with 2 phr of silanized nanoclay and 1.0 phr of para-aramid fibers treated with UV-assisted MAH grafting (T4 treatment) exhibited 34% and 6% improvement in impact strength and tensile strength respectively over the reference sample.

- Inviya fiber concentration in GFRPs was varied in the range of from 0.5–2.0 phr. For pristine Inviya fiber reinforced GFRPs, the sample containing 2 phr of silanized nanoclay and 1.5 phr of Inviya fibers showed the best results. So, 1.5 phr of Inviya fiber loading was selected to process GFRPs containing compatibilized Inviya fibers and silanized nanoclay. Epoxy based GFRP reinforced with 2 phr of silanized nanoclay and 1.5 phr of Inviya fibers treated with phosphoric acid solution followed by silanization (T6 treatment) exhibited 150%, and 3.5% improvement in impact strength and tensile strength respectively over the reference sample.

8.4 Major conclusions

The present work was envisaged on the hypothesis that reinforcement of thermoplastic fibers at a different scale (as micro-filler) to epoxy based GFRPs (glass fiber mat as macro-filler) containing clay as a nano-filler can result in significant improvements in mechanical properties, especially the impact strength. The reinforcement of nanoclay (pristine/compatibilized) to epoxy based GFRP resulted in an improvement of impact strength along with improved tensile properties. It was expected that reinforcement of thermoplastic fibers would improve the impact strength of epoxy based GFRPs owing to good ductility of thermoplastic fibers, despite their low strength and modulus. Contrary to this consideration, the impact strength of GFRPs initially decreased on reinforcement of these more elastic/ductile micro-fillers (pristine thermoplastic fibers). Further analysis showed that this decrease in impact strength was attributed to less compatibility of thermoplastic fibers with other constituents of the epoxy based GFRP nanocomposite system. To overcome this issue, thermoplastic fibers were subjected to various surface treatment procedures to improve their interfacial bonding with other constituents of GFRPs. It was noted that each specific type of thermoplastic fiber provided the best results (in terms of improvements obtained in mechanical properties of resulting GFRP containing the compatibilized fibers) with a specific type of surface treatment. From this, it can be concluded that the choice of surface treatment for a particular fiber depends upon its chemical composition, the functional groups added on its surface through a specific treatment, and the interaction of treated fiber surface with other constituents of

the composite system. Maximum improvements achieved in impact strength of multi-scale filler reinforced epoxy based GFRPs is summarized in Table 8.1. It can be concluded that more is the elastic/ductile nature of the reinforced thermoplastic fiber (Inviya fibers, para-aramid fibers, UHMWPE fibers; decreasing in this order in the present work), greater was the improvement attained in impact strength of epoxy based GFRPs. In this context, epoxy based GFRPs containing 2 phr of silanized nanoclay and 1.5 phr of surface treated Inviya fibers (treatment with phosphoric acid solution followed by silanization) exhibited maximum improvement of 150% in impact strength as compared to the reference composite.

Table 8.1. Summary of impact strength and tensile strength of GFRPs reinforced with 2 phr of silanized nanoclay and best concentrations of compatibilized polymeric fibers (percentage shown in the parenthesis represents improvement achieved for a given composition over the reference composition).

S. No.	Sample Designation3[#]	Impact Strength (kJ/m^2)	Tensile Strength (MPa)
1.	RC	153±9	338±7
2.	2PGC	189±17 (23.5%)	351±4 (4%)
3.	2PG*C	194±2 (27%)	392±9 (16%)
4.	2PG*0.25UPAC	199±10 (30%)	396±7 (17%)
5.	2PG*1.0PMC	205±6 (34%)	357±5 (6%)
6.	2PG*1.5IPAC	382±10 (150%)	350±6 (4%)

#: Details of various designations is given in nomenclature

It was a challenging task to reproducibly fabricate multi-scale filler reinforced epoxy GFRPs due to the resulting high viscosity of the system. Despite the challenges, GFRPs with significantly high impact strength and moderately improved tensile properties were successfully processed in the present research. The processing procedure established in the current research work, including (i) reinforcing compatibilized thermoplastic fibers, and (ii) processing highly viscous systems, will open up novel routes for further research to boost the mechanical properties of epoxy based GFRP nanocomposites.

8.5 Future scope

- Thermoplastic fibers including UHMWPE fibers, para-aramid fibers, and Inviya fibers were used in the present work. A wide spectrum of thermoplastic/elastomeric fillers are available having different values of ductility, impact strength, and tensile strength. These fillers with different mechanical properties can be appropriately reinforced after compatibilization into the epoxy based GFRPs to achieve further improvements in impact strength.

- The current research work used silanized nano-filler and compatibilized micro-fillers to improve their interfacial interaction with other constituents of the GFRP system. Further enhancement in mechanical properties of epoxy based GFRPs can be achieved by subjecting the glass fibers also to a suitable surface treatment.
- This study examined three different types of nanoclays in the role of a nano-filler for epoxy based GFRP systems. The nanoclays used included Cloisite®15A (CA), Nanomer® I.28E (IE), and Nanomer® PGV (PG). Out of these three nanoclays, the best results for epoxy-nanoclay system were shown by Nanomer® PGV (PG) nanoclay. So, this nanoclay was used for processing of epoxy based GFRP systems. A range of other nano-fillers are available which vary greatly in properties and characteristics. These include carbon nanotubes, graphene, graphene oxide, nano-silica, titanium oxide etc. The scope of the present research states that the effect of reinforcing these nano-fillers (other than nanoclays) on the properties of epoxy-GFRP nanocomposites can be explored in future research.
- In the current research work, the mechanical properties evaluated are tensile properties and impact strength as the focus was on increasing the impact strength of these thermoset nanocomposite systems without compromising on the tensile properties. Other properties such as fracture toughness, compressive strength, flexural properties etc. can be explored in future research.
- Apart from the surface treatment methods used in the present research for compatibilization of thermoplastic fibers, several other procedures including corona discharge treatment, plasma modification, direct fluorination, and γ-ray irradiation etc. are available and can be utilized in future research.

References

[1] Nanda T, Singh K, Shelly D, Mehta R. Advancements in multi-scale filler reinforced epoxy nanocomposites for improved impact strength: a review. Crit Rev Solid State Mater Sci 2020:1–49. https://doi.org/10.1080/10408436.2020.1777934.

[2] Azeez AA, Rhee KY, Park SJ, Hui D. Epoxy clay nanocomposites - processing, properties and applications: a review. Compos Part B Eng 2013;45:308–20. https://doi.org/10.1016/j.compositesb.2012.04.012.

[3] Alexandre M, Dubios P. Polymer-layered silicate-nanocomposities: preparation, properties, and uses of a new class of materials. Mater Sci Eng 2000;28:1–36. https://doi.org/10.1016/S0927-796X(00)00012-7.

[4] Ray SS, Okamoto M. Polymer/layered silicate nanocomposites: a review from preparation to processing. Prog Polym Sci 2003;28:1539–641. https://doi.org/10.1016/j.progpolymsci.2003.08.002.

[5] Idumah CI, Obele CM. Understanding interfacial influence on properties of polymer nanocomposites. Surfaces and Interfaces 2021;22. https://doi.org/10.1016/j.surfin.2020.100879.

[6] Li Y, Lu D Wang CP. Electrical conductive adhesives with nanotechnologies. 1st ed. Springer New York Dordrecht Heidelberg London; 2010. https://doi.org/10.1007/978-0-387-88783-8.

[7] Henrique P, Camargo C, Satyanarayana KG, Wypych F. Nanocomposites : synthesis , structure , properties and new application opportunities. Mater Res 2009;12:1–39.

[8] Bagotia N, Choudhary V, Sharma DK. Synergistic effect of graphene/multiwalled carbon nanotube hybrid fillers on mechanical, electrical and EMI shielding properties of polycarbonate/ethylene methyl acrylate nanocomposites. Compos Part B Eng 2019;159:378–88. https://doi.org/10.1016/j.compositesb.2018.10.009.

[9] Yu MF, Yakobson BI, Ruoff RS. Controlled sliding and pullout of nested shells in individual multiwalled carbon nanotubes. J Phys Chem B 2000;104:8764–7. https://doi.org/10.1021/JP002828D.

[10] Shakil UA, Abu Hassan S Bin, Yahya MY, Mujiyono, Nurhadiyanto D. A review of properties and fabrication techniques of fiber reinforced polymer nanocomposites subjected to simulated accidental ballistic impact. Thin-Walled Struct 2021;158. https://doi.org/10.1016/j.tws.2020.107150.

[11] Kumar AP, Depan D, Singh Tomer N, Singh RP. Nanoscale particles for polymer degradation and stabilization-trends and future perspectives. Prog Polym Sci 2009;34:479–515. https://doi.org/10.1016/j.progpolymsci.2009.01.002.

[12] Johnsen BB, Kinloch AJ, Mohammed RD, Taylor AC, Sprenger S. Toughening mechanisms of nanoparticle-modified epoxy polymers. Polymer (Guildf) 2007;48:530–41. https://doi.org/10.1016/J.POLYMER.2006.11.038.

[13] Zhang H, Zhang Z, Friedrich K, Eger C. Property improvements of in situ epoxy nanocomposites with reduced interparticle distance at high nanosilica content. Acta Mater 2006;7:1833–42. https://doi.org/10.1016/J.ACTAMAT.2005.12.009.

[14] Nanda T, Sharma G, Mehta R, Shelly D, Singh K. Mechanisms for enhanced impact strength of epoxy based nanocomposites reinforced with silicate platelets. Mater Res Express 2019;6:065061. https://doi.org/10.1088/2053-1591/ab1023.

[15] Shelly D, Singh K, Nanda T, Mehta R. Addition of nanomer clays to GFRPs for enhanced impact strength and fracture toughness. Mater Res Express 2018;5:105013. https://doi.org/10.1088/2053-1591/aadb0d.

[16] Sharma B, Chhibber R, Mehta R. Effect of surface treatment of nanoclay on the mechanical properties of epoxy/glass fiber/clay nanocomposites. Compos Interfaces 2016;23:623–40. https://doi.org/10.1080/09276440.2016.1165522.

[17] Aly M, Hashmi MSJ, Olabi AG, Messeiry M, Hussain AI. Effect of nano clay particles on mechanical, thermal and physical behaviours of waste-glass cement mortars. Mater Sci Eng A 2011;528:7991–8. https://doi.org/10.1016/J.MSEA.2011.07.058.

[18] Mogha A, Kaushik A. Functionalized multiwall carbon nanotubes to enhance dispersion in castor oil-based polyurethane nanocomposites. Fullerenes Nanotub Carbon Nanostructures 2021;29:907–14. https://doi.org/10.1080/1536383X.2021.1915295.

[19] Mogha A, Kaushik A. Morphological studies on renewable castor oil-based nanocomposites

with modified clay and MWCNTs as fillers. Polym Polym Compos 2021;29:740–7. https://doi.org/10.1177/0967391120935240.

[20] Asgari M, Sundararaj U. Silane functionalization of sodium montmorillonite nanoclay: the effect of dispersing media on intercalation and chemical grafting. Appl Clay Sci 2018;153:228–38. https://doi.org/10.1016/j.clay.2017.12.020.

[21] Bui TQ, Hu X. A review of phase-field models, fundamentals and their applications to composite laminates. Eng Fract Mech 2021;248:107705. https://doi.org/10.1016/j.engfracmech.2021.107705.

[22] Patil RU, Mishra BK, Singh I V., Bui TQ. A new multiscale phase field method to simulate failure in composites. Adv Eng Softw 2018;126:9–33. https://doi.org/10.1016/j.advengsoft.2018.08.010.

[23] Khanna N, Raghuram V, Munshi P, Kishore NN, Arnold W. Tomographic imaging of glass/epoxy composite with a laser based ultrasonics setup. AIP Conf. Proc 2008;1050:91–9. https://doi.org/10.1063/1.2999997.

[24] Karnati SR, Agbo P, Zhang L. Applications of silica nanoparticles in glass/carbon fiber-reinforced epoxy nanocomposite. Compos Commun 2020;17:32–41. https://doi.org/10.1016/j.coco.2019.11.003.

[25] Shelly D, Nanda T, Mehta R. Addition of compatibilized nanoclay to GFRCs for improved izod impact strength and tensile properties. Proc Inst Mech Eng Part L J Mater Des Appl 2021;235:2022–35. https://doi.org/10.1177/14644207211009923.

[26] Geboes Y, Katalagarianakis A, Soete J, Ivens J, Swolfs Y. The translaminar fracture toughness of high-performance polymer fibre composites and their carbon fibre hybrids. Compos Sci Technol 2022;221:109307. https://doi.org/10.1016/J.COMPSCITECH.2022.109307.

[27] Mesquita F, Melnikov A, Rajpurohit A, Singery V, Sanial P, Lomov S V., et al. Tensile failure strain and microstructure of unidirectional carbon fibre non-crimp fabric composites. Compos Part B Eng 2022;243:110123. https://doi.org/10.1016/J.COMPOSITESB.2022.110123.

[28] Sachan A, Choudhary V, Vimal KK, Kapur GS. Chemical treatment of cotton stalk and its

effects on mechanical, rheological and morphological properties of Polypropylene/cotton stalk bio-composites. Polym Compos 2018;39:E286–96. https://doi.org/10.1002/pc.24435.

[29] Dong C, Ranaweera-Jayawardena HA, Davies IJ. Flexural properties of hybrid composites reinforced by S-2 glass and T700S carbon fibres. Compos Part B Eng 2012;43:573–81. https://doi.org/10.1016/J.COMPOSITESB.2011.09.001.

[30] Dong C, Davies IJ. Optimal design for the flexural behaviour of glass and carbon fibre reinforced polymer hybrid composites. Mater Des 2012;37:450–7. https://doi.org/10.1016/J.MATDES.2012.01.021.

[31] Rajak DK, Wagh PH, Linul E. Manufacturing technologies of carbon/glass fiber-reinforced polymer composites and their properties: a review. Polymers (Basel) 2021;13. https://doi.org/10.3390/polym13213721.

[32] Singh K, Nanda T, Mehta R. Compatibilization of polypropylene fibers in epoxy based GFRP/clay nanocomposites for improved impact strength. Compos Part A Appl Sci Manuf 2017;98:207–17. https://doi.org/10.1016/j.compositesa.2017.03.027.

[33] Raturi M, Singh BJ, Shelly D, Singh K, Nanda T, Mehta R. Tensile behaviour and characterization of epoxy-clay-poly (ethylene terephthalate) nanocomposites. Mater Res Express 2019;6:115014. https://doi.org/10.1088/2053-1591/ab43e9.

[34] Singh K, Nanda T, Mehta R. Processing of polyethylene terephthalate fiber reinforcement to improve compatibility with constituents of GFRP nanocomposites. Mater Manuf Process 2018;33:165–73. https://doi.org/10.1080/10426914.2017.1291955.

[35] Singh K, Nanda T, Mehta R. Addition of nanoclay and compatibilized EPDM rubber for improved impact strength of epoxy glass fiber composites. Compos Part A Appl Sci Manuf 2017;103:263–71. https://doi.org/10.1016/j.compositesa.2017.10.009.

[36] Bozkurt E, Kaya E, Tanoğlu M. Mechanical and thermal behavior of non-crimp glass fiber reinforced layered clay/epoxy nanocomposites. Compos Sci Technol 2007;67:3394–403. https://doi.org/10.1016/J.COMPSCITECH.2007.03.021.

[37] Haque A, Shamsuzzoha M, Hussain F, Dean D. S2-glass/epoxy polymer nanocomposites: Manufacturing, structures, thermal and mechanical properties. J Compos Mater 2003;37:1821–38. https://doi.org/10.1177/002199803035186.

[38] Kornmann X, Rees M, Thomann Y, Necola A, Barbezat M, Thomann R. Epoxy-layered silicate nanocomposites as matrix in glass fibre-reinforced composites. Compos Sci Technol 2005;65:2259–68. https://doi.org/10.1016/J.COMPSCITECH.2005.02.006.

[39] Rafiq A, Al-Qadhi M, Merah N, Ali Y. Mechanical behavior of hybrid glass fibre/epoxy Clay nanocomposites. Adv. Mater. Res., vol. 894, 2014, p. 336–41. https://doi.org/10.4028/www.scientific.net/AMR.894.336.

[40] Isik I, Yilmazer U, Bayram G. Impact modified epoxy/montmorillonite nanocomposites: synthesis and characterization. Polymer (Guildf) 2003;44:6371–7. https://doi.org/10.1016/S0032-3861(03)00634-7.

[41] Kusmono, Wildan MW, Mohd Ishak ZA. Preparation and properties of clay-reinforced epoxy nanocomposites. Int J Polym Sci 2013;2013. https://doi.org/10.1155/2013/690675.

[42] Lim SR, Chow WS. Fracture toughness enhancement of epoxy by organo-montmorillonite. Polym - Plast Technol Eng 2011;50:182–9. https://doi.org/10.1080/03602559.2010.531427.

[43] Al-Qadhi M, Merah N, Gasem ZM. Mechanical properties and water uptake of epoxy-clay nanocomposites containing different clay loadings. J Mater Sci 2013;48:3798–804. https://doi.org/10.1007/s10853-013-7180-5.

[44] Teh SF, Liu T, Wang L, He C. Fracture behaviour of poly(ethylene terephthalate) fiber toughened epoxy composites. Compos Part A Appl Sci Manuf 2005;36:1167–73. https://doi.org/10.1016/j.compositesa.2004.08.007.

[45] Gupta R, Sharma S, Nanda T, Pandey OP. Wear studies of hybrid AMCs reinforced with naturally occurring sillimanite and rutile ceramic particles for brake-rotor applications. Ceram Int 2020;46:16849–59. https://doi.org/10.1016/j.ceramint.2020.03.262.

[46] Lu Z, Zhao Y, Su Z, Zhang M, Yang B. The effect of phosphoric acid functionalization of para-aramid fiber on the mechanical property of para-aramid sheet. J Eng Fiber Fabr 2018;13:14–22. https://doi.org/10.1177/155892501801300303.

[47] Sever K, Sarikanat M, Seki Y, Cecen V, Tavman IH. Effects of fiber surface treatments on mechanical properties of epoxy composites reinforced with glass fabric. J Mater Sci 2008;43:4666–72. https://doi.org/10.1007/S10853-008-2679-X/FIGURES/3.

[48] Asumani OML, Reid RG, Paskaramoorthy R. The effects of alkali–silane treatment on the tensile and flexural properties of short fibre non-woven kenaf reinforced polypropylene composites. Compos Part A Appl Sci Manuf 2012;43:1431–40. https://doi.org/10.1016/J.COMPOSITESA.2012.04.007.

[49] Kordoghli B, Khiari R, Dhaouadi H, Belgacem MN, Mhenni MF, Sakli F. UV irradiation-assisted grafting of poly(ethylene terephthalate) fabrics. Colloids Surfaces A Physicochem Eng Asp 2014;441:606–13. https://doi.org/10.1016/J.COLSURFA.2013.10.032.

[50] Deng T, Zhang G, Dai F. Mild surface modification of para -aramid fiber by dilute sulfuric acid under microwave irradiation. Text Res J 2017;87:799–806. https://doi.org/10.1177/0040517516639831.

[51] Mallick P. Fiber ceinforced composites, materials: manufacturing, and design. 3rd ed. CRC Press; 2007.

[52] Sathishkumar TP, Satheeshkumar S, Naveen J. Glass fiber-reinforced polymer composites - a review. J Reinf Plast Compos 2014;33:1258–75. https://doi.org/10.1177/0731684414530790.

[53] Demir B, Beggs KM, Fox BL, Servinis L, Henderson LC, Walsh TR. A predictive model of interfacial interactions between functionalised carbon fibre surfaces cross-linked with epoxy resin. Compos Sci Technol 2018;159:127–34. https://doi.org/10.1016/J.COMPSCITECH.2018.02.029.

[54] Wu Q, Zhao R, Zhu J, Wang F. Interfacial improvement of carbon fiber reinforced epoxy composites by tuning the content of curing agent in sizing agent. Appl Surf Sci 2020;504:144384. https://doi.org/10.1016/j.apsusc.2019.144384.

[55] Zhang B, Li W, Li H, Zhang H. Spontaneous infiltration and wetting behaviors of a Zr-based alloy melt on a porous SiC substrate. Int J Miner Metall Mater 2018;25:817–23.

[56] Kaushik A, Singh P, Kaushik J. The mechanical properties and chemical resistance of short glass-fiber-reinforced epoxy composites. Int J Polym Mater Polym Biomater 2006;55:425–40. https://doi.org/10.1080/009140390970404.

[57] Lin LY, Lee JH, Hong CE, Yoo GH, Advani SG. Preparation and characterization of layered silicate/glass fiber/epoxy hybrid nanocomposites via vacuum-assisted resin transfer

molding (VARTM). Compos Sci Technol 2006;66:2116–25. https://doi.org/10.1016/j.compscitech.2005.12.025.

[58] Manimaran P, Senthamaraikannan P, Sanjay MR, Marichelvam MK, Jawaid M. Study on characterization of Furcraea foetida new natural fiber as composite reinforcement for lightweight applications. Carbohydr Polym 2018;181:650–8. https://doi.org/10.1016/J.CARBPOL.2017.11.099.

[59] Thipperudrappa S, Ullal Kini A, Hiremath A. Influence of zinc oxide nanoparticles on the mechanical and thermal responses of glass fiber-reinforced epoxy nanocomposites. Polym Compos 2020;41:174–81. https://doi.org/10.1002/PC.25357.

[60] Jiao-Wang L, Loya JA, Santiuste C. Influence of cross-section on the impact and post-impact behavior of biocomposites bumper beams. Mech Adv Mater Struct 2022. https://doi.org/10.1080/15376494.2022.2072029.

[61] Robinson P, Greenhalgh E, Pinho S. Failure mechanisms in polymer matrix composites: criteria, testing and industrial applications. Woodhead Publishing; 2012. https://doi.org/10.1533/9780857095329.

[62] Schonberg WP. Hole size and crack length models for spacecraft walls under oblique hypervelocity projectile impact. Aerosp Sci Technol 1999;3:461–71. https://doi.org/10.1016/S1270-9638(99)00104-2.

[63] Fahrenthold EP, Hernandez RJ. Simulation of orbital debris impact on the space shuttle wing leading edge. Int J Impact Eng 2006;33:231–43. https://doi.org/10.1016/j.ijimpeng.2006.09.080.

[64] Bee SL, Abdullah MAA, Bee ST, Sin LT, Rahmat AR. Polymer nanocomposites based on silylated-montmorillonite: a review. Prog Polym Sci 2018;85:57–82. https://doi.org/10.1016/J.PROGPOLYMSCI.2018.07.003.

[65] Choi YY, Lee SH, Ryu SH. Effect of silane functionalization of montmorillonite on epoxy/montmorillonite nanocomposite. Polym Bull 2009;63:47–55. https://doi.org/10.1007/S00289-009-0068-5/FIGURES/9.

[66] Withers GJ, Yu Y, Khabashesku VN, Cercone L, Hadjiev VG, Souza JM, et al. Improved mechanical properties of an epoxy glass-fiber composite reinforced with surface

organomodified nanoclays. Compos Part B Eng 2015;72:175–82. https://doi.org/10.1016/j.compositesb.2014.12.008.

[67] Thongchom C, Refahati N, Saffari PR, Saffari PR, Niyaraki MN, Sirimontree S, et al. An experimental study on the effect of nanomaterials and fibers on the mechanical properties of polymer composites. Buildings 2022;12. https://doi.org/10.3390/buildings12010007.

[68] Merzah ZF, Fakhry S, Allami TG, Yuhana NY, Alamiery A. Enhancement of the properties of hybridizing epoxy and nanoclay for mechanical, industrial, and biomedical applications. Polymers (Basel) 2022;14. https://doi.org/10.3390/polym14030526.

[69] Chee SS, Jawaid M, Alothman OY, Fouad H. Effects of nanoclay on mechanical and dynamic mechanical properties of bamboo/kenaf reinforced epoxy hybrid composites. Polymers (Basel) 2021;13:1–17. https://doi.org/10.3390/polym13030395.

[70] Sivaperumal R, Jancirani J. Characterization of amino silane modified Ramie fibre, OMMT nanoclay-reinforced epoxy resin composite. Silicon 2021. https://doi.org/10.1007/s12633-021-01502-9.

[71] Nayak BA, Shubham, Prusty RK, Ray BC. Effect of nanosilica and nanoclay reinforcement on flexural and thermal properties of glass fiber/epoxy composites. Mater Today Proc 2020;33:5098–102. https://doi.org/10.1016/j.matpr.2020.02.852.

[72] Shettar M, Kini UA, Sharma S, Hiremath P, Gowrishankar GCG. Hygrothermal chamber aging effect on mechanical behavior and morphology of glass fiber-epoxy-nanoclay composites. Mater Res Express 2020;7. https://doi.org/10.1088/2053-1591/ab6405.

[73] Feiz A, Khosravi H. Multiscale composites based on a nanoclay-enhanced matrix and E-glass chopped strand mat. J Reinf Plast Compos 2019;38:591–600. https://doi.org/10.1177/0731684419836219.

[74] Kumar MA, Reddy KH, Reddy YVM, Reddy GR, Naidu SV. Improvement of tensile and flexural properties in epoxy/clay nanocomposites reinforced with weave glass fiber reel. Int J Polym Mater Polym Biomater 2010;59:854–62. https://doi.org/10.1080/00914037.2010.504144.

[75] Zunjarrao SC, Sriraman R, Singh RP. Effect of processing parameters and clay volume fraction on the mechanical properties of epoxy-clay nanocomposites. J Mater Sci

2006;41:2219–28. https://doi.org/10.1007/s10853-006-7179-2.

[76] Qi B, Zhang QX, Bannister M, Mai YW. Investigation of the mechanical properties of DGEBA-based epoxy resin with nanoclay additives. Compos Struct 2006;75:514–9. https://doi.org/10.1016/j.compstruct.2006.04.032.

[77] Wang L, Wang K, Chen L, Zhang Y, He C. Preparation, morphology and thermal/mechanical properties of epoxy/nanoclay composite. Compos Part A Appl Sci Manuf 2006;37:1890–6. https://doi.org/10.1016/j.compositesa.2005.12.020.

[78] Kim BC, Park SW, Lee DG. Fracture toughness of the nano-particle reinforced epoxy composite. Compos Struct 2008;86:69–77. https://doi.org/10.1016/j.compstruct.2008.03.005.

[79] Alamri H, Low IM. Effect of water absorption on the mechanical properties of nano-filler reinforced epoxy nanocomposites. Mater Des 2012;42:214–22. https://doi.org/10.1016/j.matdes.2012.05.060.

[80] Bakar M, Biakowska A, Molenda J, Piasek J. Preparation and properties evaluation of thermoplastic modified epoxy nanocomposites. J Macromol Sci Part B Phys 2012;51:1159–71. https://doi.org/10.1080/00222348.2011.625906.

[81] Shokrieh MM, Kefayati AR, Chitsazzadeh M. Fabrication and mechanical properties of clay/epoxy nanocomposite and its polymer concrete. Mater Des 2012;40:443–52. https://doi.org/10.1016/j.matdes.2012.03.008.

[82] Alsagayar ZS, Rahmat AR, Arsad A, binti Mustaph SNH. Tensile and flexural properties of montmorillonite nanoclay reinforced epoxy resin composites. Adv Mater Res 2015;1112:373–6. https://doi.org/10.4028/www.scientific.net/amr.1112.373.

[83] Nguyen TA. Study on the synergies of nanoclay and MWCNTs to the flame retardant and mechanical properties of epoxy nanocomposites. J Nanomater 2021;2021:5536676. https://doi.org/10.1155/2021/5536676.

[84] Timmerman JF, Hayes BS, Seferis JC. Nanoclay reinforcement effects on the cryogenic microcracking of carbon fiber/epoxy composites. Compos Sci Technol 2002;62:1249–58. https://doi.org/10.1016/S0266-3538(02)00063-5.

[85] Siddiqui NA, Woo RSC, Kim JK, Leung CCK, Munir A. Mode I interlaminar fracture behavior and mechanical properties of CFRPs with nanoclay-filled epoxy matrix. Compos Part A Appl Sci Manuf 2007;38:449–60. https://doi.org/10.1016/J.COMPOSITESA.2006.03.001.

[86] Xu Y, Hoa S Van. Mechanical properties of carbon fiber reinforced epoxy/clay nanocomposites. Compos Sci Technol 2008;68:854–61. https://doi.org/10.1016/j.compscitech.2007.08.013.

[87] Karippal JJ, Murthy HNN, Rai KS, Sreejith M, Krishna M. Study of mechanical properties of epoxy/glass/nanoclay hybrid composites. J Compos Mater 2011;45:1893–9. https://doi.org/10.1177/0021998310389087.

[88] Khan SU, Iqbal K, Munir A, Kim JK. Quasi-static and impact fracture behaviors of CFRPs with nanoclay-filled epoxy matrix. Compos Part A Appl Sci Manuf 2011;42:253–64. https://doi.org/10.1016/j.compositesa.2010.11.011.

[89] Phonthammachai N, Li X, Wong S, Chia H, Tjiu WW, He C. Fabrication of CFRP from high performance clay/epoxy nanocomposite: preparation conditions, thermal-mechanical properties and interlaminar fracture characteristics. Compos Part A Appl Sci Manuf 2011;42:881–7. https://doi.org/10.1016/j.compositesa.2011.02.014.

[90] Kanny K, Mohan TP. Resin infusion analysis of nanoclay filled glass fiber laminates. Compos Part B Eng 2014;58:328–34. https://doi.org/10.1016/j.compositesb.2013.10.025.

[91] Islam ME, Mahdi TH, Hosur M V., Jeelani S. Characterization of carbon fiber reinforced epoxy composites modified with nanoclay and carbon nanotubes. Procedia Eng 2015;105:821–8. https://doi.org/10.1016/j.proeng.2015.05.078.

[92] Sharma B, Chhibber R, Mehta R. Effect of surface treatment of nanoclay on the mechanical properties of epoxy/glass fiber/clay nanocomposites. Compos Interfaces 2016;23:623–40. https://doi.org/10.1080/09276440.2016.1165522.

[93] Jeyakumar R, Sampath PS, Ramamoorthi R, Ramakrishnan T. Structural, morphological and mechanical behaviour of glass fibre reinforced epoxy nanoclay composites. Int J Adv Manuf Technol 2017;93:527–35. https://doi.org/10.1007/s00170-017-0565-x.

[94] Annappa AR, Basavarajappa S, Davim JP. Effect of organoclays on mechanical properties

of glass fiber-reinforced epoxy nanocomposite. Polym Bull 2021;79:5085–103. https://doi.org/10.1007/s00289-021-03759-x.

[95] Tay CH, Mazlan N, Hameed Sultan MT, Abdan K, Lee CH. Mechanical performance of hybrid glass/kenaf epoxy composite filled with organomodified nanoclay. J Mater Res Technol 2021;15:4415–26. https://doi.org/10.1016/j.jmrt.2021.10.062.

[96] Steinke K, Sodano HA. Aramid nanofiber interphase for enhanced interfacial shear strength in ultra-high molecular weight polyethylene/epoxy composites. Adv Mater Interfaces 2022;9:2102030. https://doi.org/10.1002/admi.202102030.

[97] Steinke K, Sodano HA. Enhanced interfacial shear strength in ultra-high molecular weight polyethylene epoxy composites through a zinc oxide nanowire interphase. Compos Sci Technol 2022;219:109218. https://doi.org/10.1016/j.compscitech.2021.109218.

[98] Zhang B, Yin L, Wu W, Tian M, Ning N, Zhang L, et al. Functional interface with polyaniline in UHMWPE fiber-reinforced composites for enhanced interfacial adhesion and damage monitoring. Polym Compos 2022;43:311–9. https://doi.org/10.1002/pc.26375.

[99] Li W, Feng M, Liu X, Huang M, Ma R. Ultra-high molecular weight polyethylene fibers / epoxy composites : effect of fiber treatment on properties. Fibers Polym 2019;20:421–7. https://doi.org/10.1007/s12221-019-8704-7.

[100] Shanmugam L, Feng X, Yang J. Enhanced interphase between thermoplastic matrix and UHMWPE fiber sized with CNT-modified polydopamine coating. Compos Sci Technol 2019;174:212–20. https://doi.org/10.1016/j.compscitech.2019.03.001.

[101] He R, Niu F, Chang Q. The effect of plasma treatment on the mechanical behavior of UHMWPE fiber–reinforced thermoplastic HDPE composite. Surf Interface Anal 2018;50:73–7. https://doi.org/10.1002/sia.6337.

[102] Meng L, Li W, Ma R, Huang M, Cao Y, Wang J. Mechanical properties of rigid polyurethane composites reinforced with surface treated ultrahigh molecular weight polyethylene fibers. Polym Adv Technol 2018;29:843–51. https://doi.org/10.1002/pat.4193.

[103] Mohammadalipour M, Masoomi M. The effect of simultaneous fiber surface treatment and matrix modification on mechanical properties of unidirectional ultra-high molecular weight

polyethylene fiber / epoxy / nanoclay nanocomposites. J Compos Mater 2018;52:2961–2972. https://doi.org/10.1177/0021998318755542.

[104] Li W, Ma R, Huang M, Meng L, Pan Q. Surface treatment of ultra-high molecular weight polyethylene fibers using potassium permanganate and mechanical properties of its composites. Surf Interface Anal 2018;50:65–72. https://doi.org/10.1002/SIA.6336.

[105] Tang G, Hu X, Tang T, Claramunt C. Mechanical properties of surface treated UHMWPE fiber and SiO_2 filled PMMA composites. Surf Interface Anal 2017;49:898–903. https://doi.org/10.1002/sia.6240.

[106] Li W. Improved mechanical properties of epoxy composites reinforced with surface - treated UHMWPE fibers. Polym Adv Technol 2017;29:1287–93. https://doi.org/10.1002/pat.4240.

[107] Tang G, Hu X, Tang T, Claramunt C, Liu C. Enhanced interfacial adhesion of UHMWPE fibers by alkali treatment and its behavior to PI resins. J Thermoplast Compos Mater 2019;32:52–61. https://doi.org/10.1177/0892705717743296.

[108] Jin X, Wang W, Xiao C, Lin T, Bian L, Hauser P. Improvement of coating durability, interfacial adhesion and compressive strength of UHMWPE fiber/epoxy composites through plasma pre-treatment and polypyrrole coating. Compos Sci Technol 2016;128:169–75. https://doi.org/10.1016/j.compscitech.2016.03.026.

[109] Li W, Meng L, Wang L, Mu J, Pan Q. Surface modification of ultra-high molecular weight polyethylene fibers by chromic acid. Surf Interface Anal 2016;48:1316–9. https://doi.org/10.1002/SIA.6040.

[110] Ahmadi M, Masoomi M, Safi S. Mechanical property characterization of carbon nanofiber/epoxy nanocomposites reinforced by GMA-grafted UHMWPE fibers. Compos Part B Eng 2015;83:43–9. https://doi.org/10.1016/j.compositesb.2015.08.006.

[111] Firouzi D, Youssef A, Amer M, Srouji R, Amleh A, Foucher DA, et al. A new technique to improve the mechanical and biological performance of ultra high molecular weight polyethylene using a nylon coating. J Mech Behav Biomed Mater 2014;32:198–209. https://doi.org/10.1016/j.jmbbm.2014.01.001.

[112] Broujerdi MS, Masoomi M, Asgari M. Interfacial improvement and mechanical properties

of epoxy resin/ultra-high molecular weight polyethylene fibre composites compatibilized with glycidyl methacrylate. J Reinf Plast Compos 2013;32:1675–84. https://doi.org/10.1177/0731684413498520.

[113] Li ZH, Chen T. The mechanical and tribological properties of MAH- grafted HDPE-filled clay / PEI composites. Polym Plast Technol Eng 2012;51:776–9. https://doi.org/10.1080/03602559.2012.663848.

[114] Zhang Z, Wang J, Liang G, Zhao W, Lu S. Studies on surface modification of UHMWPE fibers via UV initiated grafting. Appl Surf Sci 2006;253:668–73. https://doi.org/10.1016/j.apsusc.2005.12.165.

[115] Gutowski WS, Pankevicius ER. A novel surface treatment process for enhanced adhesion of ultra-high modulus polyethylene fibres to epoxy resins. Compos Interfaces 1993;1:141–51. https://doi.org/10.1163/156855493X00031.

[116] Ogawa T, Mukai H, Osawa S. Improvement of the mechanical properties of an ultrahigh molecular weight polyethylene fiber/epoxy composite by corona-discharge treatment. J Appl Polym Sci 2001;79:1162–8. https://doi.org/10.1002/1097-4628(20010214)79:7<1162::AID-APP20>3.0.CO;2-Y.

[117] Arshad KA, Hirwani JK, Sinha SK. Effects of UHMWPE Filler on the tribological and mechanical properties of biocompatible epoxies. Tribol Trans 2020;63:382–92. https://doi.org/10.1080/10402004.2019.1700325.

[118] Belgacemi R, Derradji M, Mouloud A, Trache D, Zegaoui A, Belmehdi D, et al. On the mechanical and morphological properties of highly performant composite laminates based on epoxy resin and oxidized ultrahigh-molecular-weight polyethylene fibers. High Perform Polym 2020;32:992–1000. https://doi.org/10.1177/0954008320923385.

[119] Han L, Cai H, Chen X, Zheng C, Guo W. Study of UHMWPE fiber surface modification and the properties of UHMWPE/epoxy composite. Polymers (Basel) 2020;521:1–13. https://doi.org/10.3390/polym12030521.

[120] Wang S, Ma J, Feng X, Cheng J, Ma X, Zhao Y, et al. An effective surface modification of UHMWPE fiber for improving the interfacial adhesion of epoxy resin composites. Polym Compos 2020;41:1614–23. https://doi.org/10.1002/pc.25483.

[121] Yan R, Zhang Q, Shi B, Liu S, Qin Z, Jia L. Investigation on low-velocity impact and interfacial bonding properties of weft-knitted UHMWPE reinforced composites. J Ind Text 2020:1–19. https://doi.org/10.1177/1528083720931474.

[122] Chhetri S, Bougherara H. A comprehensive review on surface modification of UHMWPE fiber and interfacial properties. Compos Part A Appl Sci Manuf 2021;140:106146. https://doi.org/10.1016/j.compositesa.2020.106146.

[123] Pundhir N, Pathak H, Zafar S. Ballistic impact performance of ultra-high molecular weight polyethylene (UHMWPE) composite armour. Sadhana - Acad Proc Eng Sci 2021;46. https://doi.org/10.1007/s12046-021-01730-0.

[124] Tian Y, Guo L. Adhesion performance of UHMWPE fiber treated with polyethylene wax grafted methyl methacrylate alone or in conjunction with silane coupling agent. J Adhes Sci Technol 2021;35:1219–35. https://doi.org/10.1080/01694243.2020.1841998.

[125] Wu JA, Zhang Z, Dai X, Duan L, Lin Y, Sun M. Effect of stacking sequence on multi-point low-velocity impact and compression after impact damage mechanisms of UHMWPE composites. Polym Compos 2021;42:6500–11. https://doi.org/10.1002/PC.26316.

[126] Guo G, Alam S, Peel LD. An investigation of deformation and failure mechanisms of fiber-reinforced composites in layered composite armor. Compos Struct 2022;281:115125. https://doi.org/10.1016/j.compstruct.2021.115125.

[127] Wu M, Jia L, Chen Z, Wang J, Yan R. Synergetic enhancement of interfacial properties and impact resistant of UHMWPE fiber reinforced composites by oxygen plasma modification. Compos Struct 2022;292:115663. https://doi.org/10.1016/j.compstruct.2022.115663.

[128] Ahmadi M, Masoomi M, Safi S, Zabihi O. Interfacial evaluation of epoxy/carbon nanofiber nanocomposite reinforced with glycidyl methacrylate treated UHMWPE fiber. J Appl Polym Sci 2016;133. https://doi.org/10.1002/APP.43751.

[129] Belgacemi R, Derradji M, Trache D, Mouloud A, Zegaoui A, Mehelli O, et al. Effects of silane surface modified alumina nanoparticles on the mechanical, thermomechanical, and ballistic impact performances of epoxy/oxidized UHMWPE composites. Polym Compos 2020;41:4526–37. https://doi.org/10.1002/pc.25730.

[130] Liu X, Wang K. Interfacial microstructure and properties between epoxy resin and novel

organic hybrid graphene oxide modification ultra high molecular weight polyethylene fiber. Polymer (Guildf) 2020;197:122472. https://doi.org/10.1016/j.polymer.2020.122472.

[131] Shanmugam L, Kazemi ME, Qiu C, Rui M, Yang L, Yang J. Influence of UHMWPE fiber and Ti6Al4V metal surface treatments on the low-velocity impact behavior of thermoplastic fiber metal laminates. Adv Compos Hybrid Mater 2020;3:508–21. https://doi.org/10.1007/s42114-020-00189-7.

[132] Shanmugam L, Kazemi ME, Li Z, Luo W, Xiang Y, Yang L, et al. Low-velocity impact behavior of UHMWPE fabric/thermoplastic laminates with combined surface treatments of polydopamine and functionalized carbon nanotubes. Compos Commun 2020;22:100527. https://doi.org/10.1016/j.coco.2020.100527.

[133] Belgacemi R, Derradji M, Trache D, Zegaoui A, Mehelli O, Tarchoun AF. Advanced hybrid materials from epoxy, oxidized UHMWPE fibers and silane surface modified silicon nitride nanoparticles. High Perform Polym 2021;33:440–50. https://doi.org/10.1177/0954008320964547.

[134] Belgacemi R, Derradji M, Trache D, Zegaoui A, Mehelli O. Toward an efficient stress transfer with a fully connected hybrid network from epoxy, oxidized UHMWPE fibers, and silane surface modified silicon carbide nanoparticles. Polym Compos 2021;42:462–73. https://doi.org/10.1002/pc.25839.

[135] Mehelli O, Derradji M, Belgacemi R, Abdous S. Development of lightweight and highly efficient fast neutrons composites shields based on epoxy, UHMWPE fibres and boron carbide particles. Radiat Phys Chem 2022;193:109510. https://doi.org/10.1016/j.radphyschem.2021.109510.

[136] Zhang Y, Cao S, Zhou X, Kong F, Li H, Jiang G. High-performance fiber-reinforced composites with a polydopamine/epoxy silane hydrolysis-condensate bilayer on surface of ultra-high molecular weight polyethylene fiber. J Appl Polym Sci 2022;139:1–11. https://doi.org/10.1002/app.52062.

[137] M. Alsaadi. A study on the delamination and flexural behavior of carbon- and aramid-fiber reinforced epoxy composites with silicon carbide particle inclusions. Mech Compos Mater 2022;57:847–56. https://doi.org/10.22364/mkm.57.6.11.

[138] Zuo L, Wu C, Tong L, Liu X. Improving interfacial properties of polyarylene ether nitrile/aramid fiber composite through hydrogen bonding interaction combined with molecular weight adjustment. J Phys Chem Solids 2022;161:110474. https://doi.org/10.1016/j.jpcs.2021.110474.

[139] Li T, Wang Z, Zhang H, Hu Z, Yu J, Wang Y, et al. Non-destructive modification of aramid fiber by building nanoscale-coating solution to enhance the interfacial adhesion properties of the fiber-reinforced composites. J Compos Mater 2021;55:1823–34. https://doi.org/10.1177/0021998320962845.

[140] Khan MI, Umair M, Hussain R, Nawab Y. Effect of micro-fillers on the performance of thermoplastic para aramid composites for impact applications. Fibers Polym 2021;22:3120–34. https://doi.org/10.1007/s12221-021-0370-x.

[141] Lin G, Wang H, Boquan Yu, Qu G, Chen S, Kuang T, et al. Combined treatments of fiber surface etching/silane-coupling for enhanced mechanical strength of aramid fiber-reinforced rubber blends. Mater Chem Phys 2020;255:123486. https://doi.org/10.1016/j.matchemphys.2020.123486.

[142] Yang B, Zhang M, Lu Z, Luo JJ, Song S, Tan J, et al. Toward improved performances of para-aramid (PPTA) paper-based nanomaterials via aramid nanofibers(ANFs) and ANFs-film. Compos Part B Eng 2018;154:166–74. https://doi.org/10.1016/j.compositesb.2018.07.061.

[143] Fan W, Tian H, Wang H, Zhang T, Yang X, Yu Y, et al. Enhanced interfacial adhesion of aramid fiber III reinforced epoxy composites via low temperature plasma treatment. Polym Test 2018;72:147–56. https://doi.org/10.1016/j.polymertesting.2018.10.003.

[144] Akhil KT, Blaise S, Davis G, Shunmugesh K, Genuvin C, Bins P. The study of the mechanical properties of aramid fiber reinforced epoxy resin composite. Appl Mech Mater 2016;852:36–42. https://doi.org/10.4028/www.scientific.net/amm.852.36.

[145] Deng T, Zhang G, Dai F, Zhang F. Mild surface modification of para-aramid fiber by dilute sulfuric acid under microwave irradiation: Http://DxDoiOrg/101177/0040517516639831 2016;87:799–806. https://doi.org/10.1177/0040517516639831.

[146] Peng T, Cai R, Chen C, Wang F, Liu X, Wang B, et al. Surface modification of para-aramid

fiber by direct fluorination and its effect on the interface of aramid/epoxy composites. J Macromol Sci Part B Phys 2012;51:538–50. https://doi.org/10.1080/00222348.2011.609777.

[147] Park SJ, Seo MK, Ma TJ, Lee DR. Effect of chemical treatment of Kevlar fibers on mechanical interfacial properties of composites. J Colloid Interface Sci 2002;252:249–55. https://doi.org/10.1006/jcis.2002.8479.

[148] Zhang Shu-hui, Liang Guo-zheng, Zhang Wei ZJ. Effect of surface modification of fibers with a polymer coating on the interlaminar shear strength of a composite and the translation of fiber strength in an F-12 aramid/epoxy composite vessel. Mech Compos Mater 2006;42:507–12.

[149] Zhang YH, Huang YD, Liu L, Cai KL. Effects of γ-ray radiation grafting on aramid fibers and its composites. Appl Surf Sci 2008;254:3153–61. https://doi.org/10.1016/j.apsusc.2007.10.081.

[150] Zhang Y, Huang Y, He J, Wu L, Xu Z. Influence of γ-ray radiation grafting on interfacial properties of aramid fibers and epoxy resin composites. Compos Interfaces 2008;15:611–28. https://doi.org/10.1163/156855408785971281.

[151] Gu R, Yu J, Hu C, Chen L, Zhu J, Hu Z. Surface treatment of para-aramid fiber by argon dielectric barrier discharge plasma at atmospheric pressure. Appl Surf Sci 2012;258:10168–74. https://doi.org/10.1016/j.apsusc.2012.06.100.

[152] Gao J, Dai Y, Wang X, Huang J, Yao J, Yang J, et al. Effects of different fluorination routes on aramid fiber surface structures and interlaminar shear strength of its composites. Appl Surf Sci 2013;270:627–33. https://doi.org/10.1016/j.apsusc.2013.01.099.

[153] Zhao J. Effect of surface treatment on the structure and properties of para-aramid fibers by phosphoric acid. Fibers Polym 2013;14:59–64. https://doi.org/10.1007/s12221-013-0059-x.

[154] Cheng Z, Li B, Huang J, Chen T, Liu Y, Wang X, et al. Covalent modification of aramid fibers' surface via direct fluorination to enhance composite interfacial properties. Mater Des 2016;106:216–25. https://doi.org/10.1016/j.matdes.2016.05.120.

[155] Cheng Z, Zhang L, Jiang C, Dai Y, Meng C, Luo L, et al. Aramid fiber with excellent

interfacial properties suitable for resin composite in a wide polarity range. Chem Eng J 2018;347:483–92. https://doi.org/10.1016/j.cej.2018.04.149.

[156] Moraes C V., Demétrio Da Silva V, Castegnaro M V., Morais J, Schrekker HS, Amico SC. Lightweight composites through imidazolium ionic liquid enhanced aramid-epoxy resin interactions. ACS Appl Polym Mater 2020;2:1754–63. https://doi.org/10.1021/acsapm.9b01145.

[157] Zhang Y, Qu R, Wang Y, Jia X, Sun C, Sun H, et al. Enhancement of para-aramid fibers by depositing poly-p-paraphenylene terephthalamide oligomer modified multi-walled carbon nanotubes. Results Mater 2021;9:100170. https://doi.org/10.1016/j.rinma.2021.100170.

[158] Bilisik, K. Erdogan, G. Sapanci E. Flexural behaviour of 3D para-aramid/phenolic/nano (MWCNT) composites. RCS Adv 2018;8:7213–24.

[159] Bilisik K, Sapanci E. Plain para-aramid/phenolic multiwall carbon nanotubes prepreg/multistiched preform composites: experimental characterization of mode-I toughness. J Compos Mater 2019;53:1847–64. https://doi.org/10.1177/0021998318812176.

[160] Gong X, Liu Y, Wang Y, Xie Z, Dong Q, Dong M, et al. Amino graphene oxide/dopamine modified aramid fibers: preparation, epoxy nanocomposites and property analysis. Polymer (Guildf) 2019;168:131–7. https://doi.org/10.1016/j.polymer.2019.02.021.

[161] Suresh A, Bhargavi P, Kiran Kumar M. Simulation and mechanical characterization on kevlar epoxy reinforced composite with silicon carbide filler. Mater Today Proc 2020;38:2988–95. https://doi.org/10.1016/j.matpr.2020.09.321.

[162] Obradović V, Simić D, Sejkot P, Machalická K V., Vokáč M. Moisture absorption characteristics and effects on mechanical properties of Kolon/epoxy composites. Curr Appl Phys 2021;26:16–23. https://doi.org/10.1016/j.cap.2021.03.015.

[163] Zhang B, Jia L, Tian M, Ning N, Zhang L, Wang W. Surface and interface modification of aramid fiber and its reinforcement for polymer composites: a review. Eur Polym J 2021;147:110352. https://doi.org/10.1016/j.eurpolymj.2021.110352.

[164] Lei D, Zhang H, Liu N, Zhang Q, Su T. Tensible and flexible high-sensitive spandex fiber strain sensor enhanced by carbon nanotubes/Ag nanoparticles. Nanotechnology 2021;32:505509.

[165] Ali A, Sattar M, Riaz T, Khan BA, Awais M, Militky J, et al. Highly stretchable durable electro-thermal conductive yarns made by deposition of carbon nanotubes. J Text Inst 2022;113:80–9. https://doi.org/10.1080/00405000.2020.1863569.

[166] Chen Q, Li Y, Xiang D, Zheng Y, Zhu W, Zhao C, et al. Enhanced strain sensing performance of polymer/carbon nanotube-coated spandex fibers via noncovalent interactions. Macromol Mater Eng 2020;305:1–10. https://doi.org/10.1002/mame.201900525.

[167] Vo TT, Lee HJ, Kim SY, Suk JW. Synergistic effect of graphene/silver nanowire hybrid fillers on highly stretchable strain sensors based on spandex composites. Nanomaterials 2020;10:1–14. https://doi.org/10.3390/nano10102063.

[168] Kong Q, Luo Z, Wang Y, Wang B. Fabrication of super-stretchable and electrical conductive membrane of spandex/multi-wall carbon nanotube/reduced graphene oxide composite. J Polym Res 2018;25. https://doi.org/10.1007/s10965-018-1597-0.

[169] Chen Q, Xiang D, Wang L, Tang Y, Harkin-Jones E, Zhao C, et al. Facile fabrication and performance of robust polymer/carbon nanotube coated spandex fibers for strain sensing. Compos Part A Appl Sci Manuf 2018;112:186–96. https://doi.org/10.1016/j.compositesa.2018.06.009.

[170] Sun J, Xu Y, Chen Y, Liu Y, Leng J. Spandex fiber reinforced shape memory polymer composites and their mechanical properties. Adv Mater Res 2012;410:370–4. https://doi.org/10.4028/www.scientific.net/AMR.410.370.

[171] Sun J, Xu Y, Chen Y, Liu Y, Leng J. Mechanical and electrical properties of spandex reinforced GMWNT/epoxy shape memory composites. Behav Mech Multifunct Mater Compos 2012 2012;8342:83421A. https://doi.org/10.1117/12.915125.

[172] Sun J, Liu Y, Leng J. Mechanical properties of shape memory polymer composites enhanced by elastic fibers and their application in variable stiffness morphing skins. J Intell Mater Syst Struct 2015;26:2020–7. https://doi.org/10.1177/1045389X14546658.

[173] Foroughi J, Spinks GM, Aziz S, Mirabedini A, Jeiranikhameneh A, Wallace GG, et al. Knitted carbon-nanotube-sheath/spandex-core elastomeric yarns for artificial muscles and strain sensing. ACS Nano 2016;10:9129–35. https://doi.org/10.1021/acsnano.6b04125.

[174] Yang SY, Cho KH, Kim Y, Song MG, Jung HS, Yoo JW, et al. High performance twisted and coiled soft actuator with spandex fiber for artificial muscles. Smart Mater Struct 2017;26:105025. https://doi.org/10.1088/1361-665X/aa84e4.

[175] Guo YN, Gao ZY, Wang XX, Sun L, Yan X, Yan SY, et al. A highly stretchable humidity sensor based on spandex covered yarns and nanostructured polyaniline. RSC Adv 2018;8:1078–82. https://doi.org/10.1039/c7ra10474j.

[176] Montazerian H, Rashidi A, Dalili A, Najjaran H, Milani AS, Hoorfar M. Graphene-coated spandex sensors embedded into silicone sheath for composites health monitoring and wearable applications. Small 2019;15:1804991. https://doi.org/10.1002/smll.201804991.

[177] Bi S, Hou L, Dong W, Lu Y. Multifunctional and ultrasensitive-reduced graphene oxide and pen ink/polyvinyl alcohol-decorated modal/spandex fabric for high-performance wearable sensors. ACS Appl Mater Interfaces 2021;13:2100–9. https://doi.org/10.1021/acsami.0c21075.

[178] Myant C, Stewart R. Multifunctional and stretchable graphene / textile composite sensor for human motion monitoring. J Appl Polym Sci Appl 2022:1–13. https://doi.org/10.1002/app.52755.

[179] Gokuldass R, Ramesh R. Mechanical strength behavior of hybrid composites tailored by glass/Kevlar fibre-reinforced in nano-silica and micro-rubber blended epoxy. Silicon 2019;11:2731–9. https://doi.org/10.1007/s12633-018-0064-1.

[180] Gokuldass R, Ramesh R. Mechanical and low velocity impact behaviour of intra-ply glass/Kevlar fibre reinforced nano-silica and micro-rubber modified epoxy resin hybrid composite. Mater Res Express 2019;6:055302. https://doi.org/10.1088/2053-1591/aaff1e.

[181] Zhang S, Shi Z, Cui P, Duan N, Li X. Surface modification of aramid fibers with $CaCl_2$ treatment and secondary functionalization of silane coupling agents. J Appl Polym Sci 2020;137:49159. https://doi.org/10.1002/APP.49159.

[182] Czigány T, Deák T, Tamás P. Discontinuous basalt and glass fiber reinforced PP composites from textile prefabricates: effects of interfacial modification on the mechanical performance. Compos Interfaces 2008;15:697–707. https://doi.org/10.1163/156855408786778302.

[183] Asi O. An experimental study on the bearing strength behavior of Al_2O_3 particle filled glass fiber reinforced epoxy composites pinned joints. Compos Struct 2010;92:354–63. https://doi.org/10.1016/J.COMPSTRUCT.2009.08.014.

[184] Satheesh Raja R, Manisekar K. Experimental and statistical analysis on mechanical properties of nano flyash impregnated GFRP composites using central composite design method. Mater Des 2016;89:884–92. https://doi.org/10.1016/J.MATDES.2015.10.043.

[185] Liu J, Boo WJ, Clearfield A, Sue HJ. Intercalation and exfoliation: a review on morphology of polymer nanocomposites reinforced by inorganic layer structures. Mater Manuf Process 2006;21:143–51. https://doi.org/10.1080/AMP-200068646.

[186] Daud W, Bersee HEN, Picken SJ, Beukers A. Layered silicates nanocomposite matrix for improved fiber reinforced composites properties. Compos Sci Technol 2009;69:2285–92. https://doi.org/10.1016/J.COMPSCITECH.2009.01.009.

[187] Bashar M, Mertiny P, Sundararaj U. Effect of nanocomposite structures on fracture behavior of epoxy-clay nanocomposites prepared by different dispersion methods. J Nanomater 2014;2014. https://doi.org/10.1155/2014/312813.

[188] Chukov DI, Kharitonov AP, Tcherdyntsev V V., Zherebtsov DD, Maksimkin A V. Structure and mechanical properties of self-reinforced ultra-high molecular weight polyethylene. J Compos Mater 2018;52:1689–98. https://doi.org/10.1177/0021998317728781.

[189] Debnath S, Ranade R, Wunder SL, Baran GR, Zhang J, Fisher ER. Chemical surface treatment of ultrahigh molecular weight polyethylene for improved adhesion to methacrylate resins. J Appl Polym Sci 2005;96:1564–72. https://doi.org/10.1002/app.21598.

[190] Li W, Ma R, Huang M, Meng L, Pan Q. Surface treatment of ultra-high molecular weight polyethylene fibers using potassium permanganate and mechanical properties of its composites. Surf Interface Anal 2018;50:65–72. https://doi.org/10.1002/sia.6336.

[191] Peinado J, Jiao-Wang L, Olmedo Á, Santiuste C. Influence of stacking sequence on the impact behaviour of UHMWPE soft armor panels. Compos Struct 2022;286:115365. https://doi.org/10.1016/J.COMPSTRUCT.2022.115365.

[192] Vijayalakshmi KA, Karthikeyan N, Vignesh K. Surface modification of spandex fiber using

low temperature plasma. Int J Sci Res 2014:116–8.

[193] Leu CM, Wu ZW, Wei KH. Synthesis and properties of covalently bonded layered silicates/polyimide (BTDA-ODA) nanocomposites. Chem Mater 2002;14:3016–21. https://doi.org/10.1021/cm0200240.

[194] Sharma B, Chhibber R, Mehta R. Curing studies and mechanical properties of glass fiber reinforced composites based on silanized clay minerals. Appl Clay Sci 2017;138:89–99. https://doi.org/10.1016/j.clay.2016.12.038.

[195] Asgari M, Abouelmagd A, Sundararaj U. Silane functionalization of sodium montmorillonite nanoclay and its effect on rheological and mechanical properties of HDPE/clay nanocomposites. Appl Clay Sci 2017;146:439–48. https://doi.org/10.1016/j.clay.2017.06.035.

[196] Shanmugharaj AM, Rhee KY, Ryu SH. Influence of dispersing medium on grafting of aminopropyltriethoxysilane in swelling clay materials. J Colloid Interface Sci 2006;298:854–9. https://doi.org/10.1016/j.jcis.2005.12.049.

[197] Piscitelli F, Posocco P, Toth R, Fermeglia M, Pricl S, Mensitieri G, et al. Sodium montmorillonite silylation: unexpected effect of the aminosilane chain length. J Colloid Interface Sci 2010;351:108–15. https://doi.org/10.1016/j.jcis.2010.07.059.

[198] Bertuoli PT, Piazza D, Scienza LC, Zattera AJ. Preparation and characterization of montmorillonite modified with 3-aminopropyltriethoxysilane. Appl Clay Sci 2014;87:46–51. https://doi.org/10.1016/J.CLAY.2013.11.020.

[199] Su L, Tao Q, He H, Zhu J, Yuan P, Zhu R. Silylation of montmorillonite surfaces: dependence on solvent nature. J Colloid Interface Sci 2013;391:16–20. https://doi.org/10.1016/j.jcis.2012.08.077.

[200] Shen W, He HP, Zhu J, Yuan P, Frost RL. Grafting of montmorillonite with different functional silanes via two different reaction systems. J Colloid Interface Sci 2007;313:268–73. https://doi.org/10.1016/j.jcis.2007.04.029.

[201] He H, Duchet J, Galy J, Gerard JF. Grafting of swelling clay materials with 3-aminopropyltriethoxysilane. J Colloid Interface Sci 2005;288:171–6. https://doi.org/10.1016/j.jcis.2005.02.092.

[202] Herrera NN, Letoffe JM, Reymond JP, Bourgeat-Lami E. Silylation of laponite clay particles with monofunctional and trifunctional vinyl alkoxysilanes. J Mater Chem 2005;15:863–71. https://doi.org/10.1039/B415618H.

[203] Bruce AN, Lieber D, Hua I, Howarter JA. Rational interface design of epoxy-organoclay nanocomposites: role of structure-property relationship for silane modifiers. J Colloid Interface Sci 2014;419:73–8. https://doi.org/10.1016/j.jcis.2013.12.051.

[204] Ali Feiz, Hamed Khosravi ET. Effect of surface-functionalization of Na+ -montmorillonite nanoclay using 3-aminopropyl- trimethoxy silane on the mechanical properties of E-glass chopped strand mat/epoxy composites. J Part Sci Technol 2018;4:59–65. https://doi.org/10.22104/JPST.2018.2915.1125.

[205] Raji M, Mekhzoum MEM, Rodrigue D, Qaiss A el kacem, Bouhfid R. Effect of silane functionalization on properties of polypropylene/clay nanocomposites. Compos Part B Eng 2018;146:106–15. https://doi.org/10.1016/j.compositesb.2018.04.013.

[206] Li W, Meng L, Ma R. Effect of surface treatment with potassium permanganate on ultra-high molecular weight polyethylene fiber reinforced natural rubber composites. Polym Test 2016;55:10–6. https://doi.org/10.1016/j.polymertesting.2016.08.006.

[207] Li W, Liu X, Feng M, Yang J. Bamboo-like ultra-high molecular weight polyethylene fibers and their epoxy composites. Compos Sci Technol 2019;182:107716. https://doi.org/10.1016/J.COMPSCITECH.2019.107716.

[208] Sharma B, Chhibber R, Mehta R. Effect of mixing parameters on mechanical properties of organoclay epoxy nanocomposites. Mater Today Proc 2018;5:276–86. https://doi.org/10.1016/j.matpr.2017.11.083.

[209] Sharma B, Chhibber R, Mehta R. Effect of mixing parameters, postcuring, and stoichiometry on mechanical properties of fiber reinforced epoxy–clay nanocomposites. Proc Inst Mech Eng Part L J Mater Des Appl 2019;233:1363–74. https://doi.org/10.1177/1464420717752023.

[210] Pinto D, Bernardo L, Amaro A, Lopes S. Mechanical properties of epoxy nanocomposites using titanium dioxide as reinforcement – a review. Constr Build Mater 2015;95:506–24. https://doi.org/10.1016/J.CONBUILDMAT.2015.07.124.

[211] Pinto D, Bernardo L, Amaro A, Lopes S. Mechanical properties of epoxy nanocomposites using alumina as reinforcement - a review. J Nano Res 2015;30:9–38. https://doi.org/10.4028/WWW.SCIENTIFIC.NET/JNANOR.30.9.

[212] Li W, Meng L, Wang L, Mu J, Pan Q. Surface modification of ultra-high molecular weight polyethylene fibers by chromic acid. Surf Interface Anal 2016;48:1316–9. https://doi.org/10.1002/sia.6040.

[213] Meng L, Li W, Ma R, Huang M, Wang J, Luo Y, et al. Long UHMWPE fibers reinforced rigid polyurethane composites: an investigation in mechanical properties. Eur Polym J 2018;105:55–60. https://doi.org/10.1016/J.EURPOLYMJ.2018.05.021.

[214] Li W, Huang M, Ma R. Improved mechanical properties of epoxy composites reinforced with surface-treated UHMWPE fibers. Polym Adv Technol 2018;29:1287–93. https://doi.org/10.1002/PAT.4240.

[215] Moon SI, Jang J. Role of additional silane coupling agent treatment in oxygen plasma-treated UHMPE fiber/vinylester composites. J Adhes Sci Technol 2000;14:493–506. https://doi.org/10.1163/156856100742708.

[216] Jantanasakulwong K, Leksawasdi N, Seesuriyachan P, Wongsuriyasak S, Techapun C, Ougizawa T. Reactive blending of thermoplastic starch and polyethylene-graft-maleic anhydride with chitosan as compatibilizer. Carbohydr Polym 2016;153:89–95. https://doi.org/10.1016/j.carbpol.2016.07.091.

[217] Y. Abdelaal M, H. Elmossalamy E, O. S. Bahaffi S. Enhancement of polyolefins compatibility with natural fibers through chemical modification. Am J Polym Sci 2012;2:102–8. https://doi.org/10.5923/j.ajps.20120205.04.

[218] Tian YL, Guo LM. Surface modification of UHMWPE fibers by means of polyethylene wax grafted maleic anhydride treatment. J Appl Polym Sci 2018;135:1–7. https://doi.org/10.1002/app.46555.

[219] Wang C, Chen L, Li J, Sun S, Ma L, Wu G, et al. Enhancing the interfacial strength of carbon fiber reinforced epoxy composites by green grafting of poly(oxypropylene) diamines. Compos Part A Appl Sci Manuf 2017;99:58–64. https://doi.org/10.1016/J.COMPOSITESA.2017.04.003.

[220] Ma L, Li N, Wu G, Song G, Li X, Han P, et al. Interfacial enhancement of carbon fiber composites by growing TiO2 nanowires onto amine-based functionalized carbon fiber surface in supercritical water. Appl Surf Sci 2018;433:560–7. https://doi.org/10.1016/J.APSUSC.2017.10.036.

[221] Su M, Gu A, Liang G, Yuan L. The effect of oxygen-plasma treatment on Kevlar fibers and the properties of Kevlar fibers/bismaleimide composites. Appl Surf Sci 2011;257:3158–67. https://doi.org/10.1016/J.APSUSC.2010.10.133.

[222] Xing L, Liu L, Huang Y, Jiang D, Jiang B, He J. Enhanced interfacial properties of domestic aramid fiber-12 via high energy gamma ray irradiation. Compos Part B Eng 2015;69:50–7. https://doi.org/10.1016/J.COMPOSITESB.2014.09.027.

[223] Yue CY, Padmanabhan K. Interfacial studies on surface modified Kevlar fibre/epoxy matrix composites. Compos Part B Eng 1999;30:205–17. https://doi.org/10.1016/S1359-8368(98)00053-5.

[224] Cheon J, Lim SJ, Kim M. A composite RAS with an enhanced uniformity of absorbing performance using a MWCNT-anchored aramid fiber. Compos Sci Technol 2020;200:108442. https://doi.org/10.1016/j.compscitech.2020.108442.

[225] Chen J, Zhu Y, Ni Q, Fu Y, Fu X. Surface modification and characterization of aramid fibers with hybrid coating. Appl Surf Sci 2014;321:103–8. https://doi.org/10.1016/J.APSUSC.2014.09.196.

[226] Derombise G, Van Schoors LV, Messou MF, Davies P. Influence of finish treatment on the durability of aramid fibers aged under an alkaline environment. J Appl Polym Sci 2010;117:888–98. https://doi.org/10.1002/APP.31534.

[227] Abu Obaid A, Deitzel JM, Gillespie JW, Zheng JQ. The effects of environmental conditioning on tensile properties of high performance aramid fibers at near-ambient temperatures. J Compos Mater 2011;45:1217–31. https://doi.org/10.1177/0021998310381436.

[228] Guo F, Zhang ZZ, Liu WM, Su FH, Zhang HJ. Effect of plasma treatment of Kevlar fabric on the tribological behavior of Kevlar fabric/phenolic composites. Tribol Int 2009;42:243–9. https://doi.org/10.1016/J.TRIBOINT.2008.06.004.

[229] Ramasamy N, Arumugam V, Rajkumar S. Surface modification of Kevlar fibre fabric and its influence on the properties of Kevlar/epoxy composites. Bull Mater Sci 2019;42:1–9. https://doi.org/10.1007/s12034-019-1868-3.

[230] Li Z, Liu B, Kong H, Yu M, Qin M, Teng C. Layer-by-layer self-assembly strategy for surface modification of aramid fibers to enhance interfacial adhesion to epoxy resin. Polymers (Basel) 2018;10:820. https://doi.org/10.3390/polym10080820.

[231] Shelly D, Nanda T, Mehta R. Addition of compatibilized nanoclay and UHMWPE fibers to epoxy based GFRPs for improved mechanical properties. Compos Part A Appl Sci Manuf 2021;145:106371. https://doi.org/10.1016/j.compositesa.2021.106371.

[232] Patel DBH, Mandot AA, Jha PK. Extraction, characterization and application of azadirachta indica leaves for development of hygienic lycra filaments. J Int Acad Res Multidiscip 2014;393:65.

[233] Zhao Y, Huang Y, Hu W, Guo X, Wang Y, Liu P, et al. Highly sensitive flexible strain sensor based on threadlike spandex substrate coating with conductive nanocomposites for wearable electronic skin. Smart Mater Struct 2019;28. https://doi.org/10.1088/1361-665X/aaf3ce.

[234] Marjo CE, Gatenby S, Rich AM, Gong B, Chee S. ATR-FTIR as a tool for assessing potential for chemical ageing in Spandex/Lycra®/elastane-based fabric collections. Stud Conserv 2017;62:343–53. https://doi.org/10.1080/00393630.2016.1198868.

[235] Nandiyanto ABD, Oktiani R, Ragadhita R. How to read and interpret ftir spectroscope of organic material. Indones J Sci Technol 2019;4:97–118. https://doi.org/10.17509/ijost.v4i1.15806.

[236] Lee HS, Ko JH, Song KS, Choi KH. Segmental and chain orientational behavior of spandex fibers. J Polym Sci Part B Polym Phys 1997;35:1821–32. https://doi.org/10.1002/(SICI)1099-0488(199708)35:11<1821::AID-POLB13>3.0.CO;2-A.

[237] Shelly D, Nanda T, Mehta R. Novel epoxy-based glass fiber reinforced composites containing compatibilized para-aramid fibers and silanized nanoclay for improved impact strength. Polym Compos 2021. https://doi.org/10.1002/pc.26453.

Appendix-I

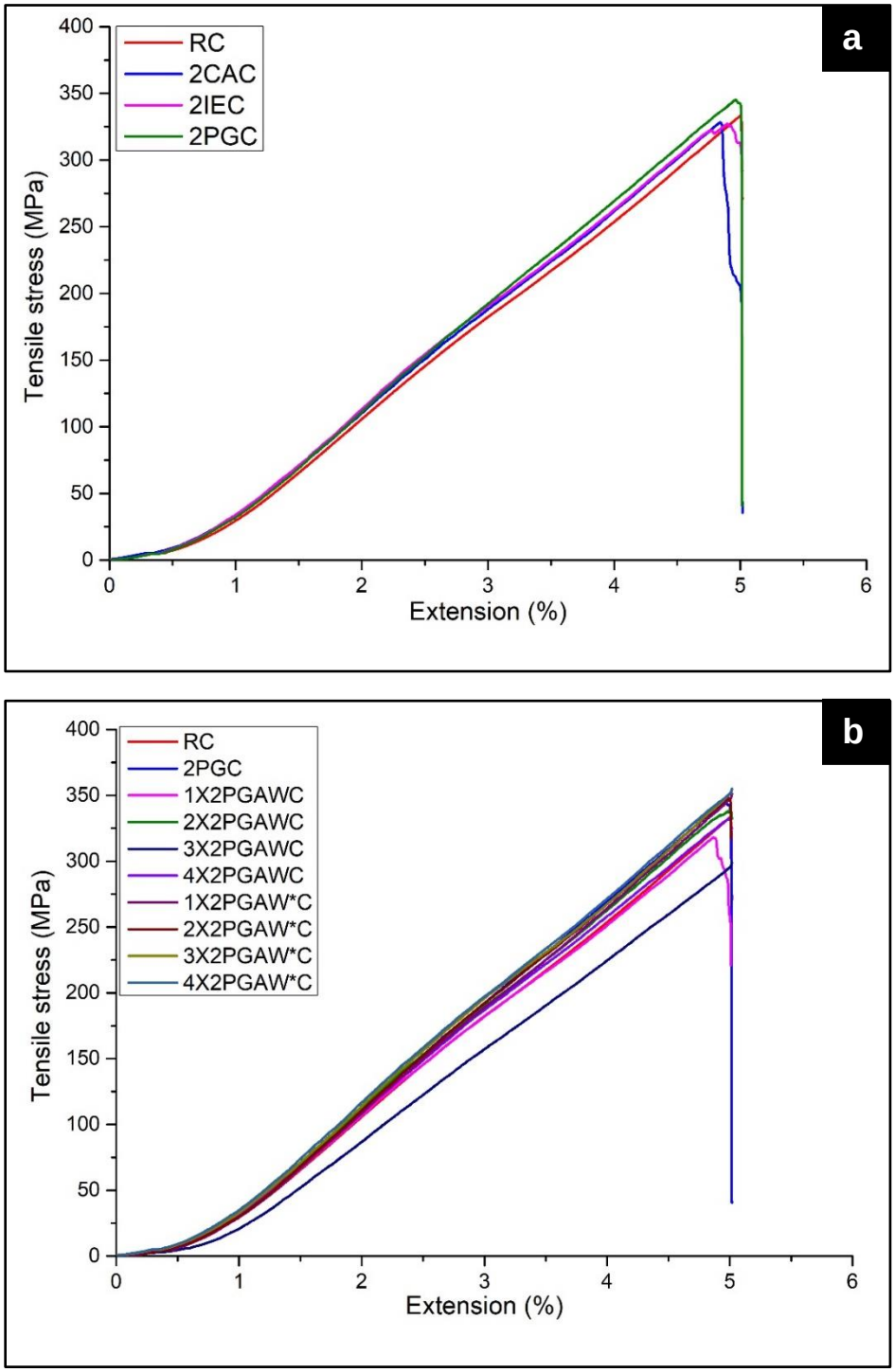

Figure A1. Stress versus extension curves under tensile loading of epoxy based GFRPs reinforced with 2 phr of (a) different pristine nanoclays, and (b) surface treated PG nanoclay under different silanization conditions.

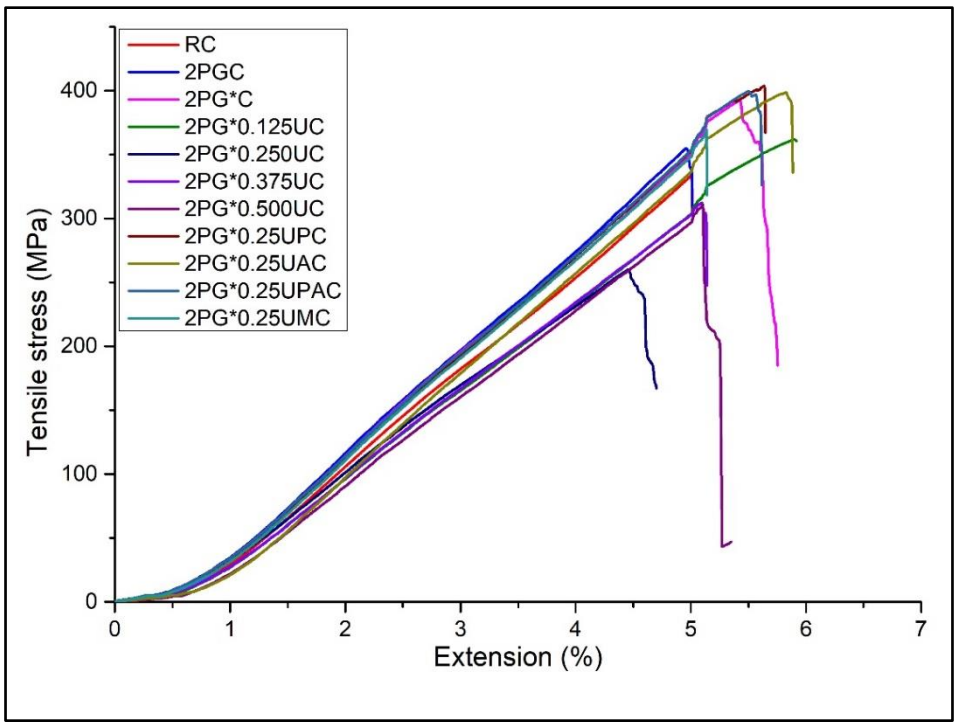

Figure A2. Stress versus extension curves under tensile loading of epoxy based GFRPs reinforced with 2 phr of silanized PG nanoclay and different concentrations of UHMWPE fibers (pristine as well as compatibilized).

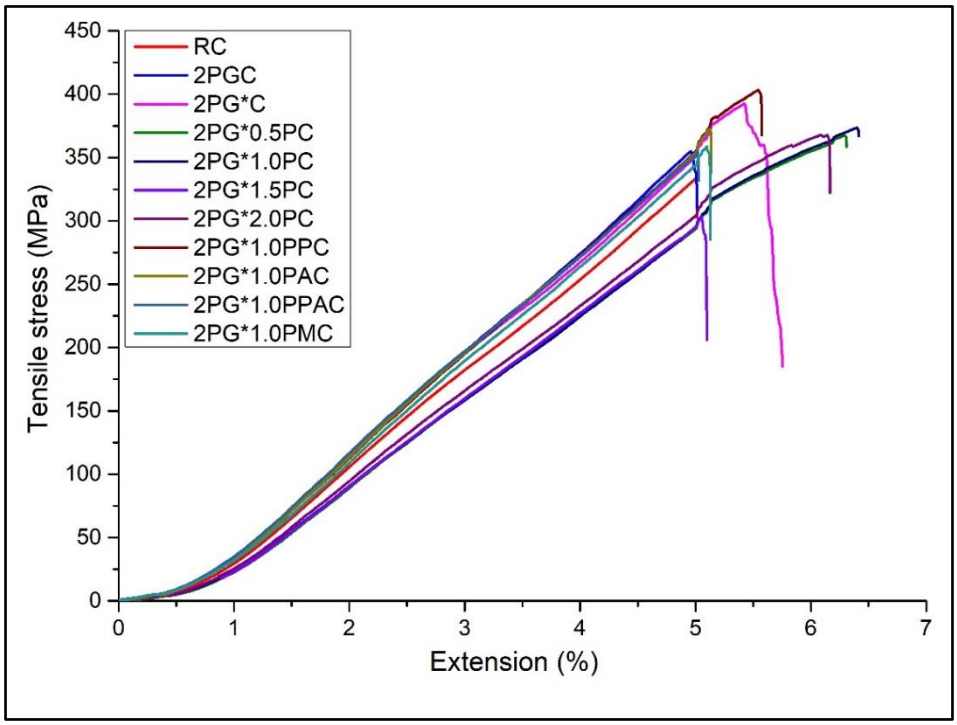

Figure A3. Stress versus extension curves under tensile loading of epoxy based GFRPs reinforced with 2 phr of silanized PG nanoclay and different concentrations of para-aramid fibers (pristine as well as compatibilized).

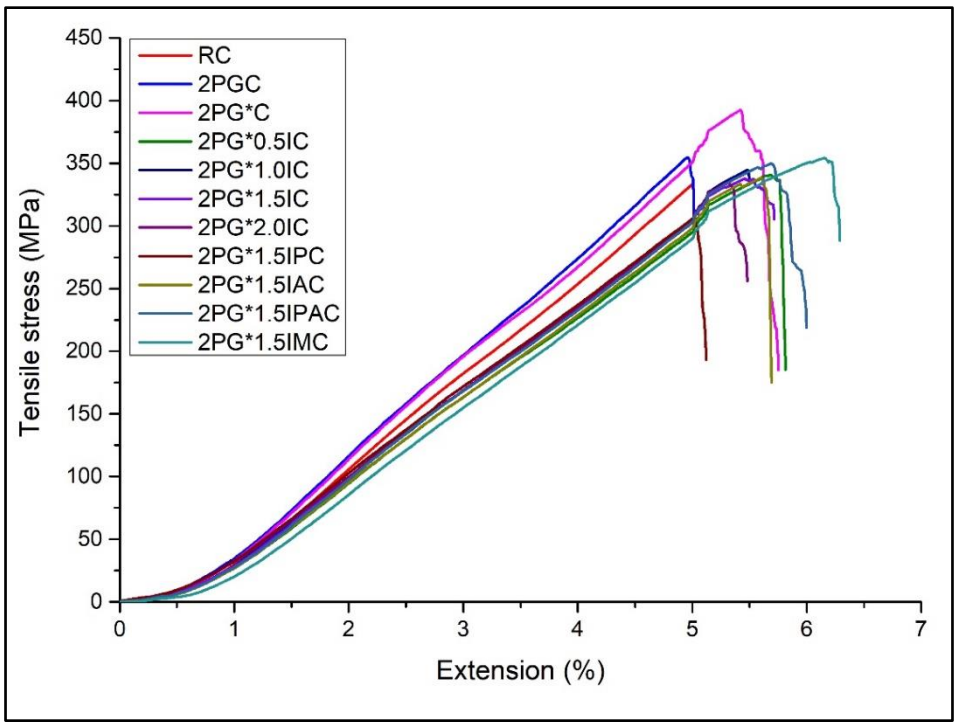

Figure A4. Stress versus extension curves under tensile loading of epoxy based GFRPs reinforced with 2 phr of silanized PG nanoclay and different concentrations of Inviya fibers (pristine as well as compatibilized).

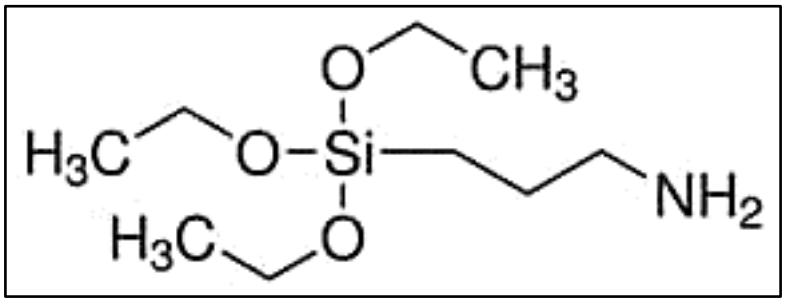

Figure A5. Chemical structure of 3-aminopropyltriethoxy silane agent.

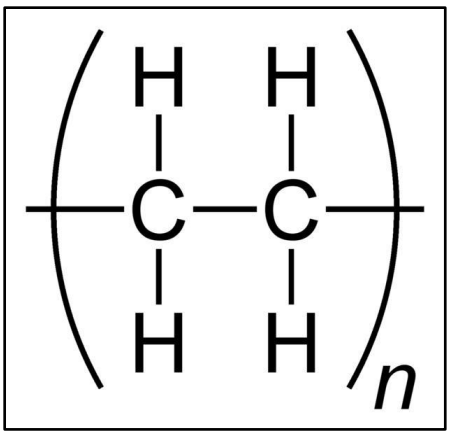

Figure A6. Chemical structure of ultra high molecular weight polyethylene (UHMWPE) fibers.

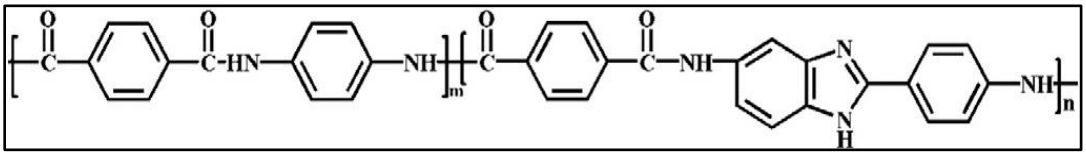

Figure A7. Chemical structure of para-aramid fibers.

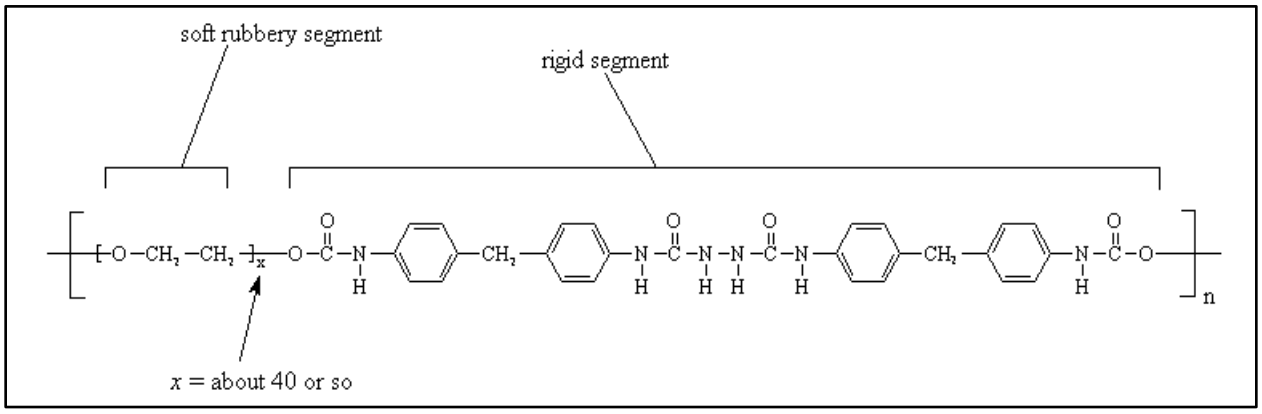

Figure A8. Chemical structure of Inviya (Spandex) fibers.